

MECHANICAL STUDIES ON THE PORCINE AORTIC VALVE: PART I

MECHANICAL STUDIES
ON THE
PORCINE AORTIC VALVE

PART I
GEOMETRICAL ASYMMETRY,
MATERIAL INHOMOGENEITY AND ANISOTROPY
IN THE
PORCINE AORTIC VALVE

By

MING CHONG (B.Sc. Queen's University, Kingston)

A Thesis

Submitted to the School of Graduate Studies
in Partial Fulfillment of the Requirements
for the Degree
Master of Engineering

Department of Engineering Physics

McMaster University

Hamilton, Ontario

(December) 1977

MASTER OF ENGINEERING (1977)
(Engineering Physics)

McMASTER UNIVERSITY
Hamilton, Ontario

TITLE: Mechanical Studies on the Porcine Aortic Valve
Part I: Geometrical Asymmetry, Material Inhomogeneity
and Anisotropy in the Porcine Aortic Valve

AUTHOR: Ming Chong, B.Sc. (Queen's University, Kingston)

SUPERVISOR: Dr. Y. F. Missirlis

NUMBER OF PAGES: x, 167, 5 Appendices

ABSTRACT

Various areas of studies on the natural and the prosthetic aortic valves are reviewed.

A microtensile technique devised to investigate the inhomogeneous and anisotropic material properties of a porcine aortic valve's leaflets is described. Also, the theory and apparatus of a new stereophotogrammetric technique to define points in space by their Cartesian coordinates is introduced. The technique is used to investigate the local surface strains and curvatures of a porcine aortic valve's leaflets from 0 to 120 mm. Hg. in-vitro.

It is found that the valve leaflets display marked inhomogeneity and anisotropy (orthotropy is assumed) in the elastic moduli and transition strains. For the non-coronary leaflet, the radial post-transition moduli vary from 42 to 215 gm/mm² with a mean of 111 gm/mm² (s.d. = 43 gm/mm²); and the radial transition strains vary from 30% to 70% with a mean of 58% (s.d. = 7%). Areas nearer the leaflet's coaptation edge tend to exhibit lower radial transition strains than the annulus edge. The central region of the leaflet is found to be the stiffest. For the same non-coronary leaflet, the circumferential post-transition moduli vary from 220 to 590 gm/mm² with a mean of 342 gm/mm² (s.d. = 118 gm/mm²);

and the circumferential transition strains vary from 22% to 47% with a mean of 33% (s.d. = 3%).

Inhomogeneity between leaflets is also observed; preliminary results seem to suggest that the non-coronary leaflet is the stiffest in the radial direction and the least stiff in the circumferential direction. In comparison, the right coronary leaflet exhibits the largest radial transition strains (~80%) and the smallest circumferential transition strains (~25%).

For the diastolic valve in-vitro, the circumferential strains are less than 10% at all pressures; therefore, this suggests pre-transition behaviour during diastole which is contrary to the general belief. Radial strains at diastole vary from 10% to well over 100% and show a definite tendency to increase from the sinus-annulus edge to the coaptation edge. The non-coronary leaflet is the least strained of the leaflets (10% to 60% at diastole).

The determination of pre- or post-transition state at diastole is discussed and the implications of the results on stress analyses and trileaflet valve designs are noted.

ACKNOWLEDGEMENTS

The author wishes to express his appreciation to his thesis supervisor, Dr. Yannis F. Missirlis, whose guidance and encouragement throughout was highly instrumental in the completion of this work; and to Denise LaMarche and Abdul Ahood, who as fellow students, have provided some valuable discussion.

The author would also like to thank Bob Hallas of Fearman Co., Burlington, Ontario for providing the porcine hearts. He also gratefully acknowledges the financial assistance provided by the Department of Engineering Physics at McMaster University.

Also a note of thanks to my family and Patricia Cox for their helpful and timely encouragement.

TABLE OF CONTENTS

	Page
ABSTRACT	iii
ACKNOWLEDGEMENTS	v
TABLE OF CONTENTS	vi
LIST OF FIGURES	viii
LIST OF TABLES	x
 Chapter	
I. INTRODUCTION	1
A. Purpose of Study	1
B. Background and Overview of Studies on the Aortic Valve	2
1. Anatomy and Geometry	2
2. The Porcine Aortic Valve	11
3. Physiological Function	13
4. Histology and Ultrastructure	17
5. Mechanical Material Properties	21
6. Flow Studies	24
7. Stress Analyses	29
8. Reasons for Aortic Valve Replacements	34
C. Aortic Valve Substitutes	36
1. Historical Review of AVR	36
2. Rigid Mechanical Prosthetic Valves	42
3. Biological Tissue Valves	44
4. Prosthetic Trileaflet Valves	52
5. Summary and Consensus	53
D. Methodology	56
II. EXPERIMENTAL METHOD	57
A. Microtensile Experiments	57
1. Dissection and Tissue Preparation	57
2. Apparatus and Testing	59
3. Data Acquisition and Processing	62
B. Whole Valve Experiments	67
1. Dissection and Tissue Preparation	67
2. Apparatus and Testing	68
3. Data Acquisition and Processing	75

Chapter		
III.	RESULTS AND DISCUSSIONS	78
	A. Microtensile Stress-Strain Experiments	78
	1. Comments on the Experimental Method	78
	2. Inhomogeneity in Material Properties	83
	3. Anisotropy in Material Properties	97
	4. Comparison with Other Microtensile Data ...	98
	5. Implications of Results	102
	B. Whole Valve Experiments	104
	1. Comments on the Experimental Method	104
	2. Radii of Curvature	111
	3. Pressure-Strain	117
	4. Iso-Strain Contour Maps	127
	5. Determination of Pre- or Post-Transition ..	134
	6. Implications of Results	140
IV.	SUMMARY OF CONCLUSIONS AND SUGGESTIONS	141
	ADDENDUM	144
	BIBLIOGRAPHY	146
APPENDIX A.	Microtensile Stress-Strain Theory and Terminology	A1
	1. Stress-Strain Relationships	A1
	2. Stress-Strain Curve Terminology	A4
	3. Determination of Elastic Moduli	A6
	4. Effect of Tissue Curvature on Errors ...	A7
APPENDIX B.	Stereophotogrammetry and Experimental Application	B1
	1. Theory	B1
	2. Application to Experiment	B7
	3. Parallax Errors	B17
	4. Curved Surface Distance Approximation ..	B19
	5. Other Error Considerations	B20
APPENDIX C.	Computer Programs for the Data Analysis ...	C1
APPENDIX D.	Method of Calculating the Local Radius of Curvature	D1
	1. Theory	D1
	2. Application to Experiment	D6
APPENDIX E.	Use of Lasers to Determine Surface Strains	E1

LIST OF FIGURES

Figure	Page
1. The Aortic Valve and the Heart	3
2. Aortic Valve Anatomy	5
3. Aortic Valve Leaflet Morphology	7
4. Aortic Valve Terminology	10
5. Typical Cardiac Pressure Cycle	14
6. Aortic Valve Leaflet Histology	18
7. Stress Analysis Methodology	31
8. Current Aortic Valve Substitutes	37
9. Microtensile Experiment Apparatus	60
10. Typical Tensilon Force-Length Curve	63
11. Microtensile Stretching of a Tissue Strip	64
12. Microtensile Strip at Rest	65
13. Microtensile Strip under Stress	66
14. Porcine Aortic Valve after Dotting	69
15. Diagram of Apparatus for Whole Valve Experiment ...	71
16. Stereophotogrammetric Set-Up	72
17. Valve Pressure and Rotator Systems	73
18. Determination of Component Strains and Radii	77
19. Effect of Storage Time on Transition Strain	84
20. Stress-Strain Curves for NC Radial Strips	85
21. Stress-Strain Curves for NC Circumferential Strips	86
22. Stress-Strain Curves for Radial Strips	87
23. Stress-Strain Curves for Circumferential Strips ...	88
24. Distribution of NC Radial Elastic Moduli	89
25. Distribution of NC Circumferential Elastic Moduli .	90
26. Distribution of NC Elastic Modulus Ratio	91
27. Comparison of Stress-Strain Curves	100
28. Pressure-Radii of Curvature Curves for NC Leaflet .	112
29. Pressure-Radii of Curvature Curves for LC Leaflet .	113
30. Pressure-Radii of Curvature Curves for RC Leaflet .	114
31. Pressure-Strain Curves for NC Leaflet	118
32. Pressure-Strain Curves for LC Leaflet	119
33. Pressure-Strain Curves for RC Leaflet	120
34. Iso-Strain Map of Porcine Valve at 20 mm. Hg.	128
35. Iso-Strain Map of Porcine Valve at 40 mm. Hg.	129
36. Iso-Strain Map of Porcine Valve at 60 mm. Hg.	130
37. Iso-Strain Map of Porcine Valve at 80 mm. Hg.	131
38. Iso-Strain Map of Porcine Valve at 100 mm. Hg.	132
39. Iso-Strain Map of Porcine Valve at 120 mm. Hg.	133
40. Aortic Ring Distension with Pressure	136

Figure	Page
A1. Microtensile Strip and Necking	A2
A2. Stress-Strain Terminology	A5
A3. Effect of Tensilon Sample Strip Curvature	A8
B1. Relationship of Point P_i with Angle of View θ	B2
B2. View of Point P at View Angles 0° and θ	B4
B3. Geometry for Derivation of Y_i	B6
B4. Porcine Aortic Valve at 0 mm. Hg.	B9
B5. Porcine Aortic Valve at 20 mm. Hg.	B10
B6. Porcine Aortic Valve at 40 mm. Hg.	B11
B7. Porcine Aortic Valve at 60 mm. Hg.	B12
B8. Porcine Aortic Valve at 80 mm. Hg.	B13
B9. Porcine Aortic Valve at 100 mm. Hg.	B14
B10. Porcine Aortic Valve at 120 mm. Hg.	B15
B11. Porcine Aortic Valve from 0 to 100 mm. Hg.	B16
B12. Parallax Errors	B18
B13. Surface Strain Approximation	B18
B14. Geometry for Derivation of Y_i - Z-Axis is not Axis of Rotation	B24
C1. Flow Charts for Computer Program VALVE	C5
D1. Illustration of Local Radii of Curvature R	D2
D2. Geometry for Derivation of R	D4

LIST OF TABLES

Table	Page
1. Assumptions used in the Stress Analyses of the Aortic Valve Leaflets	32
2. Comparison of Aortic Valve Substitutes	55
3. Comparison of Microtensile Stress-Strain Data	101
4. Comparison of Microtensile Stress-Strain Data	144

I. INTRODUCTION

A. Purpose of Study

There is a recent trend for a reversal in the design of prosthetic heart valves; the once abandoned artificial valves based on normal anatomophysiology [see Prosthetic Tri-Leaflet Valves, p. 52] are gaining renewed interest because of the recent success of the aortic valve replacements (AVR) using the stabilized glutaraldehyde-preserved porcine xenografts [see Porcine Xenograft, p. 48], and also because of the variety of unsolved problems of the second generation valves whose design features were adapted from hydrodynamic principles [see Rigid Mechanical Prosthetic Valves, p. 42].

With the rapid progress now being made in newer, stronger and more durable fibre composite biomaterials, it is anticipated by several researchers that the ultimate and ideal valve will have its basic design duplicating as much as possible the geometrical, functional, material and mechanical characteristics of the natural human aortic valve. As part of the continuous combined effort to provide contributive information to the design of a prosthetic trileaflet aortic valve, several researchers have conducted stress analyses to investigate the strength aspect of the valve leaflets while being subjected to simulated physiological

static diastolic pressures [see Stress Analyses of the Aortic Valve Leaflets, p. 29].

All of these analyses have in one way or another based their calculations on some simplifying assumptions. Some of these assumptions, such as hypothetical symmetrical leaflet surface geometry, constant leaflet thickness, and homogeneity and isotropy in material properties were in part due to the lack of suitable methods of incorporating the more exact and realistic conditions (ie., irregular surface geometry, varied leaflet thickness, inhomogeneity and anisotropy) into the various different analytical methodologies. Nevertheless, the validity of these approximations is still questionable.

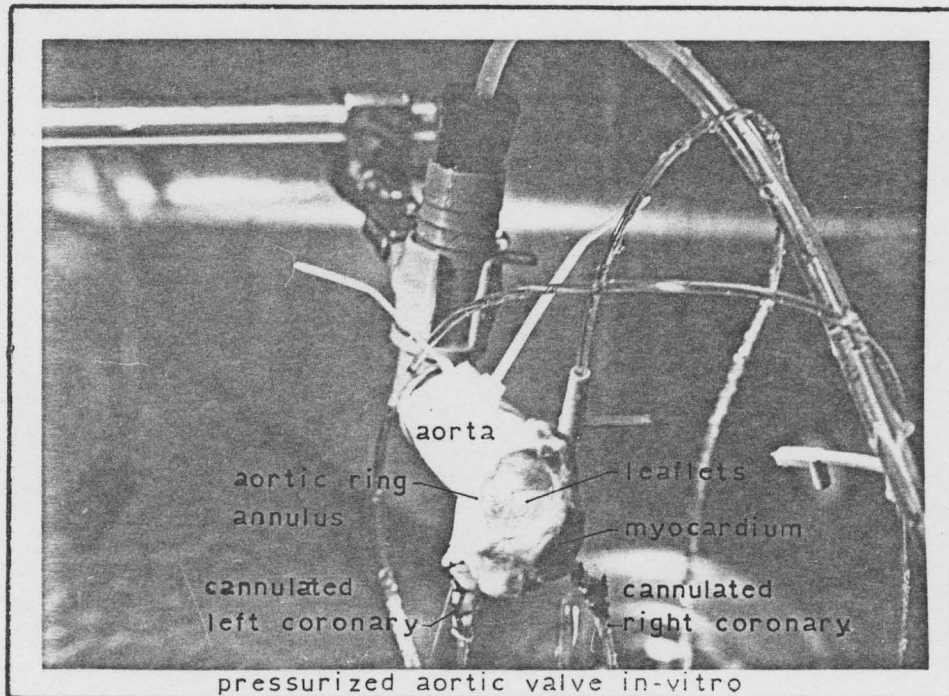
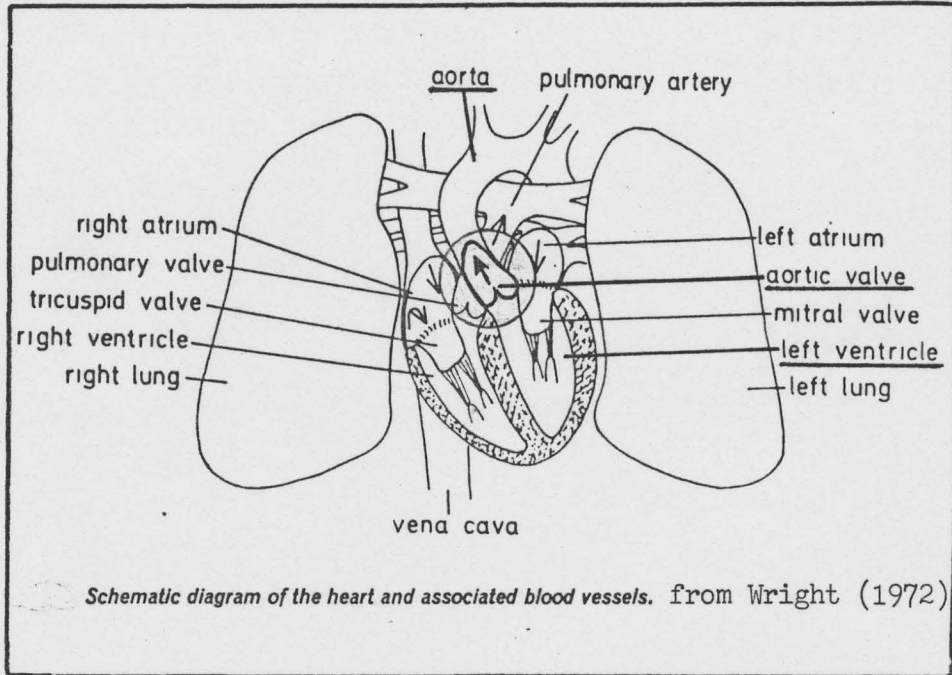
In light of the above, this research was conducted to investigate the inhomogeneity and anisotropy of the leaflet material properties with the porcine aortic valve as the in-vitro specimen. Also, the irregular local asymmetrical surface geometry of the diastolic leaflets was examined.

B. Background and Overview of Studies on the Aortic Valve

B1. Anatomy and Geometry of the Human Aortic Valve

The aortic valve acts as the unidirectional check valve for the flow of blood from the heart's left ventricle to the aorta and the systemic circulation (figure 1). The

FIGURE 1.
The AORTIC VALVE and the HEART

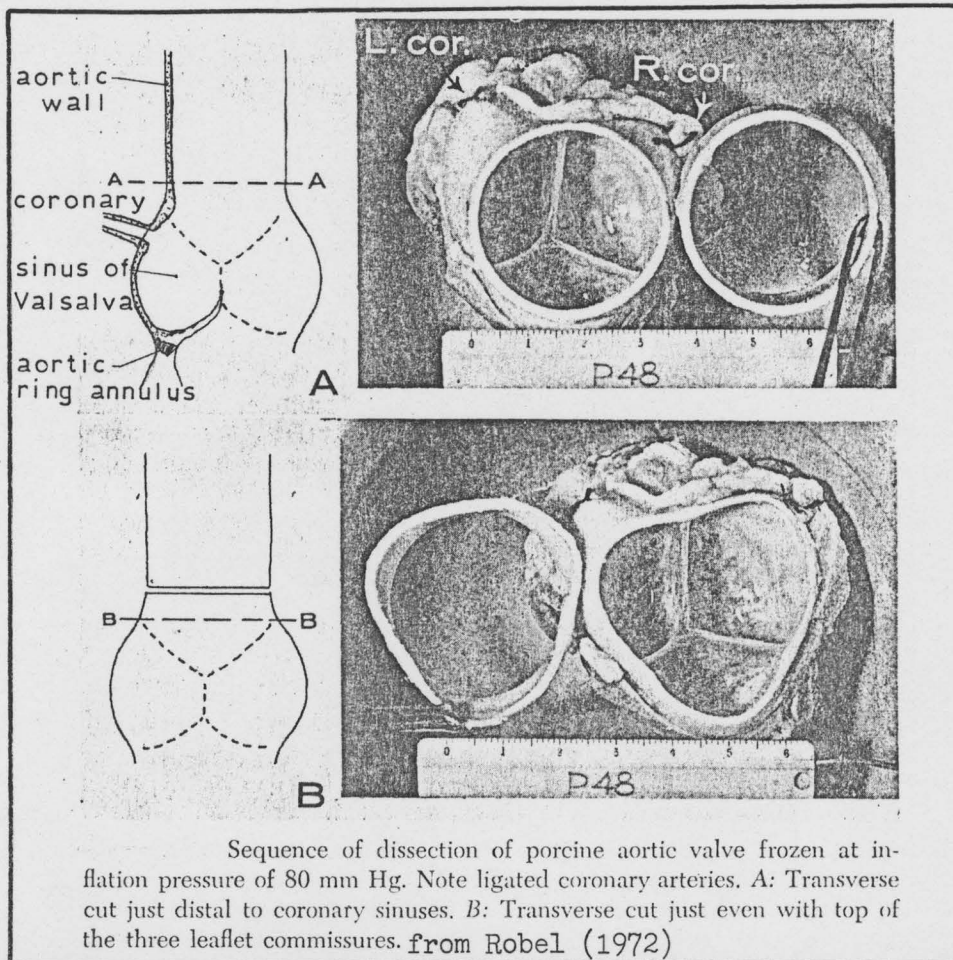


immediate anatomy of the valve as shown in figure 2 consists of three distinct regions: 1) the three sinuses of Valsalva, 2) the aortic ring or annulus fibrosus and 3) the three thin flexible cusped leaflets.

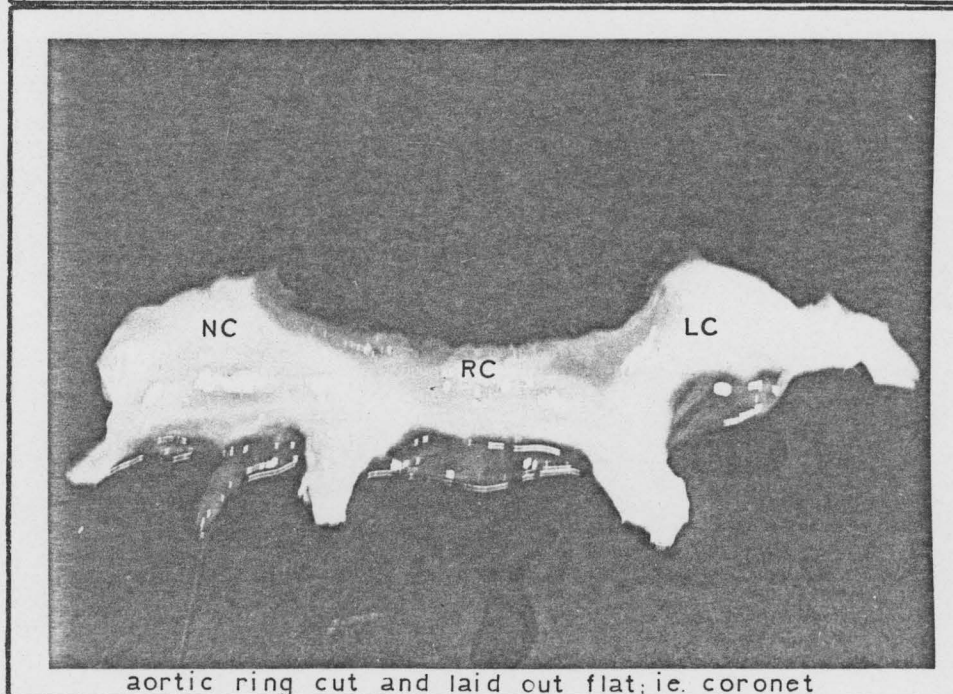
The sinuses are spherical cup cavities located behind the leaflets. They have been credited by Bellhouse (1968,1969) as being responsible for initiating valve closure by entrapping vortex eddies during the deceleration of aortic flow in late systole. The sinuses' contribution in this area has been further studied by Spaan et al (1975). Two of the sinuses have coronary ostia. The latter are the origins of the two coronary arteries which feed blood to the heart myocardium.

The aortic ring is the attachment line of the leaflets to the aortic wall. Its stiffness has led Missirlis (1973) to describe it as a circumferential clamping device that is structurally useful in maintaining proper leaflet coaptation and valve closure. Results from this research will show that the annulus might also serve to reduce the diastolic circumferential stresses. Brewer et al (1976) used strain transducers attached to a dog's aortic root at the commissures to measure the systolic and diastolic aortic radii. They found that besides being stiff, the annulus is also dynamic and serves the purpose of reducing the leaflet fatigue stresses during systole. When cut and laid out flat (figure 2), the ring assumes a coronet-like shape with three

FIGURE 2. AORTIC VALVE ANATOMY



Sequence of dissection of porcine aortic valve frozen at inflation pressure of 80 mm Hg. Note ligated coronary arteries. A: Transverse cut just distal to coronary sinuses. B: Transverse cut just even with top of the three leaflet commissures. from Robel (1972)



aortic ring cut and laid out flat; i.e. coronet

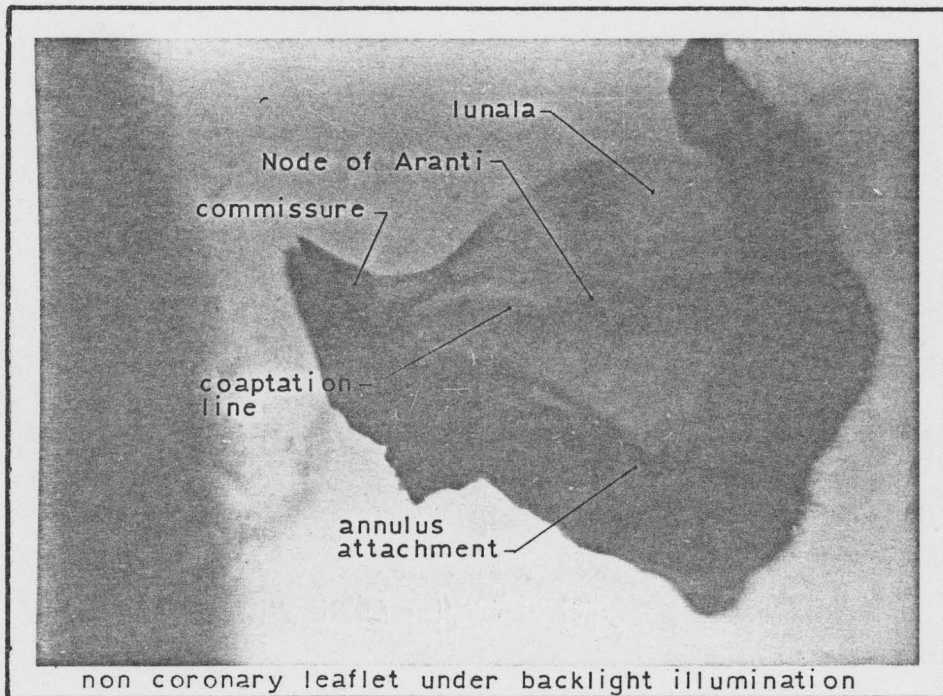
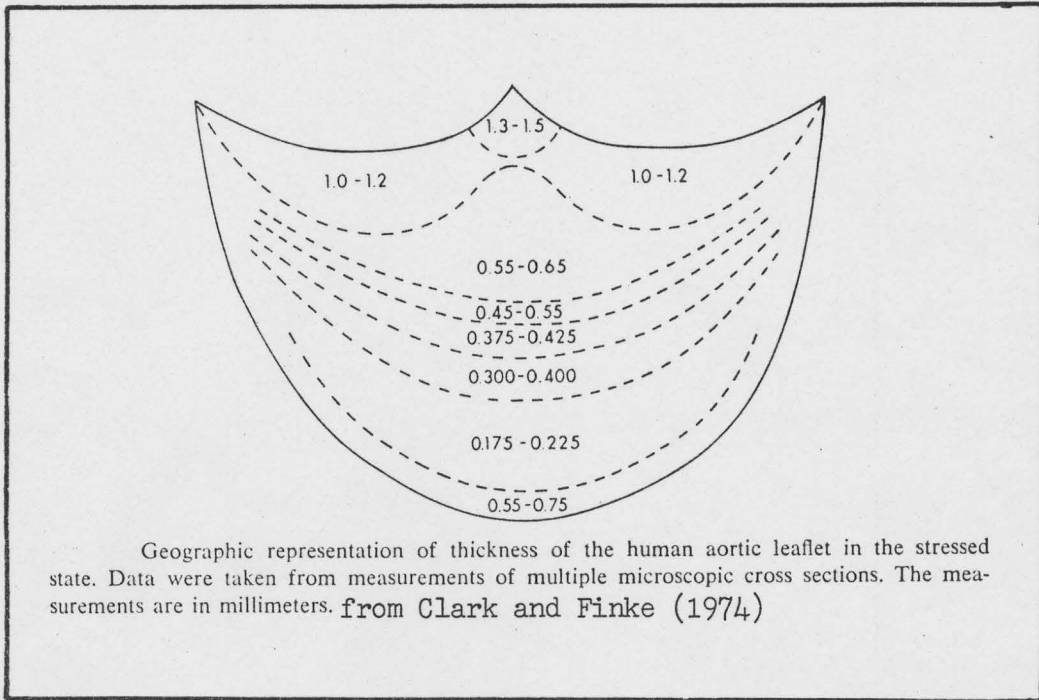
prongs. Between and external to the prongs lie the expansible elastic leaflet tissue. The leaflet attachments at the prongs are called commissures.

The leaflets are thin with a varied thickness over the entire surface. The average thickness of a relaxed leaflet is 0.5-0.6 mm. for human valves [Sands et al, 1969]. When stressed as in the diastolic state, the thickness is reduced; eg., about 0.3 mm. at 100 mm. Hg. pressure [Swanson and Clark, 1974]. Figure 3 is a distribution of the leaflet thickness for a typical leaflet in a stressed state at 80 mm. Hg. The range from 0.2 to 1.5 mm. clearly illustrates the inhomogeneity of the gross leaflet structure.

The thickened nodule at the center of the leaflet's free edge is called the Corpus or Node of Aranti. It is the point of mutual coaptation of all three leaflets. The above average thickness is structurally important in preventing central leakage of backflow through the closed diastolic valve. The crescent-shaped line just above the free edge between the node and the commissures is also thicker than the leaflet proper. This is the line of coaptation for the leaflets when the valve is first closed. The thin lunulae below this line form the surfaces of coaptation of the leaflets and are chiefly responsible for providing a competent seal when the valve is increasingly pressurized [Swanson and Clark, 1974].

The distal third or more of each leaflet attachment

FIGURE 3.
AORTIC VALVE LEAFLET MORPHOLOGY ⁷



(that portion nearest the free edge) is strengthened by collagenous fibre cords inserting perpendicularly into the prongs. These cords, which are the most predominant gross structural features on the leaflets, will be discussed in more detail later [see Histology and Ultrastructure of the Valve Leaflets, p. 17]. The proximal portion of each leaflet is connected to the fibrous coronet by a thinner sheet of collagenous tissue with an interwoven and less tendonous texture.

The first systematic study of the geometry of the aortic valve was undertaken by Robel et al (1964,1972) using freezing techniques with pressurized porcine aortic valves. More detailed analyses on the dimensions and geometry of the human aortic valves were conducted later by Swanson and Clark (1974) and Peskin (1974).

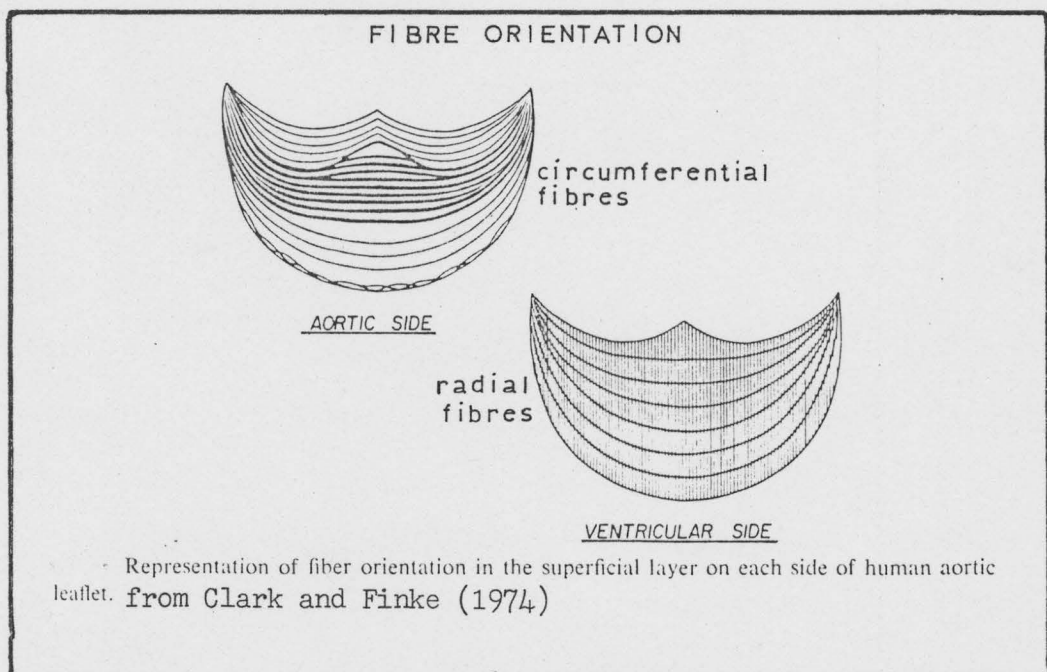
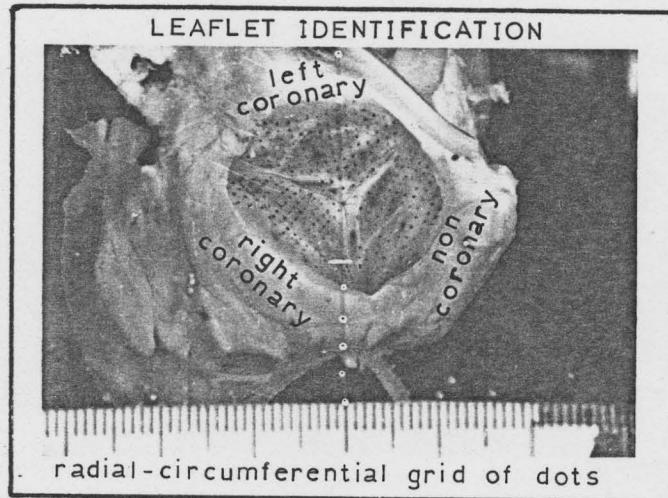
The surface geometry of the leaflets when the valve is closed and pressurized has received considerable attention following its recognition as being a critical input in stress analyses [Gould et al, 1973; Missirlis, 1973]. The stressed leaflets were once thought to be spherical segments [Retzius, 1843], and Mir Sepasi et al (1975) has constructed tissue leaflets on this premise. Robel et al (1964) and Robel (1972) viewed the leaflets as cylindrical segments, and Mercer et al (1973) constructed tissue leaflets on a paraboloid geometry assumption. Other standard geometrical surfaces such as the cylindrical paraboloid, the elliptical paraboloid and the

paraboloids of revolution have been used as inputs for various leaflet stress analyses [Chong et al, 1973; Gould et al, 1973; Missirlis, 1973; Missirlis and Armeniades, 1976].

Accurate knowledge of the leaflet surface geometry is however not essential in the construction of a valve leaflet replacement since molds of actual valves may be used in this respect [Geha et al, 1970; Carpentier et al, 1971; Reis et al, 1971]. But for reasons of refining stress analyses, techniques have been devised to describe more discretely the local surface geometry of the leaflets. Greenfield et al (1973) digitized data obtained from thin slices of human aortic valve molds in order to simulate on a computer, the changes in the three-dimensional surface of the valve with pressure. Affeld et al (1973) attempted to do the same with bovine aortic valves. Karara and Marzan (1973) and Karara (1975) described the leaflets' surface geometry by using close-range stereophotogrammetry to determine the three-dimensional coordinates of dots applied onto human aortic valve molds.

The three leaflets are not all similar and are independently named in the literature as the non-coronary (NC), the left coronary (LC) and the right coronary (RC) leaflets. Figure 4 identifies these leaflets with respect to their anatomical positions as seen from the valve's ventricular side. From time to time in this study, they will also be referred to respectively as the non-coronary (NC), the non-

FIGURE 4.
AORTIC VALVE TERMINOLOGY



muscle coronary (NMC = LC) and the muscle coronary (MC = RC) leaflets, according to the presence or absence of a coronary artery and to the amount of supporting myocardium. The dissimilarity between leaflets and the particular asymmetry of the LC leaflet are probably of functional importance since the valve surrounding anatomy is itself very asymmetrical.

The inclusion of asymmetry, although seemingly important, was ignored in all of the earlier prosthetic tri-leaflet valve designs. To employ a simple symmetrical valve in place of an obviously asymmetrical natural valve in a structurally asymmetrical environment would appear to be contrary to the rules of design optimization.

B2. The Porcine Aortic Valve

Among the animal aortic valves, the porcine aortic valve comes closest to reflecting the anatomy and dimensions of the human aortic valve [Sands et al, 1969]. Therefore, the pig is most commonly used as the source of xenograft AVRs. However, there are a few notable differences. Average center leaflet thickness for the porcine valve is 0.75 mm. as compared to 0.62 mm. for the human valve. The aortic ring diameter for both valves measure about 26 mm. but the human aortic ring is more circular due to the more equal sizing of the three leaflets. The porcine valve has a characteristically smaller NC leaflet and a more asymmetrical LC leaflet. The porcine valve also exhibits more myocardial support

along the annulus circumference; specifically, the porcine valve shows a greater percentage of myocardium along the LC leaflet annulus. Both of the valves' NC leaflet bases join a fibrous membrane immediately below the annulus without any myocardial support. This membrane is continuous with the base of the anterior mitral valve leaflet and is shared by the adjacent LC leaflet. The porcine valve's NC leaflet has however a less proportionate share of this membrane.

The recognition of these differences is important to analyzing the stress distributions in the leaflets of an in-vivo valve. It is particularly important when proper insertion of a porcine xenograft in the differing human aortic environment is considered. For example, excision of the myocardial support of porcine xenografts which is required to eliminate areas of potential calcification [Mohri et al, 1969] weakens the RC leaflet support and encourages valve incompetency. As such, researchers have devised specific means of mounting grafts; Ionescu et al (1968) tried fabric reinforcement to the muscle-excised RC leaflet and then Carpentier et al (1969) utilized an asymmetrical frame for mounting. Recent improvements in this area have included the partially flexible stent developed by Reis et al (1971) for the Hancock xenografts, the fully flexible stent introduced by Edwards Laboratories for the Carpentier-Edwards porcine xenografts [Edwards Labs Tech. Bull., 1976] and the multi-anatomical stents designed by Shiley Laboratories for the

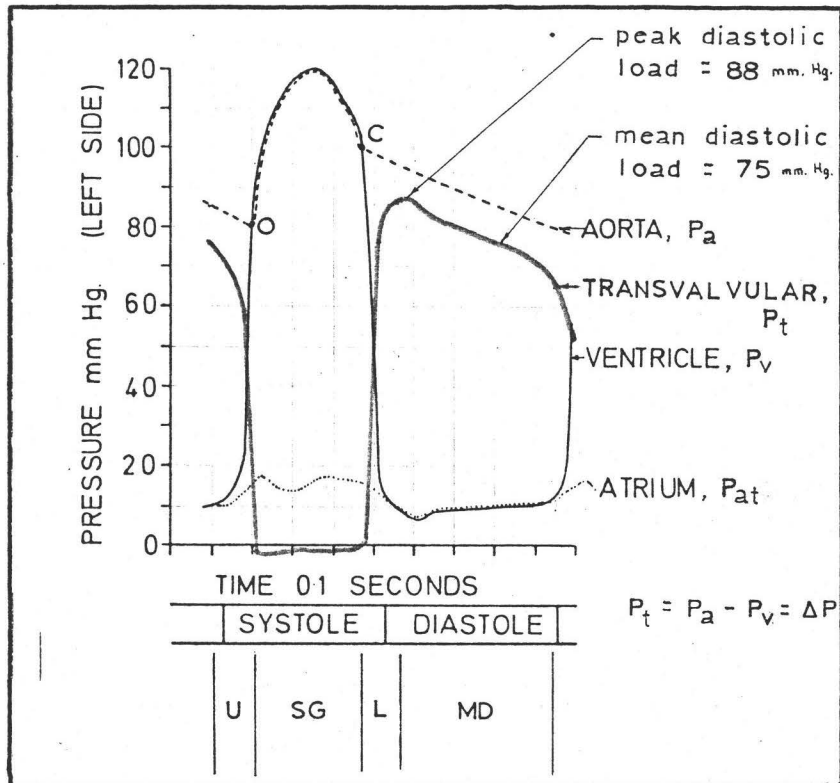
Angell-Shiley xenografts [Shiley Labs Tech. Bull., 1976].

B3. Physiological Function of the Aortic Valve

The aortic valve functioning as a unidirectional valve opens during ventricular systole (left ventricle contracts increasing ventricular pressure toward the aortic pressure) and closes during diastole (left ventricle relaxes causing ventricular pressure to drop below the aortic pressure). During systole, the valve's three leaflets fold back toward the wall of the aorta-sinus to permit blood flow through a tapered triangular orifice [McMillan et al, 1955; Davila, 1961; Robel, 1972; Brewer et al, 1976]. During diastole, the leaflets coapt and distend to prevent regurgitation.

The normal healthy valve generally opens when the left ventricle pressure just exceeds the intra-aortic pressure at the beginning of the systolic stage (figure 5). Blood flows through the opened valve with a negligible pressure gradient. The pliable leaflets flap freely in the flow of blood and observations of the aortic valve opening have indicated a wavy, buckling and whipping leaflet motion [Swanson and Clark, 1973]. Such a motion would induce bending fatigue stresses in the leaflet region with the most buckle. However, calculations of the maximum bending stresses indicated that they are only a fraction of the maximum in-plane membrane stresses developed at valve closure at about

FIGURE 5.
TYPICAL CARDIAC PRESSURE CYCLE



O : aortic valve opens when $P_t \rightarrow -0$ mm. Hg.

C : aortic valve closes when $P_t \rightarrow +0$ mm. Hg.

SG : systolic gradient ($P_v - P_a$) - for a natural human aortic valve, peak systolic gradient < 5 mm. Hg.
 - for a typical prosthetic aortic valve, peak systolic gradient > 20 mm. Hg.
 - for a diseased stenotic aortic valve, peak systolic gradient \rightarrow 100 mm. Hg.

L : valve loading period - occurs in \sim 0.1 sec with maximum strain rate up to peak load of about 90 mm. Hg.

U : valve unloading period - occurs in approximately 0.1 sec.

MD : mean diastolic loading ($P_a - P_v$) - for a natural human aortic valve, mean diastolic load = 75 mm. Hg.
 - for abnormal valve states as in hypertension and incompetency, mean diastolic load can triple.

100 mm. Hg. [Swanson and Clark, 1973,1974]. It is also interesting to note that regions of large bending stresses ($1.2 - 2.4 \times 10^4$ dynes/cm²* [Clark et al, 1974]) associated with buckling during systole coincide with the regions of valve rupture in diastole. It is possible that these two factors are interrelated.

The triangular orifice configuration of the leaflets during systole presents another complication in fatigue stresses. This configuration implies that the flapping leaflets are flat and under circumferential tension; therefore, they must have contracted along the line of coaptation. Robel (1972) using measurements from frozen pressurized porcine aortic valves showed that there is an overall change of 35% in the leaflet free edge length over a cardiac cycle of 138/104 mm. Hg. The valve leaflets are therefore remarkably durable if this cycling of tension is being repeated over 40×10^6 times per year. On the other hand, Swanson and Clark (1974) using silicone molds of pressurized aortic valves concluded that the free edge length of the leaflets varied very little with pressure. The inherent mechanism in the valve geometry which eliminates the cycling of tension implied by Robel's (1972) data was however not identified.

Prior to Bellhouse (1968), it was generally thought that the reverse aortic flow associated with increasing

* 0.17 - 0.35 psi or 0.12 - 0.24 gm/mm².

aortic pressure and decreasing ventricular pressure closed the valve. However, he showed that the valve starts to close during the deceleration phase of systole and is three-quarter closed at the end of systole [Bellhouse and Talbot, 1969]. Formations of eddy vortices in the sinuses during flow deceleration were identified as the prime mechanism of closure. Spaan et al (1975) noted that the eddy vortices also help to reduce the high tension in the leaflets at valve closure. Complete closure is obtained with a small reverse flow and the aid of the aortic root's elastic recoil [Brewer et al, 1976]. After closure and during diastole, the leaflets distend and build up in-plane membrane stresses due to the increasing aortic-ventricular differential loading pressure (figure 5). Comparatively small bending stresses due to small changes in radii of curvature are also expected.

At peak diastolic loads, the leaflets of a typical healthy human aortic valve are subjected to a transvalvular pressure ($P_{\text{tran}} = P_{\text{aorta}} - P_{\text{ventricle}}$) of about 90 to 100 mm. Hg. In conditions such as hypertension or during exercise this diastolic load may be as much as tripled.

Other features of the valve leaflets which aid in functioning are their low inertial mass and the smoothness of the ventricular side. Together with the optimized design of the valve's inflow and outflow regions, turbulence and energy losses are kept minimal; for example, the natural human aortic valve exhibits a negligible systolic pressure

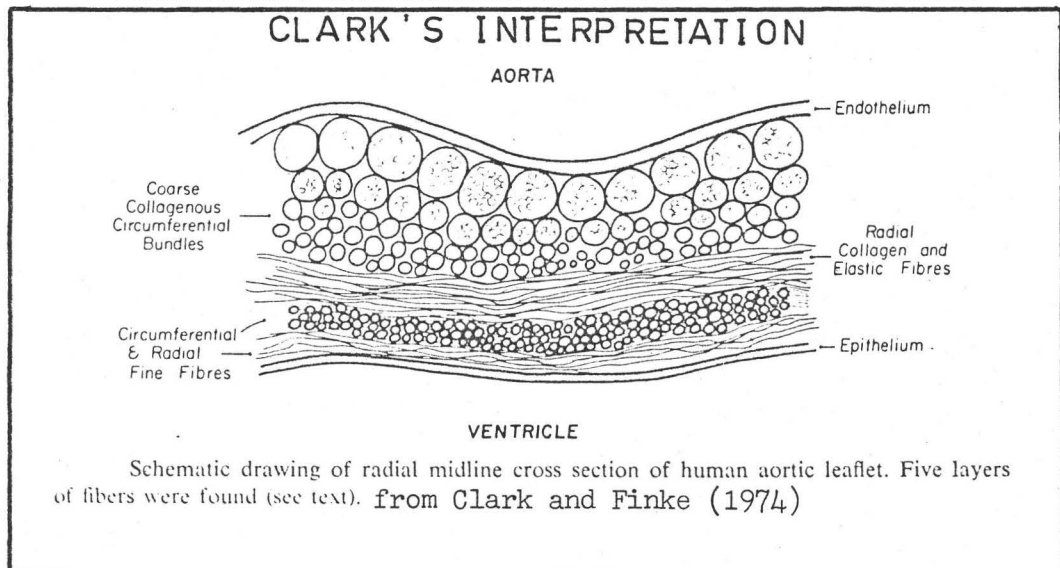
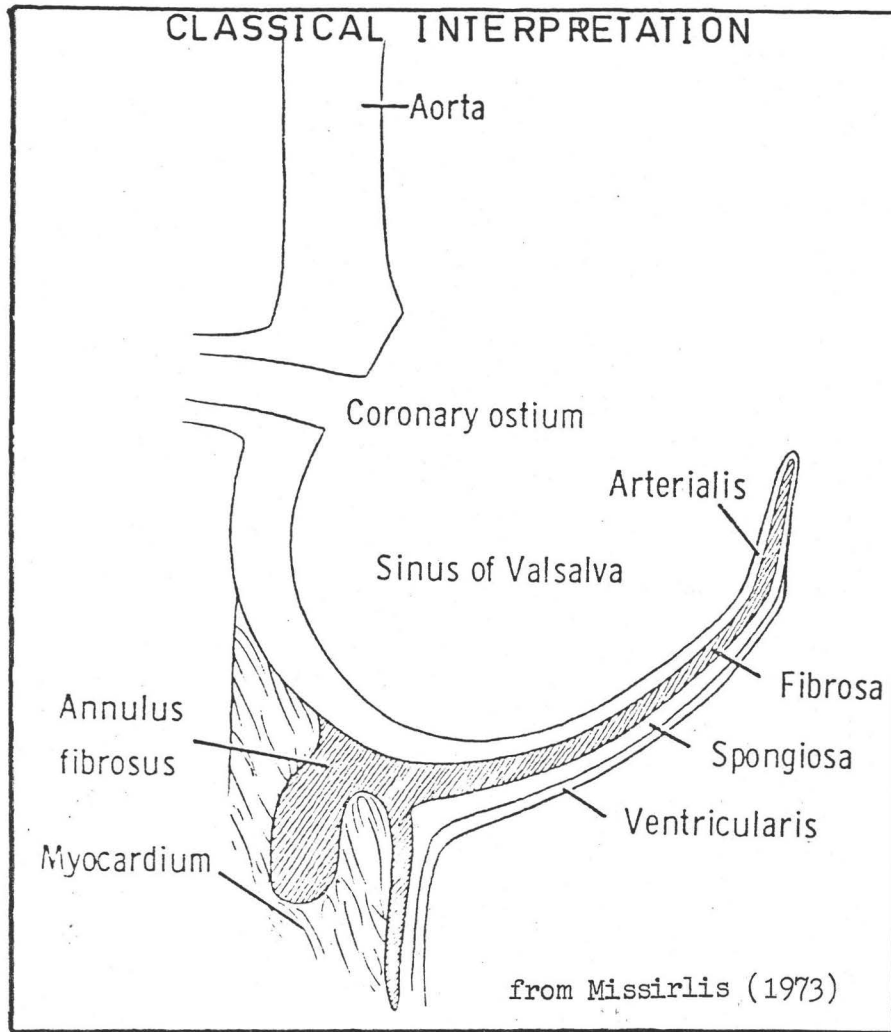
gradient (~ 5 mm. Hg.) at instantaneous peak flow rates associated with an average resting cardiac output of 5.6 litre/min [Forrester et al, 1969; Wieting et al, 1969; Viggers, 1972; Störmer et al, 1976]. At higher flow rates such as those associated with exercising, the natural human aortic valve is capable of maintaining an acceptably low systolic gradient (~ 10 mm. Hg.) [Ross Jr. et al, 1966].

B4. Histology and Ultrastructure of the Valve Leaflets

One of the earliest histological study of the leaflets was performed by Gross and Kugel (1931). It represents the classical view of the leaflet's laminate structure as depicted in figure 6. Four main constituents (cells, collagen, elastin and mucopolysaccharides) were thought to be organized into four distinct layers: 1) the fibro-elastic ventricularis which is covered with a lining of endothelial cells and has a well-organized elastic network of thick elastic fibres, 2) the spongiosa which is composed of a few fibroblasts, clumps of dense collagen and a delicate network of elastin fibrils, 3) the fibrosa which originates from the annulus fibrosus and is composed of an interlacing network of thick collagenous bundles running in the circumferential direction, and 4) the arterialis which is a thin elastic layer covered by another layer of flat endothelial cells.

More recently, more extensive histology has been performed by Missirlis [Armeniades et al, 1973; Missirlis,

FIGURE 6. AORTIC VALVE LEAFLET HISTOLOGY



1973; Missirlis and Armeniades, 1977] and by Clark and Finke (1974). Their results seem to suggest that the four classical layers can be divided into further sublayers. Observations indicated a vast inhomogeneity in the leaflets as well as a definite preferential orientation for the collagen and/or elastin fibres in the leaflets.

Clark and Finke (1974) summarized their results by describing the leaflet structure as a composite lamina with five discernible layers of fibres (figure 6): 1) a superficial aortic layer composed of large interwound bundles of circumferential fibres, 2) an adjacent zone of similarly oriented interwound fibres which change from larger to smaller diameters, 3) an intermediate layer of mixed-size interwound collagen and elastin fibres oriented in the radial direction, 4) a layer of fine interwound circumferential fibres and 5) a superficial ventricular layer of fine interwound fibres in the radial direction. Both of the superficial layers are covered by a layer of epithelium, which when peeled off reveal the definite circumferential and radial orientations of the fibres (figure 4). The latter are the main support structures for the diastolic pressure load. It was also noted that generally, the number and the diameter of the large fibre bundles nearer the aortic side become fewer and smaller toward the annulus edge while the fine fibres nearer the ventricular surface remain relatively constant. This is partially consistent with Greep's (1966)

observations that elastin is concentrated at the base of the leaflet (ie., the annulus edge) and is minimal at the free edge where the collagen content is predominant.

Missirlis' (1973,1977) observations agree with much of Clark and Finke's (1974). He did not however characterize the thin elastin and collagen fibres to be preferentially radial in orientation but instead saw them to be more randomized and anisotropic [Armeniades et al, 1973].

Recently, Broom (1978) reported an examination of relaxed and stressed porcine aortic valve leaflet collagen and elastin structures employing a non-destructive optical imaging technique. Laminate structure and fibre anisotropy are observed without the usual histological sectioning.

In another study, a group of French researchers studied porcine valve leaflets by X-ray diffraction [Huc et al, 1975]. Their technique produced results which confirmed that the collagen fibres are circumferentially oriented. Mannschott et al (1976) recently showed that these same collagen fibres are also heterogeneous in collagen chemistry.

For reasons which will become clear later in the stress analysis¹, this author will assume the orientation of the fibres in the leaflet to be approximately orthogonal to each other. The orthogonality is defined by the radial and circumferential directions as suggested by Clark and

¹ The stress analysis is covered in Part II of this study.

Finke (figure 4). Thus to a gross approximation, it may be visualized that during diastolic distension of the leaflets, the stretching (or straining) can be approximated by linearly independent stretches (or strains) in the two orthogonal directions. In other words, the leaflets are behaving as orthotropic laminae.

B5. Mechanical Material Properties of the Valve Leaflets

Basically, there have been two methods which have been used to investigate the intrinsic mechanical properties of the valve leaflet tissue: 1) pressure-volume measurements of complete aortic valve cusps and 2) microtensile stress-strain measurements of strips cut from the leaflets.

Mundth et al (1971) and Wright and Ng (1974) studied the elasticity of human aortic valve leaflets by allowing a disc of cusp tissue that is clamped to a closed saline-filled chamber to bulge under pressure. The resulting pressure-volume curves showed the characteristic phases of biological material as pointed out by Yamada (1973). An initial low elastic modulus phase is noted from 0 to 12.5 mm. Hg. with a corresponding 10% strain. Thereafter, the cusp tissue becomes relatively inelastic being characterized by a high elastic modulus. The two phases are respectively referred to as the pre-transition and post-transition regions.²

² These terms are defined and described in Appendix A.

The non-linear behaviour is attributed to the structure of the leaflets. Histology of the relaxed leaflet has shown the collagen fibres to be wavy, disoriented, rolling and interlaced over one another. Thus, the initial stage of pre-transition, characterized by a low elastic modulus, occurs as these fibres begin to straighten out with much of the strain and stress uptake being supported by the more extensible elastin fibres. The post-transition high elastic modulus is the manifestation of the collagen fibres having been straightened taut to support the in-plane stresses. This particular non-linear behaviour is regarded as being significant in aiding in valve opening and closure, in insuring a competent seal between the leaflets in diastole and in minimizing the fatigue stresses in the leaflets.

Lim and Boughner (1976) used a modified pressure-volume technique to measure the dynamic elastic modulus in order to assess the viscoelastic properties of the leaflets. The leaflets exhibited a very low loss modulus which is indicative of a high fatigue resistance. It reflects the 99% elastic recovery measured by Clark (1973).

The above methods did well to characterize the biological nature of the intact valve leaflets. However, they were deficient since they were unable to quantify the anisotropy of the leaflets. Improvements were realized following the use of microtensile stress-strain experiments on strips of human aortic valve leaflets cut in various orientations.

Clark (1973), Missirlis (1973) and Yamada (1973) performed these experiments on human valves whereas Affeld et al (1973) and Tan and Holt (1976) conducted similar tests on bovine and porcine valves respectively. Their results confirmed the two-phased nature of the tissue and also substantiated the anisotropy. The leaflet tissue exhibits a larger circumferential post-transition elastic modulus (3X to 4X greater than the radial post-transition elastic modulus), and a smaller circumferential transition strain (about 10% as compared to 25% for the radial case). This of course, is attributed to the differentiation between the stiffer collagen fibres which are circumferentially preferential and the more extensible elastin fibres which are radially preferential.

All of the above methods do however have one very important limitation; that is, they are unable to probe the inhomogeneity of the leaflet material properties. Although Wright and Ng (1974) did state that the elasticity from the different valves are comparable, they as well as others did not investigate the variation of the elastic moduli over the same leaflet. Consequently, elastic modulus inputs for the past stress analyses have been restricted to being singular homogeneous values. More study is obviously required in this area; no stress analysis appearing in the present literature has incorporated inhomogeneous elastic moduli, and only one work [Missirlis and Armeniades, 1976] has gone as far as to consider moduli anisotropy. This thesis makes a contribution

by considering both material inhomogeneity and anisotropy.

A note of interest stemming from the leaflet material non-linearity is the acknowledgement by both Clark (1973) and Wright and Ng (1974) that at normal diastolic pressures, the leaflet tissue is well into its post-transition large modulus phase. Consequently, stress analyses in the past have used the large post-transition modulus as the input for the stress calculations. The concern raised here is that the above contention was based on results obtained from individual strips or total cusps which were excised and stressed separate from the total valvular support of the stiff aortic ring and the myocardium. For the intact functional valve in-vivo, a large pressure load associated with diastole might not necessarily infer the absolute presence of the post-transition phase.

Furthermore, no detailed studies have been carried out on the inhomogeneity and the anisotropy of the Poisson's ratio. Work in this area is required since all of the stress analyses to date have either used a homogeneous isotropic value of 0.5 [Gould et al, 1973; Missirlis, 1973; Missirlis and Armeniades, 1976], or 0.3 [Clark et al, 1975; Cataloglu et al, 1975,1976,1977; Chen et al, 1977]. Leaflet thickness, another of the neglected factors, has only been incorporated in Clark's et al (1975) and Cataloglu's et al (1977) papers.

B6. Flow Studies of the Aortic Valve

Studies of the functional mechanics of the natural

aortic valve are generally of two types: 1) the flow dynamics and hydraulics of the opening and closing valve, and 2) the static stress analyses of the closed diastolic leaflets. The majority of the studies has been conducted in-vitro although other in-vivo techniques have also been used.

Flow studies have been made possible with the aid of a mechanical-hydraulic device called the pulse duplicator. Designed to simulate the physiological environment and circulatory aspects with respect to the valve as accurately as possible, it is used to study the flow performance and functional characteristics of experimental valves using water or a suitable blood analog fluid. In the earlier years of AVRs, the pulse duplicators were extremely crude, being designed primarily to cinephoto the opening and closing of the natural valve [McMillan et al, 1952,1955; Davila, 1956; Callaghan et al, 1961]. With the increasing number of prosthetic cardiac valves being designed in the 1960's, many researchers built their own pulse duplicators to assess and compare the flow patterns and the hydraulics of the many prostheses [Marx and Kittle, 1959; Leyse et al, 1961; Björk et al, 1962; Wessel et al, 1962; Starkey et al, 1963; Calvert et al, 1964; Duran et al, 1964; Steinmetz et al, 1964; Temple et al, 1964; Davey et al, 1966; Smeloff et al, 1966; Wieting et al, 1966,1969; Kaster et al, 1968,1969; Bellhouse and Talbot, 1969; Klain et al, 1969; Trimble et al, 1969; Padula et al, 1970; Love et al, 1971; Olin, 1971; Wright and Temple, 1971; Duff and

Fox, 1972; Hauf et al, 1973; Störmer et al, 1976]. The number of models is numerous to say the least. Moreover, each of the pulse duplicators is different in one way or another. As such most of the analyses performed with the pulse duplicators are non-standardized and only comparative at best.

Some of the pulse duplicators were modified to perform accelerated testing in order to investigate durability and fatigue of experimental valves. Some insight into this area may be found from the literature [Quinton et al, 1961; Steinmetz et al, 1964; Koorajian et al, 1969; Mohri et al, 1973].

A limitation of present pulse duplicators is their failure to simulate more in-vivo conditions; for example, thrombus formations, coronary flow effects and a compliant viscoelastic aorta. Nevertheless, skillful use of the pulse duplicators is essential in revealing any design flaws and deficiencies in valve performance prior to clinical applications. The most recent pulse duplicators appearing in the literature are the Cornhill (1977) model and the improved Wright model [Wright and Brown, 1977; Wright and Temple, 1977]. The former uses a collapsible silastic bag as the left ventricle and is able to simulate very accurately the physiological ventricular and aortic pressure-flow wave forms. The latter employs a curved rigid aorta to improve the aortic flow modelling and introduces a method to obtain direct measurements of valvular gradients in pulsatile flow.

The use of the pulse duplicator to study the natural human aortic valve has perhaps been best exploited by Bellhouse. His research [Bellhouse and Bellhouse, 1968,1969; Bellhouse and Talbot, 1969] were the most comprehensive studies on the human valve's fluid mechanics. Besides the usual pressure-flow measurements, valve action and flow pattern visualization, Bellhouse also investigated the effects of the sinuses and stenosis on coronary flow and turbulence. The observations formed the basis of Bellhouse's theory that the action of the sinuses' vortices on the leaflets is the major mechanism of valve closure.

Recently, a group from Holland reported results which presented a new model of valve closure [Spaan et al, 1975; Steenhoven et al, 1976]. It was noted that a transfer of rotational momentum in the sinuses is the prime valve closure mechanism. Valve closure is retarded, thereby reducing the potential tension peaks in the leaflets at complete closure.

In another study, Swanson and Clark (1973) used elements of fluid mechanics to calculate the displacement of an aortic valve leaflet during systole. They observed a retarded valve opening that resulted in a wavy buckling whipping and fluttering motion of the leaflets. Leaflet protrusion into the sinus similar to that observed in the Bellhouse model was also observed. Calculations of maximum leaflet bending and shear stresses were shown to be much smaller than the in-plane membrane stresses developed in the diastolic valve.

To this author's knowledge, there are still no in-depth theoretical analysis of the flow through the natural or prosthetic aortic valve; that is, there are no solutions to the full conservation equations of motion for time varying, viscous, axisymmetric flow through the valve with the boundary conditions of a viscoelastic aorta. It is only speculative as to whether an elastic aorta would alter the flow significantly. Kramer (1962) thought that flexible walls might prevent turbulent effects but experiments performed by Dinklelacker (1966) neither confirmed nor refuted this. No pulse duplicators to date have incorporated a viscoelastic or elastic aorta.

Until recently, flow analyses and valve performances have been assessed by conventional semi-empirical engineering parameters suitable only for steady flow; eg., 1) pressure gradient as a function of average cardiac output, 2) efficiency as measured by regurgitation relative to net forward flow, 3) energy dissipation across the valve, 4) opening and closing times of the valve and 5) degree of turbulence. A greater understanding of these parameters is given by Viggers (1972).

Aortic valve turbulence has been closely studied since it reduces flow efficiency and induces high shear stresses which lead to hemolysis [Blackshear et al, 1966, 1969; Blackshear, 1972; Suter et al, 1972, 1977; Goldsmith et al, 1974]. Also, thrombosis and atherosclerosis have been

linked with turbulence intensity [Wesolowski et al, 1962; Davila et al, 1963; Blackshear et al, 1969; Mustard et al, 1970; Stein and Sabbah, 1976]. The initial works in this area were qualitative, using the flow pattern visualization technique in the pulse duplicator as a means of assessment.

For steady flow, a critical Reynolds number of 2300 is usually used as an index for turbulence; but for pulsatile flow such as the aortic flow, the index is suspect. The peak Reynolds number just proximal to the aortic valve may be as high as 10000 [Freis and Heath, 1964]. As such, some researchers have sought other means to quantify the degree of turbulence. Much work has been done in the area of pulsatile flow turbulence and it may be found described in the literature [Yellin, 1966; Bellhouse and Talbot, 1969; Love et al, 1971; Greenfield and Kolff, 1972; Greenfield, 1976; Hwang et al, 1977].

B7. Stress Analyses of the Aortic Valve Leaflets

The healthy human aortic valve is intrinsically durable mainly because of the valve leaflets' unique biological characteristics [Clark, 1973; Wright and Ng, 1974] but also partly because of the valve's synchronous operation with the viscoelastic cardiac support structures. The prospects of designing a prosthetic flexible trileaflet aortic valve that would duplicate this durability have prompted researchers to investigate the natural aortic valve's most fundamental

functional and structural mechanics. One of the areas of this investigation has involved analyzing the stresses in the aortic valve leaflets while being subjected to simulated physiological static diastolic pressures. The information so obtained would then better enable the designers to design to what nature has constrained.

The elements of a typical stress analysis is shown in figure 7. The credibility of any analysis, regardless of the level of sophistication used in the theory, is dependent on the realistic and representative nature of the various inputs - geometry, material parameters and assumptions.

All prior stress analyses of the aortic valve leaflets have in one way or another based their calculations on some simplifying though questionable assumptions (table 1). The first three assumptions listed in the table have been generally acknowledged to be unrealistic. However, researchers have nevertheless used them due to the lack of suitable methods of incorporating the more exact situations into their analytical methodologies.

For example, K. Chong et al (1973), Ghista (1976) and Ghista and Reul (1977) referred the leaflet surface geometry to two principal radii of curvature. And Gould et al (1973) as well as Missirlis (1973,1976) approximated the leaflet surfaces with standard geometrical surfaces. Stress level calculations were found to be extremely sensitive to the geometrical surfaces being used for the approximations.

FIGURE 7.
STRESS ANALYSIS METHODOLOGY

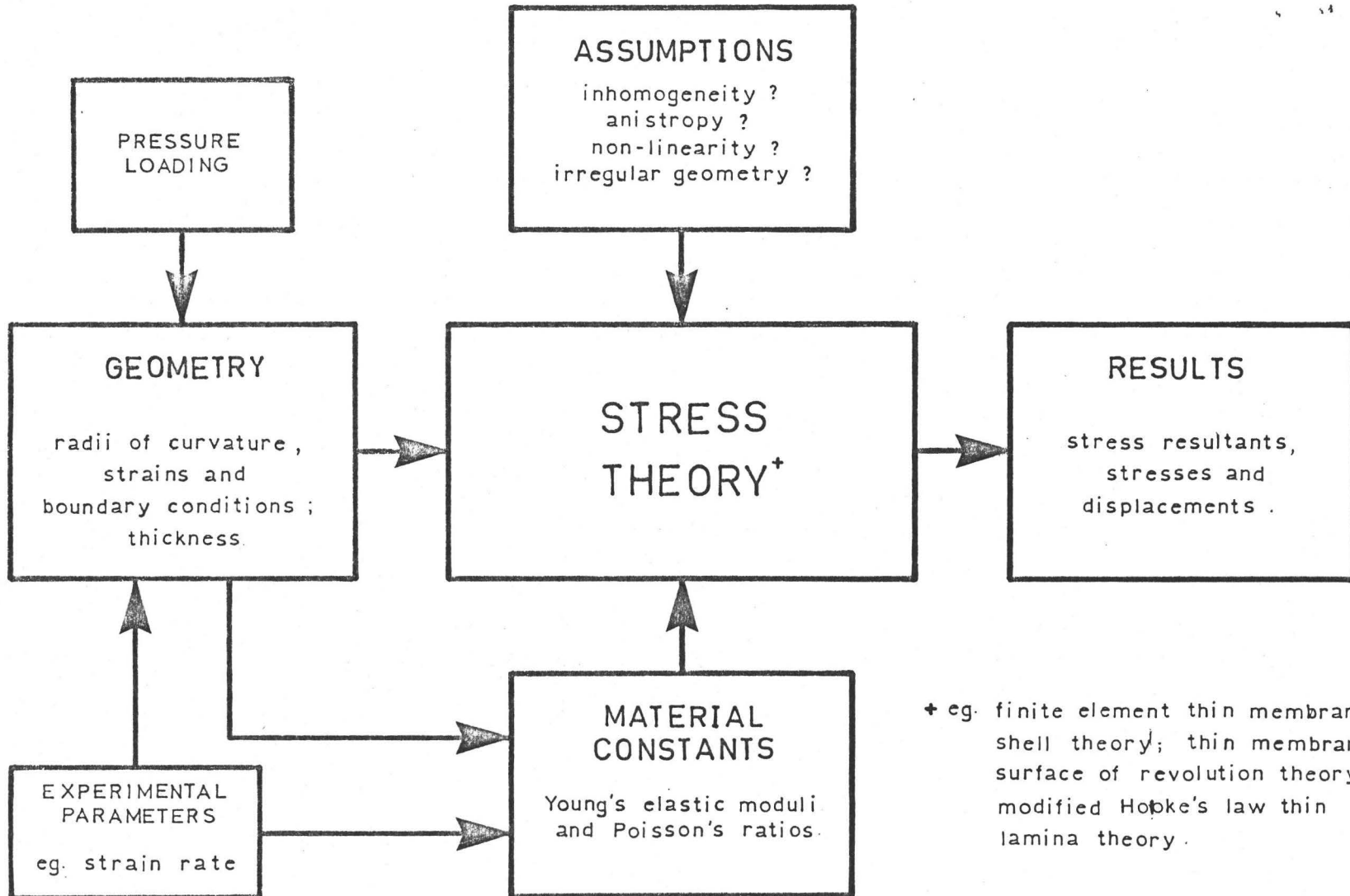


TABLE 1.
**ASSUMPTIONS used in the STRESS ANALYSES
of AORTIC VALVE LEAFLETS**

Stress Analysis	K. Chong et al (1973)	Missirlis (1973); Missirlis and Armeniades (1976)	Gould et al (1973); Clark et al (1975); Cataloglu et al (1975,1976,1977); Chen et al (1977)	M. Chong (1977)
Specimen	Human	Human	Human	Porcine
Local Surface Geometrical Symmetry	YES	YES	NO	NO
Material Homogeneity	YES	YES	YES	NO
Material Isotropy	YES	NO	YES	NO
Post-Transition Elastic Modulus	YES	YES	YES	NO

Furthermore, despite the obvious existence of leaflet material inhomogeneity and directional anisotropy, the above analyses and others [Clark et al, 1975; Cataloglu et al, 1975, 1976, 1977; Missirlis and Armeniades, 1976; Chen et al, 1977] have ignored the incorporation of one or both of these considerations into their calculations. Corroborating evidence from histological examinations of the human aortic leaflets under light, scanning and transmission electron microscopy [Armeniades et al, 1973; Missirlis, 1973, 1977; Clark and Finke, 1974] and from microtensile stress-strain experiments on human and animal aortic leaflets [Affeld et al, 1973; Armeniades et al, 1973; Clark, 1973; Missirlis, 1973; Yamada, 1973; Tan and Holt, 1976] have confirmed the anisotropy. The leaflets were observed to be orthotropic laminae with calculated post-transition elastic moduli in the circumferential direction being 3 to 4 times larger than the radial moduli.

Robel (1972) in his studies on porcine aortic valve mechanics noted that the "prosthetic replacement leaflet" must "have either a non-homogeneous or non-uniform cross-section to allow variable elasticity." However, only one work in the literature has investigated and quantified this inhomogeneity [Affeld et al, 1973]. The lack of such pertinent information, which probably arose from the lack of any suitable experimental technique for acquiring such data, is likely the main reason for assuming homogeneity in the past stress analyses.

On the other hand, the last assumption in table 1 has received scant mention. Elastic modulus inputs in past stress analyses have been invariably the post-transition moduli. The results from this study however suggest that the previously assumed inference of post-transition behaviour at diastole [Clark, 1973; Wright and Ng, 1974] is questionable. The determination of pre-transition or post-transition state for the leaflet material when subjected to diastolic conditions is certainly worthy of further investigation.

B8. Reasons for Aortic Valve Replacements

AVR is usually the result of valvular dysfunctions which cause overloading of the heart as a pump in two basic ways: pressure overload and/or volume overload. The result is work overload for the heart, which reduces the efficiency and promotes myocardial hypertrophy. Also, altered blood flow may lead to valve turbulence and subsequent hemolysis and calcification of valvular structures.

Functionally, the natural aortic valve may be altered in three ways: 1) the valve does not open fully as in the case of stiffened and shortened leaflets or an overly compliant aortic ring, 2) the valve orifice area decreases in size such as in the case of obstruction to flow due to any thrombus and 3) the valve does not close fully thus causing leakage or regurgitant backflow. Defects 1) and 2) are classified as aortic stenosis - a condition that increases the

systolic pressure gradient which in turn can result in turbulence, energy dissipation and pump inefficiency. Defect 3) is better known as aortic insufficiency or regurgitation. It is characterized by a reduced aortic pressure and a compensatory effort of the heart to recover the lost backflow by increasing its stroke volume. Oversized left ventricles are common developments.

Common causes of valvular dysfunction are: rheumatic fever and atherosclerosis (stenosis), syphilitic aortitis, ankylosing spondylitis and Marfan's syndrome (regurgitation), bacterial endocarditis (leaflet rupture and regurgitation) and congenital defects (stenotic uni-, bi- and multi-cuspid aortic valves). Further insight into these areas is given by Roberts (1974).

Prior to the developments of the heart-lung machine and extracorporeal circulation [Melrose, 1953; Lillehei and DeWall, 1958], repairs to the above dysfunctions were made by various reconstructive surgical techniques such as valvuloplasty [Murray et al, 1938; Templeton and Gibbson, 1949; Castra-Villograna et al, 1957]. Besides being risky and time consuming, these procedures were often also met with only short-term success. Thus, the availability of aortic valve substitutes became a welcomed alternative.

C. Aortic Valve Substitutes

Heart valve replacements in the United States alone numbered somewhere in the neighbourhood of 10,000 per year in 1973 [Roschke, 1973]. The number in Canada at present is estimated to be about 1000 per year.³ A fair portion of the replacements are AVRs. Brewer's (1969^a) statistical review of 3620 patients from twenty-seven centers indicated 49% AVR.

The AVRs may be categorized into three major types:

- 1) rigid mechanical prostheses with central flow occluders, which are designed to simulate the natural valve function,
- 2) flexible trileaflet prostheses which are designed to simulate the anatomophysiology of the natural human valve, and
- 3) tissue valves which include homo- or allografts (human cadavers or transplants), hetero- or xenografts (animal cadavers or transplants), and autologous and heterologous tissue valves (eg., fascia lata, pericardium, dura mater).

Groups 1) and 2) are termed prosthetic as opposed to group 3) which is referred to as being biological. Figure 8 shows some of the typical valves in the different groups.

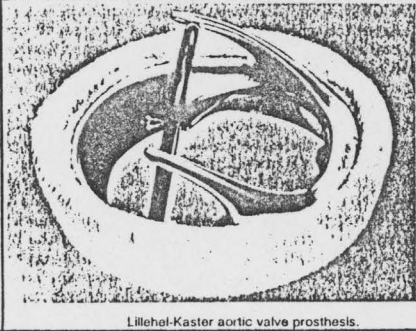
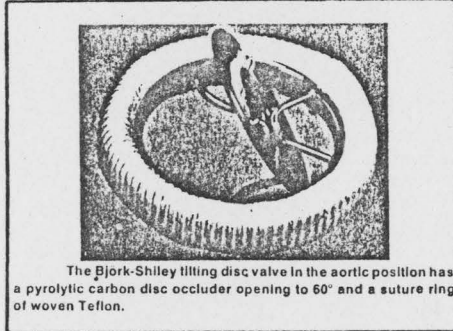
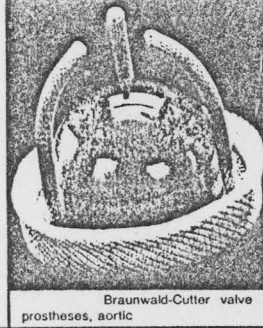
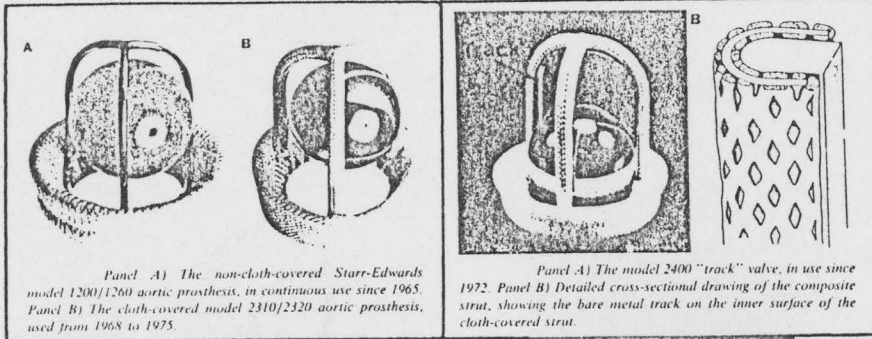
C1. Historical Review of AVR

Historically, the first implantation of a prosthetic aortic valve in a man was performed in 1952 by Hufnagel who

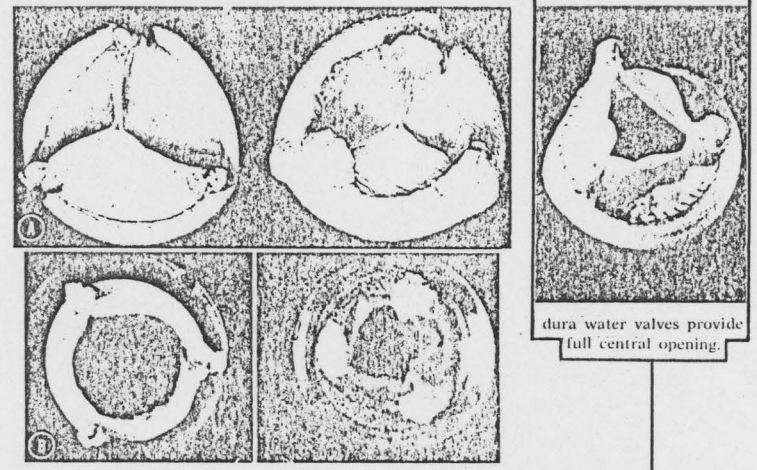
³ Personal communication with Edwards Laboratories, 1977.

FIGURE 8. CURRENT AORTIC VALVE SUBSTITUTES

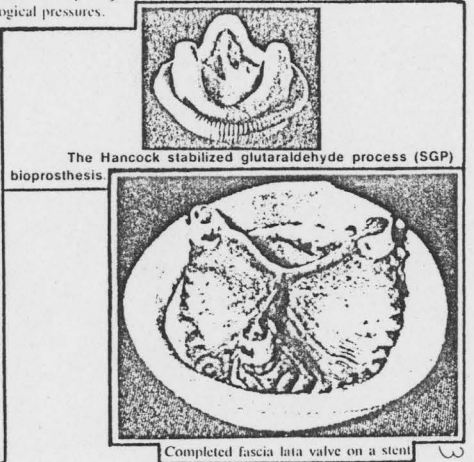
RIGID MECHANICAL PROSTHETIC VALVES



BIOLOGICAL TISSUE VALVES



Comparison between a pericardial xenograft (left) and a porcine aortic valve (right) seen from their outflow aspect. Both valves are frame mounted and both have an implantation diameter of 23 mm. A. The configuration of the valves. B. The difference in effective functional opening when the valve is tested in a pulse simulator at a flow rate of 3 L. per minute and at physiological pressures.



used a hollow rubber ball prosthesis in the descending aorta to correct aortic regurgitation [Hufnagel and Harvey, 1952, 1953]. Coronary circulation complications and the inability to correct aortic insufficiency encouraged others to develop a subcoronary prosthesis.

Over the next decade, a large number of ball valves emerged with innovative modifications, though not necessarily improvements. With the advent of open heart surgery in 1955 and extracorporeal circulation [Melrose, 1953; Lillehei and De Wall, 1958], AVR at the valve site was made possible. In 1958, Edwards and Smith described a new ball valve for aortic valve replacement. Harken et al in March 1960, and Starr and Edwards in September 1960 then performed successive AVR and MVR using caged ball valves. The subsequent work of Starr and his associates has led to the world wide acceptance of the caged ball design. The latter has since acquired numerous structural and material modifications.

Other major developments in rigid aortic prosthesis included the Smeloff-Cutter's 1965 introduction of a double-cage full-orifice ball valve, Cooley-Cutter's adaptation of the full-orifice principle with a double-cone disc, Braunwald-Cutter's 1968 introduction of cloth or fabric covering, and Wada's 1967 tilting disc concept. The latter stimulated more developments which led to the successful Bjork-Shiley tilting disc valve introduced in 1969 and the Lillehei-Kaster pivoting disc valve introduced in 1971. Cage disc valves, although

not generally employed for AVR, were introduced in 1965 and thereafter. Specific information and clinical experiences on these valves are in abundance in the available literature. Reviews, besides giving the best overview, generally provide excellent references [Braunwald and Detmer, 1968; Starr et al, 1969; Björk, 1970; Braunwald et al, 1971; Sauvage and Wood, 1972; McGoon, 1972; Wright, 1972; Behrendt and Austen, 1973; Roschke, 1973; Pluth and McGoon, 1974; Smeloff et al, 1974; Barnhorst et al, 1975; Bonchek and Starr, 1975; Björk et al, 1975^a; Braunwald, 1975; Brawley et al, 1975; Roberts, 1976; Isom et al, 1977; Starr et al, 1977]. Other excellent primary sources can be found in the 1977 March-April issue of Medical Instrumentation and in various books [Merendino, 1961; Brest, 1966; Brewer, 1969^b; Sauvage et al, 1972].

Prior to Harken's and Starr's pioneering works, many attempts were made to replace cardiac valves with prostheses that simulated the natural anatomy of the human aortic valve in hope of correcting the inefficiency of the ball valves' hemodynamics. Using materials such as polyurethane, silastic, teflon, ivalon, nylon and dacron, thin membrane leaflets were casted or cut and sewn into the configuration of the natural valve. Merendino's (1961) book covering the First Conference on Prosthetic Valves for Cardiac Surgery describes much of this early work on flexible trileaflet prostheses. Thrombus and fibrin formations, infections, hemolysis and mechanical dysfunction due to leaflet fractures and tears were found to

be the major complications. Subsequent designs produced more satisfactory early results. However, there were still high incidences of failures due to the following: hemolysis; stenosis caused by calcification, thrombus and leaflet contractures; regurgitation caused by leaflet fractures, tears and perforations; and dehiscence caused by poor insertion techniques [Björk, 1963; Björk and Hultquist, 1964; Judson et al, 1964; Bahnson et al, 1965; Baird et al, 1965; Braunwald and Morrow, 1965; Hufnagel and Conrad, 1965; Viner and Frost, 1965; Yeh et al, 1965; Roberts and Morrow, 1966; Sauvage et al, 1968; Roe, 1969; Marinescu et al, 1971]. And although Roe (1969) did report a $6\frac{1}{2}$ year survival for his valves, it was then generally accepted that prosthetic trileaflet valves be abandoned for clinical application until more durable leaflet materials were developed [Braunwald and Detmer, 1968]. The observation that not one single article, devoted to flexible leaflet design appeared in Brewer's (1969^b) book covering the Second National Conference on Prosthetic Valves for Cardiac Surgery, is supportive of the pessimism toward leaflet valves at that time. More recently in the 1970's, the search for the ideal trileaflet prosthetic valve has regained considerable interest [Clark et al, 1974].

Tissue valves first arrived on the AVR scene in 1956 when Murray and his colleagues demonstrated long term function ($\sim 6\frac{1}{2}$ years) of an aortic homograft in the descending aorta to correct aortic regurgitation. And in 1962, Barratt-Boyes and

Ross followed with the first aortic homografts in the sub-coronary position [Ross, 1962,1964; Barratt-Boyes, 1964]. The valves then appeared to be the ideal aortic valve substitute: unobstructed central flow, minimal hemolysis and no thrombo-embolism without anticoagulation. However, various technical, biological and procurement problems encouraged others to find other more suitable biological tissue valves: sterilized and/or preserved homografts and xenografts, stented homografts and xenografts, pulmonary autografts, and valves fashioned from various autologous and heterologous tissue (eg., fascia lata, pericardium, dura mater and reconstituted fibrocollagen). The description of these tissue valves is described in Ionescu's (1972) book, Biological Tissue Heart Valve Replacement and in various reviews [Braunwald and Detmer, 1968; Gerbode, 1970; Ross, 1972; Sauvage and Wood, 1972; Wright, 1972; Angell et al, 1973; Pluth and McGoon, 1974; Wallace, 1975; Kiraly and Nosé, 1976; Roberts, 1976]. Many successful experimental and clinical results were reported for short term applications. Lack of long term durability was however the major limitation for all of the tissue valves and grafts as it still remains so presently.

The major recent development in tissue valves seems to be the glutaraldehyde-preserved porcine xenograft that was first introduced by Carpentier et al (1969) and then later improved by Reis and Hancock (1971) [see The Glutaraldehyde-Preserved Porcine Xenograft, p. 48].

C2. Rigid Mechanical Prosthetic Valves

From the standpoint of mechanical reliability and durability, the rigid mechanical prostheses at present are unsurpassed, although not unchallenged. Their track record of proven clinical application with satisfactory to good results is long (eg., since the early 1960's). The most recent status reviews on ball prostheses by Barnhorst et al (1975), Bonchek and Starr (1975), Braunwald (1975), Roberts (1976), Isom et al (1977) and Starr et al (1977), and on disc prostheses by Björk et al (1975^a), Brawley et al (1975), Björk (1977) and Lillehei (1977) report the more advanced models to be nearing a decade of acceptable function with reduced operative and late mortality. In fact, one of Harken's initial patients is still alive with an original ball valve [Harken, 1977]. This durability coupled with the advantages of also being easily insertable and available has made many surgeons either firm believers in their use or users until other alternatives of equal durability become available.

Whereas natural heart valves offer central flow with low resistance, gentle acceleration and very small regurgitation, rigid prostheses obstruct and baffle the aortic flow. Regurgitation and turbulence are common occurrences. Rigid valves usually consist of three basic elements: 1) the flow occluder or poppet, 2) the valve body and sewing ring and 3) the guiding structure that limits the occluder travel (eg., cages and struts). Since the pioneering days of Harken's and

Starr's ball valves, numerous designs have been proposed and refined in response to a wide range of problems. Many of the valves, too numerous to be listed here, failed and are now of historic interest only.

At present, there remains three major designs: 1) the caged ball valve, 2) the caged disc valve and 3) the tilting/pivoting disc valves (see figure 8). However, the caged disc valves are generally not used for AVR.

Brewer's (1969^b) book and various reviews [Braunwald and Detmer, 1968; Starr et al, 1969; Björk, 1970; Braunwald et al, 1971; Sauvage and Wood, 1972; McGoon, 1972; Wright, 1972] describe the progress in developments of the various rigid mechanical prostheses during the 1960's. During this period, the design emphasis was in the area of reducing any thromboembolism. The latter was the major complication plaguing the earlier valves [Davila et al, 1966; Duvoisin et al, 1967; Akbarian et al, 1968; Matloff et al, 1969; Friedli et al, 1971; Hysten, 1972^a]. Current reviews by Dale (1976,1977) suggest that thromboembolism still remains the number one problem with prosthetic valves. Many other problems also plagued the early valves, causing a high operative mortality as well as a host of post-operative complications: noise, poor fixation, paravalvular leaks, hemolysis and hemolytic anemia, infective and fungal endocarditis, anticoagulation complications, poor hemodynamics and mechanical failures such as disc and ball variances [Herr et al, 1965; Kloster et al,

1965; Kastor et al, 1968; McHenry et al, 1968; Brewer et al, 1969; Duvoisin and McGoon, 1969; Eyster et al, 1971; Hysten, 1972^b; Roberts and Morrow, 1972; Slaughter, 1973]. More recent reviews demonstrate that some of the problems are still prevalent: infection, hemolytic anemia, mechanical dysfunctions and thromboembolism and its related anticoagulation risks are still causing deaths or re-operations [De Boer et al, 1974; Isom et al, 1974; Björk et al, 1975^b; Kloster, 1975; Arnett and Roberts, 1976; Katholi et al, 1976; Meistrell et al, 1976; Roberts et al, 1976; Dale, 1976,1977; Isom et al, 1977].

C3. Biological Tissue Valves

In comparison to the prosthetic valves, all tissue valves to date have shown a very small incidence of thromboembolism even without anticoagulants. Because of the natural trileaflet structure, the valves should possess much better hemodynamics than the prosthetic valves. Comparative in-vitro and in-vivo assessments have however shown that tissue valves are only comparable. Incidences of hemolysis are generally lower whereas incidences of infection are generally higher.

Short term results obtained with the majority of the tissue valves have been encouraging from the standpoint of satisfactory hemodynamic function and low thrombogenicity. But in general, the incidences of late post-operative tissue degeneration leading to failures have been discouragingly high. Fortunately when failures of this nature occur, the

effects are less catastrophic than with prosthetic valves, thus allowing valuable time for a selective replacement.

Biological tissue valves, despite continued changes in sources and methods of fabrication and preservation, have not matched the prosthetic valves in durability. A potential exception is the glutaraldehyde-preserved porcine xenograft. Current reviews indicate that its durability is approaching or has equalled that of the more advanced prosthetic valves.

Homografts or Allografts

Initial and early results with fresh homograft AVRs were gratifying [Barratt-Boyes, 1967; Stinson et al, 1968]. Early difficulties encountered in the time-consuming insertion of a graft by free suturing were eliminated by the use of the rigid stent and improved surgical techniques [Braunwald et al, 1968; Ionescu et al, 1968; Carpentier et al, 1969]. Unstented or improperly implanted valves often experienced dehiscence, leaks and valve incompetence.

The inconveniences of procuring fresh homografts under ideal sterile conditions initiated the use of a multitude of sterilization and preservation techniques. Mercurate, ethylene oxide, beta-propiolactone, gamma irradiation, formalin and glutaraldehyde have all been used for sterilization. Contrary to what was expected and claimed, all tissue valves so treated did not retain their viability because of cellular damages and morphological degeneration of the collagen-elastin structure

[Malm et al, 1967; Trimble et al, 1969^b; Welch et al, 1969; Innes et al, 1971; Al-Janabi et al, 1972; Gavin et al, 1973; Manhas et al, 1973; Waterworth et al, 1974; MacGregor et al, 1976]. Freezing, freeze-drying and aldehyde treatments have been used for preservation. Most valves were preserved to the time of implantation and performed satisfactorily well in the early post-operative phase. However, the majority experienced late (ie., after 4 years) failures [Barratt-Boyes and Roche, 1969; Missen et al, 1970; Barratt-Boyes, 1971; Gonzalez-Lavin et al, 1972; Pacifico et al, 1972; Davies and Roberts, 1974; Ionescu et al, 1974; Wallace et al, 1974; Moore et al, 1975]. Failures as determined from pathological studies of the leaflets were the result of infective endocarditis, perforations and tears, thinning and stretching, calcification and fibrosis [Hudson, 1966; Smith, 1967; Davies et al, 1968; Yarbrough et al, 1973].

† Availability is a major problem with the fresh aortic homografts. It alone has contributed a significant share of valve failures because of less than optimum matching of graft size [Trimble et al, 1969^a]. Compared to the preserved valves, the fresh homografts are less prone to fail [Stinson et al, 1968; Barratt-Boyes, 1971; Angell et al, 1972; Barratt-Boyes et al, 1977], but there are reservations that late failures are inevitable [Ionescu et al, 1974; Davies and Roberts, 1974; Moore et al, 1975; Anderson and Hancock, 1976]. Studies have shown that all of the various sterilization and preservation

methods adversely affect the leaflet tissue's mechanical and cellular characteristics [Harris et al, 1968; Trimble et al, 1969^b; Firor et al, 1970; Innes et al, 1971; Litwak et al, 1972; Suzuki and Ray, 1972; Clark, 1973; Yarbrough et al, 1973; Ng and Wright, 1975; Tan and Holt, 1976; Parker et al, 1977]. Comparative analyses with prosthetic AVR report similar results in the mortality and morbidity rates [Karp et al, 1974; Anderson and Hancock, 1976; Pine et al, 1976; Angell et al, 1977].

Heterografts or Xenografts

Procurement and graft-size matching problems prompted surgeons to use the preserved xenograft as an alternative for AVR. Binet and his associates (1965) reported the first successful xenograft AVR in man after Duran and Gunning (1965) performed it in a dog. Shortly thereafter, Carpentier and his colleagues (1969) reported the use of a rigid stented heterograft to eradicate the technical problems of insertion due to the differing valve anatomy between animals and man. During the same time, O'Brien and Clarebrough (1966) and Ionescu et al (1968) were examining the same technical problems. Since then, accumulating experimental and clinical experiences have helped to identify a number of technical and biological problems associated with this method of valve replacement.

As with the preserved homografts, the preserved xenografts were rendered non-viable. Thus, they experienced the

same short term success and suffered the same late failures due to degenerative changes to the tissue [Binet et al, 1967; O'Brien, 1967; Carpentier et al, 1969; Gerbode, 1970; Buch et al, 1970; O'Brien et al, 1970; Ionescu et al, 1972^a; Yarbrough et al, 1973; Zuhdi et al, 1974; Cēvese, 1975]. Clinical experiences clearly indicate that long term function is primarily dependent on the method of preservation.

The failure of formalin and other preservative agents led Carpentier et al (1969) to attempt a new method of curing and preserving xenografts using a glutaraldehyde (with sodium metaperiodate) process. Tissue so treated became more durable and less prone to late degenerative changes to the collagen structure [Strawich et al, 1974; Huc et al, 1975]. The work of Carpentier initiated a succession of developments that has resulted in the most exciting aortic valve substitute to date: the stabilized glutaraldehyde-preserved porcine xenograft. It has been coined a "bioprosthesis" by Carpentier because the glutaraldehyde process renders the tissue valve acellular and non-viable, but structurally static as an "organic plastic" [Carpentier et al, 1972].

The Glutaraldehyde-Preserved Porcine Xenograft

Glutaraldehyde has proven to be the best chemical tanning agent used to stabilize and preserve the collagen structure of natural tissue. The explanation for its effect lies in the intermolecular cross-linking of collagen fibres:

whereas natural collagen fibres possess three cross-links per tropocollagen molecule, glutaraldehyde introduces 11.5 cross-links per tropocollagen molecule.

Previous methods (eg., formalin, mercurate, chromic acid) failed because the cross-linkages were biodegradable. Their reversibility with time was the chief cause for tissue degeneration, loss of elasticity and limited durability. Chemical and mechanical tests of glutaraldehyde-treated tissue (eg., collagen shrink temperature and tension-elongation measurements) have helped to explain the unfailing stability and durability being reported for the implanted glutaraldehyde-preserved porcine xenografts [Litwak et al, 1972; Strawich et al, 1974].

When Carpentier et al (1969) first introduced the process, he included an initial pre-treatment with sodium metaperiodate that was to remove the antigen determinants in the tissues. However, the pre-treatment was found to reduce the elasticity and cross-linking irreversibility [Litwak et al, 1972], and has since been eliminated [Carpentier, 1977].

Reis and Hancock (1971) modified the treatment and introduced a porcine xenograft that was preserved by the stabilized glutaraldehyde process (SGP) without the sodium metaperiodate procedure. They also designed a semi-flexible polypropylene Dacron-covered stent which was claimed as being able to reduce leaflet closing stresses by ninety percent.

To date, many clinical experiences have reported some

extremely encouraging results for AVR as well as for MVR: satisfactory to excellent hemodynamics, no thromboembolism without anticoagulants, minimal hemolysis, high resistance to infections and extremely few structural failures [Carpentier et al, 1974; Zuhdi et al, 1974; Buch et al, 1975; Cohn et al, 1976; Hannah and Reis, 1976; Morris et al, 1976; Pipkin et al, 1976; Zuhdi, 1976; Albert et al, 1977; C evese et al, 1977; Carpentier, 1977; Hancock, 1977; Lurie et al, 1977; Stinson et al, 1977]. What few failures there have been, were not attributed to tissue degeneration and collagen denaturing but mostly to infections and technical errors. However, the long term durability is still open to question. Many patients with the initial glutaraldehyde-preserved porcine xenografts are now entering or have already entered the critical follow-up period when the homografts began to fail (eg., after four to five years). And despite Carpentier's (1974,1977) statement that the expected durability is only ten to fifteen years with a fifteen to twenty per cent failure rate, many surgeons are presently converting from the prosthetic valves to the glutaraldehyde-preserved porcine xenografts.

√ The Hancock porcine xenograft [Reis and Hancock, 1971; Hancock, 1977] has equalled or outperformed all of the other AVR substitutes. Its optimistic future has convinced two other valve manufacturing companies, which are traditionally ball and disc valve manufacturers (Edwards and Shiley Laboratories), to market their own models.

Autologous and Heterologous Tissue Valves

Availability problems with homografts, and thromboembolic and hemodynamic complications with mechanical valves were some of the reasons for resorting to valves constructed from autologous and heterologous tissues. Various sources have been used for fabricating the leaflets of the valves: pericardium [Sauvage et al, 1963; Björk, 1964], autogenous and restructured fibrocollagenous tissue [Loughridge et al, 1965; Williams et al, 1969; Geha et al, 1970; Schumacker et al, 1970; Carpentier et al, 1971; Edwards, 1971], arteries [Bailey, 1967], pulmonary autografts [Ross, 1967; Ross and Geens, 1972], fascia lata [Senning, 1967; Ionescu and Ross, 1969], peritoneum [Fadali et al, 1970], dura mater [Puig, 1972] and vena cava [Ramos et al, 1973]. In general, all of the valves gave good early hemodynamics and freedom from major thromboembolic episodes. However, fascia lata valves (unsupported, frame-supported or preserved) proved to be poor aortic valve substitutes as late failures became commonplace due to tissue degeneration and loss of elasticity [Ionescu et al, 1972^b; Rothlin and Senning, 1973; Yarbrough et al, 1973; Ionescu et al, 1974; Olsen et al, 1975; Senning et al, 1975]. Fascia lata valves are no longer used. And experiences with autogenous tissue, peritoneum and vena cava have been limited or inconclusive. On the other hand, pericardium [Ionescu et al, 1974, 1977] and dura mater valves [Nuno-Conceição et al, 1975; Puig et al, 1977] have now been implanted for more than

four years with satisfactory results. The Ionescu-Shiley (bovine) pericardial xenograft preserved by the stabilized glutaraldehyde process seems to be equally as competent as the glutaraldehyde-preserved porcine xenograft. However, it is difficult to imagine that tissues which are structurally-, functionally-, and environmentally-differentiated from the aortic valve tissue could be superior to the valve tissue.

C4. Prosthetic Trileaflet Valves

Prosthetic trileaflet valves were abandoned in the late 1960's with the claim that failures were the result of the lack of durability of the available leaflet materials [Braunwald and Detmer, 1968]. Failures however may not have been due solely to as claimed. The relatively crude methods of design lacked engineering sophistication and therefore, may have been partially at fault. For example, none of the leaflet materials displayed mechanical characteristics which are typical of the aortic valve leaflets (ie., a non-linear and two-phase stress-strain response with a high elastic recovery). These particular characteristics play important roles in determining the efficiency and durability of the natural valve [Clark, 1973; Wright and Ng, 1974], but were ignored in the designs. Furthermore, fabricating symmetrical prosthetic valves to replace the natural asymmetrical valves produced possible abnormal stress concentrations in the artificial leaflets. These stresses might have been responsible

for increased leaflet fatigue and subsequent valve failures.

It would then seem appropriate to use in a design a leaflet material that, besides being biocompatible and anti-thrombogenic, is also biological in mechanical properties (ie., non-linear and two-phase stress-strain characteristics) and inhomogeneous and anisotropic (ie., variable elasticity with respect to position and orientation).

Researchers have recently placed a new resurgence in flexible trileaflet prosthesis design. Studies on the natural leaflets' fibre structure [see Histology and Ultrastructure of the Valve Leaflets, p. 17] and mechanical properties [see Mechanical Material Properties of the Valve Leaflets, p. 21] have been conducted, and have aided in understanding how tri-leaflet prostheses can be made to be more durable. Clark and his colleagues (1974) have reported a composite leaflet woven from 10 μ polyester filaments which are microcrimped in order to simulate the non-linearity and anisotropy of the natural leaflet material. Inhomogeneity was however not incorporated.

Recent works on flexible trileaflet prostheses have also been reported by Mohri et al (1973), Gerring et al (1974), Ghista (1976), Ghista and Reul (1977) and Hufnagel (1977).

C5. Summary and Consensus

Despite all of the many advanced modifications and improved surgical techniques which to their credit did reduce some of the problems, none of the currently available valves

have been able to eliminate all of the complications which are associated with AVR. A quick look at the literature of clinical experiences reveals claims and counterclaims of each valve's performance, successes or failures. Often, the observations are clouded by the surgeon's biases and by the use of unstandardized statistical methods in the follow-up reports. At present, the situation is satisfactory but by no means acceptable. Each valve type offers its own advantages and disadvantages (table 2). The one chosen by the surgeon is usually governed by his preference, his skill and experience with the valve, and also by the patient's contraindications.

One is often faced with the following dilemma: to either choose a prosthetic valve substitute that has proven durability but also has increased thromboembolic risks and related anticoagulation complications, or to choose a tissue valve substitute that has better hemodynamic characteristics, lower thrombogenicity without anticoagulation and minimal hemolysis but has a high susceptibility to late failures. The recent success of the glutaraldehyde-preserved porcine xenografts may have somewhat reduced this "prosthetic-or-tissue" dilemma. But pending the final outcome of the late evaluations of the porcine xenografts, it would still seem that the ideal AVR substitute should be a flexible trileaflet prosthesis that is fabricated from a leaflet material which is biocompatible, non-thrombogenic and resemblant of biological tissue in its mechanical properties.

TABLE 2. COMPARISON OF AORTIC VALVE SUBSTITUTES*

	Rigid Mechanical Prosthetic Valves		Biological Tissue Valves				
			Grafts		Autologous & Heterologous Tissues		
Types	Ball S-E B-C S-C	Disc B-S L-K	Homografts	Glutaraldehyde Preserved Porcine Xenografts H , E-C , A-S	Fascia Lata	Pericardium	Dura Mater
Availability	1	1	3	1	3	1	3
Technique	1	1	3	2	3	2	2
Thromboembolism & Anticoagulation	2	2	1	1	1	1	1
Hemodynamics	2	2	1	2	2	1	1
Infection	2	2	1	1	1	1	1
Durability	1	1	3	2	3	2	2

* An arbitrary rating from good (1) to poor (3) is used in the table.
Based on a personal evaluation of the surveyed clinical literature.

S-E : Starr-Edwards

B-C : Braunwald-Cutter

S-C : Smeloff-Cutter

B-S : Björk-Shiley

L-K : Lillehei-Kaster

H : Hancock

E-C : Edwards-Carpentier

A-S : Angell-Shiley

D. Methodology

The work presented in this thesis is Part I of a two part study on the mechanics of the porcine aortic valve. It describes the acquisition, presentation and analysis of an intact porcine aortic valve leaflets' local surface geometry (ie., local surface strains and radii of curvature) as a function of the static intra-aortic pressure in-vitro. In addition, the inhomogeneity and anisotropy of the intrinsic material mechanical properties (ie., stress-strain responses and elastic moduli) of the leaflets are investigated in a set of corresponding microtensile experiments.

Part II is a presentation of the stress analysis of the porcine aortic valve leaflets in diastole, utilizing the results obtained in Part I. Specifically, considerations of geometrical asymmetry, material inhomogeneity, anisotropy and non-linearity are analysed in light of their effects on the stresses.

II. EXPERIMENTAL METHOD

Investigations were conducted following two sets of experiments: A. Microtensile stress-strain experiments on circumferentially and radially cut strips of the leaflets, and B. Analysis of the local circumferential and radial surface strains and curvatures over the leaflets of an intact whole valve. In the latter, the valve is subjected to simulated static diastolic pressures in-vitro.

A. Microtensile Stress-Strain Experiments

A1. Dissection and Tissue Preparation

Fresh porcine hearts from four months old pigs were obtained from a local slaughterhouse and the leaflets from two healthy valves were excised within the day of the kill. From valve 1, the NC leaflet¹ was cut into five parallel radial strips, each about 2.4 mm. wide. A series of surgical blades separated and spaced in parallel by washers and held together by a screw and nut was used as the cutting mechanism. Figure 20 shows the five radial strips numbered 1 to 5 as

¹ For leaflet identification, refer to figure 4, p. 10.

viewed from the ventricular side. The RC (or MC) leaflet and LC (or NMC) leaflet of the same valve 1 were cut to provide similar radial strips in a position comparable to strip 3 of the NC leaflet (figure 22).

From a second valve, valve 2, the NC leaflet was cut into four parallel circumferential² strips, each about 2.0 mm. wide (figure 21). The other two leaflets were cut to provide similar circumferential strips in a position comparable to strip 3 of the NC leaflet (figure 23).

Using a human hair as a pen, each strip after having been air-dried to a semi-moist state was then dotted with very tiny India ink dots on the smooth ventricular side. The dots are spaced along the strip length at about 1-1.5 mm. intervals. Much care was spent in arriving at the proper degree of drying; that is, the tissue is required to be not too moist as to cause the ink to run or smear, and also not too dry as to have potentially altered the tissue's mechanical characteristics.

The strips were individually stored in a 0.9% saline solution containing 600,000 U. of aqueous penicillin. They were kept at refrigerator temperatures ($\sim 4^{\circ}\text{C}$) in order to prevent bacterial growth. All strips were tested within a $1\frac{1}{2}$

² The strips were not ideally circumferential since the leaflet, when flattened to be cut, exposed the circumferential collagen fibres (see figure 4) as arcs. Therefore, the fibres did not line up with the straight-edge cutting blades. Errors due to this effect are discussed in Appendix A.

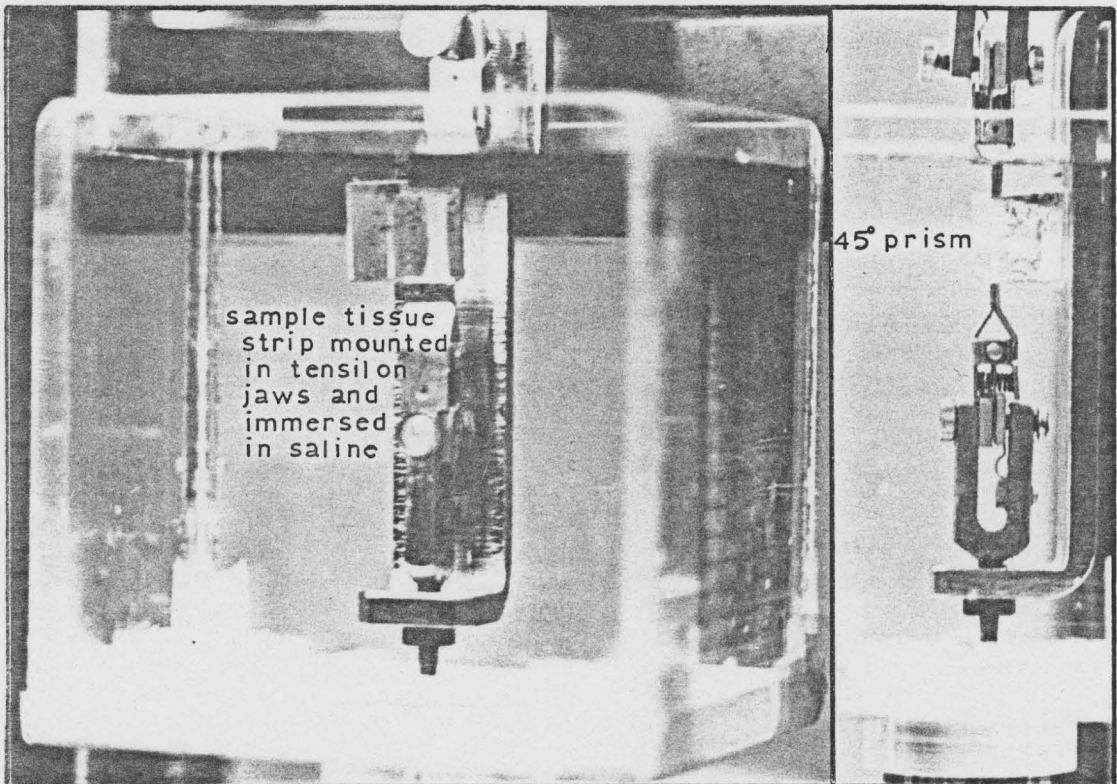
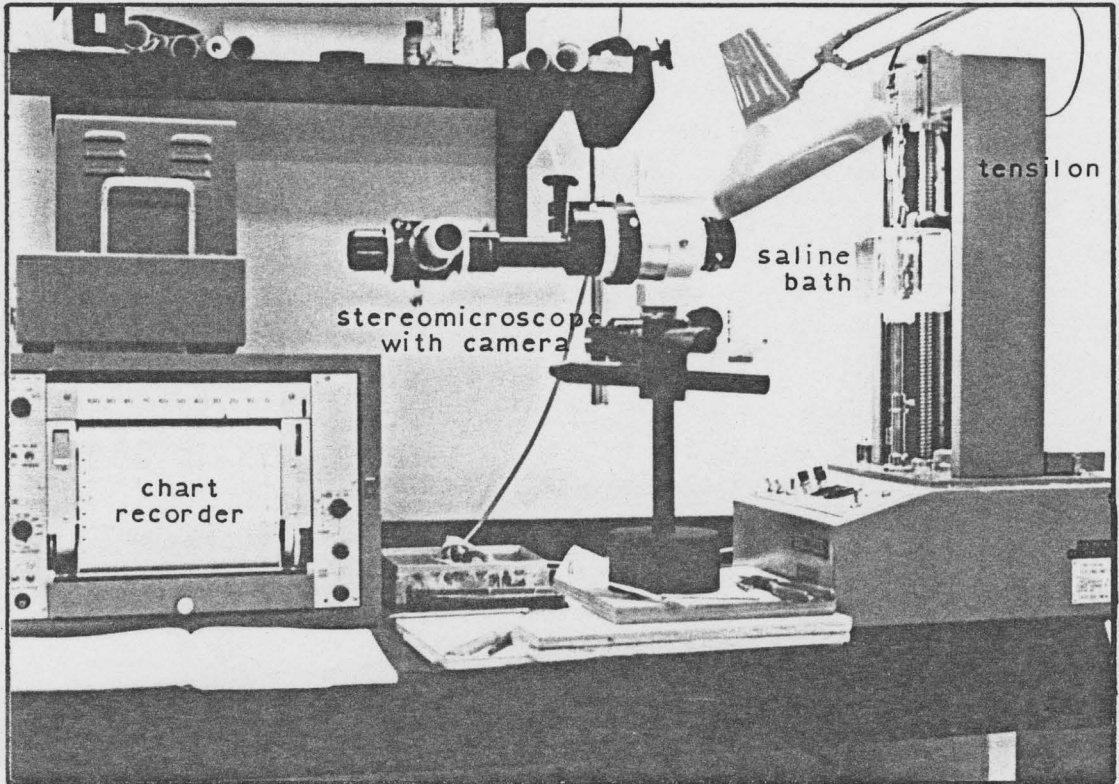
week period after dotting.

A2. Apparatus and Testing

The apparatus used for the testing is illustrated in figure 9. During the testing, all strips were kept in a normal saline solution at room temperature. For each radial strip, the ends were mounted into the jaws of a Tensilon machine (model Toyo Baldwin UTM-11-20 with a TLU-0.2L-F load cell) exposing the strip just below the sinus-annulus ridge and just above the coaptation edge. The circumferential samples were clamped approximately at their end attachments to the sinus-annulus. The crosshead speed used to stretch all the strips was 2.0 mm/min. The latter is very small when compared to the observed in-vivo strain rate of the natural valve leaflets; however, the slow speed was necessary to allow for adequate time to photograph the various phases of the stretch. The chart speed on the recorder (model Toyo Baldwin TMIBCH SS-505D-UTM) monitoring the tension-elongation data was adjusted to give 2 cm. of chart = 1 mm. of sample elongation for the radial strips and 1 cm. of chart = 1 mm. of sample elongation for the circumferential strips.

A 35 mm. camera (Praktica LLC) loaded with medium speed film (Kodak Plus-X; ASA 125) and attached to a stereomicroscope (model Wild Leitz M7) was used to photograph the strip under test at known elongations or tensions. Using the allowable aperture of the stereomicroscope, the strips were

FIGURE 9. MICROTENSILE EXPERIMENT APPARATUS 60



illuminated to require a shutter speed of one-eighth of a second. The thickness of the strip during the stretch was measured using a 45° prism attached onto the crosshead adjacent to the sample strip (see figure 9).

Zero length for the Tensilon was determined by adjusting the jaws to just touch so as to just cause the tension recorder to become sensitive. Thus, there exists a calibrated one-to-one correspondence between the sample strip length and the jaw separation. Tension was calibrated using a 20.0 gram weight.

Each strip was stretched into the stiff post-transition³ region for 3 to 5 times so that consecutive stretches gave similarly shaped tension-elongation curves with minimum load-unload hysteresis. For the final run, each strip was stretched from a slack state to well into the linear post-transition region. Photographs of the strip under test were taken at its initial length and at pre-determined elongations or tensions so as to cover the whole event of loading. The resting or initial length corresponding to zero elongation and zero tension is determined (to ± 0.1 mm.) from the chart recording by noting the point of intersection of the curve's horizontal section (which represents the zero tension that is recorded while the stretching strip is still in the slack condition) and the asymptote of the curve's pre-transition³

³ These terms are defined and described in Appendix A.

section (which represents the onset of tension). This is illustrated in figure 10. The latter is the tension-elongation chart recording for radial strip 3 of the NC leaflet. Figure 11 is a sequence of photographs associated with the curve in figure 10. The last picture in the sequence is a photograph of a 1.0 mm. scale used for calibration.

Each strip required on the average approximately 20 to 30 minutes of testing.

A3. Data Acquisition and Processing

The developed prints of the photographs, which were enlarged at about 15x to 20x* on 8" x 10" Kodak single weight Ektamatic SCF paper, were used to measure the elongations, widths and thicknesses of the individual sub-sections of each strip as defined by the spacings of the ink dots. Figures 12 and 13 are actual 8" x 10" prints from which measurements were made. They correspond to the first and seventh photographs in the sequence shown in figure 11.

The measurements combined with data obtained from the chart recordings of the tension-elongation curves provided the means to derive individual stress-strain curves for each sub-section of the leaflet in both the radial and circumferential directions. Terminologies and considerations

* This is the magnification of the actual dimensions; that is, life to print size. The negative to print enlargements were approximately 9x to 13x.

FIGURE 10.

TYPICAL TENSILON F-l CURVE

SAMPLE : NON CORONARY LEAFLET
RADIAL STRIP 3

REST LENGTH : $l_0 = 6.8 \text{ mm} \pm 0.1$

INITIAL C/S AREA : $A_0 = 2.1 \text{ mm}^2 \pm 10\%$

STRAIN RATE : $\dot{\epsilon} = 30\% / \text{min.} = 2 \text{ mm.} / \text{min.}$

PHOTOGRAPHS SHOT DURING 6th LOADING CYCLE
at LENGTHS as SHOWN

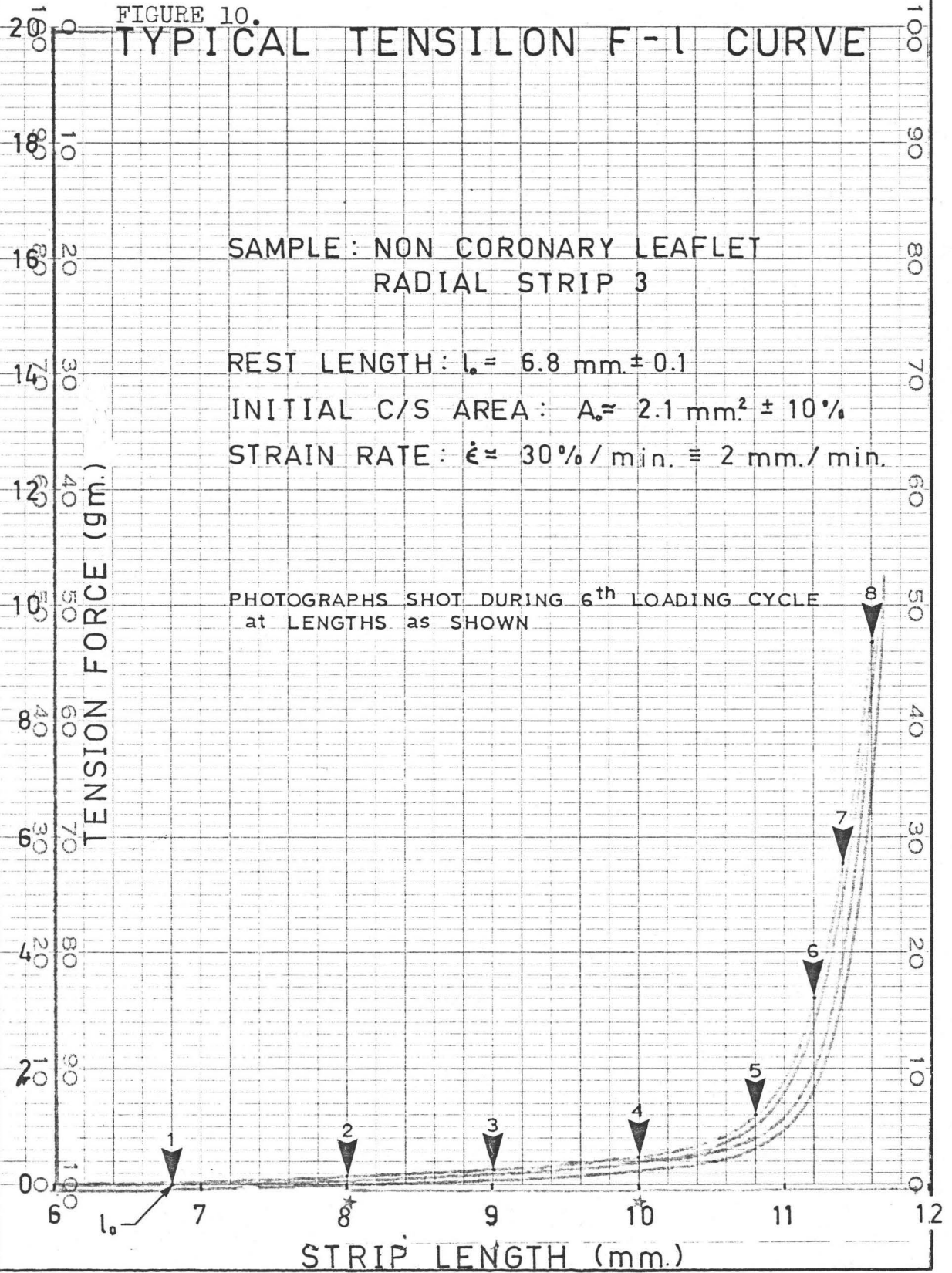
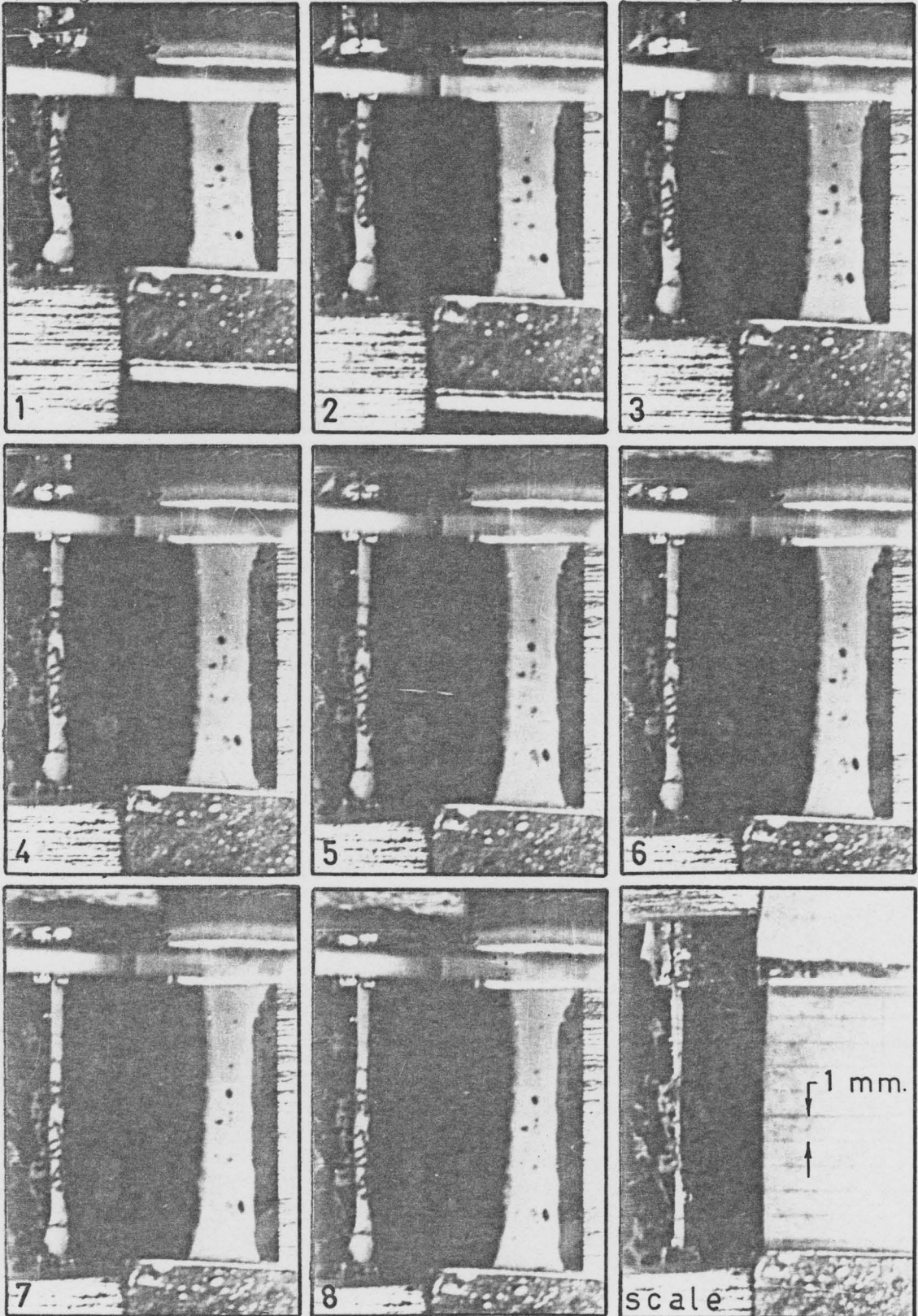


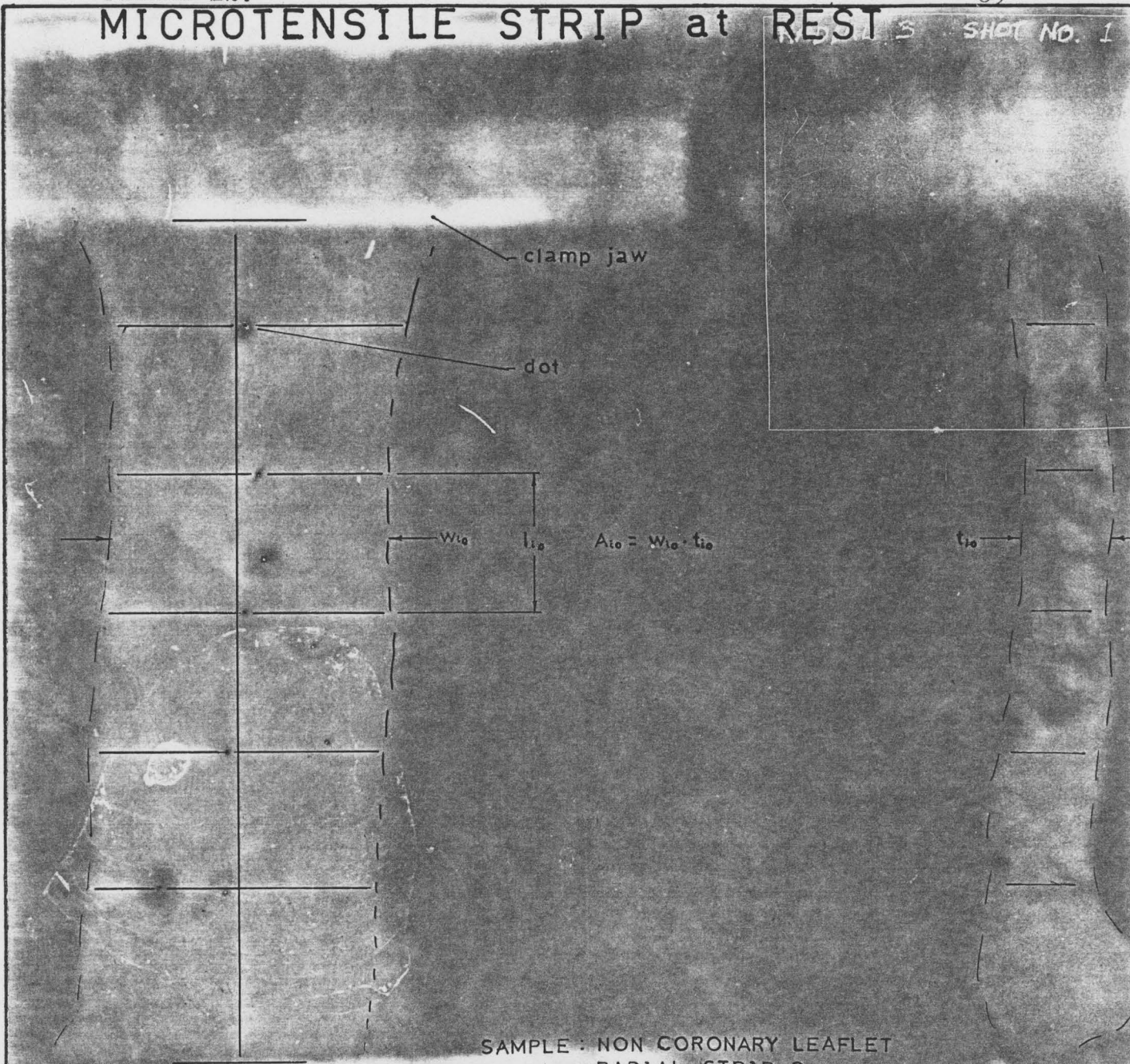
FIGURE 11.

MICROTENSILE STRETCHING of STRIP

photograph no. 1-8 are in reference to the accompanying F-l curve



MICROTENSILE STRIP at REST SHOT NO. 1



SAMPLE : NON CORONARY LEAFLET
RADIAL STRIP 3

PHOTOGRAPH NO. 1

TOTAL LENGTH : $l_0 = 6.9 \text{ mm} \pm 0.05$ (initial rest length)

ZERO STRAIN

ZERO FORCE

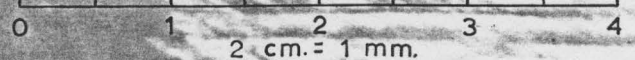
MEAN WIDTH : $w_0 = 2.5 \text{ mm} \pm 0.1$

MEAN THICKNESS : $t_0 = 0.85 \text{ mm} \pm 0.05$

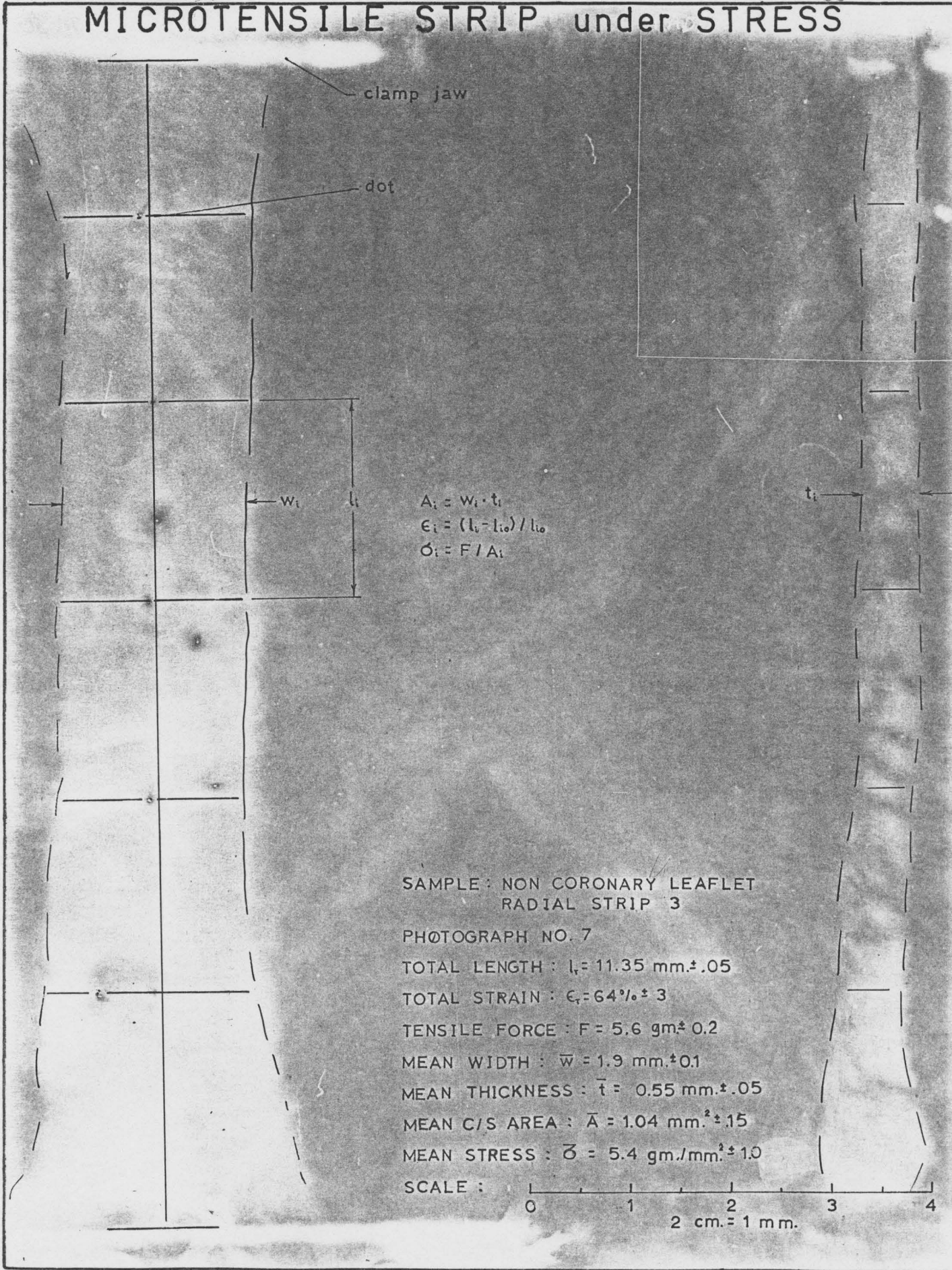
MEAN C/S AREA : $A_0 = 2.15 \text{ mm}^2 \pm 0.21$

ZERO STRESS

SCALE :



MICROTENSILE STRIP under STRESS



$$A_i = w_i \cdot t_i$$

$$\epsilon_i = (l_i - l_{i0}) / l_{i0}$$

$$\sigma_i = F / A_i$$

SAMPLE : NON CORONARY LEAFLET
RADIAL STRIP 3

PHOTOGRAPH NO. 7

TOTAL LENGTH : $l_i = 11.35 \text{ mm} \pm 0.05$

TOTAL STRAIN : $\epsilon_i = 64\% \pm 3$

TENSILE FORCE : $F = 5.6 \text{ gm} \pm 0.2$

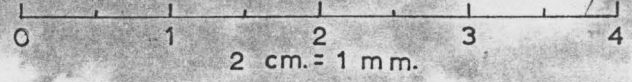
MEAN WIDTH : $\bar{w} = 1.9 \text{ mm} \pm 0.1$

MEAN THICKNESS : $\bar{t} = 0.55 \text{ mm} \pm 0.05$

MEAN C/S AREA : $\bar{A} = 1.04 \text{ mm}^2 \pm 0.15$

MEAN STRESS : $\bar{\sigma} = 5.4 \text{ gm./mm}^2 \pm 1.0$

SCALE :



involved in the conversion of a tension-elongation chart recording to a series of stress-strain curves are discussed in Appendix A.

B. Whole Valve Experiments

B1. Dissection and Tissue Preparation

A fresh porcine heart from a four months old pig was obtained from a local slaughterhouse. It was dissected the same day to give the intact aortic root specimen (figure 1). The myocardium surrounding the sinus-annulus region of the valve was left intact as much as possible in order to preserve the surrounding environment of the valve in-vivo. However, some of the muscle necessitated trimming in order to prevent blocking the ventricular view of the leaflets and also to prevent weighing down the aortic root when suspended in a horizontal position. The aorta of approximately $2\frac{1}{2}$ inch length was cannulated at its distal end. The latter was then attached to an air supply that closed the valve and distended the leaflets to their approximate diastolic configuration. The leaflets were air-dried to a semi-moist state at which point, the ventricular side of the leaflets were dotted with very tiny India ink dots. The applicator used was a human hair; but initially, a Staedtler #00 pen (diameter = 0.13 mm.) was employed. The latter proved very unsatisfactory because

of a tendency to blob. Extreme care was required to keep the dots as small (~ 0.2 mm. diameter) and as sharp as possible without any running and smearing of the ink; this was only achieved after considerable painstaking practice.

One hundred to one hundred and twenty-five dots were applied onto each leaflet's surface in an approximate 1 mm. by 1 mm. square grid that simulated the leaflet's directional anisotropy; that is, the radial and circumferential fibre directions. Each dot is identified according to its leaflet and to its column-row designation on that leaflet. The rows are oriented circumferentially and the columns are oriented radially. The dotting procedure was ceased once the leaflets and the valve exhibited excessive drying. This occurs after about ten minutes out of solution. At this point, the whole valve was then re-immersed into a normal saline solution for ten minutes in order to restore the leaflets' natural condition. The complete drying-dotting-rehydrating procedure was then repeated until all three leaflets were dotted to satisfaction. The whole dotting period spanned three days. During this period, the valve was stored at refrigerator temperatures ($\sim 4^{\circ}\text{C}$) in a normal 0.9% saline solution containing 600,000 U. of aqueous penicillin.

Figure 14 shows the experimental valve after dotting.

B2. Apparatus and Testing

On the fifth day of storage, the dotted and cannulated

valve was tested in the system shown in figures 15 to 17. The RC artery was ligated with silk suture and the LC artery was attached to a mercury manometer. The manometer which was used to monitor the static intra-aortic pressure is accurate to ± 0.5 mm. Hg. The aortic root was then immersed into a saline tank, and clamped onto a mechanical rig which suspended the valve at a fixed height (ie., fixed z coordinate) but which also allowed it to be rotated in the X-Y plane about the Z-axis. The above arrangement is schematically illustrated in figure 15. The distal end of the aortic root was joined via a rubber-stoppered cannula and tubing to a large saline reservoir (eight litres capacity). The latter was pressurized by a regulated air supply that was controlled by a needle regulator valve in conjunction with a simple clamp. The regulated pressure in turn controlled the flow of saline from the reservoir into the aortic root. A small continuous flow was made possible by some very tiny branching coronary arteries. All connections in the apparatus used suitably sized Tygon tubing.

The camera system shown in figure 15 consisted of a 35 mm. camera (Praktica LLC loaded with fine-grain Kodak Panatomic-X film: ASA 32) coupled to a 300 mm. telephoto lens (Vivitar f/4), a 2x teleconverter and a 6 cm. extension tube. The lens axis of the combination was adjusted to align with the Y-axis. A long telephoto lens was required to view the valve from a far enough distance (~ 175 cm.) to insure a

FIGURE 15.
DIAGRAM of APPARATUS for PHOTOGRAPHING
a PRESSURIZED AORTIC VALVE

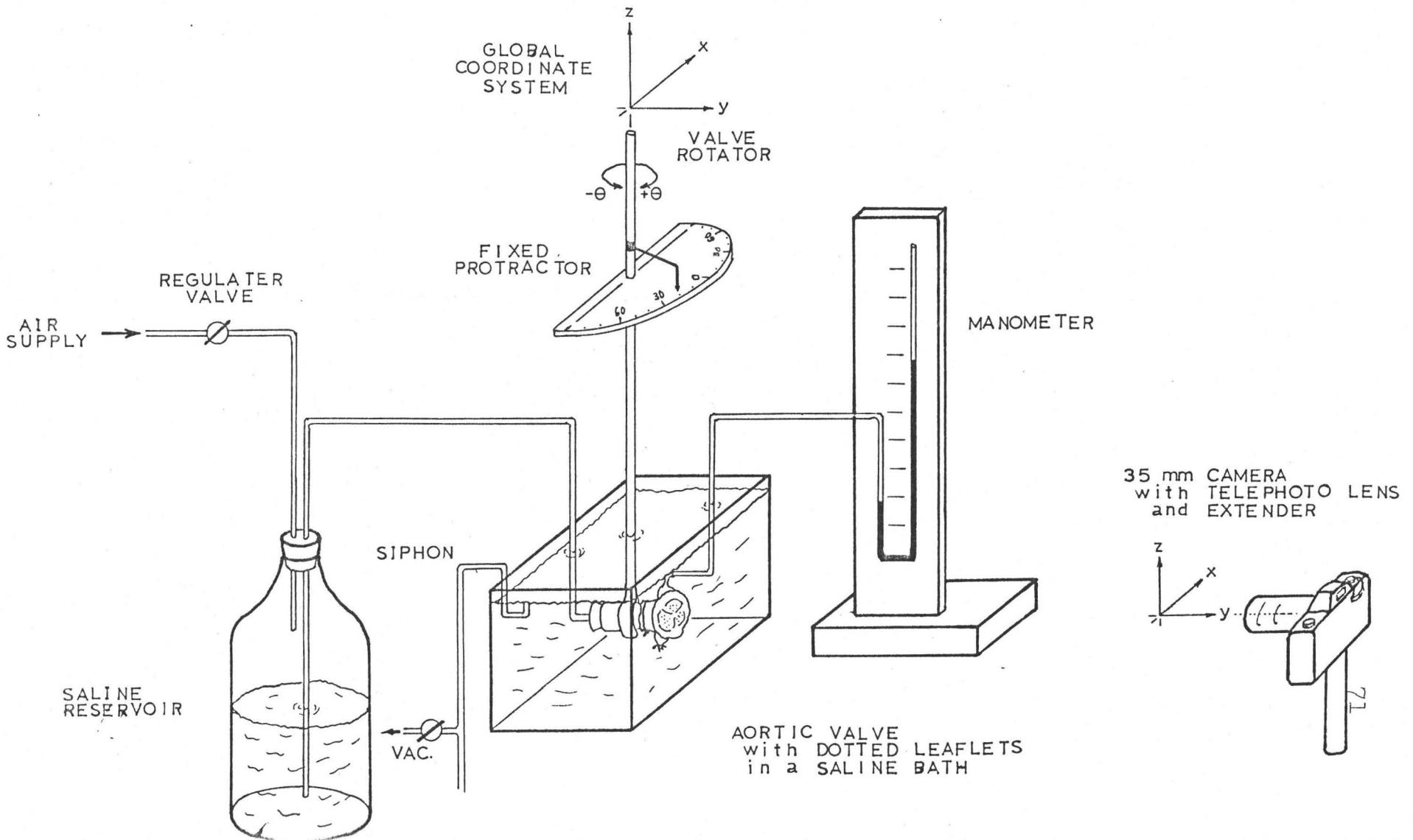
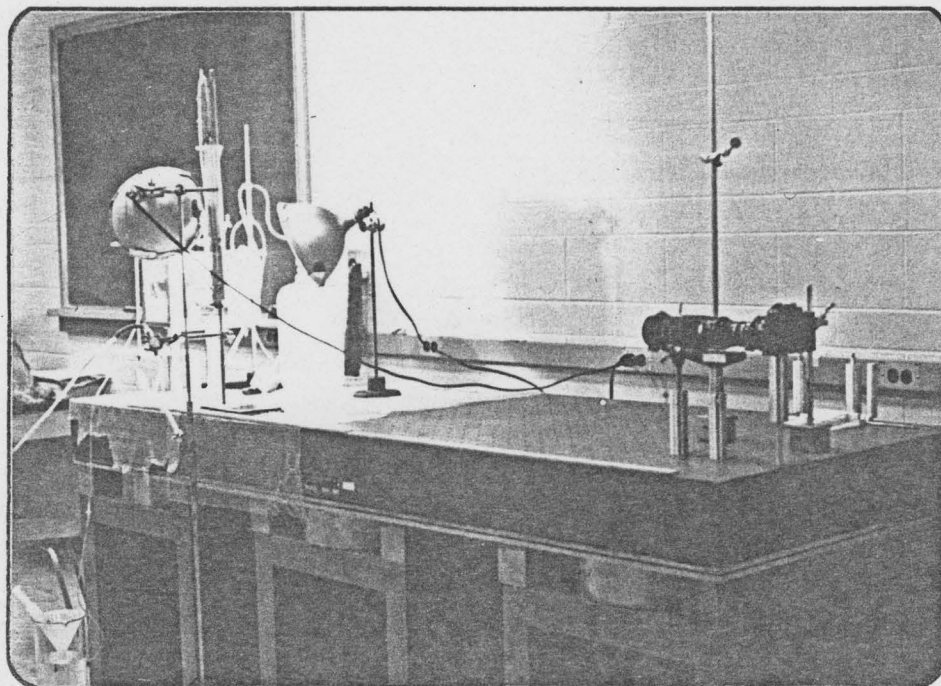


FIGURE 16. WHOLE VALVE EXPERIMENT APPARATUS ⁷²



VIEWS of STEREO-PHOTOGRAMMETRIC SET-UP

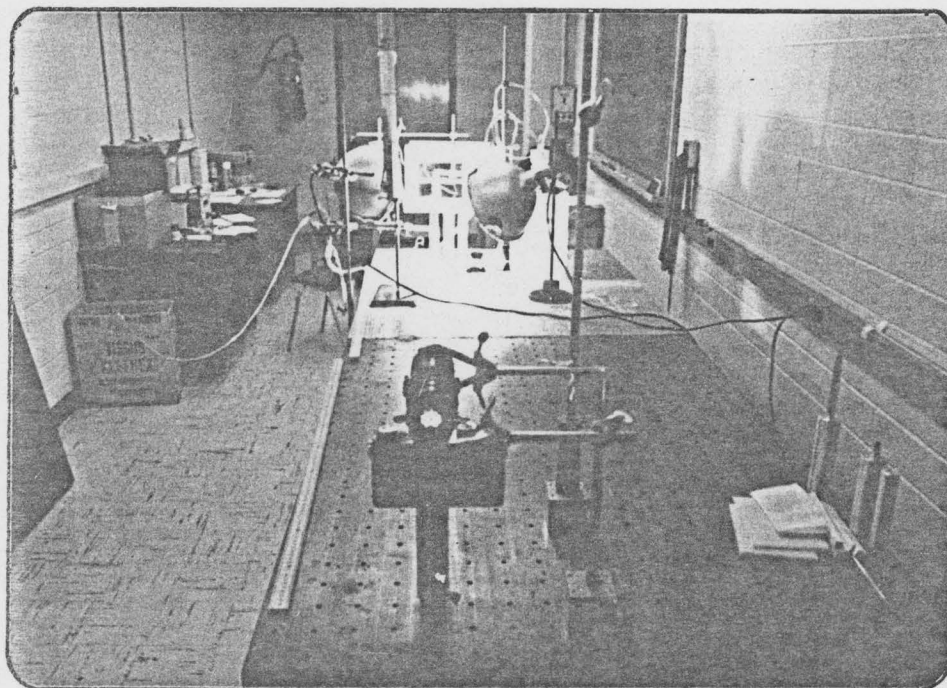
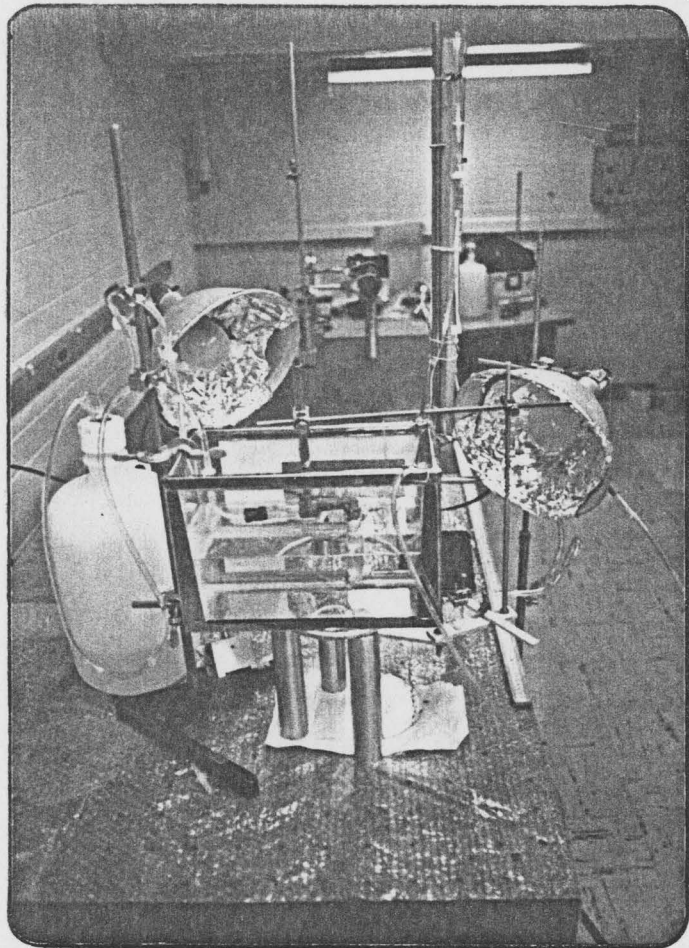
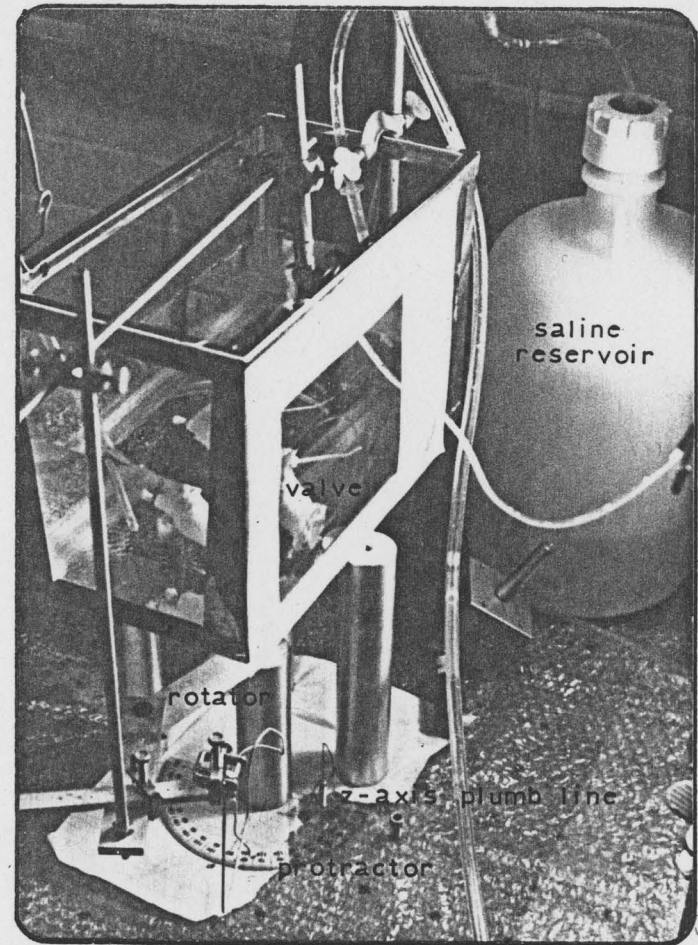


FIGURE 17.
WHOLE VALVE EXPERIMENT APPARATUS

VALVE BATH and PRESSURE SYSTEM



VALVE ROTATOR ASSEMBLY



minum of parallax. The latter is a necessary prerequisite in the theory used to determine the leaflet surface local geometry. The theory is described in detail in Appendix B. The extension tube was required to reduce the telephoto's focusable distance and also to optimize the camera magnification in order to best fill the viewfinder with the image of the valve.

The valve was focused in its unrotated reference position (ie., $\theta = 0^\circ$). With the lens aperture set at its smallest opening ($f/22$) in order to acquire the best depth of field possible (~ 2 mm.), the valve was illuminated with sufficient lighting to necessitate a $\frac{1}{2}$ second shutter speed. The whole apparatus was arranged on a sturdy 4' x 8' metal optical table in order to prevent any vibration effects or possible changes in the components' relative positioning. Any such motion would invalidate the measurements from the resulting photographs.

The valve was gradually pressurized to 140 mm. Hg. in about ten seconds and then returned to zero pressure. The procedure was repeated for five similar cycles to condition the leaflet tissue. For the final photographing run, the valve was loaded to 140 mm. Hg. and then unloaded to the lowest possible pressure required to just maintain leaflet coaptation and minimal leaflet distension. This was referenced to as the zero pressure loading corresponding to the zero stress state. Actually, the manometer was recording

approximately 3 mm. Hg. This is the intra-aortic pressure measured by the manometer at zero transvalvular pressure, which is the true loading pressure for the leaflets. Thus, transvalvular pressure equals the intra-aortic pressure measured by the manometer minus the 3 mm. Hg. The latter is the mean pressure opposing leaflet coaptation caused probably by the valve being submersed about 3 cm.* in the saline tank.

The unstressed valve was photographed at 0° , $\pm 15^\circ$, $\pm 30^\circ$ and $\pm 45^\circ$ rotations. This was repeated at 20 mm. Hg. intervals up to 120 mm. Hg. The entire photographing session required approximately ten to fifteen minutes. Throughout this time period, the saline tank was being siphoned at a rate that maintained the tank surface level constant in order to keep consistent the pressure head due to the valve submersion depth (ie., 3 mm. Hg.).

B3. Data Acquisition and Processing

The developed prints of the photographs, which were enlarged at about $8.7x^+$ on 11" x 14" Kodak single weight Ektamatic SCF paper, were used to provide the raw data measurements. The latter which are described in Appendix B were input into a computer program that output at each pressure the following: 1) the (x,y,z) coordinate data of all the dots

* 1 mm. Hg. = 1.3 cm. H_2O .

+ The corresponding negative to print enlargement is $17.5x$.

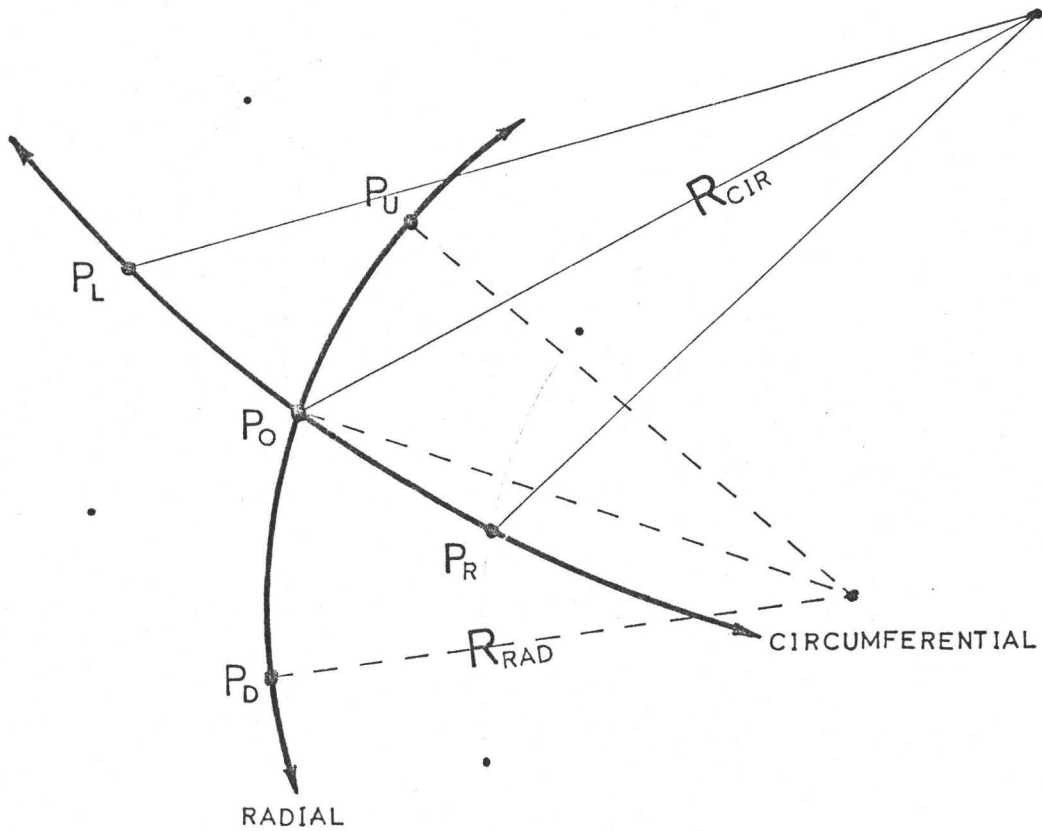
with respect to a global X-Y-Z coordinate system, 2) the local radii of curvature at each point in both the circumferential and radial directions and 3) the local circumferential and radial surface strains⁴ over the sections of the leaflets defined by the spacing of the dots (figure 18).

The theory used in converting the photograph measurements into three-dimensional coordinate data is described in Appendix B. In short, it may be described as a stereophotogrammetric method that uniquely locates a point in three-dimensional space with respect to a fixed global coordinate system. This is accomplished by recording from at least two different angles of view, a point's relative position with respect to a known coordinate axis that is perpendicular to the view directions.

The previously mentioned computer program is listed and described in Appendix C. Appendix D details the theory employed for the radii of curvature calculations. The output from the computer program are presented as local pressure-radius and pressure-strain curves to describe the local geometrical and mechanical changes in the leaflets of the valve as the loading pressure is varied.

⁴ The strains were calculated as changes in the straight-line distances between dots, although the more proper interpretation is of strain being the change in the surface distance between dots. However, the former interpretation was used in order to simplify the adaptation of the three-dimensional coordinate data to strain calculations. Further details are given in Appendix B.

FIGURE 18.
DETERMINATION of COMPONENT STRAINS and RADII



at point P_o , component strains are :

$$\epsilon_R = \frac{\Delta(\overline{P_U P_O} + \overline{P_D P_O})}{(\overline{P_U P_O} + \overline{P_D P_O})_0 \text{ mm. Hg.}}$$

$$\epsilon_C = \frac{\Delta(\overline{P_L P_O} + \overline{P_R P_O})}{(\overline{P_L P_O} + \overline{P_R P_O})_0 \text{ mm Hg.}}$$

, and radii of curvature
are R_R and R_C

III. RESULTS AND DISCUSSIONS

A. Microtensile Stress-Strain Experiments

A1. Comments on the Experimental Method

Tensile stress-strain experiments on biological tissues have been reported by several authors in recent years. Useful comments on the various methods can be found in the literature [Abrahams, 1967; Fung, 1968; Ellis, 1969; Soden and Kershaw, 1974]. The technique described in this work is fundamentally different from the other reported methods in three ways: 1) heterogeneity capability, 2) tissue cross-sectional area measurements and 3) detection of slippage.

The heterogeneity capability is rendered possible by photographing the dots on each specimen strip as the latter is being stretched. Detailed description of the technique is given in Appendix A.

Previous cross-sectional area measurements, which are required for the conversion of tension to stress, have been all similar in that a singular average area for the strip has been used [Ellis, 1969]. In Clark's (1973) and Missirlis' (1973) stress-strain studies of the human aortic valve leaflet tissue, this singular mean area was measured with the leaflet strips in their unloaded relaxed state.

The observed tendency for thin tissue, such as an aortic leaflet strip, to "neck"⁵ appreciably upon increased loading and stretching would then imply a smaller cross-sectional area than originally measured. Results from our experiments suggest that overestimation of the cross-sectional area as high as 50% to 80% is possible at post-transition⁵ strains and stresses. These figures are based on the assumption of a constant volume stretch⁵ from which it can be shown that the percent error in area is equal to the percent strain (see Appendix A). The validity of stress-strain curves converted from tension-elongation curves using a singular cross-sectional area is therefore questionable.

By photographing the tissue strip at different phases of the stretch, it is possible to determine the exact width and thickness (hence, also the area) of the strip as it necks under increasing strain. Furthermore, variations in width and thickness along the strip's length are also measurable. This is illustrated in figures 11 to 13. Thus, it is possible to obtain more exact stress and elastic modulus calculations. However, the true extent of obtaining even more exact calculations would require an analysis of the density of the load-bearing collagen fibres in the tissue.

The effect of slippage, which is a potential problem in all tensile testing equipment, is minimized in our method

⁵ These terms are defined and described in Appendix A.

since the length measurements are not singularly dependent on the Tensilon jaw separation. Instead, the lengths may be measured from the photographs.

Effects of Experimental Parameters

As with any other results determined from in-vitro tests, the results from our experiments should be interpreted with care in light of how realistic they are in comparison to the in-vivo situation. Undoubtedly, cutting the leaflet tissue into strips should theoretically damage the fibre structure integrity and weaken its load-bearing capability. It has been suggested that such damage, which can be characterized by the loss of chain branching at the fibre level or the breaking of chemical cross-linkages at the intermolecular level, would alter the mechanical response of the intact tissue [Harkness, 1961; La Ban, 1962; Missirlis, 1973]. The arcing circumferential fibres of the valve leaflet presented another significant problem in this area. Some of these circumferential fibres cut by the straight parallel blades were conceivably disabled from supporting any tension during the Tensilon stretch (see figure A3 in Appendix A). This accordingly would lead to an overestimation of the actual cross-sectional area and hence, an underestimation of the actual stress and the calculated post-transition elastic modulus. Errors as high as 10% are likely.

In other studies, Lim and Boughner (1975) working on

human chordae tendinae observed that increasing the sample cross-sectional area shifts the stress-strain curves to higher strains (ie., higher extensibility) and reduces the final post-transition elastic moduli. La Ban (1962) using canine tendons reported similar relationships with variation in tissue sample length.

The effects of strain rate on stress-strain curves has also received considerable attention. It has been noted that biological tissue becomes less extensible with increasing strain rate [Rigby et al, 1959; Abrahams, 1967; Lim and Boughner, 1975]. Rigby (1959) described it "... as a required increase in the load to produce a given strain." The degree of reduction in extensibility is seemingly dependent on the tissue characteristics; for example, the degree of visco-elasticity, the overall stiffness and the collagen-elastin proportions.

Reported effects on the elastic moduli have however been less consistent. Missirlis (1973) working on native and de-elastinated aortic valve tissue, and Lim and Boughner (1975) working with chordae tendinae observed that the final post-transition modulus is essentially independent of strain rate. On the other hand, Lake (1973) reported a 10% increase in the modulus for aortic wall elastin for each decade increase in strain rate. Others working with various animal and human tendons, which are predominantly collagen, also observed that the final post-transition modulus increases

with applied strain rate [Van Brocklin and Ellis, 1965; Abrahams, 1967].

Our experiments employed a comparatively slow stretch rate of 2 mm/min. This corresponds approximately to a strain rate of 14%/min to 21%/min for the circumferential strips ($9.4 \text{ mm.} \leq l_0^* \leq 13.9 \text{ mm.}$) and 20%/min to 45%/min for the radial strips ($4.4 \text{ mm.} \leq l_0^* \leq 9.0 \text{ mm.}$). These experimental strain rates are much smaller than the estimated in-vivo strain rate of 15,000%/min for aortic valve leaflet tissue [Missirlis, 1973]. Thus in light of the above, experimentally observed strains in-vitro would be considerably greater than the actual in-vivo strains. Post-transition moduli would probably be invariant. The first supposition agrees in part with data recently reported by Brewer et al (1977) on canine aortic valves: 16% strains in-vitro as compared to 2% strains in-vivo. The reported strains are circumferential.

Another important consideration in our experiments is the potential adverse effects of the drying-dotting-rehydrating procedure on the mechanical properties of the tissue strips. The hair used in dotting the strips is unlikely to cause excessive damage to the tissue. And although Clark (1973) reported significant alteration to the stress-strain response after drying, our preliminary tests apparently showed no obvious differences between stress-strain curves

* l_0 is the tissue strip rest or initial length.

obtained from tissues before and after the drying-dotting-rehydrating procedure. The manner of tissue preparation used in our experiments is therefore considered acceptable. Furthermore, figure 19, which shows the effect of the length of storage of leaflet tissue in 0.9% saline, suggests that the means of storage used in our experiments is also satisfactory in preserving the tissues' intrinsic mechanical characteristics. However, the effects of testing under non-physiological temperatures and pH were not investigated and therefore can only be speculated.

In retrospect, maybe a few comments could be made in regards to some improvements which can be incorporated into the experimental method. Foremost in mind is the possible use of a video-record system. The latter would help to minimize or eliminate the difficulties involved in synchronizing the camera exposures with the chart recording, and also in maintaining scale constancy in the developed photographs. Another invaluable aid would be a computerized Tensilon that could perform tension-elongation to stress-strain conversions.

A2. Inhomogeneity in Leaflet Material Properties

The results, shown in figures 20 to 23 as spatially distributed stress-strain curves, clearly illustrate the marked inhomogeneity and directional orthotropy in the leaflets' material properties. Also, each of the tested strips and their individual sub-sections demonstrate the two-phase

FIGURE 19.
EFFECT of STORAGE TIME on TRANSITION STRAIN

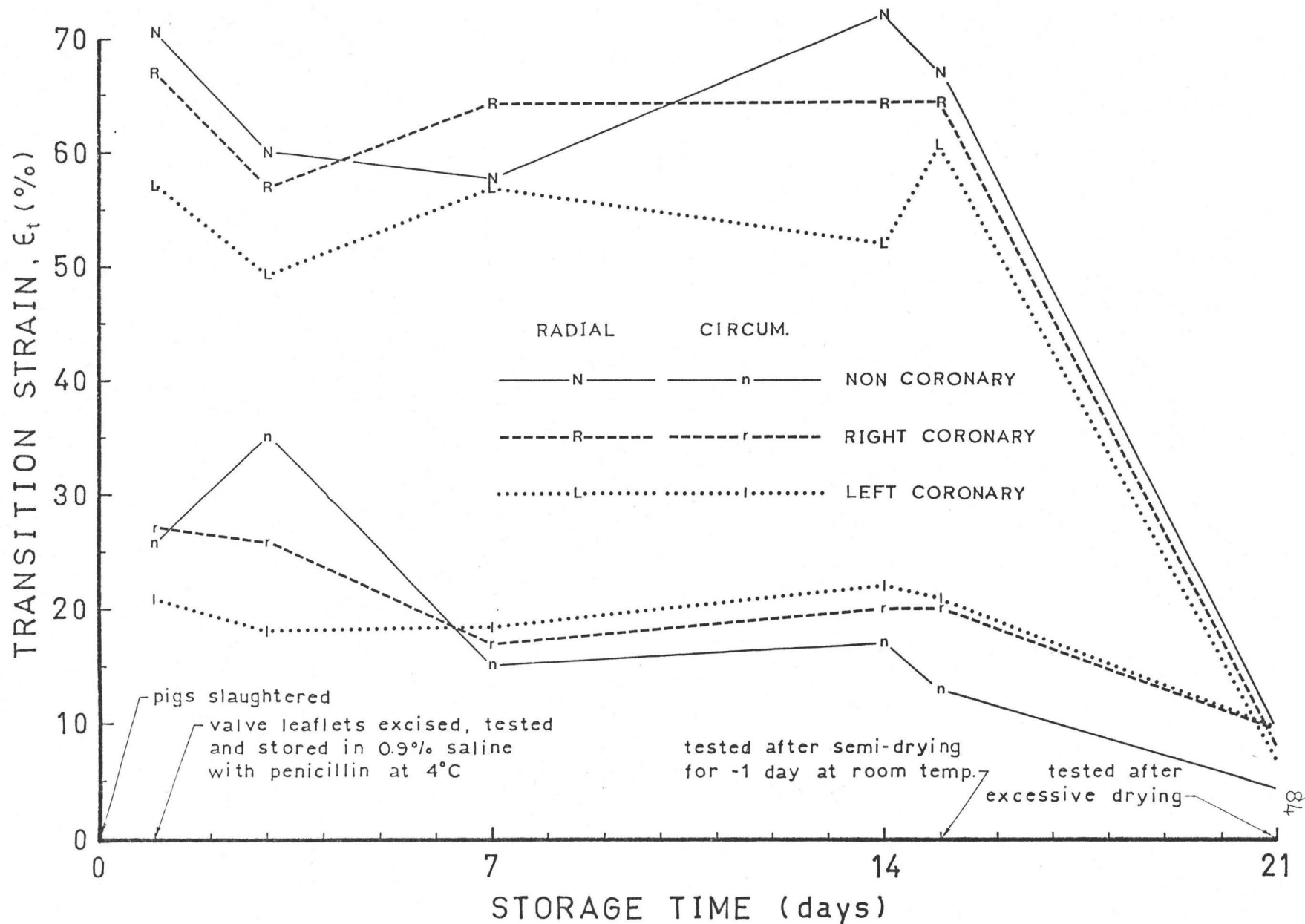
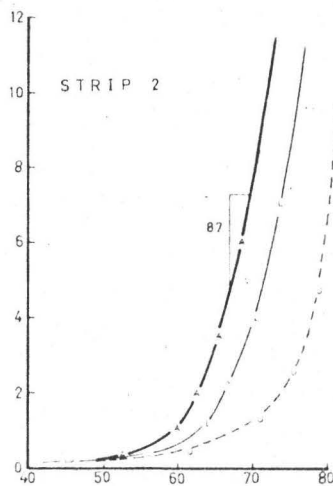
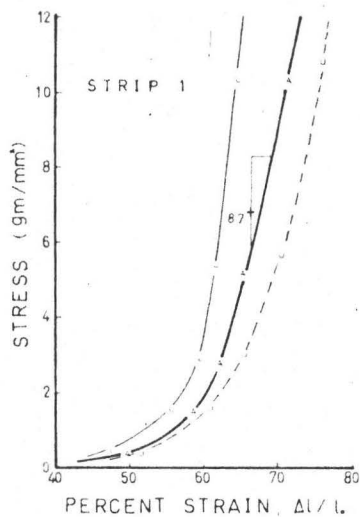


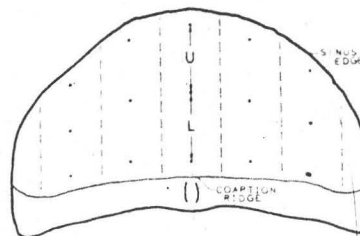
FIGURE 20. RADIAL STRESS-STRAIN CURVES
 for a PORCINE AORTIC VALVE
 NON-CORONARY LEAFLET
 at DIFFERENT POSITIONS

* POST TRANSITION ELASTIC MODULI in gm/mm²



NON-CORONARY LEAFLET STRIPS
 IDENTIFICATION as viewed
 from the VENTRICULAR SIDE

STRIP 1	STRIP 2	STRIP 3	STRIP 4	STRIP 5
---------	---------	---------	---------	---------



A: CURVE for TOTAL STRIP
 U, L: CURVES for STRIP SECTIONS

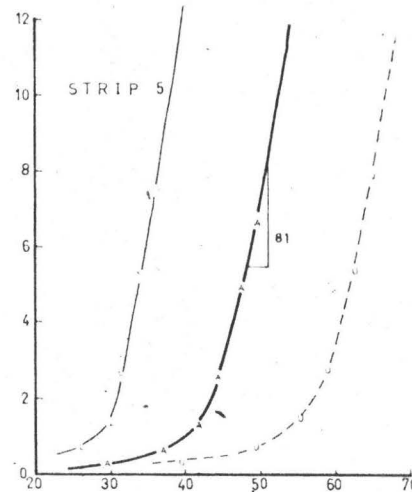
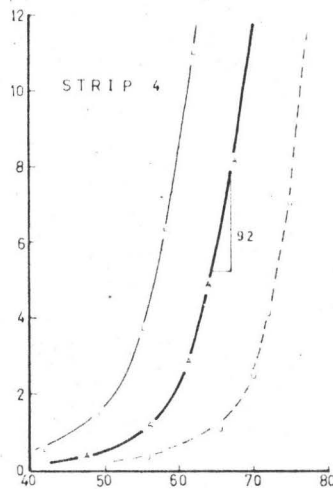
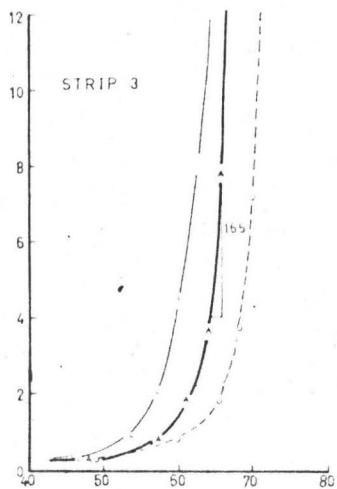
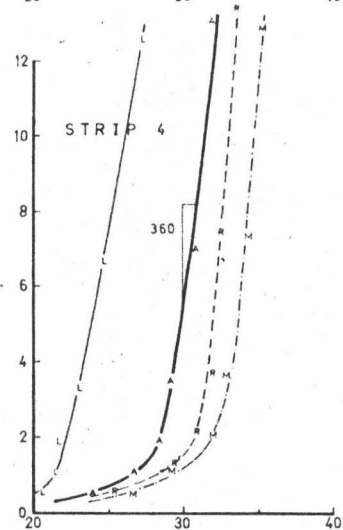
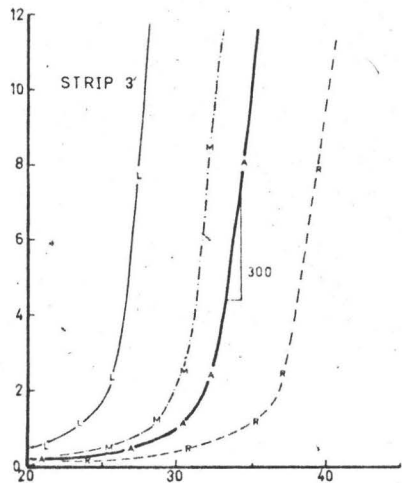
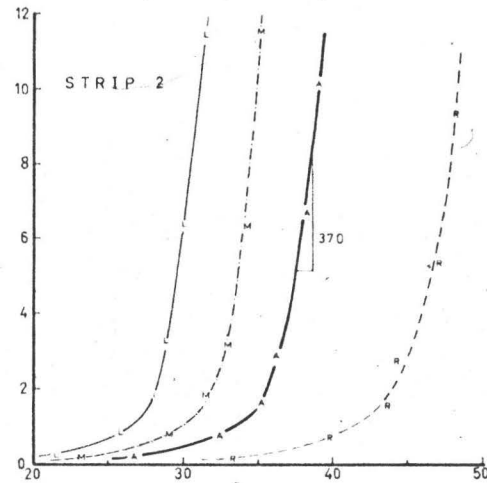
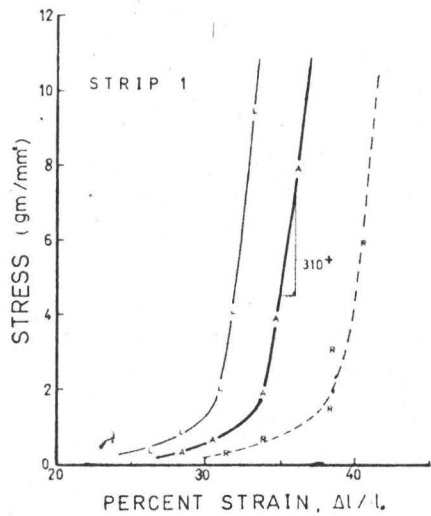
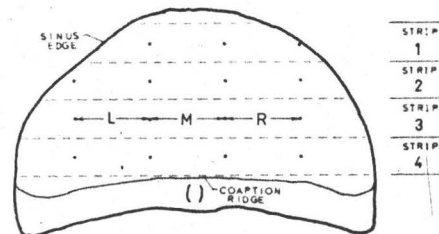


FIGURE 21. CIRCUMFERENTIAL STRESS-STRAIN CURVES
 for a PORCINE AORTIC VALVE
 NON-CORONARY LEAFLET
 at DIFFERENT POSITIONS * POST TRANSITION ELASTIC MODULI in gm/mm²



NON-CORONARY LEAFLET STRIPS
 IDENTIFICATION as viewed
 from the VENTRICULAR SIDE



A: CURVE for TOTAL STRIP
 LMR: CURVES for STRIP SECTIONS

FIGURE 22.
 COMPARISON of STRESS-STRAIN CURVES
 of SIMILARLY POSITIONED RADIAL
 STRIPS from the THREE LEAFLETS
 of a PORCINE AORTIC VALVE

* POST TRANSITION ELASTIC MODULI in gm/mm²

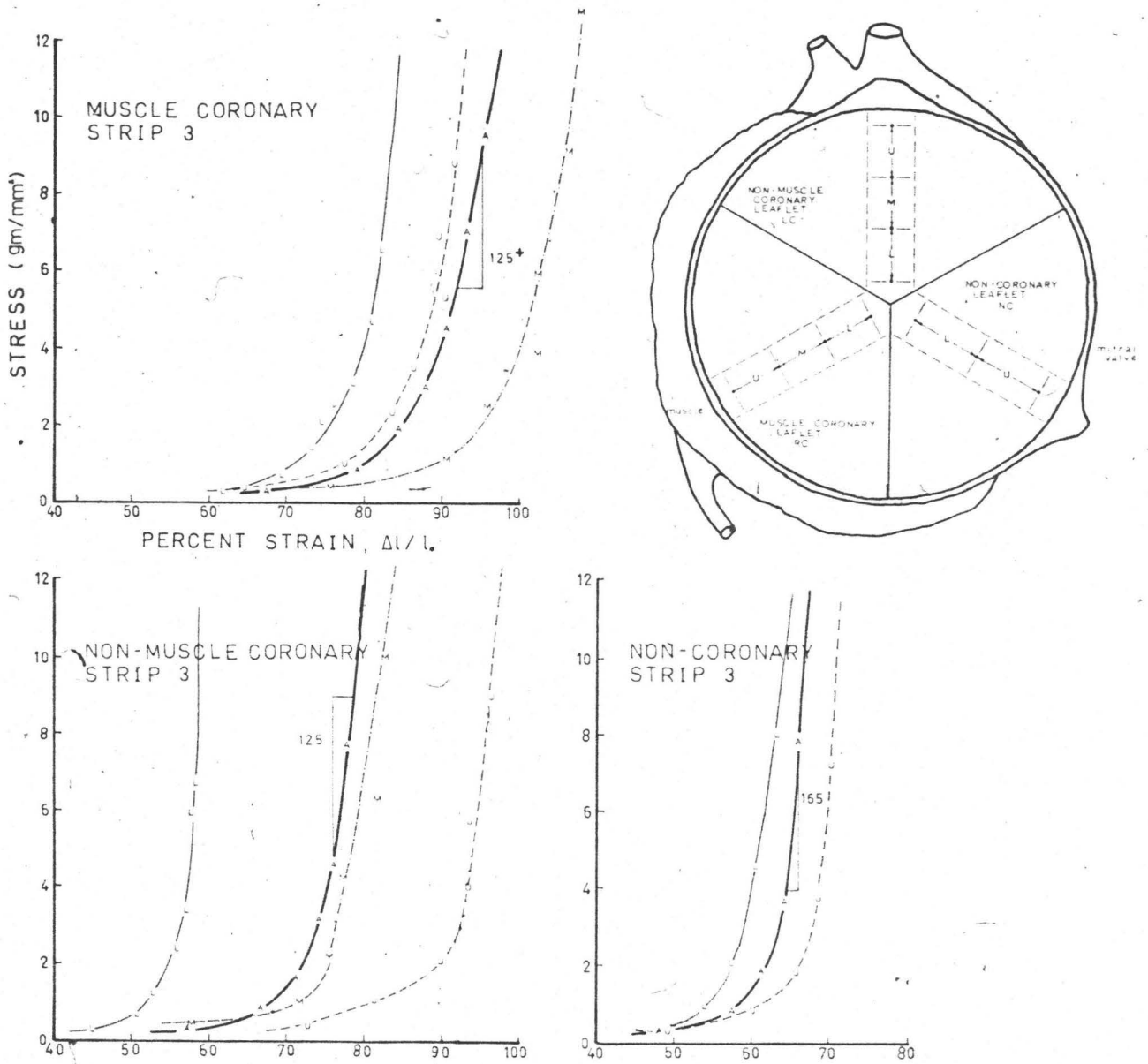


FIGURE 23.
 COMPARISON of STRESS-STRAIN CURVES
 of SIMILARLY POSITIONED CIRCUMFERENTIAL
 STRIPS from the THREE LEAFLETS
 of a PORCINE AORTIC VALVE * POST TRANSITION ELASTIC MODULI in gm/mm²

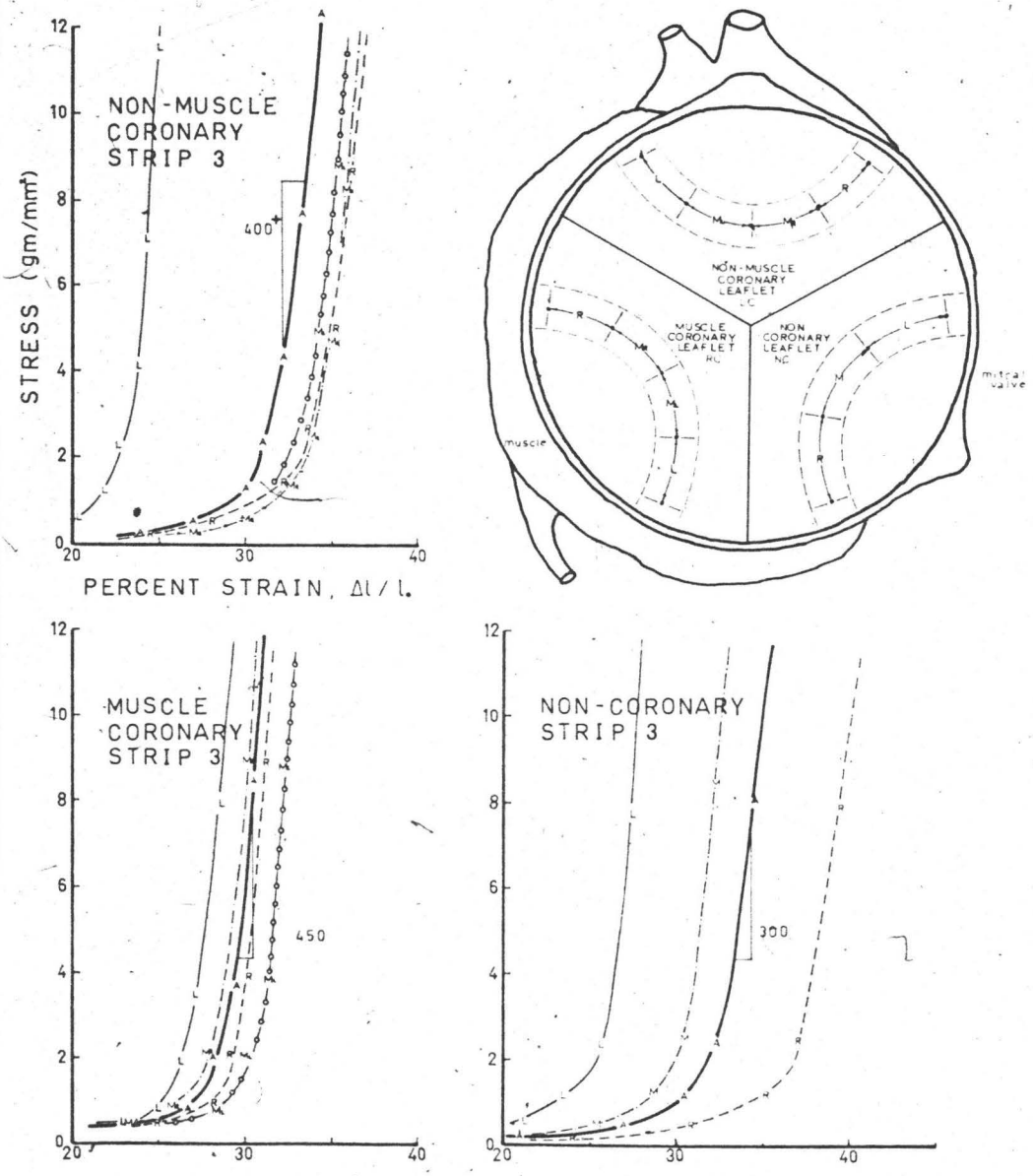


FIGURE 24.

DISTRIBUTION of POST-TRANSITIONAL ELASTIC MODULI in the RADIAL DIRECTION for the NON-CORONARY LEAFLET of a PORCINE AORTIC VALVE (units in $9m/mm^2$)

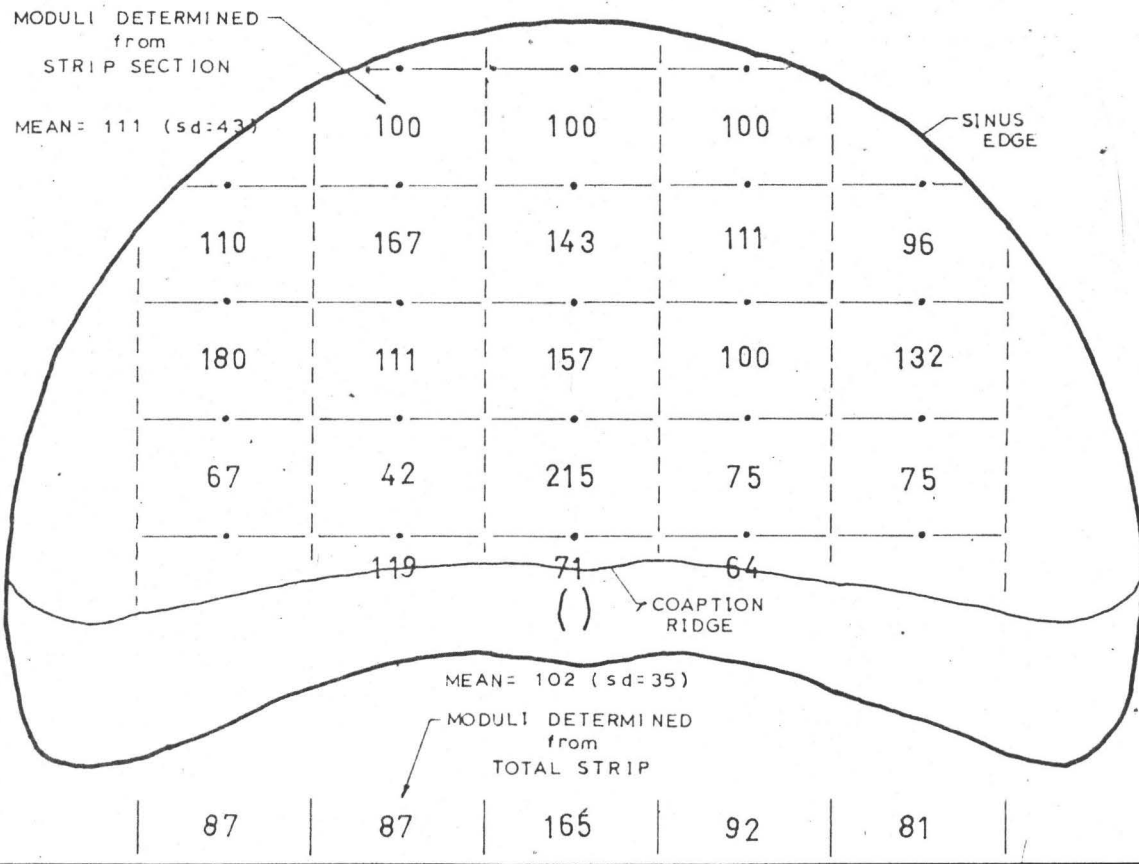


FIGURE 25.

DISTRIBUTION of POST-TRANSITIONAL ELASTIC MODULI in the CIRCUMFERENTIAL DIRECTION for the NON-CORONARY LEAFLET of a PORCINE AORTIC VALVE (units in gm/mm²)

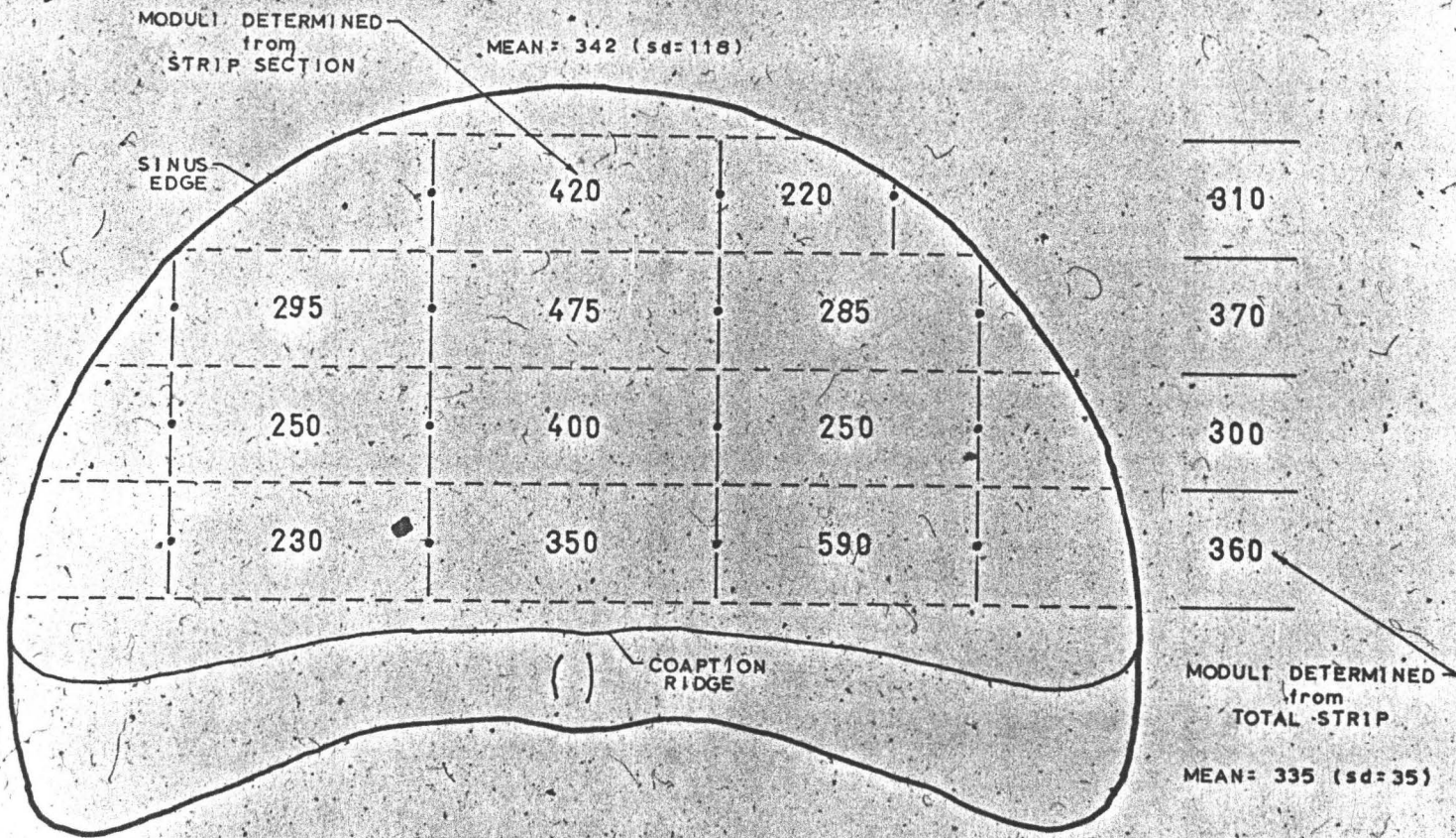
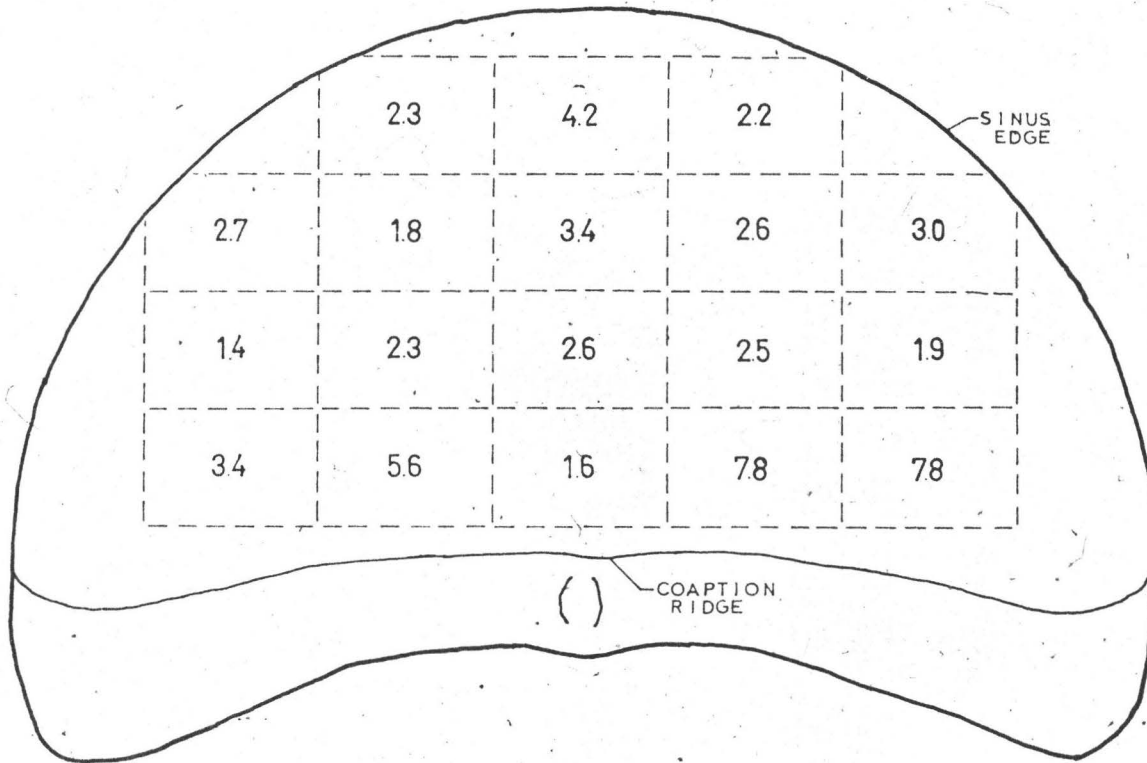


FIGURE 26.

VARIATION of ELASTIC MODULI RATIO (E_{CIRC}/E_{RAD}) for the
NON-CORONARY LEAFLET of a PORCINE AORTIC VALVE

MEAN RATIO = 33 (sd=1.9, se=.05)



non-linear stress-strain response characteristic of all biological material [Yamada, 1973].

The inhomogeneity is obvious from the results for the NC leaflet (figures 20 and 21). Wide variations in post-transition elastic moduli, E_{post}^* , and transition strains, ϵ_{tran}^* , are evident from strip to strip and from sub-section to sub-section for each strip. This is observed for both the radial and circumferential directions. Figures 24 to 26 show a wide variation for the NC leaflet in the spatial distribution of post-transition moduli and modulus ratio in both the radial and circumferential directions. Similar inhomogeneity may also be expected for the pre-transition modulus, E_{pre}^* . As expected, the post-transition moduli are much larger than the pre-transition moduli. Typically, the pre-transition moduli for either directions are less than 1.5 gm/mm^2 .

Inhomogeneity between leaflets of the same valve is illustrated in figures 22 and 23. Comparison of stress-strain curves for similarly positioned strips for both the radial and circumferential directions show distinct differences in the post-transition moduli and transition strains.

Radial Moduli and Strains

Radially, it appears that the stiffest region of the NC leaflet is the middle strip (eg., middle $E_R = 165 \text{ gm/mm}^2$

* These terms are defined and described in Appendix A.

as opposed to a mean of $E_R = 88 \text{ gm/mm}^2$ for the other four adjacent radial strips).^{*} Affeld (1973) reported a similar relationship for bovine pulmonic valve leaflets (ie., middle $E_R = 263 \text{ gm/mm}^2$ and side $E_R = 165 \text{ gm/mm}^2$). However, Missirlis (1973) observed the reverse for human aortic valve leaflets; that is, the smaller E_R is in the middle of the leaflet.

A closer examination of the results would reveal that the middle strip of the NC leaflet is stiffest near the coaptation edge ($E_R = 215 \text{ gm/mm}^2$) and becomes less stiff toward the sinus edge ($E_R = 100 \text{ gm/mm}^2$). In contrast, Affeld (1973) found no appreciable variation. The decrease in E_R from the coaptation to the sinus region is also observed in the LC and RC leaflets of the porcine valve; however, the NC leaflet is on the average stiffer in the radial direction than the other two leaflets (eg., NC $E_R = 165 \text{ gm/mm}^2$ whereas LC and RC $E_R = 125 \text{ gm/mm}^2$).

Transition strains for the NC leaflet's five radial strips are relatively constant; respectively for strips 1 to 5, they are 60%, 62%, 63%, 60% and 45%. Therefore, the mean radial transition strain for the NC leaflet is $\overline{\epsilon}_{tR} = 58\%$ (s.d. = 7%). Sectionally, the transition strains range from 30% to 70%.

There is also a distinct trend for the leaflet

^{*} Unless otherwise indicated, E_R is the post-transition modulus in the radial direction. Similarly, E_C is the post-transition modulus in the circumferential direction.

section near the coaptation edge to reach transition well before the section near the sinus edge. However, different regions of the leaflet and different leaflets exhibit this behaviour to varying degree. This is readily shown in the radial stress-strain curves (figures 20 and 22). Perhaps, the above property is important to the natural valve design. For example, valve opening and closing delays are minimal if the coaptation edge exhibits early (ie., smaller) transition strains; and the support of the whole valve structure is best accomplished with sinus region tissue possessing late (ie., larger) transition strains. Delayed transition implies increased extensibility which helps to reduce radii of curvature and hence also systolic bending stresses. Furthermore, the high stiffness and small transition strains observed in the region adjacent to the Node of Aranti are possibly functional in providing firm mutual coaptation at the nodes, as well as in reducing the bending stresses in this highly-curvated region of the leaflets.

The early transition strains of coaptation edge tissue and the late transition strains of sinus edge tissue are also consistent with Greep's (1966) and Clark and Finke's (1974) histology of the human aortic valve leaflets. The latter noted that the number and diameter of the stiffer collagen fibres become more and larger toward the coaptation edge. The former observed that the more extensible elastin is concentrated at the leaflet's sinus edge and is minimal

at the coaptation edge where the collagen proportion is greater. Clark and Finke (1974) also reported a progressive decrease in the thickness of a stressed human aortic valve leaflet from the coaptation to the sinus edge. Thus, Lim and Boughner's (1975) statement that increasing cross-sectional area (hence, also increasing thickness) delays the transition strain and reduces the final post-transition elastic modulus is apparently consistent with our findings.

Functional application might also explain the larger overall transition strains in the RC leaflet's middle strip (eg., RC $\epsilon_{tR} = 90\%$; LC $\epsilon_{tR} = 70\%$; NC $\epsilon_{tR} = 63\%$). A conjecture is that the myocardial support of the RC leaflet enables the leaflet tissue to delay its transition into the high stress region by absorbing the transferred diastolic load. However, a more plausible explanation is that the collagen content at the sinus edge is least in the RC leaflet. Collagen exhibits smaller transition strains than elastin.

Circumferential Moduli and Strains

Circumferentially, the NC leaflet shows fewer trends. One is the observation that the stiffest region of each circumferential strip is the middle (figure 25), and another is that the left side of the leaflet adjacent to the LC leaflet reveals a consistently smaller transition strain (figure 22). The first observation reflects the concentration of the stiff circumferential collagen fibre bundles in the said region.

The latter might reflect the lack of myocardial support on the LC side of the NC leaflet; for example, support in this region consists mainly of tougher and stiffer cartilage-like annulus.

The circumferential post-transition moduli determined for each total strip are relatively constant. However, the modulus for the strip adjacent to the free coaptation edge ($E_C = 360 \text{ gm/mm}^2$) is slightly greater than the sinus edge counterpart ($E_C = 310 \text{ gm/mm}^2$). Missirlis' (1973) results for human aortic leaflets are similar. Affeld's (1973) data for bovine pulmonic valves also agree but are more dramatic (eg., coaptation $E_C = 1030 \text{ gm/mm}^2$; sinus $E_C = 260 \text{ gm/mm}^2$). Again, these results are consistent with Clark and Finke's (1974) histological findings on human aortic leaflets.

Whereas the NC leaflet is stiffer in the radial direction than the other two leaflets, it is the least stiff in the circumferential direction (eg., NC $E_C = 300 \text{ gm/mm}^2$; RC $E_C = 450 \text{ gm/mm}^2$; LC $E_C = 400 \text{ gm/mm}^2$). However, the importance of the above to the functional operation of the valve leaflets is not exactly clear.

Transition strains for the NC leaflet's circumferential strips are also relatively constant; respectively for strips 1 to 4 as shown in figure 22, they are 34%, 37%, 32% and 29%. The mean is $\overline{\epsilon}_{tC} = 33\%$ (s.d. = 3%). The observation of increasing circumferential transition strains from the coaptation edge (ie., strip 4) to the sinus edge is again

consistent with Clark and Finke's (1974) histological observations. Sectionally, the circumferential transition strains for the NC leaflet range from 22% to 47%.

Apparently, there are less variations in transition strains and post-transition elastic moduli between leaflets as well as between different regions of the same leaflet in the circumferential direction than in the radial direction. Perhaps this is suggestive of a greater inhomogeneity factor in the radial orientation.

A3. Anisotropy in Leaflet Material Properties

The anisotropy, orthotropy being assumed, of the leaflets' mechanical characteristics is evident from figures 24 to 26. All of the NC leaflet's radial strips and their individual sub-sections exhibit smaller post-transition moduli than their circumferential counterparts. The E_C/E_R ratio ranges from 1.4 to 7.8 with a mean of 3.3 (s.d. = 1.9). The latter agrees very well with results for human aortic leaflets [Armeniades et al, 1973; Clark, 1973; Missirlis, 1973]. And although the circumferential and radial post-transition moduli are derived from two different NC leaflets, the wide range in the modulus ratio does nevertheless illustrate the inhomogeneity in the leaflet material properties.

Transition strains in the radial direction are on the average greater. Based on the data obtained from the five radial strips and the four circumferential strips of the NC

leaflet, the mean radial and circumferential strains are:

$$\overline{\epsilon}_{tR} = 58\% \text{ (s.d. = 7\%)}; \overline{\epsilon}_{tC} = 33\% \text{ (s.d. = 3\%)}.$$

The basis of the mechanical orthotropy is a direct consequence of the directional differentiation between the collagen and elastin fibres of the leaflet tissue. Collagen fibres, which are characteristically stiffer and show early transition strains, are predominantly circumferential. In contrast, the elastin fibres, which are characteristically pre-transitionally extensible, are interwoven with the circumferential collagen fibres either in parallel or obliquely.

A4. Comparison with Other Microtensile Data

Since porcine valves were used for our experiments, comparisons with data obtained from similar microtensile tests using human valves should be carefully undertaken. The porcine and human aortic valves are similar but there are notable differences.⁶ These differences could reflect differences observed in other microtensile data.

On the basis of the porcine valves tested, it appears that porcine leaflet tissue possesses less stiffness and a longer pre-transition stage than human leaflet tissue. This would suggest that porcine valve tissue in comparison to human valve tissue, has a larger elastin content and is different in the collagen fibre cross-linking. Comparisons with

⁶ The differences have been previously discussed; see p. 11.

Clark's (1973), Missirlis' (1973) and Wright and Ng's (1974) microtensile data on human valve tissue are summarized in figure 27 and table 3. Since it has already been established that the stress-strain response is dependent on various experimental parameters (eg., strain rate, sample size and tissue preparation)*, the comparisons should be interpreted considering also the differences of the methods employed.

The larger transition strains for the porcine valve tissue as compared to the human tissue is an interesting result. Originally thought suspect since the strains of the two valve types were expected to be comparable, the stress-strain data were rechecked by testing several other typical porcine valves which were prepared and stored similarly as for the experimental valves. A sampling of ten radial strips and ten circumferential strips gave the following results: $50\% \leq \epsilon_{tR} \leq 85\%$ with a mean of $\overline{\epsilon_{tR}} = 67\%$ (s.d. = 10%) and $18\% \leq \epsilon_{tC} \leq 45\%$ with a mean of $\overline{\epsilon_{tC}} = 30\%$ (s.d. = 10%).⁺

The only information found in the available literature reporting data on tensile studies on porcine aortic valve leaflets is given by Litwak et al (1972) and Robel (1972)[±]. Comparative results are shown in table 3. There is an agreement with Robel's value for ϵ_{tC} which he reported

* see Effects of Experimental Parameters, p. 80.

⁺ Sampling of transition strains consisted of the following:
radial: 50%, 57%, 60%, 65%, 65%, 67%, 70%, 71%, 80%, 85%.
circum: 18%, 21%, 23%, 26%, 26%, 27%, 30%, 43%, 45%, 45%.

[±] see Addendum for additional comparative data, p. 144.

FIGURE 27.
COMPARISON of STRESS-STRAIN CURVES

of AORTIC VALVE TISSUE

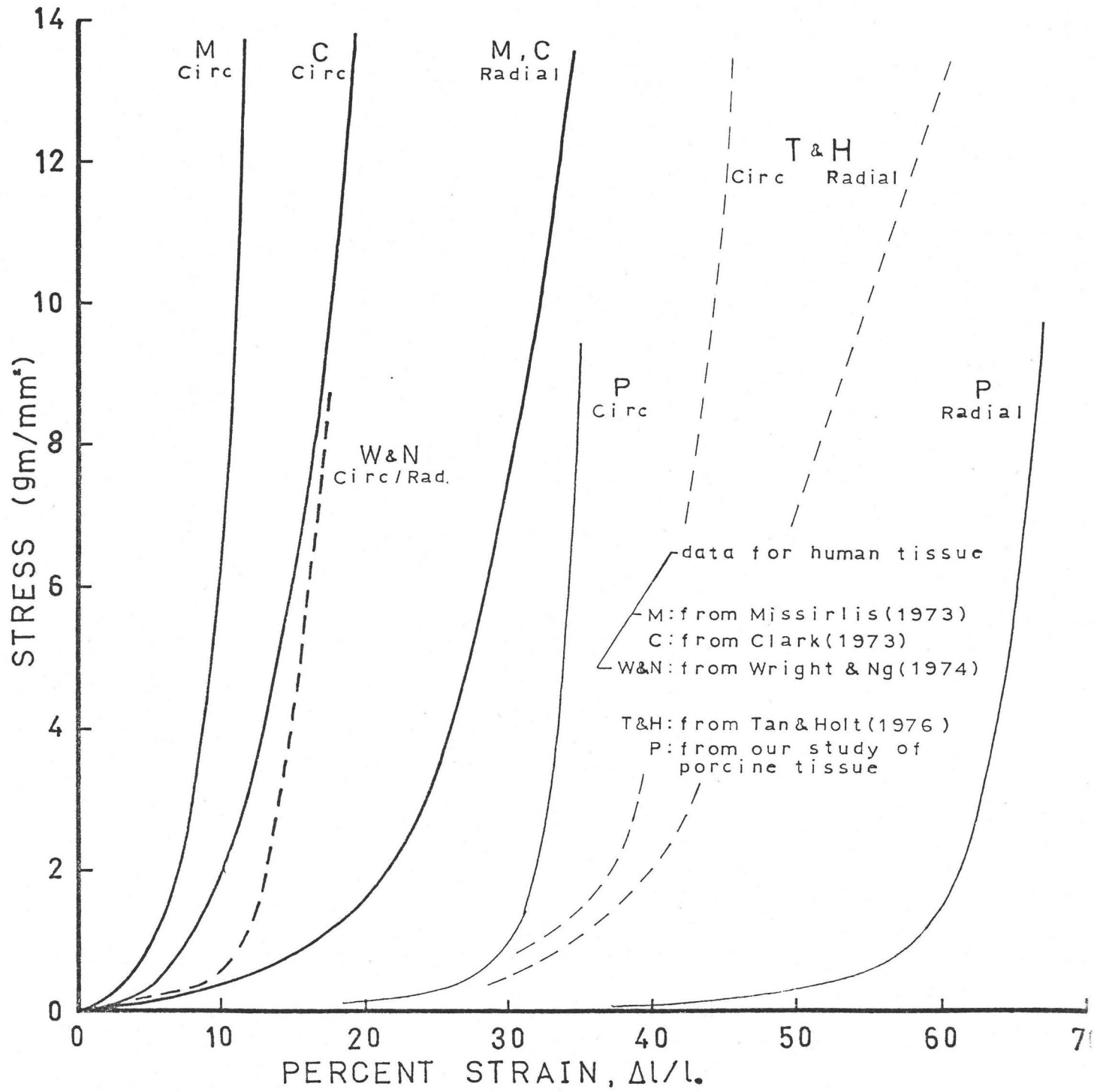


TABLE 3. COMPARISON OF MICROTENSILE STRESS-STRAIN DATA

	Strain Rate (%/min)	E_{CIR} (gm/mm ²)	E_{RAD} (gm/mm ²)	E_{CIR}/E_{RAD} (-)	ϵ_{tR} (%)	ϵ_{tC} (%)	$\epsilon_{tR}/\epsilon_{tC}$ (-)
Clark	8-13	598 ± 301	174 ± 70	3.4 ± 3.1	13 ± 6	24 ± 8	1.9 ± 1.5
Missirlis	20-100	723 , 35	232 , 14	3.1 , 0.3	11 ± 2	28 ± 2	2.5 ± 0.6
Yamada	-	14000 ± 1000	810 ± 50	17 ± 3	10 ± 1	18 ± 1	1.8 ± 0.3
Wright and Ng	130-160	165 ± 15	-	-	13 ± 2	-	-
Litwak et al	-	240 ± 20	-	-	-	-	-
Robel	-	5000 ± 1000	-	-	30 ± 5	-	-
Tan and Holt	10-15	944 , 147	233 , 110	4.0 , 1.5	51 , 14	39 , 5	1.3 , 0.3
Chong	15-45	342 , 113	111 , 42	3.3 , 0.4	58 , 7	33 , 3	1.8 , 0.4

Clark's (1973) data are reproduced from his table; standard errors are based on N = 50. Missirlis' (1973) elastic moduli data are reproduced from his table; standard deviations are based on 20 radial samples and 28 circumferential samples. Transition strains are extrapolated from reported typical stress-strain curves for human aortic leaflets. Yamada's (1973) data are extrapolated from reported typical stress-strain curves for human aortic leaflets; results for post-transition elastic moduli seem large. Wright and Ng's (1974) data are extrapolated from a reported typical curve. There are no designation as to fibre orientation since a pressure-volume technique was used. The latter tests total aortic cusps non-destructively unlike the microtensile method. Litwak et al's (1972) data is derived from a reported typical stress-strain curve for a porcine aortic leaflet. The transition region of the curve is however not shown. Robel's (1972) data are extrapolated from a reported typical stress-strain curve for a porcine aortic leaflet. The experimental method used is not described. Tan and Holt's (1976) data are extrapolated from 4 radial and 4 circumferential stress-strain curves obtained from porcine aortic leaflets. Chong's (1977) data are results determined from our experiments on porcine aortic valve leaflets. Elastic modulus data are based on averaging 11 different circumferential areas of a NC leaflet and 23 different radial areas of another NC leaflet. Transition strain data are based on 5 circumferential and 4 radial strips from NC leaflets.

as approximately 30%. However, he also reported unusually large uniaxial stresses (eg., $\sim 100 \text{ gm/mm}^2$ at $\epsilon_C = 25\%$ as compared to $< 1 \text{ gm/mm}^2$ at $\epsilon_C = 25\%$ from our results). The post-transition circumferential modulus as determined from Robel's (1972) data is also large at 5000 gm/mm^2 . It is not exactly clear as to what experimental method was employed by Robel in recording tension and elongation. Data of Litwak et al (1972) on fresh porcine tissue do not differentiate the fibre orientation of the leaflet sample; and the transition region of his curves is not clearly delineated. However, the tissue is shown to withstand strains just above 100% with a final post-transition modulus of about 240 gm/mm^2 .

A5. Implications of Results

Employing one valve and one leaflet is sufficient to illustrate inhomogeneity and anisotropy since no variances due to different valves being used are introduced. However, a much wider sampling of valves is an absolute prerequisite for obtaining greater confidence in the absolute and relative magnitudes of elastic moduli and transition strains.

The inhomogeneous and anisotropic properties of the aortic leaflet tissue are undoubtedly important to the total valve functioning in-vivo. These properties, if shown to be consistent in more valves, must be considered when designing a trileaflet prosthesis - especially if the durability and efficiency of the natural valve is to be approached.

Modelling the mechanical characteristics of biological tissue with composite fibre biomaterials is certainly a realizable technology [Skeleton, 1974]. Clark et al (1974) has already reported a leaflet designed from a composite material that simulates the natural leaflet's non-linearity and anisotropy. It only remains for the inhomogeneity of the leaflet to be incorporated into the design. It is for the latter that data, such as those presented in this study, are considered necessary.

The current xenografts which are experiencing encouraging success are the stabilized glutaraldehyde-preserved porcine aortic valves [see Porcine Xenograft, p. 48]. As of yet, there has been no intensive work reported on the effect of glutaraldehyde on the stress-strain response of porcine aortic leaflet tissue or any other tissue. Strawich et al (1974) did however show that the glutaraldehyde treatment increases the tensile strength of fresh tissue by as much as $2\frac{1}{4}$ times. Litwak et al (1972) reported similar results. In addition, he observed that the final post-transition elastic modulus is also increased.

A speculation by this author is that glutaraldehyde besides stiffening the valve tissue also promotes earlier transition strains, especially in the circumferential direction. This conjecture, which is based on the theory of glutaraldehyde acting as a cross-linking agent for collagen [Cater, 1963; Carpentier et al, 1969], would then suggest

that the glutaraldehyde-treated porcine valves are rendered to be more "human-like". The effect of glutaraldehyde on stress-strain certainly warrants further investigations.

B. Whole Valve Experiments

B1. Comments on the Experimental Method

The experimental method used to investigate the porcine aortic valve leaflets' surface geometry is the culmination of a year of experience with various other methods and refinements. Some of these methods are described in Appendix E. The resulting method is a refined technique that incorporates features which are adapted from Karara's (1973,1975) and Missirlis' [1973; Armeniades et al, 1973] experiments.

Missirlis (1973) used a Polaroid camera coupled to a stereomicroscope to analyze the surface strains in a human aortic valve leaflet as defined by ink microdots which had been aspirated onto the leaflets. In essence, it was attempted to measure from photographs the changes in the straight-line distances between dots as the valve underwent pressure loading. The method has however several major limitations. One, the dots randomly aspirated onto the leaflets do not lend themselves to a systematic and flexible approach in analyzing the inhomogeneity and anisotropy in the leaflets. Two, the use of a Polaroid camera and stereomicroscope is suspect to

parallax errors. The latter become significant when the dots undergo changes in the object-to-lens distance.* Another limitation of Missirlis' (1973) method is the neglect of the effects due to curvatures and changes in curvature of the leaflet surface. For example, in choosing the dots suitable for photographing, the camera was positioned and focused on points which lie most closely to the plane perpendicular to the lens axis. Because of strains and curvature changes due to increased pressure, it is very possible that the valve bulges causing the dots under consideration to leave the plane of focus. The plane containing the dots is shifted so that the camera's angle of view with respect to this plane becomes changed. Tests performed on this author's apparatus indicated that a difference of 15° ⁺ in the angle of view for two points separated approximately by 2 mm. in the plane of focus, would result in discrepancies as high as 5% for length measurements. Furthermore, errors incurred by changes in magnification due to focus shifts are also possible. Strains which are calculated using the above method are therefore questionable.

Karara's (1975) stereophotogrammetric method of determining the three-dimensional coordinates of dots applied

* Parallax errors are discussed in Appendix B.

⁺ A 15° shift in the angle of view is not unlikely. In fact, it is quite conservative when large pressure increments, such as 0 to 120 mm. Hg., are used.

on silicone aortic molds eliminates the problems associated with randomized dots, curvature effects and parallax. However, the use of silicone molds poses some potential adverse consequences. Although the same valve may be used to provide a series of molds which presumably are representative of the progressive changes in the diastolic valve configuration at different molding pressures, the molds cannot be produced in one continuous loading cycle. Thus, such inconsistent conditioning of the valve prior to each molding step may lead to inconsistent valve geometry. And since each mold is individually loaded to its own loading pressure, Karara's (1975) method is unable to follow the displacement of a fixed point on the valve through a complete loading cycle. Furthermore, it is conceivable that the long curing process required for the silicone may alter the true surface geometry through tissue over-relaxation.

Our experimental method was devised to incorporate the best aspects of Missirlis' (1973) and Karara's (1975) techniques. A porcine aortic valve was prepared with a systematic circumferential-radial grid of India ink dots on each leaflet surface. Whereas Karara found a Rapidograph #00 pen (diameter = 0.1 mm.) to be satisfactory for the application of dots on the silicone molds' surfaces, the particularly moist condition of the valve leaflets prohibited the use of the pen for our purposes. Instead, an ordinary hair was found more suitable, but only after considerable painstaking hours

of practice. Initially, air was used to pressurize the valve but problems stemming from vibrations caused by bubbling air leaks via the coronaries necessitated changes. Besides being responsible for immeasurable pressure fluctuations ($\pm 3-4$ mm. Hg.), the vibrations also caused excessive movements of the valve which proved to be a nuisance for still photography. Hence, the final method employed a continuous flow of saline to pressurize the valve. The saline flow is more representative of the in-vivo environment, but it also helps to dampen the pressure fluctuations and stabilize the valve vibrations. The flow was small (~ 30 ml/min at 120 mm. Hg.); therefore, pressure corrections due to dynamic heads are negligible. The stereophotogrammetric method used to record the leaflets' surface geometry is described in Appendix B.

Recently, Thompson and Barratt-Boyes (1977) reported an attempt to measure strains in a glutaraldehyde-treated porcine aortic valve also by photographing dots applied on the valve leaflets. However, they abandoned the idea stating that the measurement errors, being in the same order as the strains, were too large.

Raw Data Measurements

Whereas Karara (1975) was able to use specialized stereophotogrammetric equipment to make the two-dimensional measurements from the negatives, we lacked such equipment and therefore decided to convert the negatives into slides.

The slides were then projected on a wall at $\sim 40x$ magnification. Measurements made in this manner were found to be extremely sensitive to slight movements of the projector and to the position of the slide in the projector. Difficulties were also encountered in positioning the projector so that all points on the slide are magnified at the same scale on the wall (ie., oblique projection problems). Maintaining scale constancy from slide to slide was another nuisance. The long painstaking hours spent measuring in the dark (eg., approximately 12,000 measurements), and the inability to permanently record pictures from which measurements may be made and rechecked more conveniently, added to the list of disadvantages of using slides.

The decision to develop prints from our negatives on 11" x 14" paper proved to be a satisfactory alternative. The tendency for the single weight photographic paper to buckle and curl during exposures was a source of concern. Fortunately, the problem was minor; scale constancy as determined from the final prints is accurate to 0.1 %. Of course, much of the aforementioned difficulties could have been eliminated by using a video-record system.

The diameters of the dots on the prints are approximately 1 to 1.5 mm. Since the magnification used is 8.7x, the hair is able to apply dots of diameters ~ 0.15 mm. The dots were then re-identified by finer dots with a Staedtler #00 pen. The raw data measurements are made using these

dots. The photograph measurement errors are in the order of ± 0.3 mm.; this corresponds approximately to ± 0.03 mm. actual scale. Errors in the scale calibration and in estimating the dots' centres would probably compound the latter to ± 0.04 mm. actual scale (see Appendix B).

Data Reduction and Computer Programs

Karara (1975) used a linear transformation matrix method to convert the stereo-measurements into the dots' three-dimensional coordinates. The method was assessed as being satisfactory. The standard deviations and medians of differences are respectively: x: 0.10 mm. and 0.08 mm.; y: 0.06 mm. and 0.02 mm.; z: 0.05 mm. and 0.02 mm. In comparison, the technique used in our experiments is estimated to produce errors in x and z of the order of ± 0.04 mm., and standard deviations and standard errors for y of the order of ± 0.15 mm. and ± 0.09 mm. respectively (see Appendix B).

The stereophotogrammetric theory described in the Appendix B is translated into a Fortran computer program named VALVE. The program calculates the (x,y,z) coordinates and employs them to further calculate the local strains and radii of curvature at each coordinate position. The program listing, its description, the means of processing and preparing the raw data for input, and a sample output is given in Appendix C. Appendix D outlines the theory from which the subprogram RAD was written to calculate radii of curvature.

Effects of Experimental Parameters

In regards to the relationship between the in-vitro observations and the in-vivo function of the valve, much of what was said for the microtensile experiments is also applicable to the whole valve experiments. However, the process of drying-dotting-rehydrating was perhaps more detrimental in the latter since the procedure lasted much longer. The valve often spent several hours out of cold storage.

Any distortion to the in-vivo state of the valve caused by trimming the myocardial support around the valve annulus is left much to conjecture. During diastole, the ventricular myocardium is relaxed, and therefore offers only passive support to the loaded valve. One might then reason that the amount of muscular support does not affect the valve's diastolic configuration but would be determinant to the systolic configuration. Unfortunately, no experiments were conducted to investigate the changes in strains in the leaflets as a result of excision of myocardial support.

During the experiment, central leakage through the valve was observed at about 80 mm. Hg. (see figure B8 in Appendix B). The insufficiency was also observed in several other fresh porcine valves tested as checks. It is suspected that the source of the insufficiency is due to the long loading period required for photographing (~10 minutes). Such an extended period may adversely affect the mechanism of coaptation of the leaflets. Indeed, when the same porcine valves

were subjected to rapid pulsatile loads, valve leakages were eliminated. The explanation lies in the observation that the extensibility of biological tissue varies inversely as the strain rate [Rigby et al, 1959; Abrahams, 1967; Lim and Boughner, 1975]. At large in-vivo strain rates, the leaflets are rendered more inextensible and thus are able to sustain the sudden diastolic load without experiencing large strains. Comparatively, the experimental in-vitro strain rate was essentially nil ($\sim 10\%/min$). The leaflet tissue becomes more extensible resulting in larger strains. The latter at the leaflets' coaptation surfaces causes a "peel back" effect that leads to leakage through the valve.

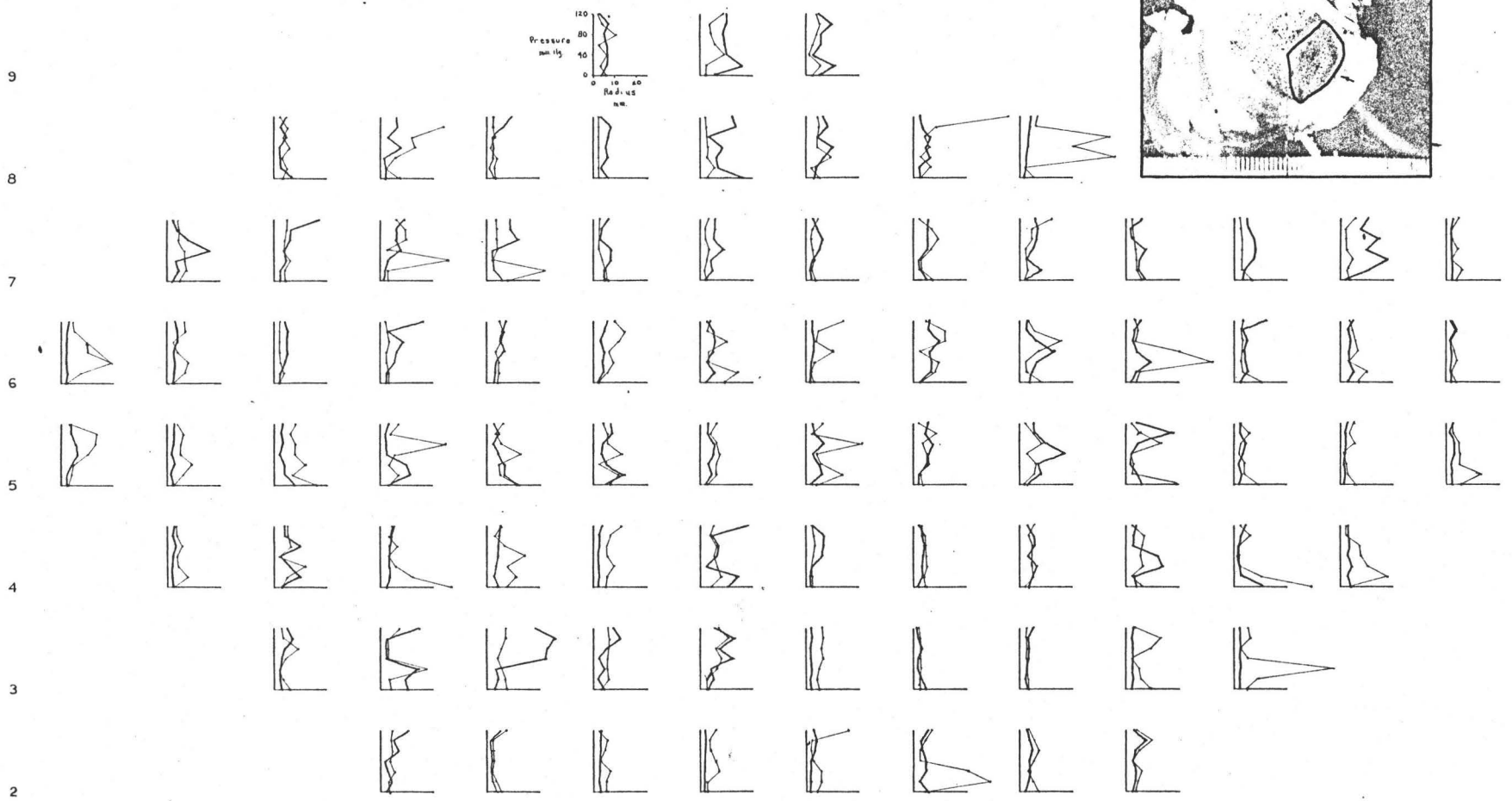
Employing a video-record system would obviously aid in improving the credibility of extrapolating near-static in-vitro results to the dynamic in-vivo situation. Nevertheless, results obtained from quasi-static experiments such as the whole valve experiments are valuable in helping to understand other aspects of the mechanics of valve leaflets; eg., leaflet fatigue and valve transition.

B2. Radii of Curvature

The local P - R (ie., pressure - radii of curvature) curves over the three leaflets of the valve are shown in figures 28 to 30. The curves show no discernible conclusion, and the rather rapid fluctuations in curvature from pressure to pressure are unlikely. Errors in the method of calculating

FIGURE 28. LOCAL PRESSURE-RADIUS CURVES for the NON CORONARY LEAFLET

— CIRCUMFERENTIAL RADII
— RADIAL RADII



9

8

7

6

5

4

3

2

2

3

4

5

6

7

8

9

10

11

12

13

14

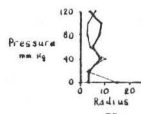
15



FIGURE 29. LOCAL PRESSURE-RADIUS CURVES for the LEFT CORONARY LEAFLET

— CIRCUMFERENTIAL RADII
— RADIAL RADII

*or NON MUSCLE CORONARY



2

3

4

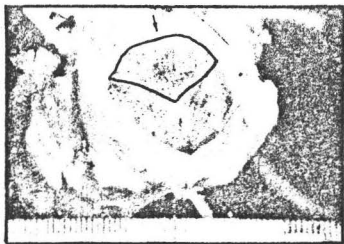
5

6

7

8

9



2

3

4

5

6

7

8

9

10

11

12

13

14

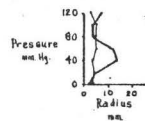
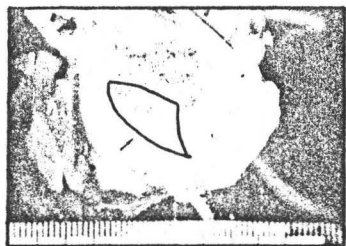
15

16

FIGURE 30. LOCAL PRESSURE-RADIUS CURVES for the RIGHT CORONARY LEAFLET

— CIRCUMFERENTIAL RADII
— RADIAL RADII

• of MUSCLE CORONARY

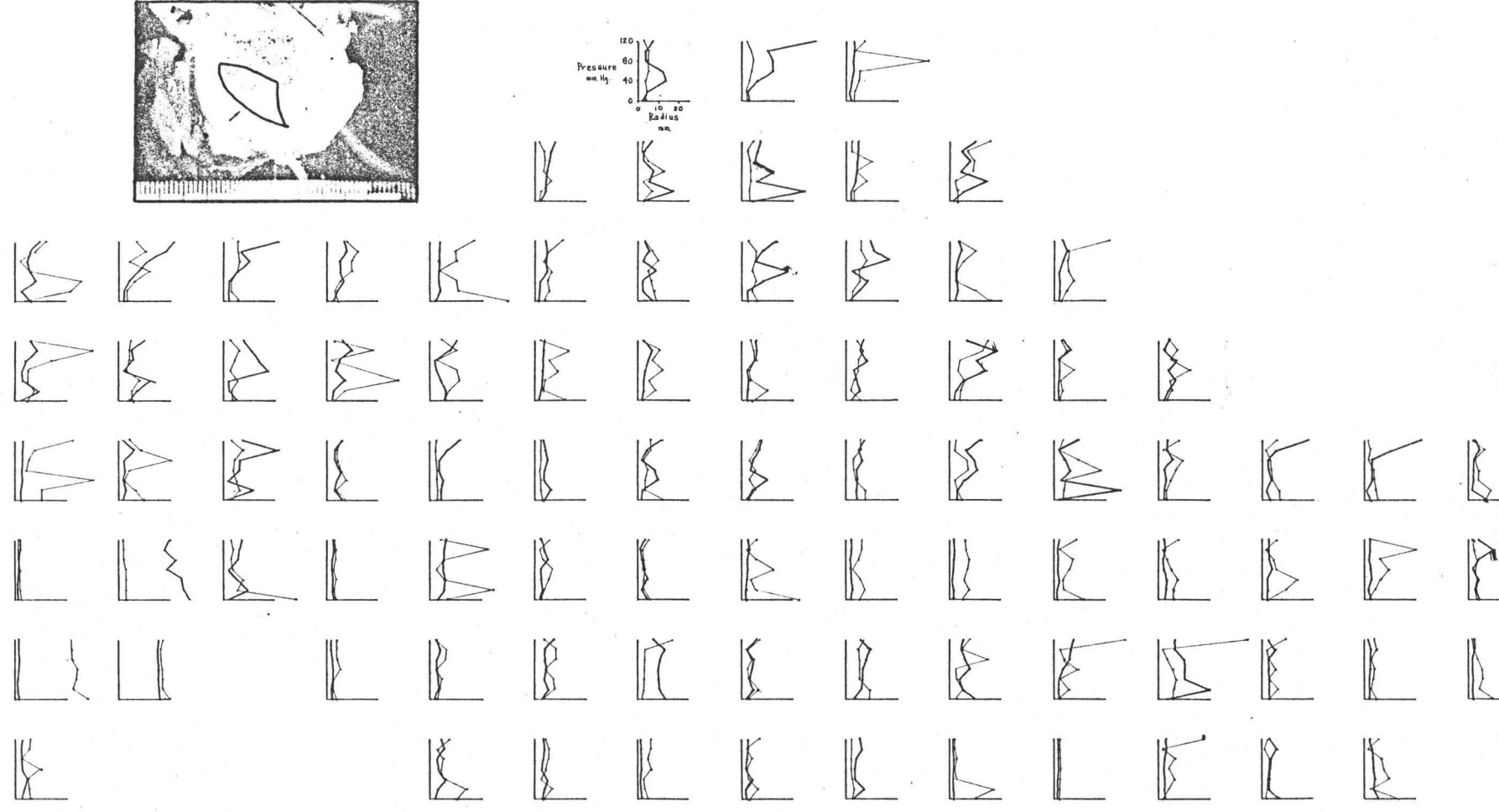


9
8
7
6
5
4
3
2

2 3 4 5 6 7 8 9 10 11 12 13 14 15 16 17



114



the radii are estimated to be 50% or more (see Appendix D). The errors and the insufficient mesh size of the grid of dots on the leaflets are the major reasons for the fluctuations in radii. Insufficient mesh size is explained in Appendix D.

The local radial and circumferential radii of curvature vary from 1 mm. to 4 cm. with the majority within the 5 to 10 mm. range. Cross-sectional profiles of human aortic valve molds illustrated in Karara's (1975) research suggest that the wide variation in radii may not be too unrealistic. Since the radii are determined from a curve connecting three consecutive dots which are spaced approximately at 1 mm., the 1 mm. radii are therefore theoretically impossible.

Originally, the radii calculations were required as inputs for a stress analysis that is based on a thin shell membrane surface of revolution [Timoshenko, 1959]. The radii are also useful in checking the validity of the thin membrane assumption (ie., thickness/radius ratio, $t/R \leq 0.1$), and the validity of interpreting the straight-line distance changes between dots as being representative of the curved surface strains (see Appendix B). However, the weak precision of the method prohibits these checks. But it is estimated that the straight-line approximation is valid to 1% for $R > 2$ mm., a criterion that is satisfied by a high majority of the valve leaflets.

The method as described in Appendix D does have one limitation; that is, it fails to consider the sense of the

curvatures (ie., negative or positive). However, it may be assumed by simple observation of the diastolic valve that the curvatures are all convex outward (ie., positive R).

Previous analyses have assumed approximate homogeneous and/or orthotropic radii of curvature for estimating the leaflet stresses. Assuming a cylindrical geometry Laplace law relationship (ie., $\sigma = PR/t$), Swanson and Clark (1973) estimated the maximum membrane stresses at $\sigma_{\max} = 27 \text{ gm/mm}^2$ for a human aortic valve at pressure $P = 100 \text{ mm. Hg.}$, thickness $t = 0.5 \text{ mm.}$, and radius $R = 10 \text{ mm.}$ Gould et al (1973) employed $R = 11.3 \text{ mm.}$ to estimate $\sigma_{\max} = 21 \text{ gm/mm}^2$ for a human valve with $P = 115 \text{ mm. Hg.}$ and $t = 0.4 \text{ mm.}$ Chong et al (1973) differentiated between the radial and circumferential radii. Using a range of $7.5 \text{ mm.} \leq R_R, R_C \leq 12.5 \text{ mm.}$, he found that the maximum radial and circumferential stresses are respectively 18 gm/mm^2 and 5 gm/mm^2 for a human valve at $P = 80 \text{ mm. Hg.}$ and $t = 0.5 \text{ mm.}$ And Missirlis (1973,1976) used $R = 10 \text{ mm.}$ to estimate $\sigma_{\max} = 16 \text{ gm/mm}^2$ for a human valve at $P = 120 \text{ mm. Hg.}$ and $t = 0.5 \text{ mm.}$ The consensus seems to be that the aortic valve leaflets' geometry cannot be truly described by a single homogeneous radius of curvature.

Robel (1972) is the only researcher to have reported radii data for porcine valves. He assumed a cylindrical geometry Laplace relationship and calculated $\sigma_{\max} = 100 \text{ gm/mm}^2$ for a porcine aortic valve at $P = 140 \text{ mm. Hg.}$, $t = 0.3 \text{ mm.}$ and $R = 16 \text{ mm.}$

B3. Pressure-Strain

Circumferential Strains

The local $P - \epsilon$ (ie., pressure - strain) curves over the three leaflets are shown in figures 31 to 33.

The circumferential strains in all three leaflets are small, even at the higher pressures corresponding to maximum diastole. On the average, the strains lie between 5% and 10%. Since the dots' three-dimensional coordinates are accurate to ± 0.05 mm. implying that straight-line dot-to-dot lengths can at best be accurate to ± 0.1 mm. (see Appendix B), the calculated circumferential strains, being determined over a 2 mm. to 2.5 mm. span of three consecutive dots, are in the same order as the errors. Therefore, the strains should be interpreted with caution. Thompson and Barratt-Boyes (1977) made this same conclusion from their studies of the leaflet strains in glutaraldehyde-treated porcine aortic valves.

Comparable circumferential strain data have been reported by Brewer et al (1976) and Missirlis [1973; Armeniades et al, 1973]. Brewer observed canine aortic valves' maximum circumferential strains corresponding to a full cardiac cycle to be about 16%. Under in-vivo conditions (ie., much higher strain rates), the strains are reduced to approximately 2% [Brewer et al, 1977]. Missirlis' $P - \epsilon_C$ data on human valves reported both positive and negative strains which are no larger than $\pm 2\%$ even at 160 mm. Hg. However, since Missirlis

FIGURE 31. LOCAL PRESSURE-STRAIN CURVES for the NON CORONARY LEAFLET

— CIRCUMFERENTIAL STRAINS
— RADIAL STRAINS

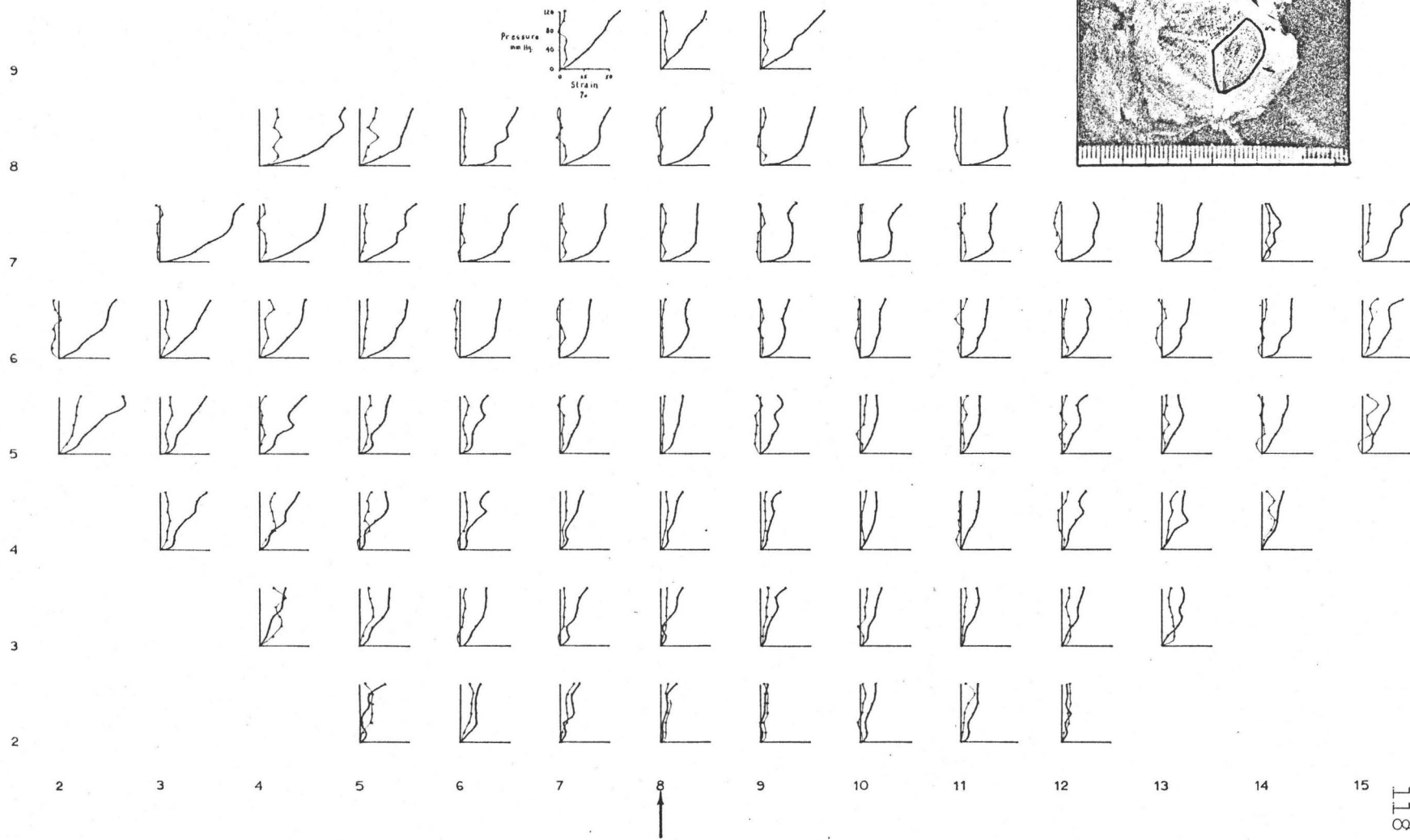
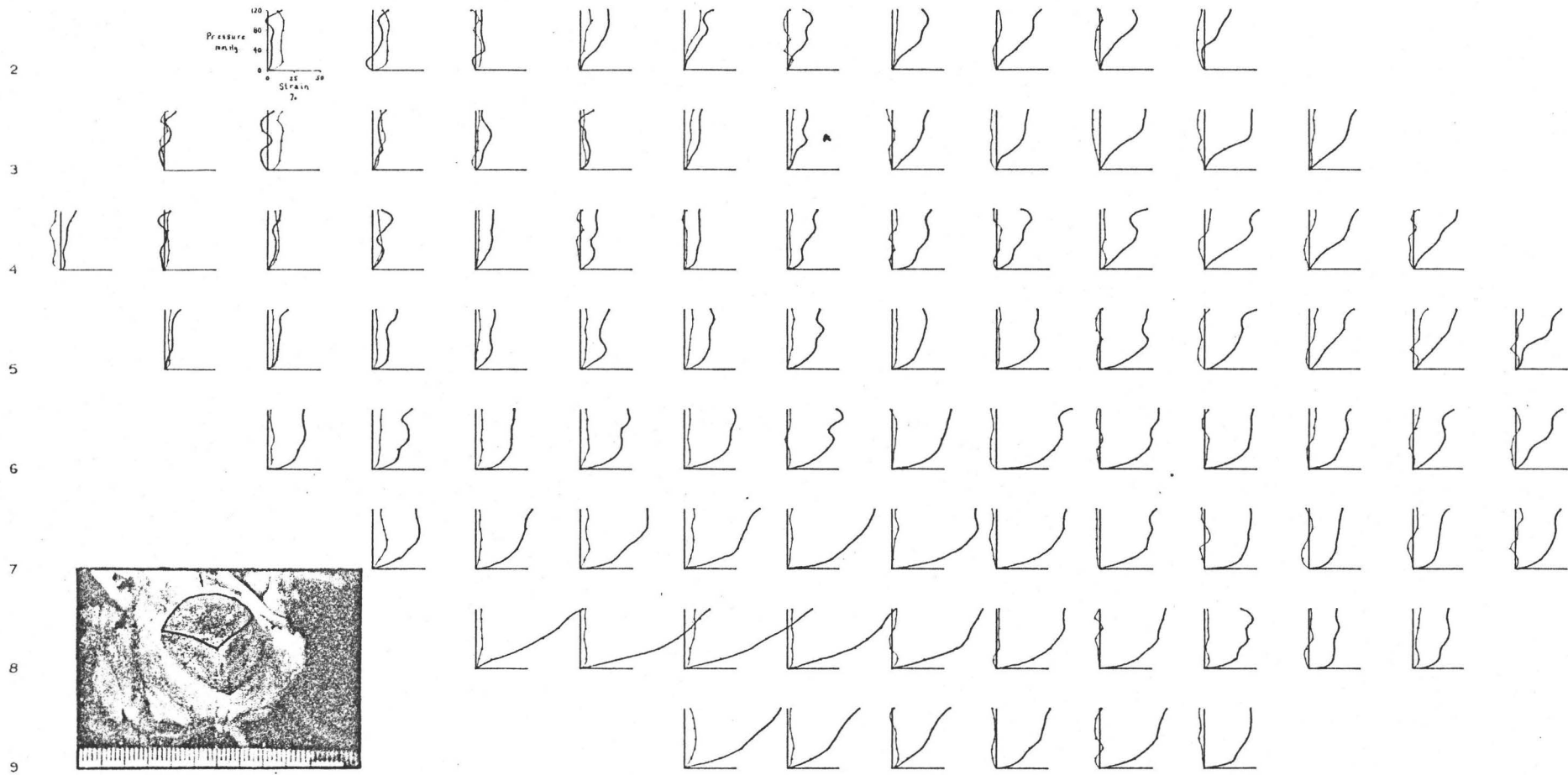


FIGURE 32. LOCAL PRESSURE-STRAIN CURVES for the LEFT CORONARY LEAFLET

— CIRCUMFERENTIAL STRAINS
— RADIAL STRAINS

*or NON MUSCLE CORONARY

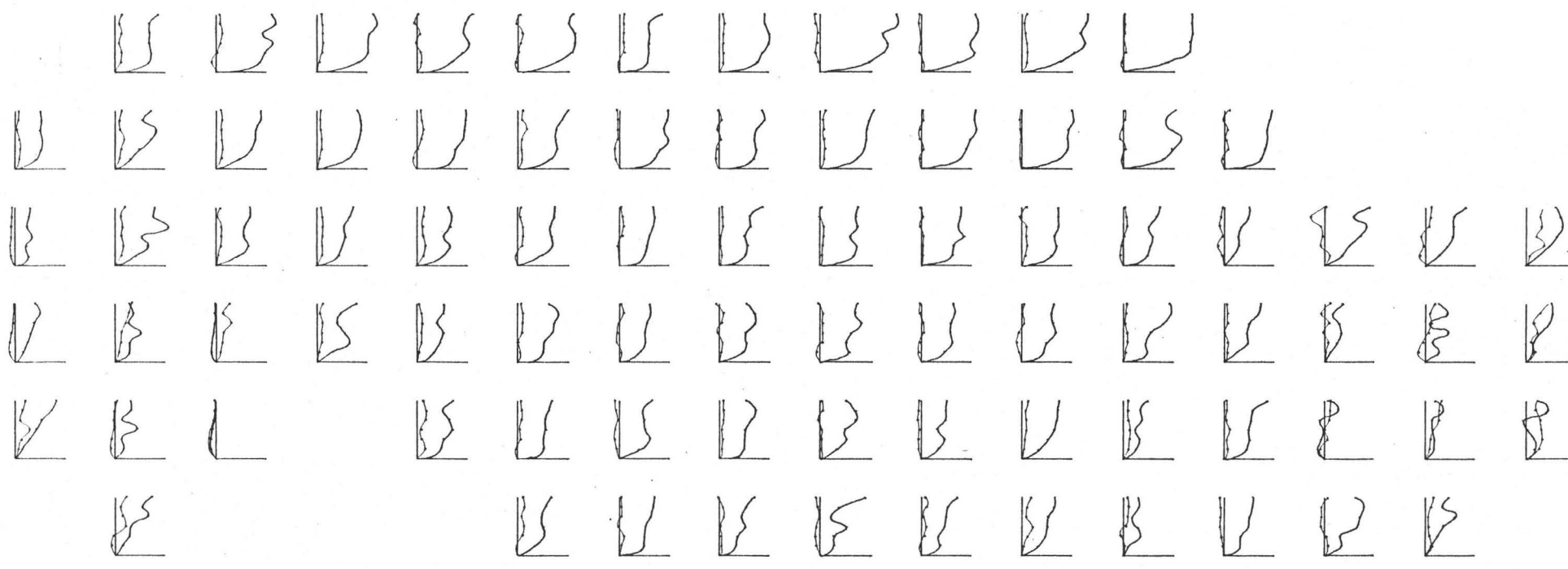
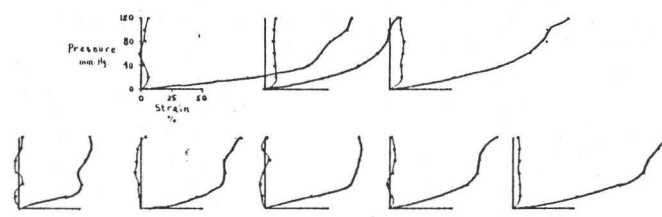
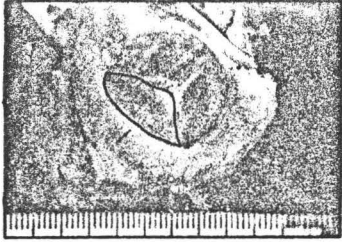


2 3 4 5 6 7 8 9 10 11 12 13 14 15 16

FIGURE 33. LOCAL PRESSURE-STRAIN CURVES for the RIGHT CORONARY LEAFLET

— CIRCUMFERENTIAL STRAINS
— RADIAL STRAINS

*or MUSCLE CORONARY



2 3 4 5 6 7 8 9 10 11 12 13 14 15 16 17

based the strains on a reference pressure of 38 mm. Hg. instead of the standard 0 mm. Hg., the true strains are indeterminate. And since it has already been established that the largest strain uptake ($\sim 10\%$) occurs during the first 15 mm. Hg. of transvalvular pressure [Mundth et al, 1971; Wright and Ng, 1974], it is likely that Missirlis' (1973) reported strains are underestimated.

The shapes of the $P - \epsilon_C$ curves show no distinct monotonic trends. In particular, the non-linear two-phase loading-deformation response of biological tissue is absent. Although erratic, the shapes of the curves do resemble those of Missirlis' [1973; Armeniades et al, 1973] curves.

For some points on the leaflets, negative circumferential strains (ie., compression) are observed. They occur randomly at different positions and at different pressures. Missirlis observed similar distension-compression behaviour for a RC leaflet [Armeniades et al, 1973; Missirlis, 1973].

Negative strains imply compressive stresses. Clark et al (1975) and Cataloglu et al (1976,1977) reported randomized areas of compressive stresses for the human aortic valve NC leaflet. The stresses were generally smaller than the tensile stresses and were observed for both the radial and circumferential directions. Our results show only negative circumferential strains. Cataloglu et al (1976,1977) reasoned that some compressive stresses near the coaptation region are plausible because of coaptation forces. However,

isolated compressive states in the middle of the leaflets are unlikely. Anomalies introduced by the silicone molding process and unsmoothed geometrical data were identified as possible explanations for the isolated compressive states. This is to be expected since the silicone molds are representative of the bumpy and undulating aortic surface of the leaflets. In comparison, our strains are calculated using geometrical data obtained from the smooth ventricular surface of the porcine valve leaflets. Similar circumferential compressive states are however still observed near the coaptation edge and at various isolated positions. Negative strains are also present in the LC leaflet's sinus-annulus region. With the exception of three points on the LC leaflet, all of the negative strains are circumferential.

Using three different hypothetical geometries for the aortic leaflet, Gould et al (1973) reported circumferential compression at the coaptation edge. Radial compression was observed in only one of the geometries (paraboloid of revolution). For the elliptical paraboloid geometry, Gould reported circumferential compression at the center of the leaflet nearer the coaptation edge. Our results for the NC and RC leaflets produced the same observation.

Radial Strains

In contrast to the circumferential strains, the radial strains are considerably much larger. If the valve

leaflet material properties were homogeneous, isotropic and linear according to Hooke's law (ie., $\sigma = E\epsilon$), then the observed strains would be sufficient to conclude that the radial stresses are larger than the circumferential stresses. However, since the microtensile experiments proved otherwise, the determination of the stress distribution in the leaflets requires a closer analysis.⁷

Furthermore, the shapes of the $P - \epsilon_R$ curves are more definitive than the $P - \epsilon_C$ curves. For much of each leaflet and noticeably in the middle, the $P - \epsilon_R$ curves are characteristically non-linear and two-phased, with transition into the stiff post-transition phase having occurred or beginning to do so by 20 mm. Hg. By 60 mm. Hg., these regions are into the post-transition phase for the radial direction. There exists a wide variation in the transition and post-transition strains from leaflet to leaflet as well as from region to region on the same leaflet. The nature of the transitions vary from being sharp (eg., nearer the sinus-annulus edges) to being gradual (eg., nearer the coaptation edges). These variations are probably due partly to the inhomogeneity of the leaflet material properties, and partly also to the dissimilar and asymmetrical support structures of the leaflets. In contrast, Wright and Ng (1974) and Ng and Wright (1975),

⁷ The analysis of the leaflet stresses is covered in Part II of this study [Chong, 1977]. The analysis incorporates data obtained from the microtensile and whole valve experiments.

using the pressure-volume technique, observed less variation in the transitions for human aortic leaflets. Transitions were found to occur at 25 to 30 mm. Hg., and 25% strain. Inhomogeneity and anisotropy were however not considered. Also, their results are independent of myocardial support effects.

The post-transition phase of the $P - \epsilon_R$ curves, being non-monotonic, do not resemble the linear post-transition phase of the stress-strain curves observed in the micro-tensile experiments. Many of the curves exhibit strains which first increase, then decrease and increase again with increasing pressure. Missirlis observed this same behaviour for the radial strains in the LC leaflet [Armeniades et al, 1973; Missirlis, 1973]. The non-monotonic behaviour is speculated to be either a result of a tissue relaxation process⁸ caused by the irregular and prolonged period of loading used in the experiment, or an effect of the leaflet support structure being non-rigid and viscoelastic.

Deviations from the non-linear two-phase response do exist in certain regions of the leaflets. At the coaptation edges, particularly toward the Node of Aranti, the $P - \epsilon_R$ curves exhibit more gradual transitions with a tendency to

⁸ In the relaxation process, a sample of tissue, that is simply supported by non-rigid supports and maintained at a constant load, will attempt to recover some of its deformation. This is a corollary of the stress-relaxation phenomena described by Abrahams (1967).

become linear and elastic. Near the sinus-annulus regions, the curves tend to show smaller strains without the appearance of any transitions, similar to Missirlis' (1973) curves for radial strains in a NC leaflet [Armeniades et al, 1973]. The behaviour may be interpreted as a reflection of the role of the annulus in offering support and in reducing stresses at the leaflet base attachment region. The annulus maintains the leaflet tissue in this region in its pre-transition low-strain and low-stress condition. The surrounding myocardium might also offer a similar effect; however, just how much of an effect would be difficult to assess.

At all pressures, the radial strains are smallest in the sinus-annulus regions. The strains also show a trend to increase toward the coaptation edges. Near the coaptation edges and especially in the area of the Nodes of Aranti, the radial strains are unexpectedly large - some are in excess of 100%. These large strains were not observed in the micro-tensile experiments. Strains greater than 100% would have ruptured the radial tissue strips. This discrepancy is either due to the natural variance in mechanical properties between valves or more logically, due to the following explanation. There is a possibility that at zero transvalvular pressure, the valve leaflets at the coaptation edges were slightly compressed, folded or buckled. If so, then these regions were not in a true "zero stress - zero strain" state, but instead a "zero stress - slacked" state. Consequently, initial length

measurements corresponding to zero transvalvular pressure are underestimated. Hence, with increasing pressure, these regions begin to unfold prior to distending and straining in the radial direction. Calculated strains as a result are larger than the actual strains. Photographs of the valve at zero transvalvular pressure (figures B4 and B5 in Appendix B) seem to confirm the above conjecture. The highly elastic-shaped $P - \epsilon_R$ curves in the regions of the Nodes of Aranti would also comply with the reasoning.

Another interesting observation concerning the radial strains is the following: whereas the microtensile experiments revealed increasing leaflet stiffness and decreasing transition strains from the sinus-annulus edge to the coaptation edge, the whole valve experiments revealed the reverse. This contrasting behaviour of the leaflet tissue is possibly the result of the differing tissue support used in the two types of experiments. In the microtensile experiments, the radial tissue strips are supported by the rigid Tensilon jaws; hence, data so obtained reflect the leaflet tissue's intrinsic mechanical properties. In the whole valve experiments, the leaflet tissue in the radial direction is supported by the coaptation surfaces and the aortic ring. Apparently, these valvular structures can be influential in determining the operational mechanical properties of the leaflet tissue. For example, the stiff aortic ring maintains a pre-transition low-strain and low-stress diastolic state in the adjacent

leaflet tissue that is intrinsically capable of larger diastolic strains.

B4. Iso-Strain Contour Maps

Another means of presenting pressure-strain data is the iso-strain contour map. Figures 34 to 39 show iso-strain maps illustrating the changes in the distribution of radial strains in the three leaflets as the valve is progressively loaded from 20 to 120 mm. Hg. The maps suggest two general observations: 1) the NC leaflet exhibits the least overall strains at all pressures, and 2) there is a graded increase in the strains from the sinus-annulus ring to the coaptation edges. The latter explains in part why the valve leaflets do not bulge but instead, fold inward toward the center. This aids in maintaining a competent coaptation and facilitates sinus flushing during late diastole. By preventing bulging, bending stresses and cusp prolapse are also minimized.

The iso-strain contours are not to be extrapolated as being representative of the iso-stress contours without considering the inhomogeneity of the leaflet material properties.⁹ For a linear homogeneous material, areas of largest strains correspond directly to areas of largest stresses (ie., $\sigma = E\epsilon$). A non-linear inhomogeneous material, such as

⁹ The calculation of stresses from strains incorporated with leaflet material inhomogeneities is described in Part II of this study [Chong, 1977].

FIGURE 34.

ISO-STRAIN[†] MAP of PORCINE AORTIC VALVE at 20 mm. Hg.

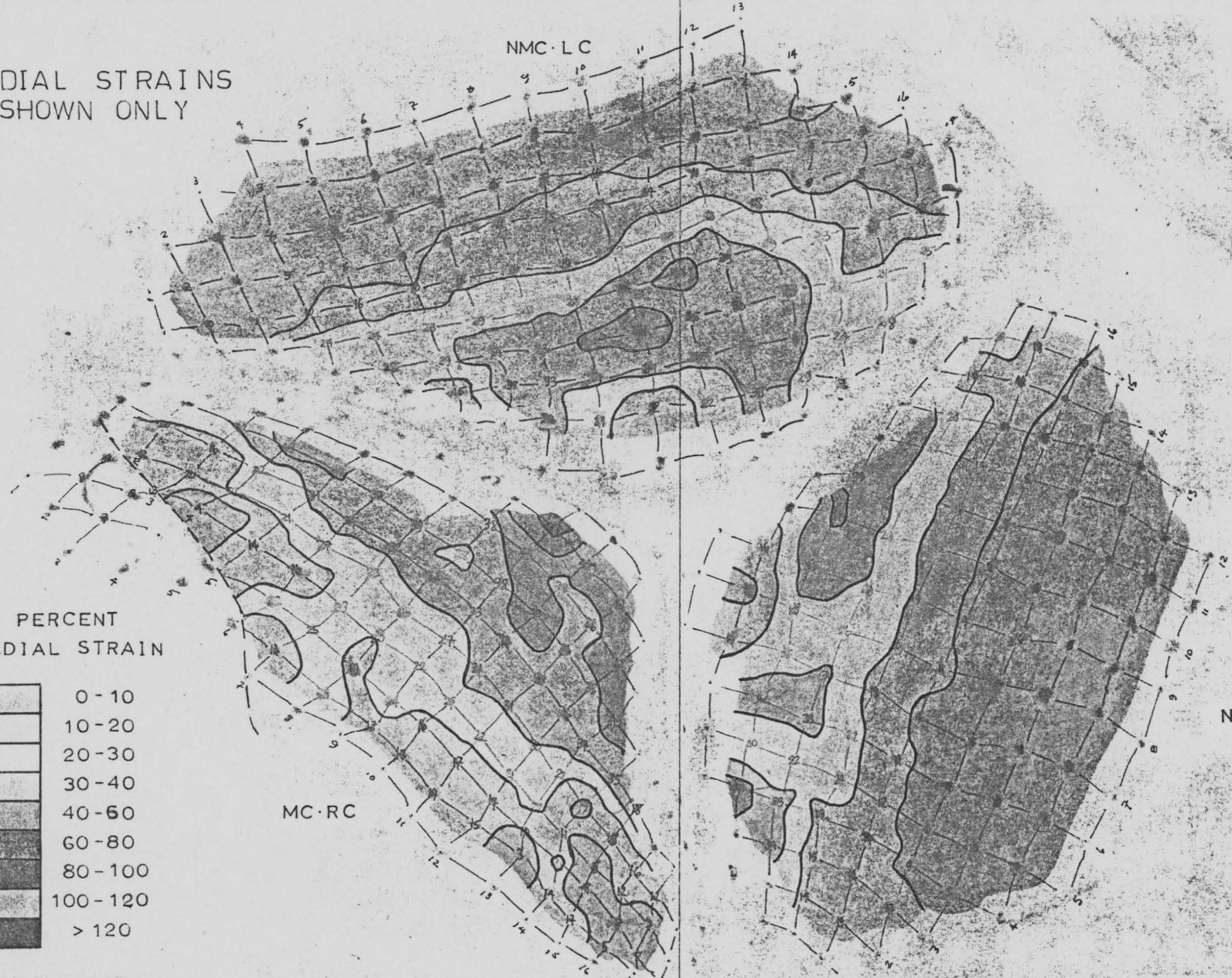
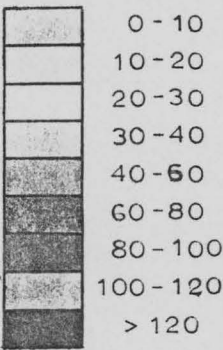
*RADIAL STRAINS SHOWN ONLY

NMC · LC

MC · RC

NC

PERCENT RADIAL STRAIN



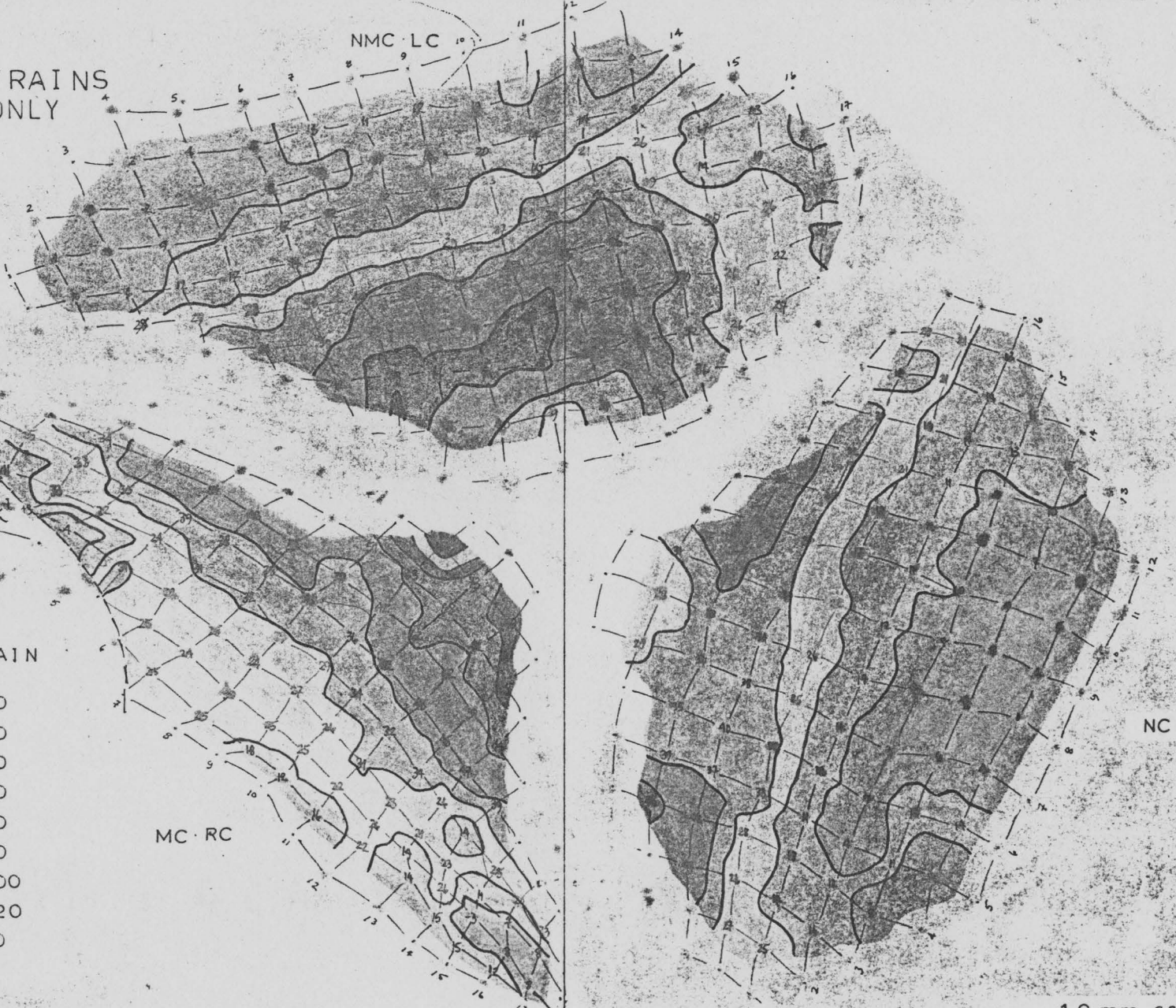
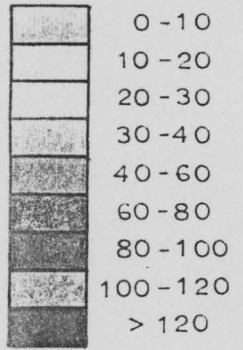
1.0 mm. scale

FIGURE 35.

ISO-STRAIN MAP of PORCINE AORTIC VALVE at 40 mm. Hg.

*RADIAL STRAINS SHOWN ONLY

PERCENT RADIAL STRAIN



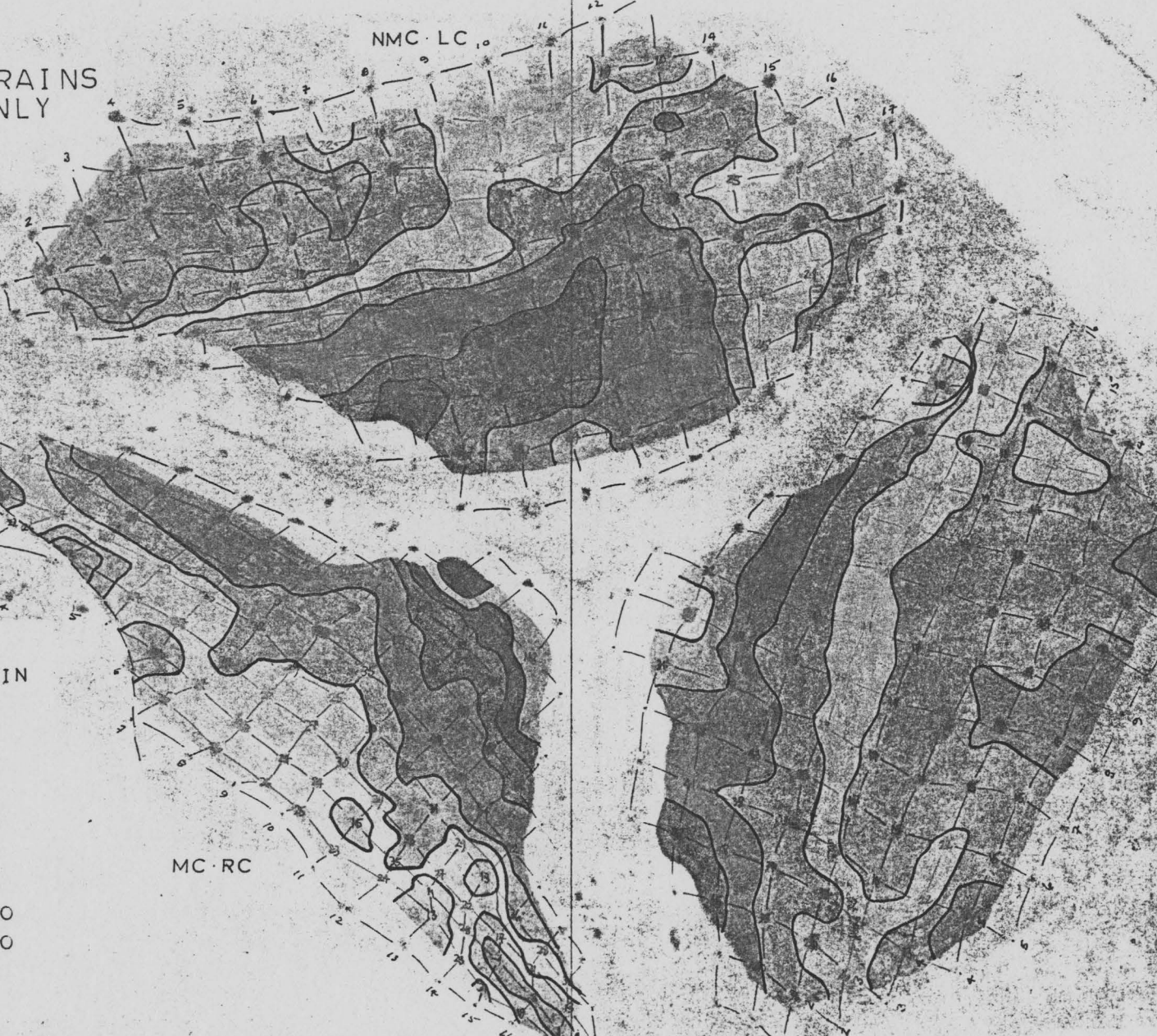
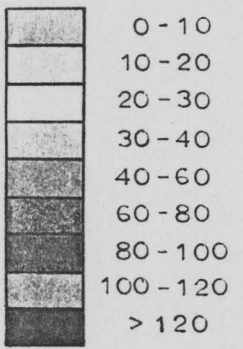
1.0 mm. scale

FIGURE 36.

ISO-STRAIN MAP of PORCINE AORTIC VALVE at 60 mm. Hg.

*RADIAL STRAINS SHOWN ONLY

PERCENT RADIAL STRAIN



1.0 mm. scale

FIGURE 37.

ISO-STRAIN MAP of PORCINE AORTIC VALVE at 80 mm. Hg.

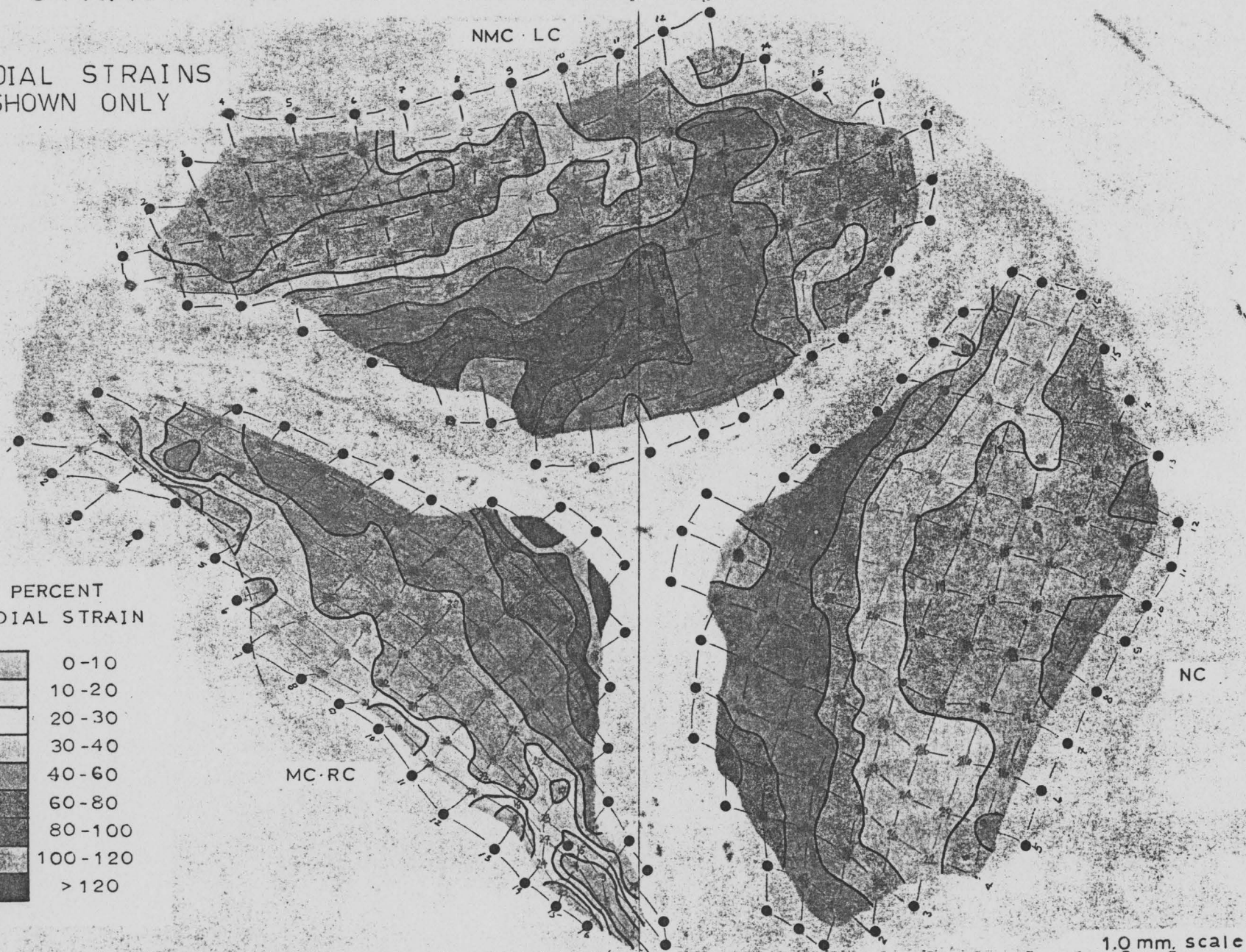
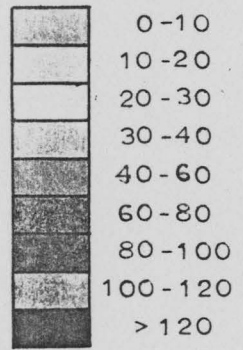
*RADIAL STRAINS SHOWN ONLY

NMC · LC

NC

MC · RC

PERCENT RADIAL STRAIN



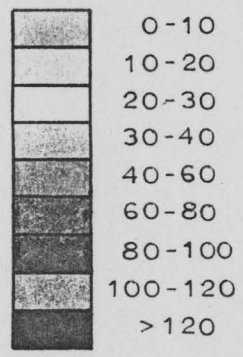
1.0 mm. scale

FIGURE 38.

ISO-STRAIN MAP of PORCINE AORTIC VALVE at 100 mm. Hg.

*RADIAL STRAINS SHOWN ONLY

PERCENT RADIAL STRAIN



10 mm. scale

FIGURE 39.

ISO-STRAIN MAP of PORCINE AORTIC VALVE at 120 mm. Hg.

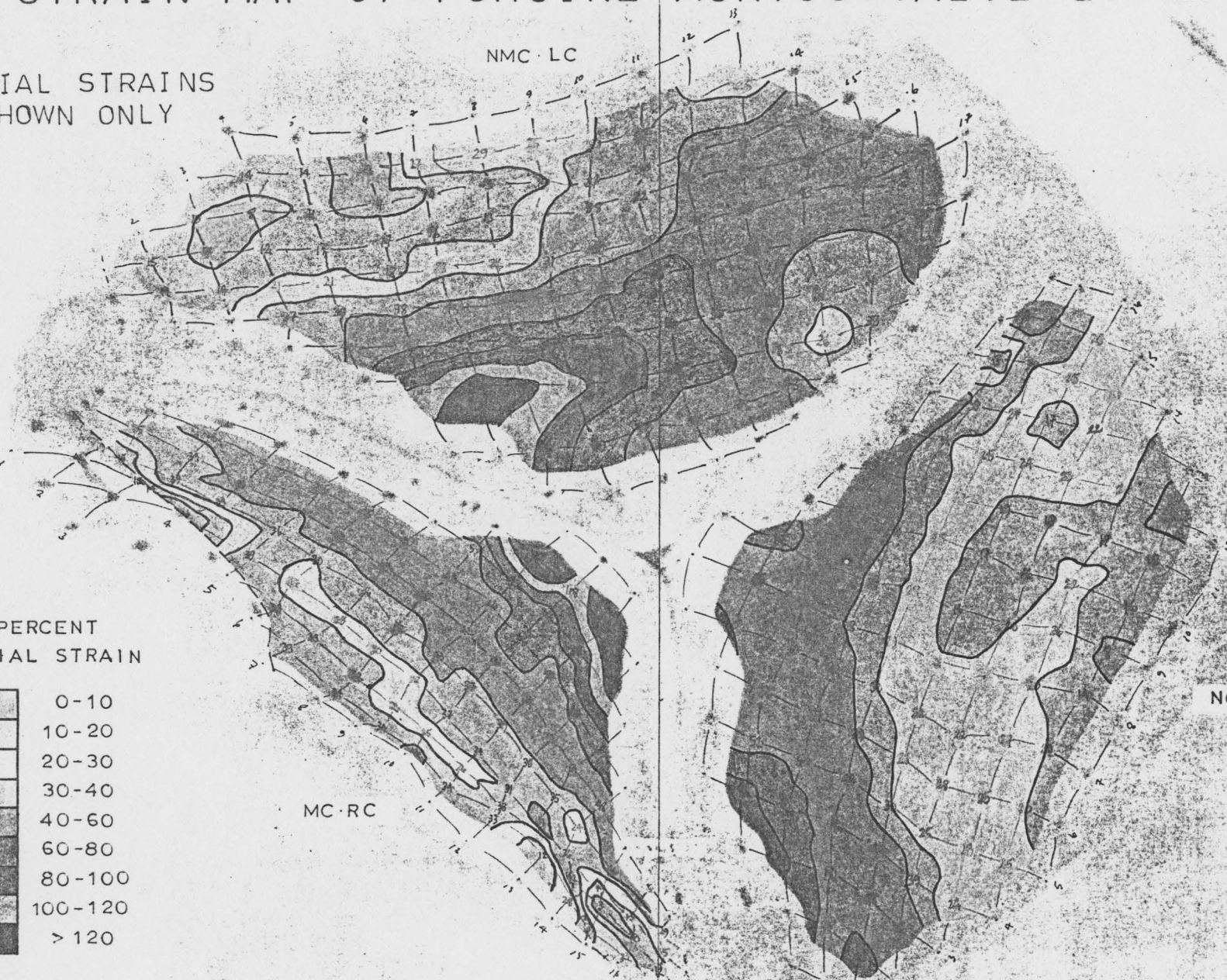
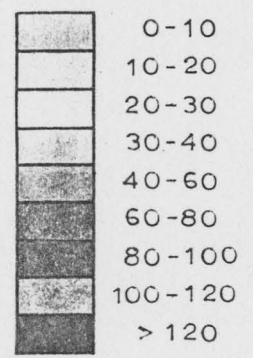
*RADIAL STRAINS SHOWN ONLY

NMC · LC

MC · RC

NC

PERCENT RADIAL STRAIN



1.0 mm. scale

an aortic valve leaflet, does not however imply this one-to-one correspondence. For example, the smaller radial strains in the NC leaflet do not infer absolutely that the NC leaflet has the smallest radial stresses; interestingly, Clark et al (1975) reported that the maximum membrane stresses are the largest in the NC leaflet.

Corresponding contour maps for the circumferential strains are not presented since the results were thought to be inconclusive.

Again, it is reiterated that because of the almost static method of testing, the observed experimental strains are probably larger than the actual strains in-vivo.

B5. Determination of Pre- or Post-Transition Status

Our data lead us to believe that the diastolic valve exhibits differentiated mechanical behaviour for its leaflets' circumferential and radial directions. Circumferentially, the leaflet tissue seems to be in the low-stress pre-transition state. Radially, the leaflet tissue, with the possible exception of the sinus-annulus regions, seems to be in the high-stress post-transition state.

Status of Circumferential Strains - Effect of Aortic Ring

The maximum circumferential strain at diastolic pressures (~80 mm. Hg.) that was observed in the whole valve experiments is 10%. None of the circumferential microtensile

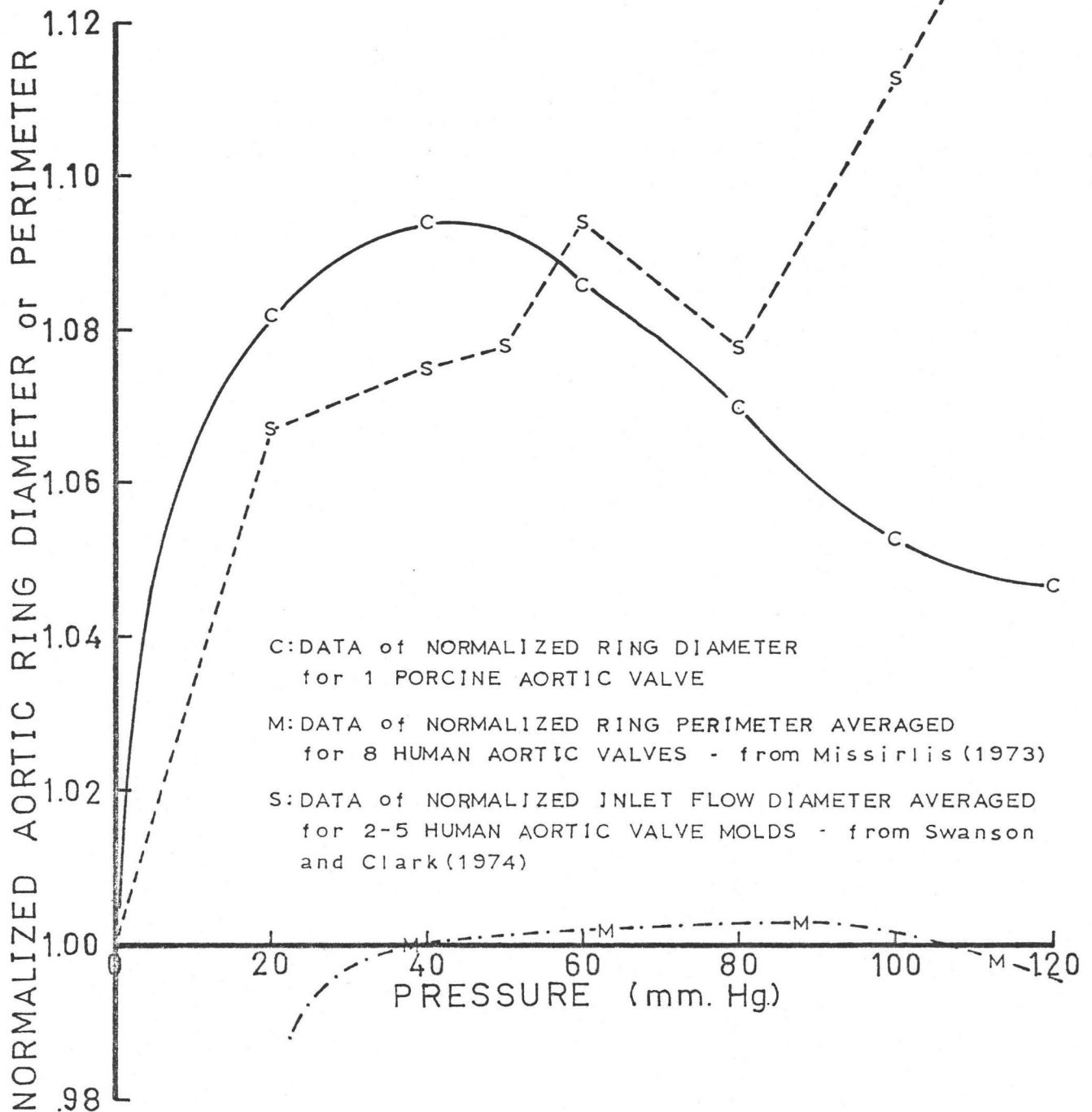
strips or sections thereof showed any post-transition behaviour at this strain. Missirlis' (1973) pressure-strain data reported diastolic circumferential strains to be about 1%. However, since the strain calculations were referenced to 38 mm. Hg., pre- or post-transition status is indeterminant.

Using silicone molds of human aortic roots formed at various physiological pressures, Swanson and Clark (1974) showed that the inlet flow diameter of the valve varies very little with pressure. The increase in diameter at 120 mm. Hg. referenced to the 0 mm. Hg. diameter is approximately 10% (figure 40). The inlet diameter varies directly as the aortic ring circumference. The latter is concentric with the leaflets' circumferential fibres whose ends are anchored in the ring. Hence, Swanson and Clark's (1974) results lend support to the contention that the diastolic leaflets are in pre-transition in the circumferential direction.

Missirlis (1973) showed that the photographed perimeter of the human aortic ring remains essentially constant with pressure up to 120 mm. Hg. He reported less than 0.5% aortic ring strain; again, the reported low strain is the result of using 38 mm. Hg. as the "zero-load" pressure. In our work with the porcine aortic valves, the aortic ring diameter at various pressures was measured from photographs. The results as shown in figure 40 imply that the circumferential strains are no larger than 10% (ie., pre-transition).

Thus, if the contention concerning circumferential

FIGURE 40.
AORTIC RING DISTENSION with PRESSURE



pre-transition strains is true, then the aortic ring may be attributed to as being responsible for maintaining the valve leaflets in a circumferentially low-strain state. This would be particularly important in minimizing the leaflet stresses during diastole. Reduction of strains in-vivo also implies a reduction of the strain rate in-vivo. Both of the above are important factors in determining the fatigue rate and hence also, the durability of the valve.

The decrease in aortic ring size after 40 mm. Hg. is puzzling. Missirlis (1973) observed the same behaviour for human aortic valves, but only after 90 mm. Hg. (figure 40). The source of the associated compressive forces remains to be identified. However, we can speculate that the same causes, which were described as being responsible for the $P - \epsilon_R$ curves' non-monotonic shape, are somehow related.

Status of Radial Strains

The status of the porcine valve's radial strains at diastolic pressures is more complicated than the case for the circumferential strains. Interpolating from the shapes of the $P - \epsilon_R$ curves, the leaflets at diastolic pressures, with the possible exception of the sinus-annulus regions, seem to be in the stiff post-transition phase. However, with reference to the NC leaflet at 80 mm. Hg. (see figure 37), it appears that the majority of the leaflet exhibits strains which correspond to microtensile pre-transition or transition strains

(see figure 20). For example, the green, yellow, orange and red regions of the 80 mm. Hg. iso-strain contour map comprise a large majority of the leaflets and correspond to the areas with $\epsilon_R \leq 40\%$. Microtensile radial transition strains for the NC leaflet lie in the range of $30\% < \epsilon_{tR} < 70\%$ with a mean of $\overline{\epsilon_{tR}} = 58\%$ (s.d. = 7%). The same discrepancy is observed for the other two leaflets' middle strip region for which microtensile data were available. Missirlis' (1973) microtensile and whole valve experiments on human aortic valves also gave similar results [Armeniades et al, 1973; Missirlis, 1973].

The above contradiction is most bothersome and awaits to be resolved. It is unlikely that the whole valve is in its pre-transition state at 80 mm. Hg. Whereas it may be possible to support the contention of pre-transition status for the circumferential strains at diastole (ie., the effect of the aortic ring), the same cannot be said for the radial strains. A feasible explanation is to attribute the discrepancy to possible variances in the mechanical properties between the valves used for the experiments. It is conceivable that the valves used for the microtensile experiments had characteristically above-average strains and that the valve used for the whole valve experiment had below-average strains. Further explanations may be rooted in the differing experimental methods.

As a means of checking, several other typical porcine valves stored similarly to the experimental valves were tested

for microtensile transition strains. Ten random radial and ten circumferential strips produced the following results: $50\% \leq \epsilon_{tR} \leq 85\%$ with a mean of $\overline{\epsilon_{tR}} = 67\%$ (s.d. = 10%) and $18\% \leq \epsilon_{tC} \leq 45\%$ with a mean of $\overline{\epsilon_{tC}} = 30\%$ (s.d. = 10%). Three other valves subjected to the whole valve experiment, but using a less accurate technique¹⁰ similar to that used by Missirlis (1973), produced results similar to the experimental valve's results. Local circumferential strains were consistently less than 10%, thus reconfirming the contention of pre-transition circumferential strains at diastole. Local radial strains at diastolic pressures ranged from 20% to 30%. And although the shapes of the $P - \epsilon_R$ curves again suggested post-transition, the question as to whether the diastolic radial strains are in pre-transition, transition or post-transition is still very much left open to speculation.

In summary, we believe that the valve leaflets are circumferentially in the low-stress pre-transition state at diastole. Radially, the majority of the leaflets seem to be in the high-stress post-transition state, but regions of pre-transition and transition are possible. These final observations are fundamental to the stress calculations which follow in Part II of this study [Chong, 1977].

¹⁰ The less accurate technique involved using single Polaroid photographs to measure the changes in distance between the dots applied onto the valve leaflets. The mesh size of the dots (3 to 4 mm.) was however larger than that used in the main whole valve experiment.

B6. Implications of Results

As noted earlier, stress analyses of the diastolic aortic valve leaflets have been limited by the use of one or more of the following assumptions:

- 1) hypothetical symmetrical geometry for the leaflets;
- 2) homogeneity in the leaflet material properties;
- 3) isotropy in the leaflet material properties; and
- 4) post-transition status for the leaflets in diastole.

This study so far has shown that the first three assumptions are clearly invalid and unacceptable. Assumption four is certainly open to question. Its resolution warrants further investigations.

And although the conducted whole valve experiment may not have been very representative of the in-vivo conditions and of the human aortic valve, the results nevertheless do illustrate a means of modelling the leaflets' operational mechanical properties. Whereas the microtensile experiments serve to explain the leaflets' intrinsic mechanical properties, the whole valve experiment elucidates as to how these properties are utilized under the influence of the other valvular structures. An excellent example is the effect of the aortic ring on the diastolic circumferential strains.

IV. SUMMARY OF CONCLUSIONS AND SUGGESTIONS

1. A new photographic technique has been used to obtain the inhomogeneous and anisotropic microtensile stress-strain data for aortic valve leaflets by observing the sectional strains between dots applied onto the circumferential and radial strips.
2. The porcine aortic valve leaflets exhibit marked inhomogeneity and anisotropy in the post-transition elastic moduli and transition strains. Microtensile measurements revealed a distinct variation in the two parameters from position to position on the same leaflet, from leaflet to leaflet of the same valve, and from valve to valve.
3. The porcine valve leaflets are noticeably less stiff than the human valve leaflets. This is observed for both of the circumferential and radial directions. It is speculated that the glutaraldehyde used to preserve and stabilize the porcine aortic xenografts has the effect of "humanizing" the bioprostheses for adaptation to human physiological flow and stress conditions. It would be most informative and advantageous to prosthetic trileaflet valve design to investigate and understand this effect.

4. A new stereophotogrammetric method has been devised to obtain three-dimensional Cartesian coordinate data for points on an irregular surface. The method has been used to determine the local strains and radii of curvature on the leaflets of a pressurized porcine aortic valve *in vitro*. Improved accuracy in the method requires further refinements to the stereophotogrammetric apparatus.
5. In the whole valve experiment, the stiff aortic ring and the magnitude of the observed circumferential strains at diastolic pressures ($\leq 10\%$) suggest that the valve leaflets during diastole are in the low-stress pre-transition state in the circumferential direction. The shapes of the local pressure-strain curves suggest that for the majority of the valve leaflets during diastole, the tissue is in the high-stress post-transition state in the radial direction. However, the magnitudes of the whole valve radial strains, when spatially matched to the microtensile strains, infer pre-transition. The discrepancy awaits to be resolved. It certainly warrants further investigation since its understanding is important to the determination of more realistic input parameters for stress analyses.
6. Both of the microtensile and the whole valve experiments should be conducted on the same valve in order to improve the procedure for determining pre- or post-transition

status by comparing spatially-matched strains from the two experiments. Specifically, a more precise and systematic approach to spatially match the strains from the experiments is required. Furthermore, since it is not possible with the present method to test for both circumferential and radial behaviour on the same leaflet, a better technique to obtain inhomogeneous and anisotropic stress-strain data without altering the leaflet ultrastructure by cutting is also required.

7. In order to arrive at typical or average leaflet material properties which then can be used for trileaflet valve designs, inhomogeneous and anisotropic data should be accumulated from a much wider spectrum of leaflet samples.

ADDENDUM

A paper by Tan and Holt (1976) recently reported microtensile stress-strain data for porcine aortic leaflet tissue. It was observed that the stress-strain curves vary from leaflet to leaflet in a single valve as well as from valve to valve - an observation of inhomogeneity which is also present in our experiments. Post-transition elastic moduli and transition strains extrapolated from Tan and Holt's stress-strain curves are summarized and compared to our results below in table 4.

TABLE 4. COMPARISON OF MICROTENSILE STRESS-STRAIN DATA

	Tan & Holt	Chong	
E_{CIR} gm/mm ²	944 , 147 (4)	342 , 113 (11)*	number of specimen standard deviation
E_{RAD}	233 , 110 (4)	111 , 42 (21)*	
E_C/E_R —	4.0 , 1.5	3.3 , 0.4	
ϵ_{tC} %	39 , 5 (4)	33 , 3 (4)*	30 , 10 (10) ⁺
ϵ_{tR}	51 , 14 (4)	58 , 7 (5)*	67 , 10 (10) ⁺
$\epsilon_{tR}/\epsilon_{tC}$ —	1.3 , 0.3	1.8 , 0.4	2.2 , 1.1
* results averaged for different sections of a NC leaflet + results averaged for randomly chosen leaflets and valves			

Sample strip size (6 mm. x 19 mm.) used by Tan and Holt is larger than ours (~2 mm. x 10 mm.). The strain rates (~13%/min) are in the same order as ours (15%/min - 45%/min).

These variances along with possible differences in tissue storage and preparation might account for any discrepancies in the two sets of results.

Transition strain data are comparable; however, Lim and Boughner's (1975) observation of increased transition strains and extensibility with sample cross-sectional area does not seem to apply to the results.

Tan and Holt's post-transition elastic modulus data are much larger than ours. A possible explanation is that Tan and Holt stretched their samples further into the post-transition region; that is, the modulus increases with increasing stress.

BIBLIOGRAPHY

- Abrahams, M. (1967). Mechanical Behaviour of Tendon In-Vitro. *Med. Biol. Eng.* 5(4):433-442.
- Affeld, K. et al (1973). Analysis of the Shape and Stress of Aortic and Pulmonary Leaflets from Cows (Translated). Source Unknown:85-88.
- Akbarian, M. et al (1968). Thromboembolic Complications of Prosthetic Cardiac Valves. *Circ.* 37(5):826-831.
- Albert, H.M. et al (1977). Seven-Year Experience with Mounted Porcine Valves. *Ann. Surg.* 185(6):717-723.
- Al-Janabi, N. et al (1972). Viability of Fresh Aortic Valve Homografts: A Quantitative Assessment. *Thorax* 27(1):83-86.
- Anderson, E.T. and Hancock, E.W. (1976). Long Term Follow-Up of Aortic Valve Replacement with the Fresh Aortic Homograft. *J. Thorac. Cardiovasc. Surg.* 72(1):150-156.
- Angell, W.W. et al (1972). A Five-Year Study of Viable Aortic Homografts. *J. Thorac. Cardiovasc. Surg.* 64(3):329-339.
- Angell, W.W. et al (1973). Valve Replacement: Present Status of Homograft Valves. *Prog. Cardiovasc. Dis.* 15(6):589-622.
- Angell, W.W. et al (1977). Selection of Tissue or Prosthetic Valve: A Five-Year Prospective Randomized Comparison. *J. Thorac. Cardiovasc. Surg.* 73(1):43-52.
- Armeniades, C.D. et al (1973). Histologic Origin of Aortic Tissue Mechanics. *Appl. Polymer Symposium* 22:319-339.
- Arnett, E.N. and Roberts, W.C. (1976). Prosthetic Valve Endocarditis. *Amer. J. Cardiology* 38(3):281-292.
- Bahnson, H.T. et al (1965). Replacement of the Aortic Valve with Individual Teflon Leaflets. *J. Thorac. Cardiovasc. Surg.* 49(5):719-730.
- Bailey, C.P. (1967). Discussion in Malm, J.R. (1967). *J. Thorac. Cardiovasc. Surg.* 54(4):486.

- Baird, F.J. et al (1965). An Evaluation of the Late Results of Aortic Valve Repair. *J. Thorac. Cardiovasc. Surg.* 49(4):562-573.
- Barnhorst, D.A. et al (1975). Isolated Replacement of the Aortic Valve with the Starr-Edwards Prosthesis: A 9 Year Review. *J. Thorac. Cardiovasc. Surg.* 70(1):113-118.
- Barratt-Boyes, B.G. (1964). Homograft Aortic Valve Replacement in Aortic Incompetence and Stenosis. *Thorax* 19(2): 131-150.
- Barratt-Boyes, B.G. (1967). Homograft Replacement for Aortic Valve Disease. *Mod. Concepts Cardiovasc. Dis.* 36(1):1-9.
- Barratt-Boyes, B.G. and Roche, A.H.G. (1969). A Review of Aortic Valve Homografts Over a Six and One-Half Year Period. *Ann. Surg.* 170(3):483-490.
- Barratt-Boyes, B.G. (1971). Long Term Follow-Up of Aortic Valvular Grafts. *Brit. Heart J.* 33(Suppl.):60-65.
- Barratt-Boyes, B.G. et al (1977). Six-Year Review of the Results of Freehand Aortic Valve Replacement Using an Antibiotic Sterilized Homograft Valve. *Circ.* 55(2): 353-361.
- Bellhouse, B.J. and Bellhouse, F.H. (1968). Mechanism of Closure of the Aortic Valve. *Nature* 217:86-87.
- Bellhouse, B.J. and Bellhouse, F.H. (1969). Fluid Mechanics of Model Normal and Stenosed Aortic Valves. *Circ. Res.* 25(6):693-704.
- Bellhouse, B.J. and Talbot, L. (1969). The Fluid Mechanics of the Aortic Valve. *J. Fluid Mechanics* 35(4):721-735.
- Behrendt, D.M. and Austen, W.G. (1973). Current Status of Prosthetics for Heart Valve Replacement. *Prog. Cardiovasc. Dis.* 15(4):369-401.
- Binet, J.P. et al (1965). Heterologous Aortic Valve Transplantation. *Lancet* 2:1275.
- Binet, J.P. et al (1967). Clinical Use of Heterografts for Replacement of the Aortic Valve. *J. Thorac. Cardiovasc. Surg.* 55(2):238-254.
- Björk, V.O. et al (1962). A Mechanical Pulse Duplicator for Testing Prosthetic Mitral and Aortic Valves. *Thorax* 17 (3):280-283.

- Björk, V.O. et al (1963). Aortic Valve Prosthesis (Teflon): Two-Year Follow-Up. *J. Thorac. Cardiovasc. Surg.* 45(5): 635-644.
- Björk, V.O. and Hultqvist, G. (1964). Teflon and Pericardial Aortic Valve Prostheses. *J. Thorac. Cardiovasc. Surg.* 47(6):693-701.
- Björk, V.O. (1970). The Present Status of Artificial Heart Valves. *Adv. Biomed. Eng. Med. Phys.* 3(7):259-260.
- Björk, V.O. et al (1975a). Five-Year Experience with the Bjork-Shiley Tilting Disc Valve in Isolated Aortic Valve Disease. *J. Cardiovasc. Surg. (Torino)* 16(5):451-457.
- Björk, V.O. et al (1975b). Management of Thromboembolism after Aortic Valve Replacement with the Bjork-Shiley Tilting Disc Valve. *Scand. J. Thorac. Cardiovasc. Surg.* 9(3):183-191.
- Björk, V.O. (1977). The History of the Bjork-Shiley Tilting Disc Valve. *Med. Instrum.* 11(2):80-81.
- Blackshear, P.L. et al (1966). Shear, Wall Interaction and Hemolysis. *Trans. Amer. Soc. Artif. Int. Org.* 12:113-120.
- Blackshear, P.L. et al (1969). Effects of Flow and Turbulence on the Formed Elements of Blood, in Prosthetic Heart Valves (editor: L.A. Brewer III). Springfield, Ill.: C.C. Thomas. Chapter 5:52-67.
- Blackshear, P.L. (1972). Mechanical Hemolysis in Flowing Blood, in Biomechanics: Its Foundation and Objectives (editor: Y.C. Fung). Englewood Cliffs, New Jersey: Prentice Hall. Chapter 19:501-528.
- Bonchek, L.I. and Starr, A. (1975). Ball Valve Prostheses: Current Appraisal of Late Results. *Amer. J. Cardiology* 35(6):843-854.
- Braunwald, N.S. and Morrow, A.G. (1965). A Late Evaluation of Flexible Teflon Prostheses Utilized for Total Aortic Valve Replacement. *J. Thorac. Cardiovasc. Surg.* 49(3): 485-496.
- Braunwald, N.S. and Detmer, D.E. (1968). A Critical Analysis of the Status of Prosthetic Valves and Homografts. *Prog. Cardiovasc. Dis.* 11(2):113-132.
- Braunwald, N.S. et al (1968). Simplified Insertion of Aortic Homograft Valves with Non-thrombogenic Prosthetic Frames. *Surgery* 63(1):38-43.

- Braunwald, N.S. et al (1971). New Developments in the Design of Fabric-Covered Prosthetic Heart Valves. *J. Thorac. Cardiovasc. Surg.* 62(5):673-682.
- Braunwald, N.S. (1975). The Fabric-Covered Prosthetic Heart Valve: Present Status and Future Development. *Ann. Thorac. Surg.* 20(3):360-363.
- Brawley, R.K. et al (1975). Current Status of the Beall, Björk-Shiley, Braunwald-Cutter, Lillehei-Kaster and Smeloff-Cutter Cardiac Valve Prostheses. *Amer. J. Cardiology* 35(6):855-865.
- Brest, A.N. (1966). editor: Heart Substitutes: Mechanical and Transplants. Springfield, Illinois: C.C. Thomas.
- Brewer, L.A. (1969a). Statistical Survey of 3620 Cases of Heart Valve Replacement, in Prosthetic Heart Valves (editor: L.A. Brewer III). Springfield, Ill.: C.C. Thomas. Chapter 60:838-845.
- Brewer, L.A. (1969b). editor: Prosthetic Heart Valves. Springfield, Illinois: C.C. Thomas. (Second National Conference on Prosthetic Heart Valves, LA, California)
- Brewer, L.A. et al (1969). Current Clinical Problems in Prosthetic Heart Valves, in Prosthetic Heart Valves (editor: L.A. Brewer III). Springfield, Ill.: C.C. Thomas. Chapter 62:856-872.
- Brewer, R.J. et al (1976). The Dynamic Aortic Root: Its Role in Aortic Valve Function. *J. Thorac. Cardiovasc. Surg.* 72(3):413-417.
- Brewer, R.J. et al (1977). An In-Vivo Study of the Dimensional Changes of the Aortic Valve Leaflets During the Cardiac Cycle. *J. Thorac. Cardiovasc. Surg.* 74(4):645-650.
- Broom, N.D. (1978). The Observation of Collagen and Elastin Structures in Wet Whole Mounts of Pulmonary and Aortic Leaflets. *J. Thorac. Cardiovasc. Surg.* 75(1):121-130.
- Buch, W.S. et al (1970). Deterioration of Formalin-Treated Aortic Valve Heterografts. *J. Thorac. Cardiovasc. Surg.* 60(5):673-682.
- Buch, W.S. et al (1975). Hancock-Stabilized Glutaraldehyde Valve: Clinical and Laboratory Evaluation. *Arch. Surg.* 110(11):1408-1415.

- Callaghan, J.C. et al (1961). Visualization of the Function of Human Heart Valves with an External Pulse Duplicator, in Prosthetic Valves for Cardiac Surgery (editor: K.A. Merendino). Springfield, Ill.: C.C. Thomas. Chap. 1:48-55.
- Calvert, G. et al (1964). An Aortic Pulse Duplicator of Simple Design. *J. Thorac. Cardiovasc. Surg.* 47(5):633-643.
- Carpentier, A. et al (1969). Biological Factors Affecting Long Term Results of Valvular Heterografts. *J. Thorac. Cardiovasc. Surg.* 58(4):467-483.
- Carpentier, A. et al (1971). Collagen-Derived Heart Valves. *J. Thorac. Cardiovasc. Surg.* 62(5):707-713.
- Carpentier, A. et al (1972). From Xenograft to Bioprosthesis, in Biological Tissue in Heart Valve Replacement (editor: M.I. Ionescu). London: Butterworth & Co. Chap. 22:514-541.
- Carpentier, A. et al (1974). Six-Year Follow-Up of Glutaraldehyde-Preserved Heterografts. *J. Thorac. Cardiovasc. Surg.* 68(5):771-782.
- Carpentier, A. (1977). From Valvular Xenograft to Valvular Bioprosthesis (1965-1977). *Med. Instrum.* 11(2):98-101.
- Castra-Villograna, B. et al (1957). An Experimental Surgical Treatment for Aortic Insufficiency. *Surg. Forum* 8:371-375.
- Cataloglu, A. et al (1975). Validation of a Simplified Mathematical Model for the Stress Analysis of Human Aortic Heart Valves. *J. Biomechanics* 8(5):347-348.
- Cataloglu, A. et al (1976). Refined Stress Analysis of Human Aortic Heart Valves. *J. Engr. Mechanics Division, Proc. ASCE* 102(EM1):135-150.
- Cataloglu, A. et al (1977). Stress Analysis of Aortic Valve Leaflets with Smooth Geometrical Data. *J. Biomechanics* 10(3):153-158.
- Cater, C.W. (1963). The Evaluation of Aldehydes and Other Difunctional Compounds as Crosslinking Agents for Collagen. *J. Soc. Leath. Trades Chem.* 47:259.
- Cèvese, P.G. (1975). Long Term Results of 212 Xenograft Valve Replacements. *J. Cardiovasc. Surg. (Torino)* 16(6):639-642.
- Cèvese, P.G. et al (1977). Heart Valve Replacement with the Hancock Bioprosthesis: Analysis of Long Term Results. *Circ.* 56(Suppl. II):111-116.

- Chen, M.T. et al (1977). Finite Element Stress Analysis of a Human Aortic Valve. *Applied Math. Modelling* 1:218-220.
- Chong, K.P. et al (1973). Stress Analysis of Normal Human Aortic Valve Leaflets During Diastole. *Biomat. Med. Dev. Artif. Org.* 1(2):307-321.
- Chong, M. (1977). Mechanical Studies on the Porcine Aortic Valve. Part II: A Stress Analysis of the Porcine Aortic Valve Leaflets in Diastole. M. Eng. Thesis, McMaster University, Hamilton, Ontario.
- Clark, R.E. (1973). Stress-Strain Characteristics of Fresh and Frozen Human Aortic and Mitral Leaflets and Chordae Tendinae: Implications for Clinical Use. *J. Thorac. Cardiovasc. Surg.* 66(2):202-208.
- Clark, R.E. and Finke, E.H. (1974). Scanning and Light Microscopy of Human Aortic Leaflets in Stressed and Relaxed States. *J. Thorac. Cardiovasc. Surg.* 67(5):792-804.
- Clark, R.E. et al (1974). Design and Fabrication of Prosthetic Leaflet Heart Valves. *Biomat. Med. Dev. Artif. Org.* 2(4):379-385.
- Clark, R.E. et al (1975). Close-Range Stereophotogrammetry and Coupled Stress Analysis as Tools in the Development of Prosthetic Devices. *Trans. Amer. Soc. Artif. Int. Org.* 21:71-78.
- Cohn, L.H. et al (1976). Aortic Valve Replacement with the Hancock Porcine Xenograft. *Ann. Thorac. Surg.* 22(3):221-227.
- Cornhill, J.F. (1977). An Aortic-Left Ventricular Pulse Duplicator Used in Testing Prosthetic Aortic Heart Valves. *J. Thorac. Cardiovasc. Surg.* 73(4):550-558.
- Dale, J. (1976). Arterial Thromboembolic Complications in Patients with Starr-Edwards Aortic Ball Valve Prostheses. *Amer. Heart J.* 91(5):653-659.
- Dale, J. (1977). Arterial Thromboembolic Complications in Patients with Bjork-Shiley and Lillehei-Kaster Aortic Disc Valve Prostheses. *Amer. Heart J.* 93(6):715-722.
- Davey, T.B. et al (1966). Design of Heart Valves. *Mechanical Engineering* 88(7):22-26.
- Davies, H. et al (1968). Homograft Replacement of the Aortic Valve: A Clinical and Pathologic Study. *Amer. J. Cardiol.* 22(2):195-217.

- Davies, H. and Roberts, C.I. (1974). Homograft Valves Ten Years Later: The Physician's Viewpoint. *Adv. Cardiology* 11:198-210.
- Davila, J.C. et al (1956). A Simple Mechanical Pulse Dupli-
cator for Cinematography of Cardiac Valves in Action.
Ann. Surg. 143(4):544-551.
- Davila, J.C. (1961). The Mechanics of the Cardiac Valves,
in Prosthetic Valves for Cardiac Surgery (editor: K.A.
Merendino). Springfield, Ill.: C.C. Thomas. Chap. 1:3-47.
- Davila, J.C. et al (1963). Thrombosis in Artificial Heart
Valves: Role of Turbulence Due to Design. *Circ.* 28(4):
708-709.
- Davila, J.C. et al (1966). The Problem of Thrombosis in Arti-
ficial Cardiac Valves, in Heart Substitutes: Mechanical
and Transplants (editor: A.N. Brest). Springfield, Ill.:
C.C. Thomas. Chapter 3:25-53.
- De Boer, A. et al (1974). Isolated Aortic Valve Replacement:
Analysis of Factors Influencing Survival after Replacement
with the Starr-Edwards Prosthesis. *Ann. Thorac. Surg.*
17(4):360-367.
- Duvoisin, G.E. et al (1967). Factors Affecting Thromboembo-
lism Associated with Prosthetic Heart Valves. *Circ.* 35
(Suppl. I):70-76.
- Duvoisin, G.E. and McGoon, D.C. (1969). Advantages and Dis-
advantages of Prosthetic Valves for Aortic Valve Replace-
ment. *Prog. Cardiovasc. Dis.* 11(4):294-303.
- Dinklelacker, A. (1966). Preliminary Experiments on the
Influence of Flexible Walls on Boundary Layer Turbulence.
J. Sound Vib. 4(2):187-214.
- Duff, W.R. and Fox, R.W. (1972). Prosthetic Cardiac Valves:
An In-Vitro Study. *J. Thorac. Cardiovasc. Surg.* 63(1):
131-142.
- Duran, C.G. et al (1964). A Simple Versatile Pulse Duplicator.
Thorax 19(6):503-506.
- Duran, C.G. and Gunning, A.J. (1965). Heterologous Aortic
Valve Transplantation in the Dog. *Lancet* 2:114-115.
- Edwards, W.S. and Smith, L. (1958). Aortic Valve Replacement
with a Subcoronary Ball Valve. *Surgical Forum* 9:309-313.

- Edwards, W.S. (1971). Late Results with Autogenous Tissue Heart Valves. *Ann. Thorac. Surg.* 12(4):385-390.
- Ellis, D.G. (1969). Cross-Sectional Area Measurements for Tendon Specimen: A Comparison of Several Methods. *J. Biomechanics* 2(2):175-186.
- Eyster, E. et al (1971). Chronic Intravascular Hemolysis after Aortic Valve Replacement: Long Term Study Comparing Different Types of Ball Valve Prostheses. *Circ.* 44(4):657-665.
- Fadali, A.M. et al (1970). The Use of Autogenous Peritoneum for Heart Valve Replacement. *J. Thorac. Cardiovasc. Surg.* 60(2):188-195.
- Firor, W.B. et al (1970). Effect of Sterilization and Preservation on the Tensile Properties of Aortic Cusp Tissue. *Can. J. Surg.* 13(6):434-438.
- Forrester, J.H. et al (1969). A Comparative Study of the Fluid Flow Resistance of Prosthetic Heart Valves. *Cardiovasc. Res. Cen. Bull. (Baylor College of Medicine)* 7(3):83-99.
- Freis, E.D. and Heath, W.C. (1964). Hydrodynamics of Aortic Blood Flow. *Circ. Res.* 14(2):105-116.
- Friedli, B. et al (1971). Thromboembolic Complications of Heart Valve Prostheses. *Amer. Heart J.* 81(5):702-708.
- Fung, Y.C. (1968). Biomechanics. *Appl. Mech. Rev.* 21:1.
- Gavin, J.B. et al (1973). Pathology of Antibiotic Treated Human Heart Valve Allografts. *Thorax* 28(4):473-481.
- Geha, A.S. et al (1970). Replacement of the Aortic Valve with Moulded Autogenous Grafts Grown in Response to Implanted Silastic. *J. Thorac. Cardiovasc. Surg.* 60(5):661-672.
- Gerbode, F. (1970). Proceedings of the First International Workshop on Tissue Valves. *Ann. Surg.* 172(Supplement).
- Gerring, E.L. et al (1974). Long Term Animal Trials of the Oxford Aortic/Pulmonary Valve Prosthesis without Anticoagulants. *Trans. Amer. Soc. Artif. Int. Org.* 20B:703-706.
- Ghista, D.N. (1976). Toward An Optimum Prosthetic Trileaflet Aortic Valve Design. *Med. Biol. Eng.* 14(2):122-128.

- Ghista, D.N. and Reul, A. (1977). Optimal Prosthetic Aortic Leaflet Valve: Design Parameters and Longevity Analyses. Development of the Avcothane-51 Leaflet Valve Based on the Optimal Design Analysis. *J. Biomechanics* 10(5):313-324.
- Goldsmith, H.L. et al (1974). The Effects of Flow and Fluid Mechanical Stress on Red Blood Cells and Platelets. *Trans. Amer. Soc. Artif. Int. Org.* 20A:21-26.
- Gonzalez-Lavin, L. et al (1972). Long Term Results after Aortic Valve Replacement with Preserved Aortic Homografts. *Ann. Thorac. Cardiovasc. Surg.* 13(6):594-606.
- Gould, P.L. et al (1973). Stress Analysis of the Human Aortic Valve. *J. Comp. & Struct.* 3:377-384.
- Greenfield, H. and Kolff, W. (1972). The Prosthetic Heart Valve and Computer Graphics. *J. Amer. Med. Assoc.* 219(1):69-74.
- Greenfield, H. et al (1973). Computer Simulation of the Natural Heart Valve. *Trans. Amer. Soc. Artif. Int. Org.* 19:216-223.
- Greenfield, H. (1976). Computer Visualization of Flow Pattern for Prosthetic Heart Valves. *Scand. J. Thorac. Cardiovasc. Surg.* 10(3):197-204.
- Greep, R.O. (1966). editor: Histology. 2nd edition. New York: McGraw Hill Book Co. Chapter 4:99-133.
- Gross, L. and Kugel, M.A. (1931). Topographic Anatomy and Histology of the Valves in the Human Heart. *Amer. J. Path.* 7(5):445-473.
- Hancock, W.D. (1977). The Porcine Heart Valve Prosthesis. *Med. Instrum.* 11(2):102-103.
- Hannah, H. and Reis, R.L. (1976). Current Status of Porcine Heterograft Prostheses: A Five-Year Appraisal. *Circ.* 54 (Suppl. III):27-31.
- Harken, D.E. et al (1960). Partial and Complete Prostheses in Aortic Insufficiency. *J. Thorac. Cardiovasc. Surg.* 40(6):744-762.
- Harken, D.E. (1977). Prosthetic Heart Valves. *Med. Instrum.* 11(2):70-71.
- Harkness, R.D. (1961). Biological Function of Collagen. *Biol. Rev.* 36(4):399-463.

- Harris, P.D. et al (1968). Factors Modifying Aortic Homograft Structure and Function. *Surgery* 63(1):45-52.
- Hauf, E. et al (1973). Comparative Study of In-Vitro Hydrodynamic Behaviour between Three Differently Designed Fascia Lata Valves and the Starr-Edwards Prosthesis in the Aortic Position. *Eur. Surg. Res.* 5(1):37-51.
- Herr, R.H. et al (1965). Special Problems Following Valve Replacement: Embolus, Leak, Infection, Red Cell Damage. *Ann. Thorac. Surg.* 1(4):403-415.
- Huc, A. et al (1975). Study of Pig Valve Heterografts by X-Ray Diffraction. *J. Biomed. Mat. Res.* 9(1):79-95.
- Hudson, R.E.B. (1966). Pathology of the Human Aortic Valve Homograft. *Brit. Heart J.* 28(3):291-301.
- Hufnagel, C.A. and Harvey, W.P. (1952). The Surgical Correction of Aortic Regurgitation. *Bull. Georgetown Univ. Med. Centre* 5:128-130.
- Hufnagel, C.A. and Harvey, W.P. (1953). The Surgical Correction of Aortic Insufficiency: Preliminary Report. *Bull. Georgetown Univ. Med. Centre* 6:60-61.
- Hufnagel, C.A. and Conrad, P.W. (1965). Comparative Study of Some Prosthetic Valves for Aortic and Mitral Replacement. *Surgery* 57(1):205-210.
- Hufnagel, C.A. (1977). Reflections on the Development of Valvular Prostheses. *Med. Instrum.* 11(2):74-76.
- Hwang, N.H.C. et al (1977). Turbulent Flow Through a Natural Human Mitral Valve. *J. Biomechanics* 10(1):59-67.
- Hysten, J.C. (1972a). Mechanical Malfunction and Thrombosis of Prosthetic Heart Valves. *Amer. J. Cardiology* 30(3):396-404.
- Hysten, J.C. (1972b). Mechanical Malfunction and Hemolysis with Prosthetic Heart Valves. *Adv. Cardiology* 7:187-212.
- Innes, B.J. et al (1971). Effect of Sterilization Methods on Endothelium of Homograft and Heterograft Valves. *J. Surg. Res.* 11(3):111-118.
- Ionescu, M.I. et al (1968). Heart Valve Replacement with Reinforced Aortic Heterografts: Technique and Results. *J. Thorac. Cardiovasc. Surg.* 56(3):333-350.

- Ionescu, M.I. and Ross, D.N. (1969). Heart Valve Replacement with Autologous Fascia Lata. *Lancet* 2:335-338.
- Ionescu, M.I. (1972). editor: Biological Tissue in Heart Valve Replacement. London: Butterworth & Co.
- Ionescu, M.I. et al (1972a). Heart Valve Replacement with Aortic Heterografts: Follow-Up Study. *Ann. Thorac. Surg.* 13(1):1-14.
- Ionescu, M.I. et al (1972b). Results of Aortic Valve Replacement with Frame-Supported Fascia Lata and Pericardial Grafts. *J. Thorac. Cardiovasc. Surg.* 64(3):340-353.
- Ionescu, M.I. et al (1974). Long Term Evaluation of Tissue Valves. *J. Thorac. Cardiovasc. Surg.* 68(3):361-378.
- Ionescu, M.I. et al (1977). Heart Valve Replacement with the Ionescu-Shiley Pericardial Xenograft. *J. Thorac. Cardiovasc. Surg.* 73(1):31-41.
- Isom, O.W. et al (1974). Factors Influencing Long Term Survival after Isolated Aortic Valve Replacement. *Circ.* 50 (Suppl. II):154-162.
- Isom, O.W. et al (1977). Long Term Results in 1375 Patients Undergoing Valve Replacement with the Starr-Edwards Cloth-Covered Steel Ball Prosthesis. *Ann. Surg.* 186(3):310-322.
- Judson, W.E. et al (1964). Post-Operative Evaluation of Prosthetic Replacement of Aortic and Mitral Valves. *Circ.* 29(Suppl. I):14-29.
- Karara, H.M. and Marzan, M.T. (1973). Determination of the Geometry of Trileaflet Aortic Heart Valves. Proc. 17th Ann. Tech. Meeting of the Soc. Photo-Optical Instrum. Engrs. San Diego, CA. August, 1973.
- Karara, H.M. (1975). Geometry of Aortic Heart Valves. Proc. of the Amer. Soc. of Photogrammetry, 41st Ann. Meeting, Washington, D.C. March.
- Karp, R.B. et al (1974). Comparison of Three Devices to Replace the Aortic Valve. *Circ.* 50(Suppl. II):163-169.
- Kaster, R.L. et al (1968). Analysis of Dynamic Characteristics of Heart Valves in a Pulse Duplicator-Analog Computer System. *Biomed. Sci. Instrum.* 4:112.

- Kaster, R.L. et al (1969). Comparative Analysis of In-Vitro Flow Characteristics of Seven Types of Prosthetic Heart Valves, in Prosthetic Heart Valves (editor: L.A. Brewer). Springfield, Illinois: C.C. Thomas. Chapter 9:137-147.
- Kastor, J.A. et al (1968). Paravalvular Leaks and Hemolytic Anemia Following Insertion of Starr-Edwards Aortic and Mitral Valves. *J. Thorac. Cardiovasc. Surg.* 56(2):279-288.
- Katholi, R.E. et al (1976). Living with Prosthetic Heart Valves. Subsequent Non-Cardiac Operations and the Risk of Thromboembolism or Hemorrhage. *Amer. Heart J.* 92(2): 162-167.
- Kiraly, R.J. and Nosé, Y. (1976). Natural Tissue as a Bio-material. *Biomat., Med. Dev., Artif. Org.* 2(3):207-224.
- Klain, M. et al (1969). Comparative Testing of Artificial Heart Valves in a Mock Circulation, in Prosthetic Heart Valves (editor: L.A. Brewer III). Springfield, Illinois: C.C. Thomas. Chapter 8:114-136.
- Kloster, F.E. et al (1965). Medical Problems in Mitral and Multiple Valve Replacement. *Prog. Cardiovasc. Dis.* 7(6):504-529.
- Kloster, F.E. (1975). Diagnosis and Management of Complications of Prosthetic Heart Valves. *Amer. J. Cardiology* 35(6):872-885.
- Koorajian, S. et al (1969). Criteria and Systems for Testing Artificial Heart Valves In-Vitro, in Prosthetic Heart Valves (editor: L.A. Brewer III). Springfield, Illinois: C.C. Thomas. Chapter 7:92-111.
- Kramer, M.O. (1962). Boundary Layer Stabilization by Disturbed Damping. *J. Amer. Soc. Nav. Engr.* 74:341.
- La Ban, M.M. (1962). Collagen Tissue: Implications of Its Response to Stress In-Vitro. *Arch. Phys. Med. & Rehab.* 43(9):461-466.
- Lake, L.W. (1973). Structure-Property Relations of the Aortic Wall and Its Tissue Components. Ph. D. Thesis, Rice Univ., Houston, Texas, 1973.
- Leyse, R.M. et al (1961). A System for the Study of Cardiovascular Flow Patterns, in Prosthetic Valves for Cardiac Surgery (editor: K.A. Merendino). Springfield, Illinois: C.C. Thomas. Chapter 1:56-70.

- Lim, K.O. and Boughner, D.R. (1975). Mechanical Properties of Human Mitral Valve Chordae Tendinae: Variation with Size and Strain Rate. *Can. J. Physiol. Pharmacol.* 53(3):330-39.
- Lim, K.O. and Boughner, D.R. (1976). The Low Frequency Dynamic Viscoelastic Properties of Human Aortic Valve Tissue. *Circ. Res.* 39(2):209-214.
- Lillehei, C.W. and De Wall, R.A. (1958). Design and Clinical Application of the Helix Reservoir Pump-Oxygenator System for Extracorporeal Circulation. *Post. Med.* 23(5):561-573.
- Lillehei, C.W. (1977). Heart Valve Replacement with the Pivoting Disc Prosthesis: Appraisal of Results and Description of a New All-Carbon Model. *Med. Instrum.* 11(2):85-94.
- Litwak, R.L. et al (1972). Results of Mitral Valve Replacement with Formalin-Fixed Porcine Xenografts. *Adv. Cardiology* 7:119-137.
- Loughridge, B.P. et al (1965). Use of Fibro-Collagenous Tissue in Cardiac Valves. *Surgical Forum* 16:168-170.
- Love, J.S. et al (1971). Comparative Turbulence of Heart Valves (Natural and Prosthetic). *Trans. Amer. Soc. Artif. Int. Org.* 17:497-507.
- Lurie, A.J. et al (1977). Hemodynamic Assessment of the Glutaraldehyde-Preserved Porcine Heterograft in the Aortic and Mitral Positions. *Circ.* 56(Suppl. III):104-110.
- MacGregor, C.G. et al (1976). Viability in Human Heart Valves Prepared for Grafting. *Cardiovasc. Res.* 10(3):394-397.
- Malm, J.R. et al (1967). An Evaluation of Aortic Valve Homografts Sterilized by Electron Beam Energy. *J. Thorac. Cardiovasc. Surg.* 54(4):471-477.
- Manhas, D.R. et al (1973). Late Results of Beta-Propiolactone Sterilized Aortic Homograft Valves: A Study of 51 Patients Followed Up to Seven and a Half Years. *Amer. J. Surg.* 126(2):255-262.
- Mannschott, P. et al (1976). Collagen Heterogeneity in Pig Heart Valves. *Biochimica & Biophysica Acta* 434:177-183.
- Marinescu, V. et al (1971). Long Term Biological Fate of Polyurethane Aortic Prostheses. *Thorax* 26(1):108-111.
- Matloff, J.M. et al (1969). Control of Thromboembolism from Prosthetic Heart Valves. *Ann. Thorac. Surg.* 8(2):133-145.

- Marx, T.I. and Kittle, C.F. (1959). A Cardiovascular Simulator for the Evaluation of Prosthetic Aortic Valves. *J. Thorac. Cardiovasc. Surg.* 38(3):412-418.
- McGoon, D.C. (1972). The Status of Prosthetic Cardiac Valves, in Biological Tissue in Heart Valve Replacement (editor: M.I. Ionescu). London: Butterworth & Co. Chapter 1:3-19.
- McHenry, M.M. et al (1968). Complications of Heart Valve Replacement: Embolism, Bleeding and Hemolysis. *Calif. Med.* 109(1):1-8.
- McMillan, I.K.R. et al (1952). The Movement of the Aortic and Pulmonary Valves Studied Post-Mortem by Colour Cinematography. *Brit. Heart J.* 14(1):42-46.
- McMillan, I.K.R. et al (1955). Aortic Stenosis: A Post-Mortem Cinematographic Study of Valve Action. *Brit. Heart J.* 17(1):56-62.
- Meistrell, M.L. et al (1976). Thromboembolic Complications after Aortic Valve Replacement - Comparative Study. *Brit. Heart J.* 38(3):314-315.
- Melrose, D.G. (1953). A Mechanical Heart-Lung for Use in Man. *Brit. Med. J.* 2(1):57-62.
- Mercer, J.L. et al (1973). The Geometry and Construction of the Aortic Leaflet. *J. Thorac. Cardiovasc. Surg.* 65(4): 511-518.
- Merendino, K.A. (1961). editor: Prosthetic Valves for Cardiac Surgery. Springfield, Ill.: C.C. Thomas. (Conference on Prosthetic Valves for Cardiac Surgery, Chicago, Ill., 1960).
- Mir Sepasi, M.H. et al (1975). The Construction of Individual Leaflets for Aortic Valve Replacement. *J. Surg. Res.* 18(1):75-80.
- Missen, G.A. et al (1970). Calcification and Cusp Rupture in Human Aortic Valve Homografts Sterilized by Ethylene Oxide and Freeze-Dried. *Lancet* 2:962-964.
- Missirlis, Y.F. (1973). In-Vitro Studies of Human Aortic Valve Mechanics. Ph. D. Thesis, Rice Univ., Houston.
- Missirlis, Y.F. and Armeniades, C.D. (1976). Stress Analysis of the Aortic Valve During Diastole: Important Parameters. *J. Biomechanics* 9(7):477-480.
- Missirlis, Y.F. and Armeniades, C.D. (1977). Ultrastructure of the Human Aortic Valve. *Acta Anat.* 98(2):199-205.

- Mohri, H. et al (1969). Viable Aortic Valve Heterotransplantation. *Circ.* 39,40(Suppl. I):1-11.
- Mohri, H. et al (1973). Design and Durability of Silastic Trileaflet Aortic Valve Prosthesis. *J. Thorac. Cardiovasc. Surg.* 65(4):576-582.
- Moore, C.H. et al (1975). Analysis of Homograft Valve Failure in 311 Patients Followed Up to Ten Years. *Ann. Thorac. Surg.* 20(3):274-281.
- Morris, D.C. et al (1976). Hemodynamic Evaluation of the Porcine Xenograft Aortic Valve. *Amer. J. Cardiology* 37(1):157.
- Mundth, M.D. et al (1971). Development of a Method for Stress-Strain Analysis of Cardiac Valvular Tissue. *Curr. Topics in Surg. Res.* 3(1):67-72.
- Murray, G. et al (1938). Reconstruction of the Valves of the Heart. *Can. Med. Assoc. J.* 38(4):317-319.
- Murray, G. et al (1956). Homologous Aortic Valve Segment Transplants as Surgical Treatment for Aortic and Mitral Insufficiency. *Angiology* 7(5):466-471.
- Mustard, J.F. et al (1970). Thromboembolism: Manifestation of Blood to Injury. *Circ.* 42(1):1-21.
- Ng, Y.L. and Wright, J.E.C. (1975). Effect of Preservation on the Elasticity of Human Aortic Valve Homografts. *Thorax* 30(3):266-270.
- Nuno-Conceição, A. et al (1975). Homologous Dura Mater Cardiac Valves. Structural Aspects of Eight Implanted Valves. *J. Thorac. Cardiovasc. Surg.* 70(3):499-508.
- O'Brien, M.F. and Clarebrough, J.K. (1966). Heterograft Aortic Valve Transplantation for Human Valve Disease. *Med. J. Aust.* 2(5):228-230.
- O'Brien, M.F. (1967). Heterograft Aortic Valves for Human Use: Valve Bank, Techniques of Measurement and Implantation. *J. Thorac. Cardiovasc. Surg.* 53(3):392-397.
- O'Brien, M.F. et al (1970). Heterograft Valves: An Analysis of Clinical Results of Valve Replacement. *Circ.* 41 (Suppl. II):16-19.
- Olin, C. (1971). Pulsatile Flow Studies of Prosthetic Aortic Valves. *Scand. J. Thorac. Cardiovasc. Surg.* 5(1):1-12.

- Olsen, E.G.J. et al (1975). Fascia Lata Valves: A Clinico-pathological Study. *Thorax* 30(5):528-534.
- Pacifico, A.D. et al (1972). Homografts for Replacement of the Aortic Valve. *Circ.* 45(Suppl. I):36-43.
- Padula, R.T. et al (1970). In-Vivo Cinephotographic Analysis of the Hydrodynamics of Prosthetic Cardiac Valves. *Surgery* 68(6):1018-1025.
- Parker, R. et al (1977). Elasticity of Frozen Aortic Valve Homografts. *Cardiovasc. Res.* 11(2):156-159.
- Peskin, C.S. (1974). The Differential Geometry of Heart Valves. *J. Franklin Inst.* 297:355.
- Pine, M. et al (1976). Homograft and Prosthetic Aortic Valve Replacement: A Comparative Study. *Circ.* 54(Suppl. III): 84-89.
- Pipkin, R.D. et al (1976). Evaluation of Aortic Valve Replacement with a Porcine Xenograft without Long Term Anticoagulation. *J. Thorac. Cardiovasc. Surg.* 71(2):179-186.
- Pluth, J.R. and McGoon, D.C. (1974). Current Status of Heart Valve Replacement. *Mod. Concepts Cardiovasc. Dis.* 48: 65-70.
- Puig, L.B. (1972). Homologous Dura Mater Cardiac Valves: Preliminary Study of 30 Cases. *J. Thorac. Cardiovasc. Surg.* 64(1):154-160.
- Puig, L.B. et al (1977). Four Years Experience with Dura Mater Cardiac Valves. *J. Thorac. Cardiovasc. Surg.* 18(3):247-255.
- Quinton, W.E. et al (1961). An Accelerated Fatigue Pump for Testing Prosthetic Aortic Valves, in Prosthetic Valves for Cardiac Surgery (editor: K.A. Merendino). Springfield, Illinois: C.C. Thomas. Chapter 3:234-241.
- Ramos, G. et al (1973). Evaluation of Physical Properties of Biological Tissues that can be used for Reconstruction of Cardiac Valves. An Experimental Study. *J. Thorac. Cardiovasc. Surg.* 65(3):359-363.
- Reis, R.L. et al (1971). The Flexible Stent. A New Concept in the Fabrication of Tissue Heart Valve Prostheses. *J. Thorac. Cardiovasc. Surg.* 62(5):683-689.
- Retzius, A. (1843). Uber den Mechanismus des Zschliessens der Halbmond Formigen Klappen. *Muller Arch.*:14-18.

- Rigby, B.J. et al (1959). The Mechanical Properties of Rat Tail Tendon. *J. Gen. Physiol.* 43(2):265-283.
- Robel, S.B. et al (1964). The Effect of Pressure on the Configuration of the Aortic Valve. *Trans. Amer. Soc. Artif. Int. Org.* 10:218-222.
- Robel, S.B. (1972). Structural Mechanics of Aortic Valve, in Prosthetic Replacement of the Aortic Valve. Springfield, Illinois: C.C. Thomas. Chapter 1:3-37.
- Roberts, D.L. et al (1976). Long Term Survival Following Aortic Valve Replacement. *Amer. Heart J.* 91(3):311-319.
- Roberts, W.C. and Morrow, A.G. (1966). Renal Hemosiderosis in Patients with Prosthetic Aortic Valves. *Circ.* 33(3):390-398.
- Roberts, W.C. and Morrow, A.G. (1972). Causes of Death and Other Anatomic Observations after Cardiac Valve Replacement. *Adv. Cardiology* 7:226-247.
- Roberts, W.C. (1974). Left Ventricular Outflow Tract Obstruction and Aortic Regurgitation, in The Heart (editor: J.E. Edwards). Baltimore: William & Wilkin Co. Chapter 7:110-175.
- Roberts, W.C. (1976). Choosing a Substitute Cardiac Valve: Type, Size, Surgeon. *Amer. J. Cardiology* 38(5):633-644.
- Roe, B.B. (1969). Late Follow-Up Studies on Flexible Leaflet Prosthetic Valves. *J. Thorac. Cardiovasc. Surg.* 58(1):59-61.
- Roschke, E.J. (1973). An Engineer's View of Prosthetic Heart Valve Performance. *Biomat., Med. Dev., Artif. Org.* 1(2):249-290.
- Ross, D.N. (1962). Homograft Replacement of the Aortic Valve. *Lancet* 2:487.
- Ross, D.N. (1964). Homotransplantation of the Aortic Valve in the Subcoronary Position. *J. Thorac. Cardiovasc. Surg.* 47(6):713-719.
- Ross, D.N. (1967). Replacement of Aortic and Mitral Valves with a Pulmonary Autograft. *Lancet* 2:956-958.
- Ross, D.N. (1972). Biologic Valves: Their Performance and Prospects. *Circ.* 45(6):1259-1272.

- Ross, D.N. and Geens, M. (1972). Heart Valve Replacement with Pulmonary Autografts, in Biological Tissue in Heart Valve Replacement (editor: M.I. Ionescu). London: Butterworth & Co. Chapter 25:575-599.
- Ross Jr., J. et al (1966). Left Ventricular Performance During Muscular Exercises. Circ. 34(4):597-608.
- Rothlin, M. and Senning, A. (1973). Ten Years Follow-Up after Fascia Lata Replacement of the Aortic Valve. J. Cardiovasc. Surg. (Torino) Spec. Issue:339-343.
- Sands, M.P. et al (1969). An Anatomical Comparison of Human, Pig, Calf, and Sheep Aortic Valves. Ann. Thorac. Surg. 8(5):407-414.
- Sauvage, L.R. et al (1963). Pericardial Autografts in Clinical Surgery. Surgery 53(2):213-221.
- Sauvage, L.R. et al (1968). Prosthetic Heart Valve Replacements. Ann. N.Y. Acad. Sci. 146(1):289-313.
- Sauvage, L.R. et al (1972). Prosthetic Replacement of the Aortic Valve. Springfield, Illinois: C.C. Thomas.
- Sauvage, L.R. and Wood, S.J. (1972). Prosthesis Development, in Prosthetic Replacement of the Aortic Valve. Springfield, Illinois: C.C. Thomas. Chapter 5:157-209.
- Schumacker, H.B. et al (1970). Autogenous Tissue Cardiac Valves. Surgery 70(6):848-855.
- Senning, A. (1967). Fascia Lata Replacement of Aortic Valves. J. Thorac. Cardiovasc. Surg. 54(4):465-470.
- Senning, A. et al (1975). The Late Fate of Autologous Fascia Lata Valve Grafts in the Aortic Position. Isr. J. Med. Sci. 11(2-3):179-184.
- Skeleton, J. (1974). Textiles in Biomedical Devices - Some Unrecognized Variables. Biomat., Med. Dev., Artif. Org. 2(4):345-352.
- Slaughter, L. (1973). Prosthetic Valvular Endocarditis: A Twelve-Year Review. Circ. 47(6):1319-1326.
- Smeloff, E.A. et al (1966). Comparative Study of Prosthetic Heart Valves. J. Thorac. Cardiovasc. Surg. 52(6):841-848.
- Smeloff, E.A. et al (1974). Isolated Single Valve Replacement with the Smeloff-Cutter Prosthesis: 1966-1972. Adv. Cardiology 11:211-215.

- Smith, J.C. (1967). The Pathology of Human Aortic Valve Homografts. *Thorax* 22(2):114-118.
- Soden, P.D. and Kershaw, I. (1974). Tensile Testing of Connective Tissues. *Med. Biol. Eng.* 12(7):510-523.
- Spaan, J.A.E. et al (1975). Hydrodynamic Factors Causing Large Mechanical Tension Peaks in Leaflets of Artificial Triple Leaflet Valves. *Trans. Amer. Soc. Artif. Int. Org.* 21:396-404.
- Starkey, W.L. et al (1963). The Design and Development of a Cardiac Simulator for the Evaluation of Heart Valve Prostheses. *J. Thorac. Cardiovasc. Surg.* 46(2):207-211.
- Starr, A. and Edwards, M.L. (1961). Mitral Replacement: Clinical Experience with a Ball Valve Prosthesis. *Ann. Surg.* 154(4):726-740.
- Starr, A. et al (1969). Accumulated Experience with the Starr-Edwards Prostheses: 1960-68, in Prosthetic Heart Valves (editor: L.A. Brewer III). Springfield, Ill.: C.C. Thomas. Chapter 31:468-478.
- Starr, A. et al (1977). Aortic Valve Replacement: A Ten-Year Follow-Up of Non-Cloth-Covered versus Cloth-Covered Caged Ball Prostheses. *Circ.* 56(Suppl. II):133-138.
- Steenhoven, A.A. et al (1976). Two-Dimensional Model Experiments on the Closing of the Aortic Valve. Dept. Mech. Eng. & Physics, Eindhoven Univ. of Tech., the Netherlands.
- Stein, P.D. and Sabbah, H.N. (1976). Turbulent Blood Flow in the Ascending Aorta of Human in Normal and Diseased Aortic Valves. *Circ. Res.* 39(1):58-65.
- Steinmetz, G.P. et al (1964). An Improved Accelerated Fatigue Machine and Pulse Duplicator for Testing and Developing Prosthetic Cardiac Valves. *J. Thorac. Cardiovasc. Surg.* 47(2):186-198.
- Stinson, E.B. et al (1968). Aortic Valve Replacement with the Fresh Valve Homograft. *Amer. J. Surg.* 116(2):204-209.
- Stinson, E.B. et al (1977). Long Term Experience with Porcine Aortic Valve Xenografts. *J. Thorac. Cardiovasc. Surg.* 73(1):54-63.
- Störmer, B. et al (1976). Comparative Study of In-Vitro Flow Characteristics between a Human Aortic Valve and a Designed Aortic Valve and Six Corresponding Types of Prosthetic Heart Valves. *Eur. Surg. Res.* 8(2):117-131.

- Strawich, E. et al (1974). Chemical Composition and Biophysical Properties of Porcine Cardiovascular Tissues. *Biomat., Med. Dev., Artif. Org.* 3(3):309-318.
- Swanson, W.M. and Clark, R.E. (1973). Aortic Valve Leaflet Motion During Systole. *Circ. Res.* 32(1):42-48.
- Swanson, W.M. and Clark, R.E. (1974). Dimensions and Geometry Relationships of the Human Aortic Valve as a Function of Pressure. *Circ. Res.* 35(6):871-882.
- Sutera, S.P. et al (1972). Hemodynamic and Sub-Hemodynamic Alterations of Human Red Blood Cell Induced by Turbulence. *Trans. Amer. Soc. Artif. Int. Org.* 18:335-341.
- Sutera, S.P. et al (1977). Flow Induced Trauma to Blood Cells. *Circ. Res.* 41(1):2-8.
- Tan, A.J.K. and Holt, D.L. (1976). The Effects of Sterilization and Storage Treatments on the Stress-Strain Behaviour of Aortic Valve Leaflets. *Ann. Thorac. Surg.* 22(2):188-194.
- Temple, L.J. et al (1964). Principles of Fluid Mechanics Applied to Some Situations in the Human Circulation and particularly to the Testing of Valves in a Pulse Duplicator. *Thorax* 19(3):261-267.
- Templeton, J.Y. and Gibbson, J.H. (1949). Experimental Reconstruction of Cardiac Valves by Venous and Pericardial Grafts. *Ann. Surg.* 129(2):161-176.
- Thompson, F.J. and Barratt-Boyes, B.G. (1977). The Glutaraldehyde-Treated Heterograft Valve. Some Engineering Observations. *J. Thorac. Cardiovasc. Surg.* 74(2):317-321.
- Timoshenko, S. and Woinowsky-Krieger, S. (1959). Theory of Plates and Shells. 2nd edition. New York: McGraw Hill Book Co. p. 533-534.
- Trimble, A.S. et al (1969a). Cinematographic Evaluation of Homograft Aortic Valve Function Using an Internal Pulse Duplicator. Part I: The Importance of Donor Valve Size. *J. Thorac. Cardiovasc. Surg.* 58(1):48-53.
- Trimble, A.S. et al (1969b). Cinematographic Evaluation of Homograft Aortic Valve Function Using an Internal Pulse Duplicator. Part II: The Effects of Sterilization and Storage. *J. Thorac. Cardiovasc. Surg.* 58(1):54-58.
- Van Brocklin, J.D. and Ellis, D.G. (1965). Study of the Mechanical Behaviour of Toe Extensor Tendons under Applied Stress. *Arch. Phys. Med. & Rehab.* 46(5):369-373.

- Viggers, R.F. (1972). Hydraulics of the Aortic Valve, in Prosthetic Replacement of the Aortic Valve. Springfield, Illinois: C.C. Thomas. Chapter 2:38-80.
- Viner, E.D. and Frost, J.W. (1965). Hemolytic Anemia Due to a Defective Teflon Aortic Valve Prosthesis. *Ann. Int. Med.* 63(2):295-301.
- Wallace, R.B. et al (1974). Aortic Valve Replacement with Preserved Aortic Valve Homografts. *J. Thorac. Cardiovasc. Surg.* 67(1):44-52.
- Wallace, R.B. (1975). Tissue Valves. *Amer. J. Cardiology* 35(6):866-871.
- Waterworth, P.M. et al (1974). A Critical Investigation into the Antibiotic Sterilization of Heart Valve Homografts. *Thorax* 29(4):432-436.
- Welch, W. et al (1969). A Comparative Study of Different Methods of Processing Aortic Homografts. *Thorax* 24(9):746-749.
- Wesolowski, S.A. et al (1962). The Production and Significance of Turbulence in Hemic Systems. *Trans. Amer. Soc. Artif. Int. Org.* 8:11-16.
- Wessel, H.U. et al (1962). A Simple External Pulse Duplicator for Observation of Cardiac Valvular Action. *J. Thorac. Cardiovasc. Surg.* 43(4):513-516.
- Wieting, D.W. et al (1966). Design of a System for Analyzing Flow Behaviour of Prosthetic Human Heart Valves. *Cardiovasc. Res. Cen. Bull. (Baylor Coll. of Med.)* 5:41.
- Wieting, D.W. et al (1969). Dynamic Flow Behaviour of Artificial Heart Valves, in Prosthetic Heart Valves (editor: L.A. Brewer III). Springfield, Illinois: C.C. Thomas. Chapter 4:34-49.
- Williams, G.R. et al (1969). The Use of Structured Fibrocollagenous Tissue as Partial and Complete Replacement of Cardiac Valves, in Prosthetic Heart Valves (editor: L.A. Brewer III). Springfield, Illinois: C.C. Thomas. Chapter 59:832-836.
- Wright, J.E.C. and Ng, Y.L. (1974). Elasticity of Human Aortic Valve Cusps. *Cardiovasc. Res.* 8(3):384-390.
- Wright, J.T.M. and Temple, L.J. (1971). An Improved Method for Determining the Flow Characteristics of Prosthetic Mitral Heart Valves. *Thorax* 26(1):81-88.

- Wright, J.T.M. (1972). The Heart, Its Valves and Their Replacement. *Bio-Medical Engineering* 7(1):26-33.
- Wright, J.T.M. and Brown, M.C. (1977). A Method for Measuring the Mean Pressure Gradient Across Prosthetic Heart Valves under In-Vitro Pulsatile Flow Conditions. *Med. Instrum.* 11(2):110-113.
- Wright, J.T.M. and Temple, L.J. (1977). A Flow Visualization Study of Prosthetic Aortic and Mitral Valves in a Model of the Aorta and Left Heart. *Eng'g. in Medicine* 6(2):31-45.
- Yamada, H. (1973). Tensile Properties of Cardiac Valves, in Strength of Biological Materials (editor: F.G. Evans). Huntington, New York: R.E. Krieger Publ. Co. p. 109-110.
- Yarbrough, J.W. et al (1973). Structural Alterations in Tissue Cardiac Valves Implanted in Patients and in Calves. *J. Thorac. Cardiovasc. Surg.* 65(3):364-375.
- Yeh, T.J. et al (1965). Hemolytic Anemia Due to a Ruptured Prosthetic Aortic Cusp. *J. Thorac. Cardiovasc. Surg.* 49(6):963-967.
- Yellin, E.L. (1966). Laminar-Turbulent Transition Process in Pulsatile Flow. *Circ. Res.* 19(6):791-804.
- Zuhdi, N. et al (1974). Porcine Aortic Valves as Replacements for Human Heart Valves. *Ann. Thorac. Surg.* 17(5):479-491.
- Zuhdi, N. (1976). The Porcine Aortic Valve Bioprosthesis: A Significant Alternative. *Ann. Thorac. Surg.* 21(6):573-576.

APPENDIX A

Microtensile Stress-Strain Theory and Terminology

1. Stress-Strain Relationships

A tissue strip in its relaxed state and in its loaded state is shown in figure A1. However, the illustration of the "necking" shown as a variable area along the strip length is exaggerated. Inhomogeneity is investigated by dividing the total strip length into individual sections as defined by the dots. The instantaneous tension force (F), cross-sectional area (A) and length (l) are the primary variables. Subscript 'o' denotes the initial unloaded state. Subscript 'T' denotes total strip whereas subscript 'i' denotes the i^{th} section.

The instantaneous strains (ϵ) are defined by:

$$\epsilon_T = \frac{l_T - l_{oT}}{l_{oT}} = \frac{l_T}{l_{oT}} - 1 \quad (1)$$

$$\epsilon_i = \frac{l_i - l_{oi}}{l_{oi}} = \frac{l_i}{l_{oi}} - 1 \quad (2)$$

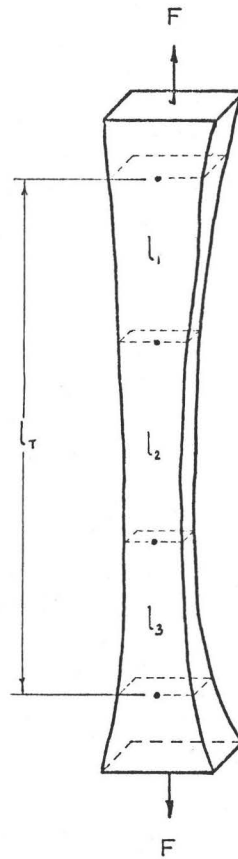
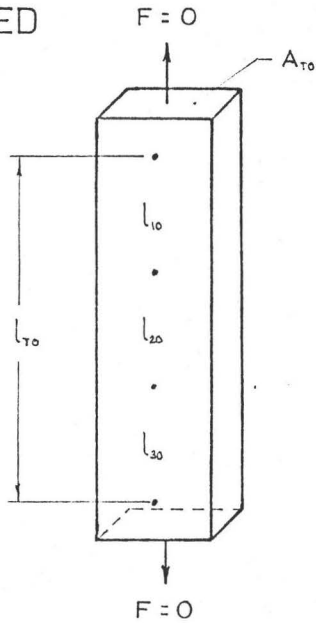
and the instantaneous stresses (σ) are defined by:

$$\sigma_T = \frac{F_T}{A_T} \quad (3)$$

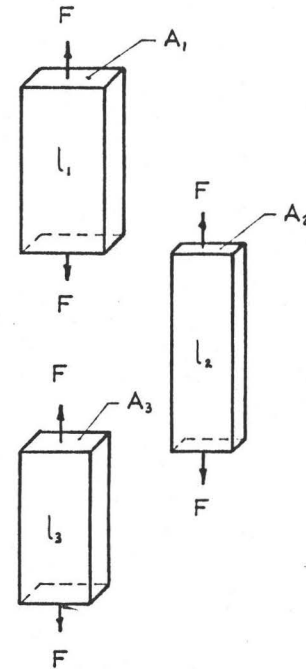
$$\sigma_i = \frac{F_i}{A_i} = \frac{F_T}{A_i} \quad \begin{array}{l} \text{since } F_i = F_j = F_k = \dots = F_T \\ \text{because of tension continuity} \end{array} \quad (4)$$

FIGURE A1.
MICROTENSILE STRIP and NECKING

UNSTRESSED STATE



STRESSED STATE



$$F = F_1 = F_2 = F_3$$

$$l_T = l_1 + l_2 + l_3$$

A_i and A_{i0} are length-averaged

$$\epsilon_i = \frac{l_i - l_{i0}}{l_{i0}}, \quad i = 1, 2, 3$$

$$\epsilon_T = \frac{l_T - l_{T0}}{l_{T0}} = \sum_i^3 \frac{l_{i0}}{l_{T0}} \cdot \epsilon_i$$

$$\sigma_i = \frac{F}{A_i}, \quad i = 1, 2, 3$$

$$\frac{1}{\sigma_T} = \sum_i^3 \frac{l_i}{l_T} \cdot \frac{1}{\sigma_i}$$

Because of necking, A_i and A_T are determined by averaging over their respective lengths. If necking is severe, then

$$A_{i-1} \neq A_i \neq A_{i+1} \quad (5)$$

A constant volume (V) tissue strip is assumed; hence

$$V = A \cdot l = A_0 \cdot l_0 = \text{constant} \quad (6)$$

and

$$A = A_0 \cdot \frac{l_0}{l} = \frac{A_0}{1 + \epsilon} \quad (7)$$

Differentiating equation (6) gives

$$dV = dA \cdot l + A \cdot dl = 0 \quad (8)$$

where dA is a decrease in the cross-sectional area and

dl is an increase in the length due to straining.

From equation (8), the following relationships are derived.

$$\frac{dA}{A} = - \frac{dl}{l_0} = -\epsilon \quad (9)$$

$$\frac{dl}{l} = - \frac{dA}{A_0} \quad (10)$$

Herein, the subscripts 'T' and 'i' are omitted for clarity.

The instantaneous stresses may be rearranged as

$$\sigma = \frac{F}{A} = \frac{F}{A_0} \cdot (1 + \epsilon) \quad (11)$$

If the instantaneous area (A) is not used for the F - l to σ - ϵ conversions (eg., as in the case where there are difficulties in monitoring a continuously changing A), then the usual procedure is to use a single A for the calculations. One method has been to use A_0 which is the average cross-sectional area

at zero load [Clark, 1973; Missirlis, 1973]. The stress so calculated underestimates the true stress. It is referred to as the nominal stress,

$$\sigma^* = \frac{F}{A_0} \quad (12)$$

Thus, the true stress using equations (11) and (12) becomes

$$\sigma = \sigma^* \cdot (1 + \epsilon) \quad (13)$$

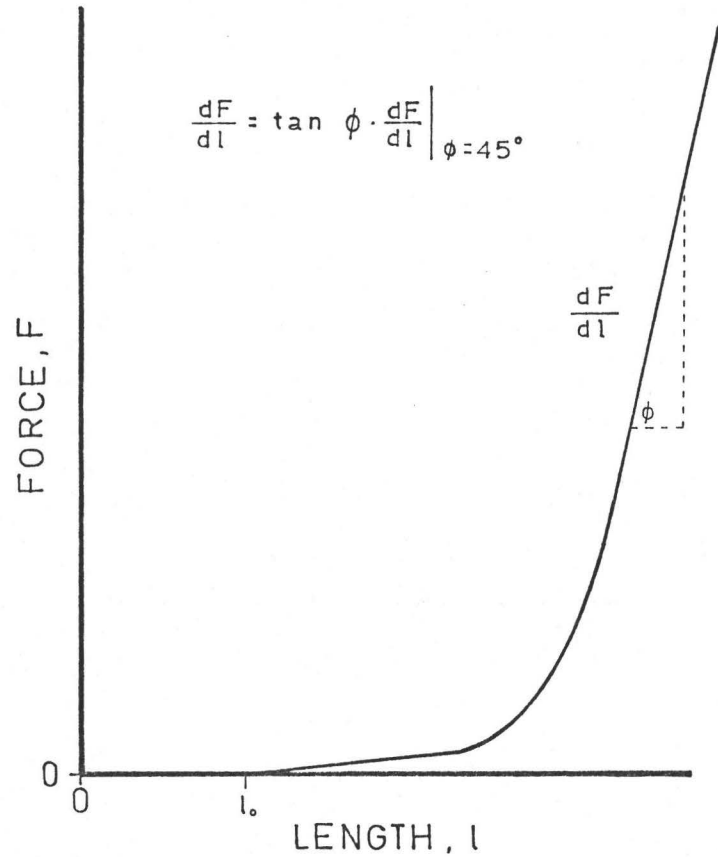
Stress calculations are therefore dependent on the strain level and on the amount of necking. For small strains and minimal necking, the error between the true stress and the nominal stress is negligible. But for large strains for which there is considerable associated necking, the error can be large being in the same order as the strain; that is,

$$\frac{\Delta\sigma}{\sigma} = \frac{\sigma - \sigma^*}{\sigma} = \frac{\epsilon}{1 + \epsilon} \quad (14)$$

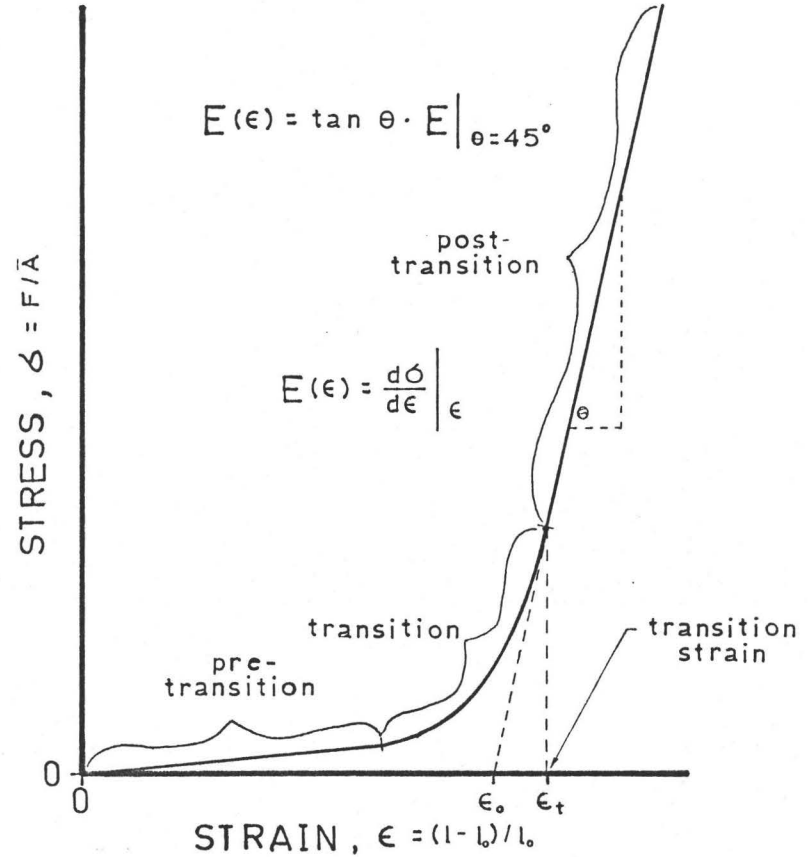
2. Stress-Strain Curve Terminology

A typical non-linear two-phase stress-strain curve for a biological tissue is illustrated in figure A2. The key parameters consist of the low pre-transition elastic modulus (E_{pre}), the high post-transition elastic modulus (E_{post}), the transition stress (σ_t), the transition strain (ϵ_t) and the zero-stress extrapolated strain (ϵ_0). The particular shape of the σ - ϵ curve is biological in origin being based on the content and structure of the collagen and elastin network. For example, a large content in elastin or a highly wavy collagen

FIGURE A2.
STRESS-STRAIN TERMINOLOGY



$$\sigma = \frac{F}{A} = \frac{F(1 + \epsilon)}{A_0}$$



$$E = \frac{d\sigma}{d\epsilon} = \frac{1 + \epsilon}{A_0} \cdot \left[\frac{dF}{dl} \cdot l_0 + F \right]$$

structure increases ϵ_t , and a higher density of the collagen cross-linking increases E_{post} . A sharp "knee" at transition is indicative of a high similarity in the cross-linkages.

The corresponding force-length curve is also shown. For the i^{th} section of a microtensile strip in a state that is described by (F_i, l_i, A_i) , strains and stresses are given by equations (2) and (4).

3. Determination of Elastic Moduli

In engineering, the elastic modulus is defined as the slope of a stress-strain curve (ie., $E = d\sigma/d\epsilon$). Since there are incurrent errors in the $F-l$ to $\sigma-\epsilon$ conversions, errors in calculating the instantaneous E from the slope of the $\sigma-\epsilon$ curve are compounded. The following is a derivation that can be used to determine the instantaneous E directly from the force-length curve:

$$E = \frac{\partial \sigma}{\partial \epsilon} = \frac{\partial (F/A)}{\partial ((l - l_0)/l_0)} = \frac{(\partial F \cdot A - \partial A \cdot F)/A^2}{\partial l/l_0} \quad (15)$$

$$E = \frac{\partial F}{\partial l} \cdot \frac{l_0}{A} - \frac{\partial A}{\partial l} \cdot \frac{F \cdot l_0}{A^2} \quad (16)$$

Using equation (9) from the constant volume assumption,

$$E = \frac{\partial F}{\partial l} \cdot \frac{l_0}{A} + \frac{A}{l_0} \cdot \frac{F \cdot l_0}{A^2} \quad (17)$$

$$E = \frac{1}{A} \cdot \left[\frac{\partial F}{\partial l} \cdot l_0 + F \right] \quad (18)$$

Thus, the calculation of the instantaneous elastic modulus

for the i^{th} section (E_i) in the state (F_i, l_i) requires the slope ($\partial F_T / \partial l_i$) and the instantaneous area A_i . If the initial area A_{0i} is used, then the elastic modulus can be shown to be a function of the strain (ϵ_i), the tension force ($F_i = F_T$) and the force-length slope ($\partial F_T / \partial l_i$); that is,

$$E = \frac{1 + \epsilon}{A_0} \cdot \left[\frac{\partial F}{\partial l} \cdot l_0 + F \right] \quad (19)$$

Inhomogeneity is observed if $E_{i-1} \neq E_i \neq E_{i+1}$ (20)

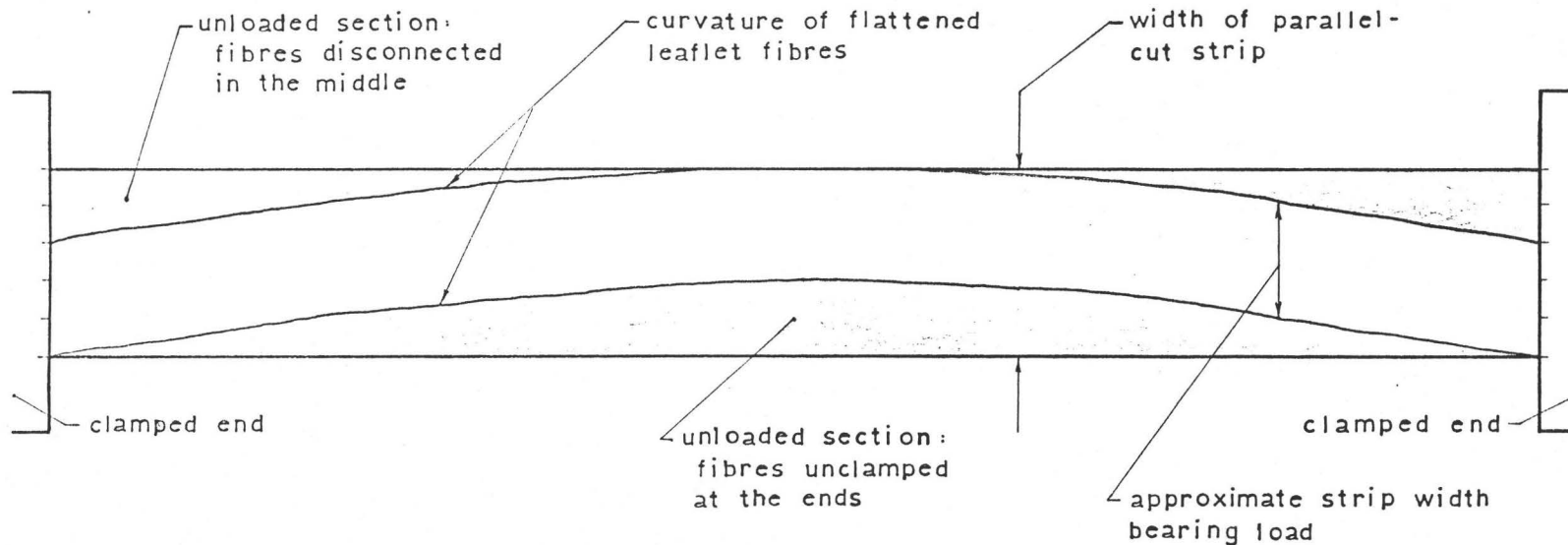
Note that the elastic modulus determined from nominal stress calculations (E^*) underestimates the actual elastic modulus as determined from using equation (19),

$$E^* = \frac{\partial \sigma^*}{\partial \epsilon} = \frac{\partial (F/A_0)}{\partial ((l - l_0)/l_0)} = \frac{\partial F}{\partial l} \cdot \frac{l_0}{A_0} \quad (21)$$

4. Effect of Tissue Curvature on Errors

Tissues with curved arcing fibres do not lend themselves to be cut as microtensile tissue strips by straight-edged blades. This is observed for the aortic valve leaflet and its circumferential collagen fibres. Figure A3 shows how some of the circumferential fibres can be cut. The cut fibres do not support any tension and do not contribute to the true cross-sectional area that supports the tension. However, they do contribute to the measured area. This area overestimation therefore results in an underestimation of the calculated stresses and elastic moduli. The extent of the discrepancy varies inversely as the radii of curvature

FIGURE A3.
EFFECT of TENSILON SAMPLE STRIP CURVATURE



fibre curvature leads to necking and overestimation of the width, w and hence also of the C/S area, A ; accordingly, calculated stresses ($\sigma = F/A$) and elastic moduli ($E = d\sigma/d\epsilon$), are underestimated.

ie. $\frac{\Delta w}{w} = \frac{\Delta A}{A} = -\frac{\Delta \sigma}{\sigma} = -\frac{\Delta E}{E} = \text{error} \approx \frac{l_0}{wR}$ (as illustrated above, error = 40%)

of the fibres, and directly as the length of the microtensile strip (see figure A3).

The cut fibres also encourage the tissue strips to neck. If the instantaneous area of a strip is continuously monitored for the complete loading cycle such as in the case with our experiments, then the effect of necking serves to give truer cross-sectional area measurements. This therefore would compensate for the area overestimation.

In view of the above, it is estimated that errors of this nature in our experiments are no more than 5%. Other errors inherent in the experimental method consist of: 1) errors in the determination of l_0 and 2) measurement errors of the dot-to-dot distance on the photographs of the microtensile strips. Errors associated with l_0 are minimized by slack loading the tissue strip; that is, l_0 is determined (to ± 0.2 mm.) by noting the length on the F-l curve at which tension begins to increase (see figure 10, p. 63 in the main text). Errors of the second type are governed by the size and sharpness of the dots, and also by the mesh size of the dots. An increase in the mesh size of the dots reduces the related errors but it compromises the ability of the experimental method to investigate the inhomogeneity in the tissue strip.

APPENDIX B

Stereophotogrammetry and Experimental Application

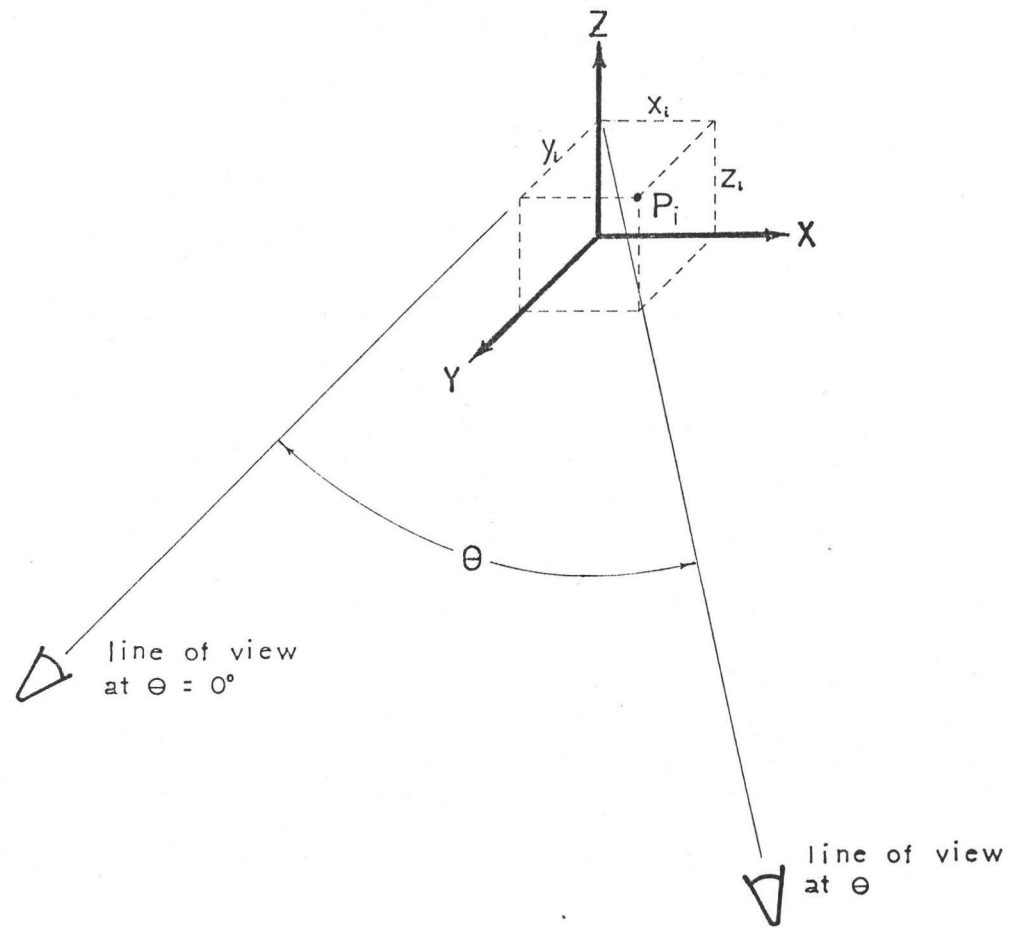
The technique of stereophotogrammetry to identify a point in a fixed global Cartesian coordinate system is well established. Karara and Marzan (1973) and Karara (1975) have used the technique to define the irregular surface geometry of the human aortic valve leaflets. This appendix describes an alternative stereophotogrammetric method that is used in our experiments.

1. Theory

By producing two-dimensional photographs of a three-dimensional object (eg., the valve) for at least two angles of view (θ), the three-dimensional Cartesian coordinates of a point on the object's surface can be determined with the use of simple geometrical relationships. Consider figure B1 which illustrates a point P_i with the coordinates (x_i, y_i, z_i) being viewed from a direction that is defined by the angle θ . The latter is scanned along the horizontal X-Y plane at a constant z ; hence, the coordinate z_i is independent of θ .

From a scaled two-dimensional photograph of point P_i at any angle θ , the coordinate z_i is measured with respect to an arbitrarily fixed reference X-Y plane. The other two

FIGURE B1.
RELATIONSHIP of POINT P_i with ANGLE of VIEW, θ



coordinates (x_i, y_i) can be determined by correlating various linear measurements from photographs of the point P_i for at least two angles of view. One of the angles for reference reasons is labelled as 0° , and it corresponds to the view direction parallel to the Y-axis as shown in figure B1. The other angle is chosen so that its corresponding photograph is also able to record the point P_i . However, more than two angles of view may be used to improve the accuracy of the correlation.

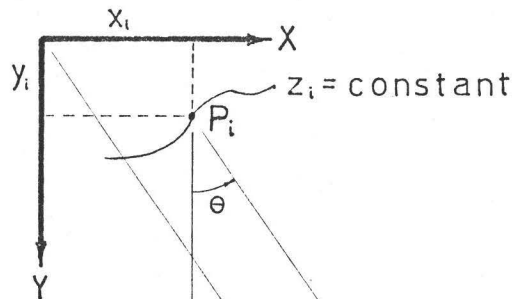
All measurements are relative to an arbitrarily fixed global X-Y-Z axis system to which the object surface and its points are maintained at a constant orientation. As noted previously, z_i is independent of θ and therefore can be measured from any θ photograph; eg., the $\theta = 0^\circ$ photograph. In order to determine the coordinates (x_i, y_i) , refer to figure B2 which shows the top perpendicular view (ie., parallel to the Z-axis) of a X-Y plane slice of the object through the point P_i . Thus, a $\theta = 0^\circ$ photograph of figure B2 will appear as shown in figure B2a, with the measurement d_i directly giving the coordinate x_i ; that is, $d_i(\theta = 0^\circ) = x_i$. The measurement d_i is defined as the perpendicular distance between the Z-axis and the point P_i .

Coordinate y_i is indeterminate from the single $\theta = 0^\circ$ photograph. Its determination requires the use of a θ photograph such as the one illustrated in figure B2b. When x_i is known, the measurement $d_i(\theta)$ may be used to obtain y_i . The

FIGURE B2.
 VIEW of POINT P at VIEW ANGLES 0° and θ°

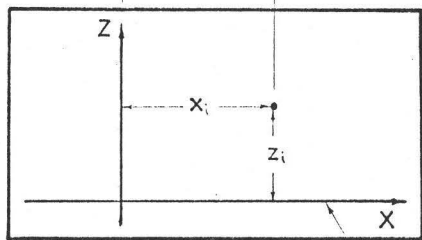
top perpendicular
 view of point P_i
 on surface of
 constant z_i

z -axis is axis
 of rotation

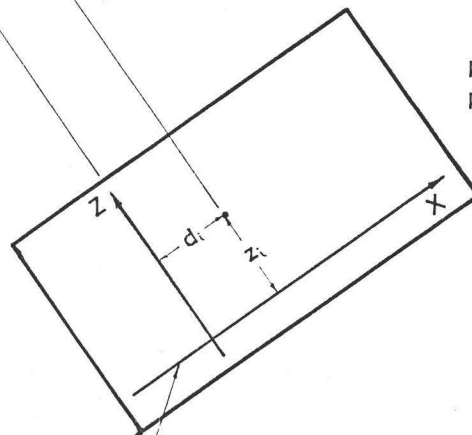


$$y_i = \frac{x_i}{\tan \theta} - \frac{d_i}{\sin \theta}$$

photograph of
 point P_i at $\theta = 0^\circ$



photograph of
 point P_i at θ



arbitrary
 x-y plane

derivation for $y_i = y_i(\theta, x_i, d_i)$ is as follows:

With reference to figure B3, the following geometrical relationships exist:

$$b_i = y_i \cdot \tan \theta \quad (1)$$

$$a_i = x_i - b_i = x_i - y_i \cdot \tan \theta \quad (2)$$

$$d_i = a_i \cdot \cos \theta = (x_i - y_i \cdot \tan \theta) \cdot \cos \theta \quad (3)$$

Solving for y_i ,

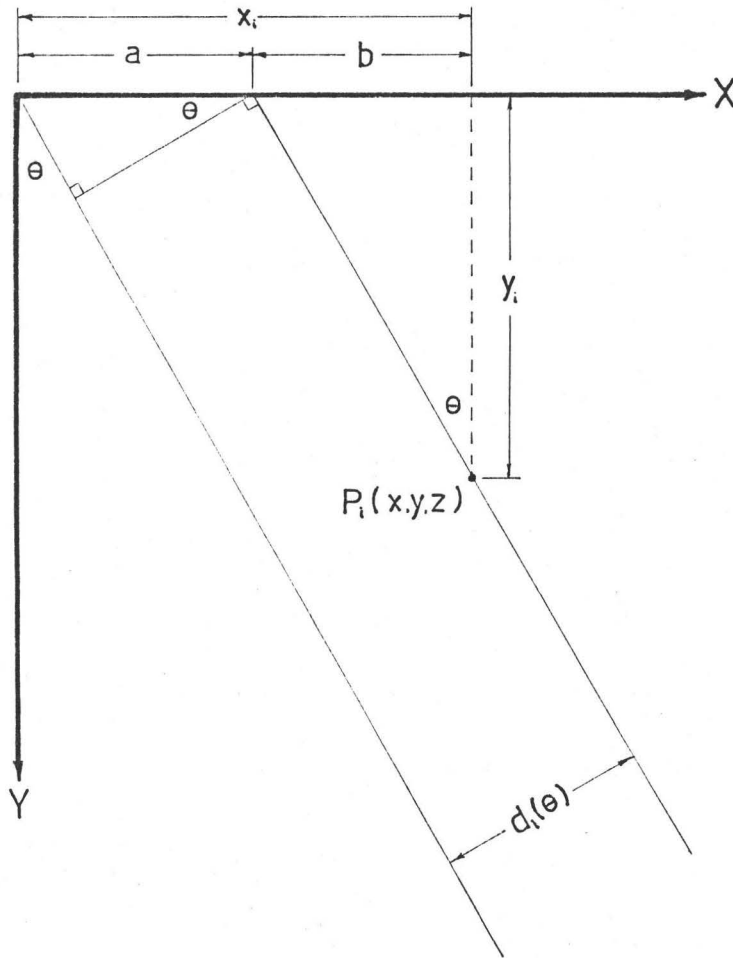
$$y_i = \frac{x_i}{\tan \theta} - \frac{d_i}{\sin \theta} \quad (4)$$

Positive θ is measured counter-clockwise (see figure B2).

The validity of the above derivation depends on the requirement that the light from the points on the surface of the object (ie., the valve) arrives at the camera lens as parallel rays. This would then require the valve to be a far distance from the camera, thus necessitating the use of a telephoto lens. In effect, the telephoto lens helps to reduce any parallax.

Theoretically, it is also conceivable to determine (x_i, y_i, z_i) by using the close-range stereophotogrammetric technique with a shorter lens [Karara, 1975]. The close-range method carries with it the advantages of better depth of field, better resolution and less complicated equipment. A main disadvantage is the required correction for parallax which results in a more complicated geometrical analysis. Also important to consider is the higher quality required of the lens and of the camera in such a system.

FIGURE B3.
GEOMETRY for DERIVATION of y_i
Z-AXIS is the AXIS of ROTATION



$$b = y_i \cdot \tan \theta$$

$$a = x_i - y_i \cdot \tan \theta \quad , \quad x_i = d_i(\theta')$$

$$d_i = a \cdot \cos \theta = (x_i - y_i \cdot \tan \theta) \cdot \cos \theta$$

$$y_i = \frac{x_i}{\tan \theta} - \frac{d_i}{\sin \theta}$$

2. Application to Experiment

The above theory is based on the fact that the variation in the angle θ is produced by rotating the camera about the Z-axis that is situated near the object (ie., the valve). The large lens-to-valve distance (~ 175 cm.) of the telephoto system made the task of constructing the apparatus to perform the rotation particularly difficult. It is more convenient instead to rotate the valve about the Z-axis while keeping the camera fixed with its lens axis aligned in parallel with the Y-axis. However, the global X-Y-Z axis system does not rotate with the valve. This alteration to the theory introduces only one change to the derivation for y_i . Equation (4) for y_i remains unchanged, but positive θ is now measured in the clockwise direction; that is, a CW rotation of the valve is equivalent to an equal CCW rotation of the camera.

In the actual experiment, a 35 mm. camera is coupled to a 300 mm. telephoto ($f/4$), a 2X teleconverter and a 6 cm. extension tube. The camera is height adjusted so that the lens axis is approximately aligned in parallel with the axis of the suspended aortic root as well as with the Y-axis (see figure 15 on p. 71). The valve is suspended at a constant height in a saline tank but it is free to rotate at this height. The orientation of the valve at the reference 0° is such that the number of points on the valve leaflets appearing in the viewfinder of the camera is maximized. The valve suspending jig is fixed onto a valve rotator to which is

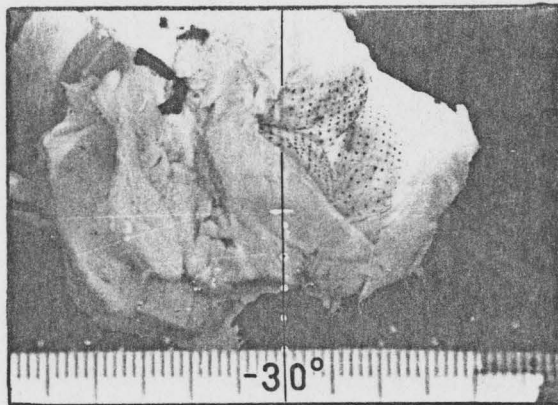
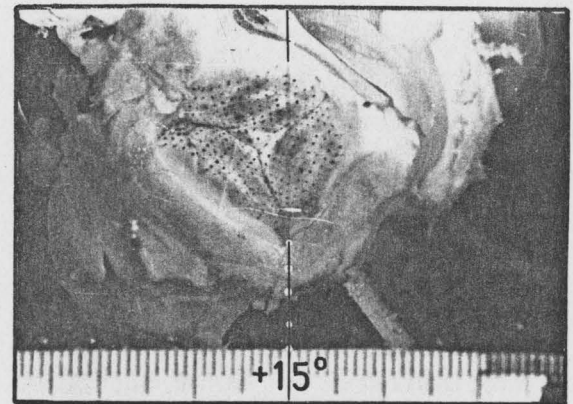
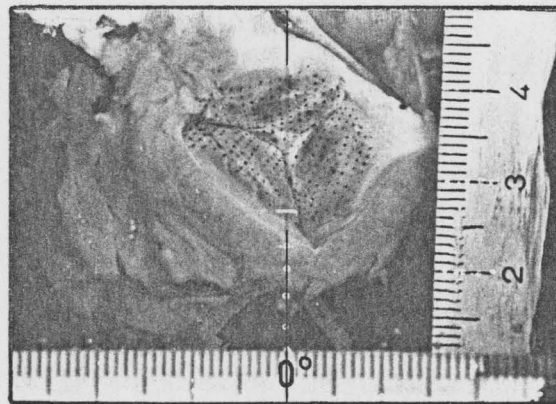
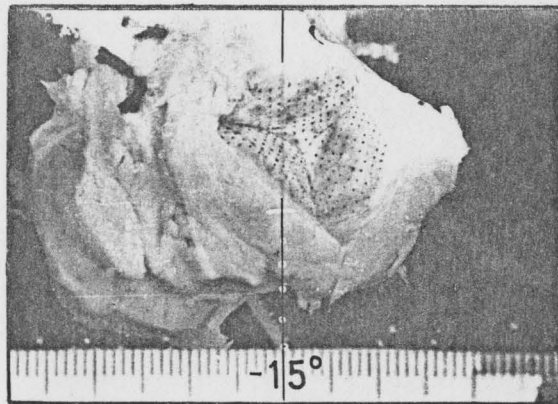
attached a pointer. The latter measures θ from a protractor that is centered at the axis of rotation (see figure 17 on p. 73). The whole apparatus is arranged on a 4 ft. x 8 ft. heavy metal table (see figure 16 on p. 72). The table has a 2 inch grid of threaded holes in which component parts are secured in order to minimize any vibration effects and also to prevent any changes in the relative positioning of the parts. The 6 cm. extension tube is required to reduce the telephoto lens' focusable range to within the confines of the table. It also optimizes the camera magnification so as to best fill the viewfinder with the image of the valve.

A thin thread is plumb-lined in front of the saline tank so that it hangs in the Y-Z plane (see figure 17). When photographed with the valve, the thread appears as a thin line that is coincident with the Z-axis. The latter is the reference line from which the dimensions d_1 are measured.

Kodak Panatomic-X film (ASA 32) is used because the large negative enlargements require its fine grain and high resolving power. Its slow speed coupled with the reduction of light due to the telephoto and the extension tube necessitate very bright illumination of the valve. Two 300 watt photoflood light sources are used. And in order to acquire the maximum depth of field possible (~ 2 mm.), the lens is stopped down to its smallest aperture (f/22). Despite this, some points on the valve leaflets are still rotated out of focus. It is found that the optimum shutter speed is $\frac{1}{4}$ to $\frac{1}{2}$

FIGURE B4.
PORCINE AORTIC VALVE at 0** mm. Hg.

**ZERO LOAD STATE ACTUALLY 3 mm. Hg.



note folding and buckling in the
leaflets' Node of Aranti regions

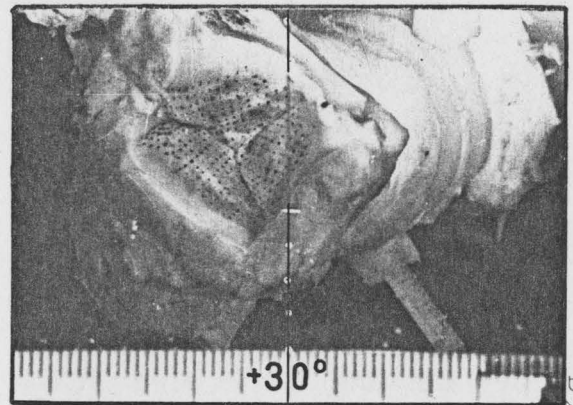


FIGURE B5.
PORCINE AORTIC VALVE at 20 mm. Hg.

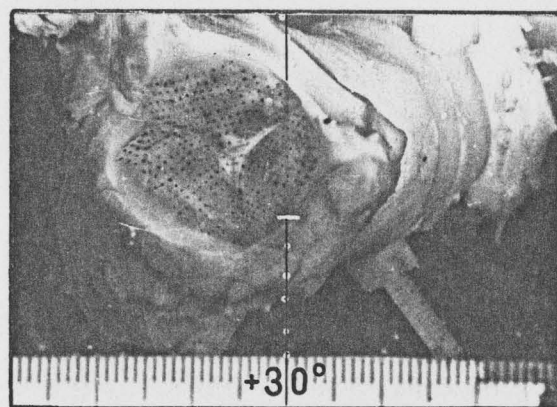
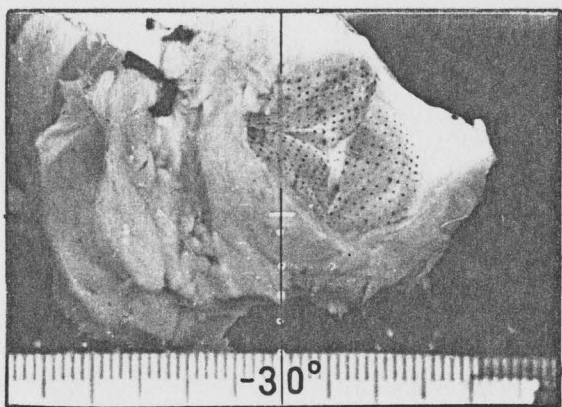
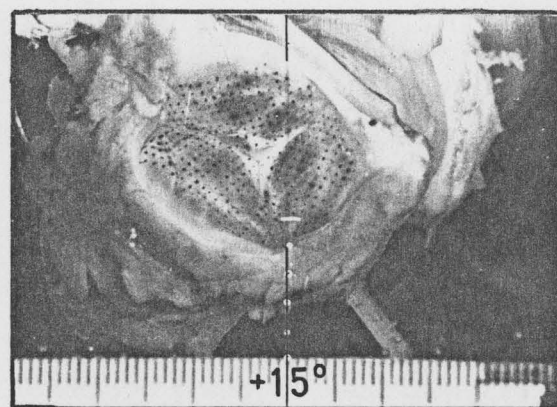
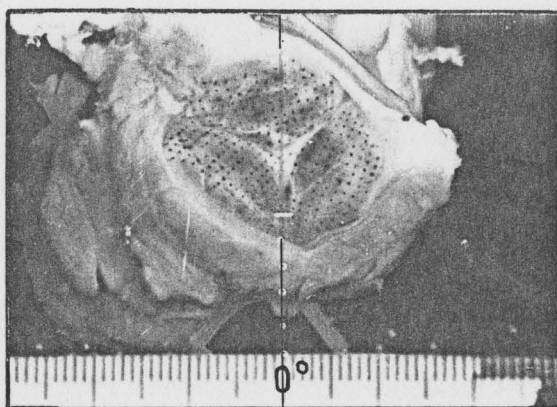
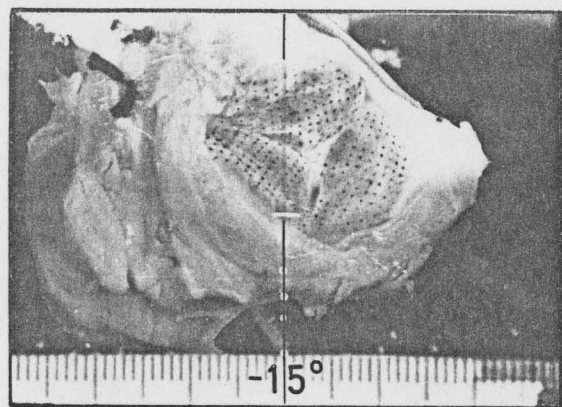


FIGURE B6.
PORCINE AORTIC VALVE at 40 mm. Hg.

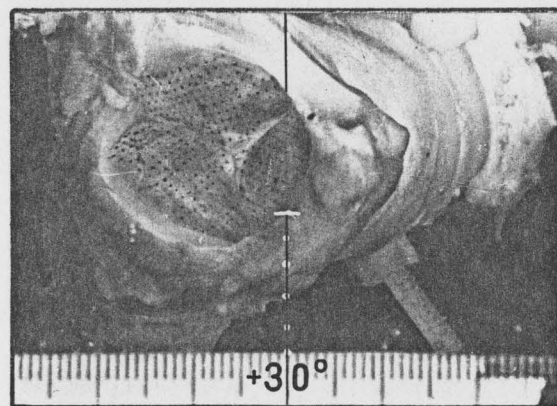
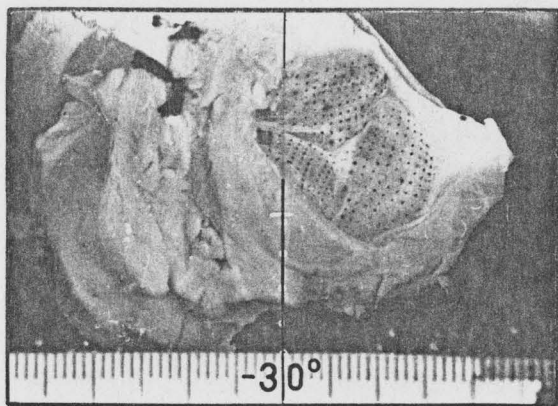
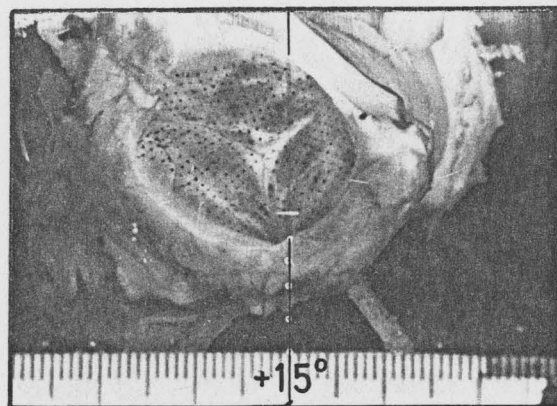
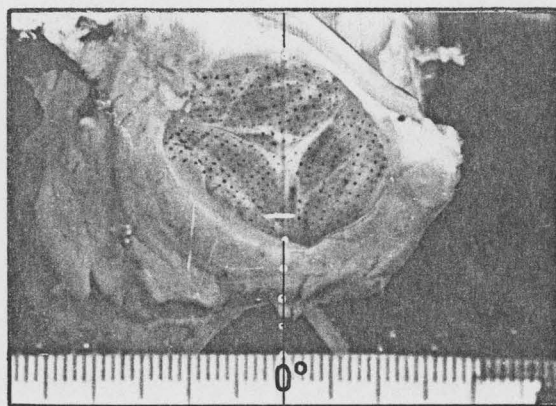
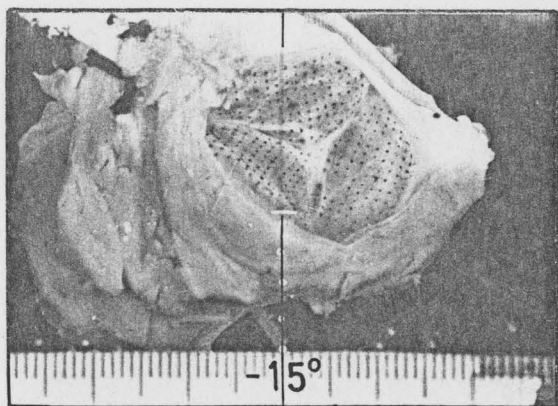


FIGURE B7.
PORCINE AORTIC VALVE at 60 mm. Hg.

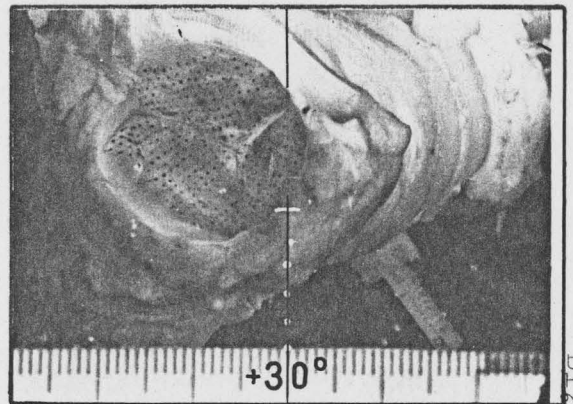
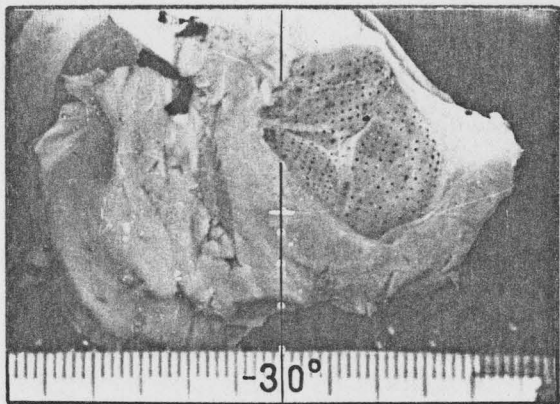
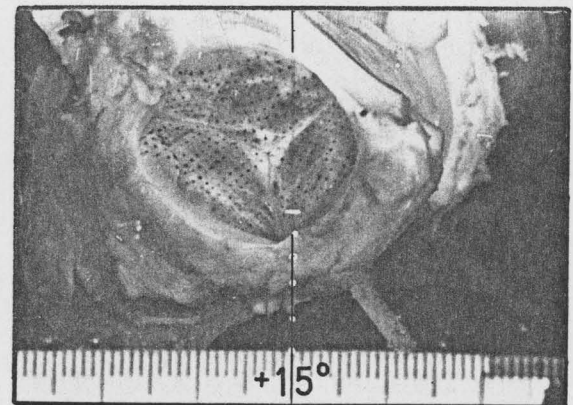
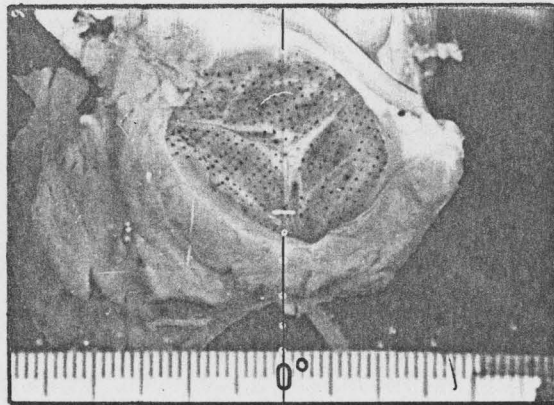
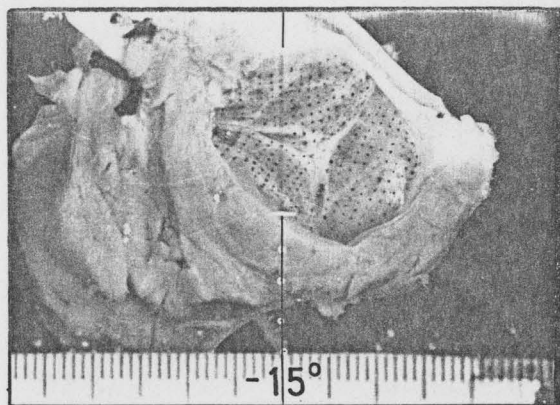


FIGURE B8.
PORCINE AORTIC VALVE at 80 mm. Hg.

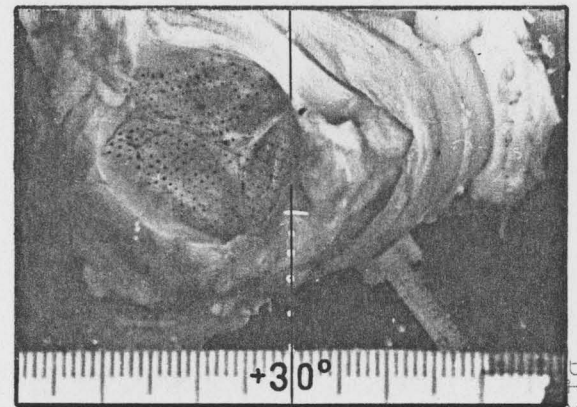
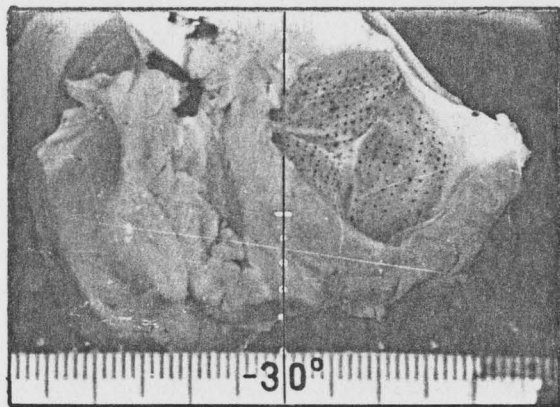
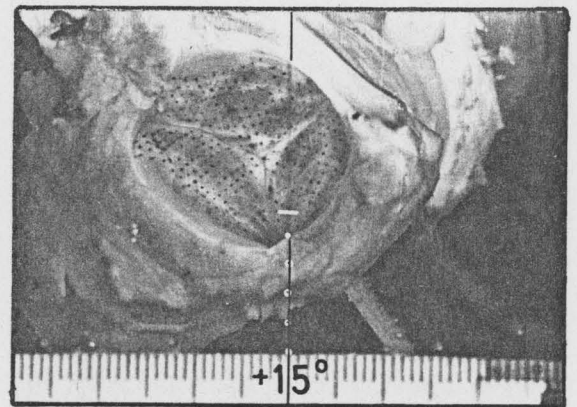
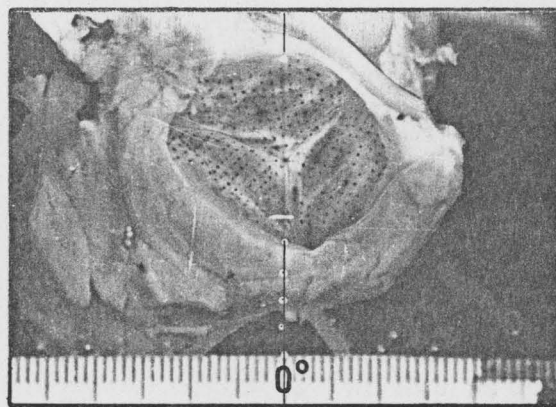
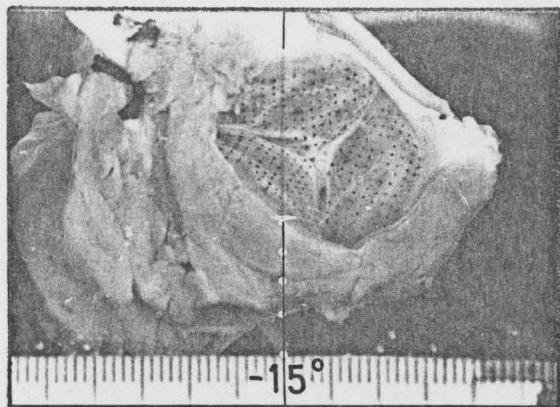


FIGURE B9.
PORCINE AORTIC VALVE at 100 mm. Hg.

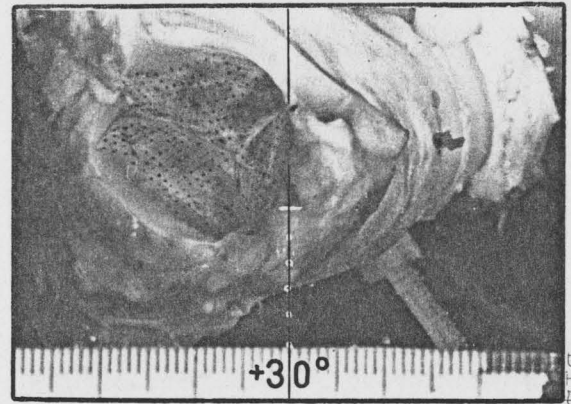
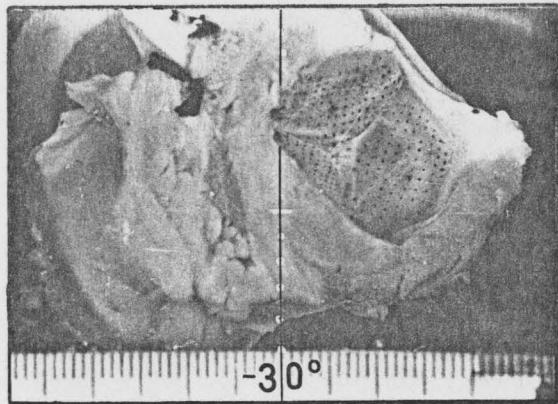
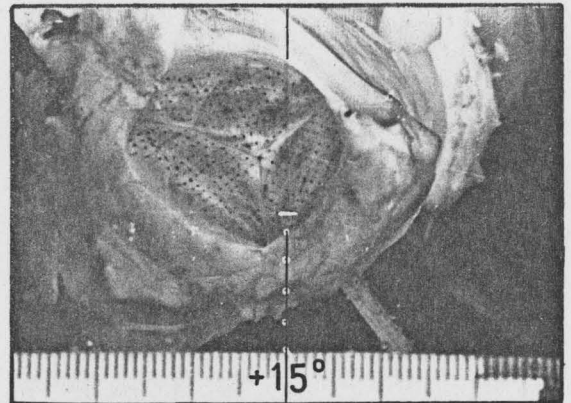
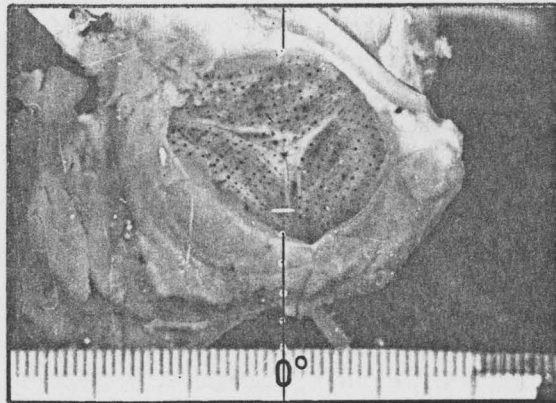
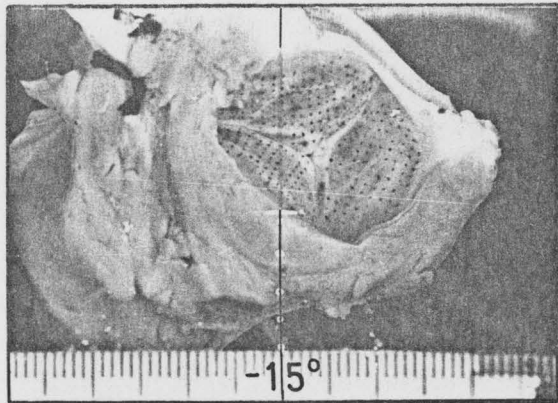


FIGURE B10.
PORCINE AORTIC VALVE at 120 mm. Hg.

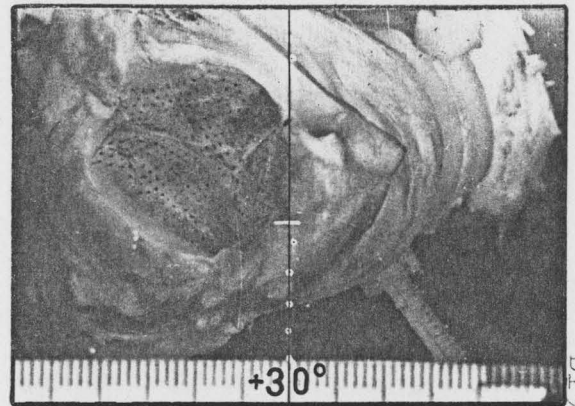
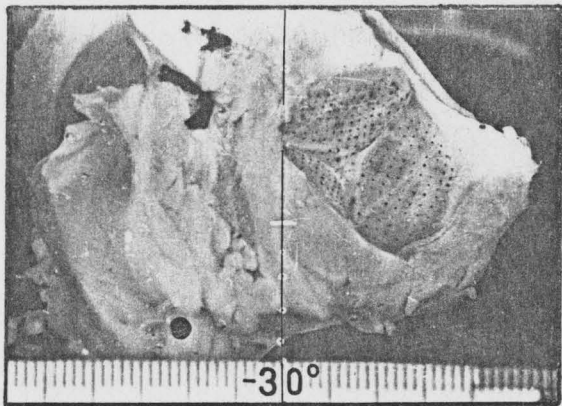
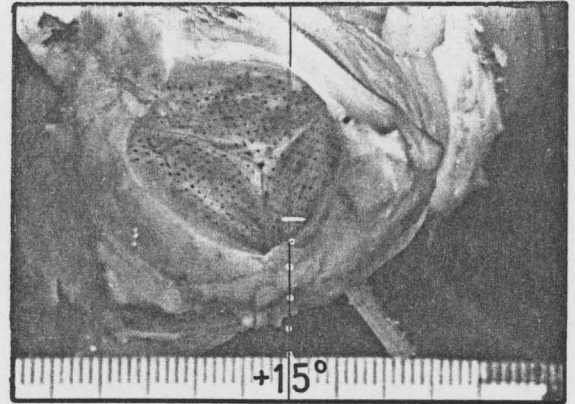
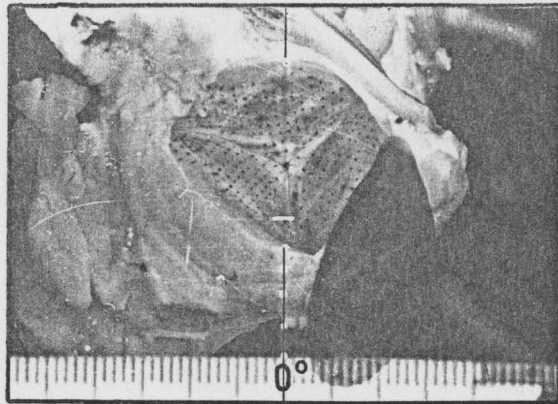
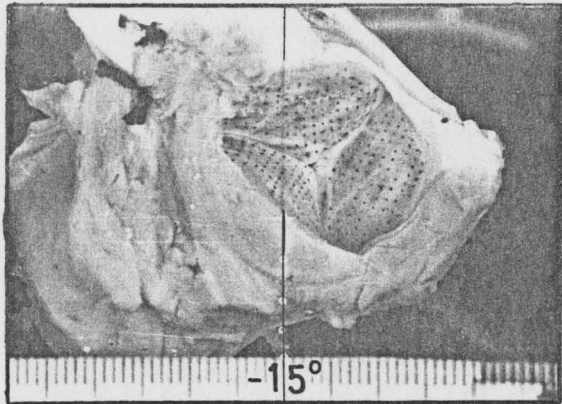
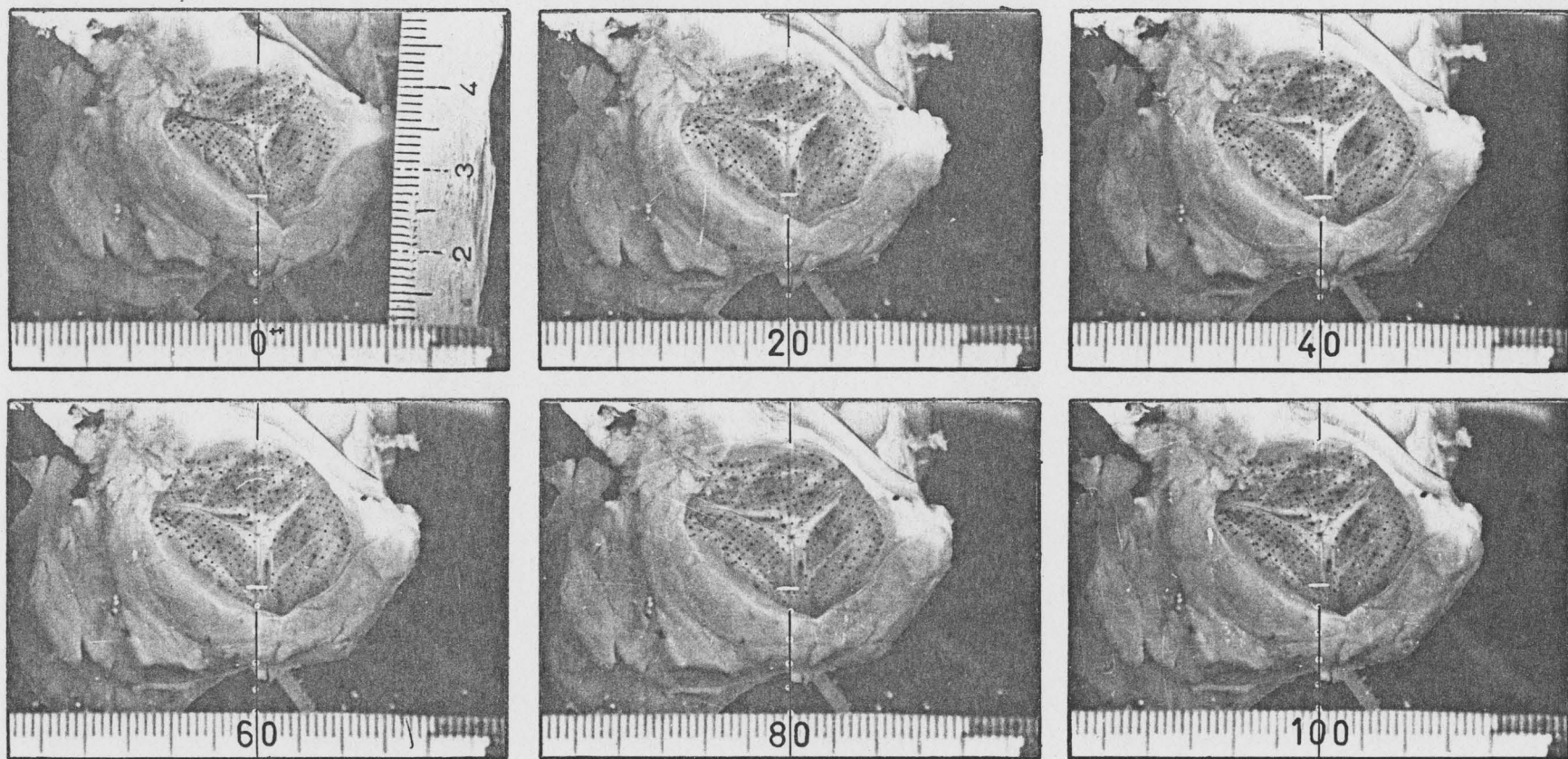


FIGURE B11.
PORCINE AORTIC VALVE from 0** to 100 mm. Hg.

**ZERO LOAD STATE ACTUALLY 3 mm Hg



second. A millimetre rule placed near the valve serves as a calibration scale.

Figure B4 is the series of photographs of the dotted experimental valve at $P = 0$ mm. Hg. for $\theta = 0^\circ, \pm 15^\circ, \pm 30^\circ$. Figures B5 to B10 are similar series for $P = 20, 40, 60, 80, 100$ and 120 mm. Hg. respectively. Figure B11 shows the valve (at the 0° orientation) during the course of a loading cycle from 0 mm. Hg. to 100 mm. Hg.

3. Parallax Errors

The parallax errors in the experimental method may be described as magnification errors. The latter arise from the fact that distances between points which are closer to the camera are recorded at a greater magnification than the distances between points which are more distant. For a photo system with a fixed lens-to-film distance (I), the percent change in the magnification ($\Delta M/M$) is equal to the percent change in the lens-to-object distance ($\Delta O/O$). This is illustrated in figure B12 and is shown as follow. By definition, the magnification (M) is

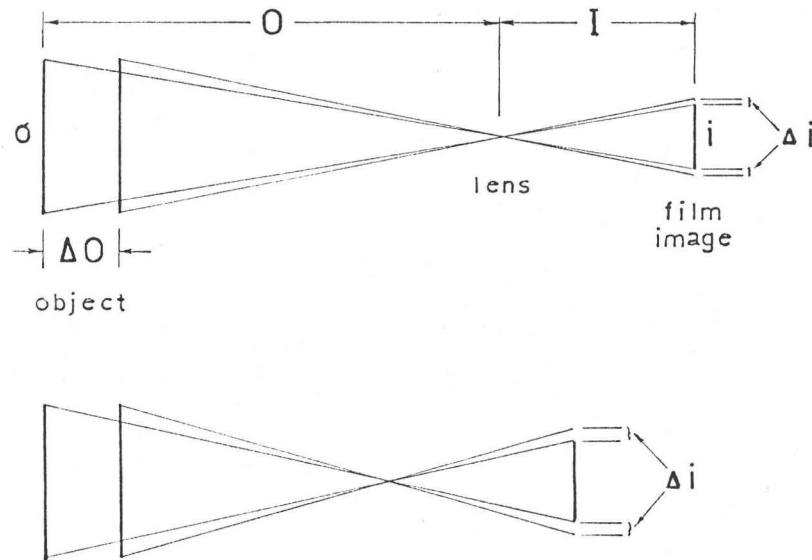
$$M = \frac{i}{o} = \frac{I}{O} \quad (5)$$

where o and i are respectively the object and the film image dimensions, and

O and I are respectively the lens-to-object and the lens-to-film distances.

ERROR CONSIDERATIONS in THEORY

FIGURE B12.
PARALLAX ERRORS

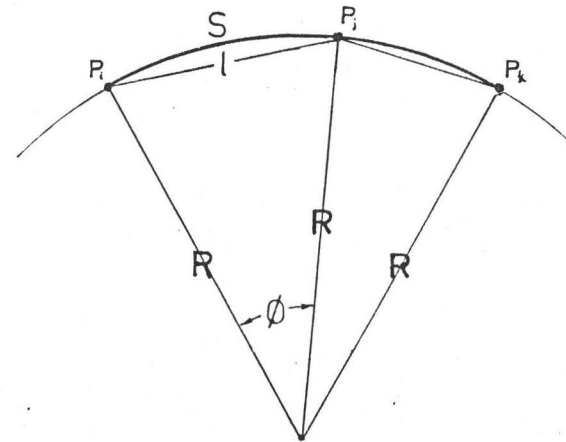


$$M = \frac{i}{o} = \frac{I}{O}$$

$$\Delta i \approx \frac{\Delta O}{O} = -\frac{\Delta M}{M}$$

if $I = \text{constant}$

FIGURE B13.
SURFACE STRAIN APPROXIMATION



$$S = R \cdot \phi \quad ; \quad l = R \cdot 2 \sin \frac{\phi}{2}$$

ϕ	ϕ (RAD)	$2 \cdot \sin \frac{\phi}{2}$	error
10°	.1745	.1743	0.1 %
20°	.3491	.3473	0.5 %
30°	.5236	.5176	1.1 %

for $<1\%$ error, $\frac{S}{R} = \frac{l}{R} < 0.5$

If $I = \text{constant}$, then

$$\frac{\Delta M}{M} = - \frac{\Delta O}{O} \quad (6)$$

$$\Delta M = - \Delta O \cdot \frac{I}{O^2} \quad (7)$$

Variations in the magnification (hence, also the measurement) of the surface distances on the valve leaflets are therefore minimized by increasing the lens-to-valve distance (O).

In the experiment, ΔO arises from three sources:

- 1) because of the three-dimensional nature of the valve, different points on the valve have different O ;
- 2) because of deformation due to pressure changes, the same point changes in its O ; and
- 3) because of valve rotation, the same point changes its O .

For a 600 mm. lens + a 6 cm. extension tube, it was estimated that $O = 175$ cm., $I = 29$ cm. and $(\Delta O)_{\text{max}} = 1$ cm. Thus, $(\Delta M/M)_{\text{max}} = (\Delta O/O)_{\text{max}} = 0.6\%$ which is negligible.

For comparison, a trial system using a 100 mm. lens, that gave similar magnifications at a reduced $O = 35$ cm. and $I = 11$ cm., has a maximum magnification error of 3%.

4. Curved Surface Distance Approximation

Figure B13 shows a schematic sectioned curve of the valve leaflet containing P_i , P_j and P_k . Calculated strains of the surface distance $P_i P_k$ are approximated by the straight line distances $\overline{P_i P_j} + \overline{P_j P_k}$. Both sections are in the order of

1 mm. The approximation is good if the radius of curvature of the curve $P_i P_j P_k$ is sufficiently large so that the angle subtended by each pair of points is small enough for the $\phi = 2 \cdot \sin(\phi/2)$ approximation as shown in figure B13. It is good to less than 1% for $\phi < 28^\circ$; that is, $1/R < 0.5$. Since l is in the order of 1 mm., the condition of "sufficiently large radius of curvature" is defined as: $R \geq 2$ mm. This stipulation is satisfied by a high majority of the valve.

The accuracy of the approximation is governed by the mesh size of the dots on the valve leaflets. Minimization of the curvature effects on strain calculations is achieved by using the smallest possible mesh size. However, the "smallness" is limited by the errors incurred in measuring small distances.

5. Other Error Considerations

As determined by the sharpness of the valve dots on the photographs (diameter = 1 to 1.5 mm.), the measurement errors are in the order of ± 0.3 mm. Hidden errors which can not be accounted for quantitatively (eg., film and photographic paper warpage during exposure and printing) are considered negligible.

The scale calibration error is negligible ($\sim 0.5\%$); hence, the errors in x_i and z_i may be determined directly from the error in d_i . Based on a scale enlargement of 8.7X, $\Delta x = \Delta z = \Delta d = \pm 0.3 \text{ mm.} / 8.7 = \pm 0.035 \text{ mm.}$ actual scale. The

error in calculating y_i using equation (4) is determined by

$$\Delta y = \left| \frac{\partial y}{\partial x} \cdot \Delta x \right| + \left| \frac{\partial y}{\partial d} \cdot \Delta d \right| + \left| \frac{\partial y}{\partial \theta} \cdot \Delta \theta \right| \quad (8)$$

$$\Delta y = \left| \frac{1}{\tan \theta} \cdot \Delta x \right| + \left| \frac{1}{\sin \theta} \cdot \Delta d \right| + \left[\left| \frac{x}{\sin^2 \theta} \right| + \left| \frac{d}{\sin \theta \cdot \tan \theta} \right| \right] \cdot \Delta \theta \quad (9)$$

where $\Delta \theta$ is the error in the angle ($\pm 0.5^\circ$ or ± 0.01 radian). Calculations for Δy give large errors, especially for small angles because of the denominators $\tan \theta$ and $\sin \theta$. Errors as high as 20% are observed for $\theta = \pm 15^\circ$. The errors could be reduced if a more accurate micrometric means is used for measuring θ . The protractor used in the experiment is comparatively crude.

A fairer assessment of the error in y_i is found in the standard deviation of the calculations for y_i using the four different view angles (ie., $\pm 15^\circ$ and $\pm 30^\circ$). The mean s.d. = ± 0.15 mm., ranging from ± 0.1 mm. to ± 0.5 mm. Hence, the average standard error* for y_i is $\overline{\Delta y} = \pm 0.09$ mm. The standard deviations also serve as a means of spotting incorrect data; that is, an unusually large standard deviation indicates a possible incorrect measurement.

Estimated errors in the strain calculations are high because of the accumulative effects of the above. The error

* standard error = $(N - 1)^{-\frac{1}{2}}$ · standard deviation

in the straight-line distance (l_{ij}) between two points P_i and P_j is derived as follows:

From geometry,

$$l_{ij}^2 = (\delta x_{ij})^2 + (\delta y_{ij})^2 + (\delta z_{ij})^2 \quad (10)$$

where $\delta x_{ij} = x_i - x_j$.

The error in l_{ij} is therefore

$$\Delta l_{ij} = \frac{\delta x_{ij}}{l_{ij}} \cdot \Delta(\delta x_{ij}) + \frac{\delta y_{ij}}{l_{ij}} \cdot \Delta(\delta y_{ij}) + \frac{\delta z_{ij}}{l_{ij}} \cdot \Delta(\delta z_{ij}) \quad (11)$$

where $\Delta(\delta x_{ij}) = \Delta(\delta z_{ij}) = 2 \cdot \Delta x = 0.07 \text{ mm.}$, and

$$\Delta(\delta y_{ij}) = 2 \cdot \Delta y = 0.18 \text{ mm.}$$

Since the error multipliers in equation (11) are all less than one, Δl_{ij} is at most 0.32 mm. A more realistic figure is $\Delta l_{ij} = \pm 0.1 \text{ mm.}$ which is approximately 5% to 10% of l_{ij} .

The experimental circumferential strains for the porcine aortic valve leaflets are less than 10%. This means that the elongations of the distances between points on the leaflets are about 0.1 mm. Accordingly, it may be seen why the circumferential strains do not result in smooth pressure-strain curves whereas the radial strains do (see figures 31 to 33 on p. 118-120 in the main text).

The accuracy of calculating strains therefore varies inversely as the mesh size of the valve dots. However, the ability to observe inhomogeneity and the reduction of curvature effects on strains vary directly as the mesh size. One therefore must compromise between accuracy and inhomogeneity considerations.

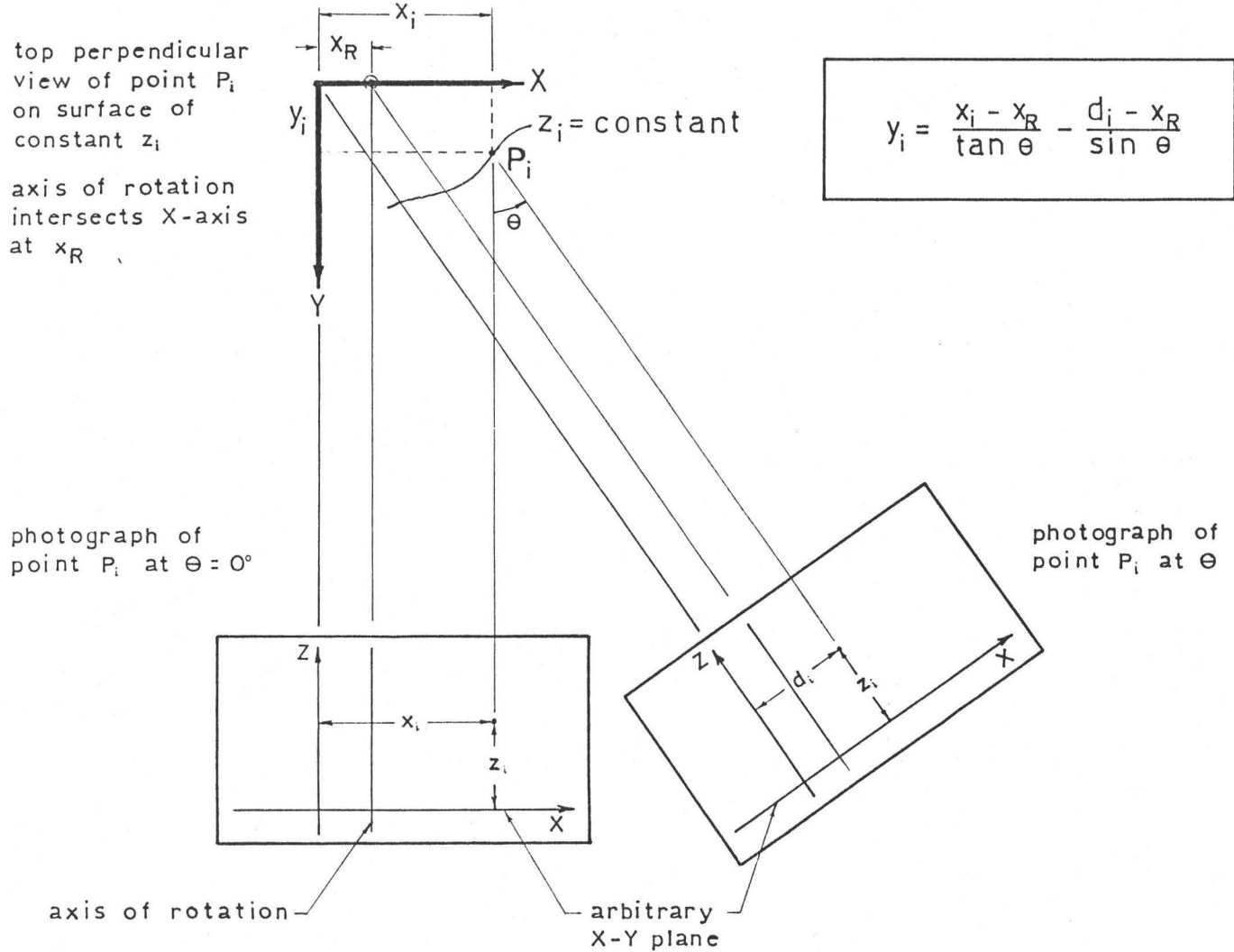
The theory and experimental method were first tested by using them to determine the (x_i, y_i, z_i) coordinates of the visible corners of a 10 mm. (± 0.01 mm.) machined cube, from which the cube's edge lengths may be calculated and compared. The visible edges were calculated to be 10.0 mm., 10.3 mm., 10.8 mm., 10.2 mm. and 10.3 mm. (mean = 10.32 mm. with a s.d. = 0.2 mm.). Hence, the 10 mm. lengths are approximately accurate to 3%. Coordinate determinations are thus accurate to about 1%.

Addendum

The plumb-lined thread is intended to hang so that when photographed with the valve, it appears as the projection of the axis of rotation as well as the Z-axis; that is, $x_{\text{ROT}} = 0$ as illustrated in figure B3. However, in the actual experiment, the thread did not hang as planned. The thread representing the axis of rotation was shifted relative to the Z-axis such that $x_{\text{ROT}} \neq 0$, as shown in figure B14. It may be shown that with this altered geometry, the result of the derivation for $y_i = y_i(\theta, x_i, d_i, x_{\text{ROT}})$ becomes:

$$y_i = \frac{(x_i - x_{\text{ROT}})}{\tan \theta} - \frac{(d_i - x_{\text{ROT}})}{\sin \theta} \quad (12)$$

FIGURE B14
GEOMETRY for DERIVATION of y_i
Z-AXIS is not AXIS of ROTATION



APPENDIX C

Computer Programs for the Data Analysis

Program VALVE is written to perform the data reduction and analysis. At the end of this appendix is a list of the program variables and the complete program listing. Also included are the flow charts (figure 1), a description of an input data deck preparation and a sample output from the RC leaflet analysis.

Inputs for the program are of two types. The first consist of the stereophotogrammetric system and experimental constants; these are internal to the program and are therefore self-explanatory from the listing. The second type is the data deck that consists of the photographic measurements for the points on the leaflet at each different pressure (L) and at each different view angle (θ). Identification of each point is by its row (R) and by its column (C).

The key output variables are the calculated Cartesian coordinates (ie., $X(R,C,L)$, $Y(R,C,L)$, $Z(R,C,L)$) for all the points on the leaflet at each different pressure. Error calculations for (X,Y,Z) are also provided but are not included in the sample output. However, they may be printed if needed. The standard deviations for Y, as discussed in Appendix B, are included in the sample output.

The main program uses these coordinate calculations in several ways to investigate the geometry of the leaflet being analysed. The net displacements of each point from its 0 mm. Hg. position (ie., TDISX, TDISY, TDISZ), and the incremental displacements of each point from its position at the previous pressure (ie., DISX, DISY, DISZ) are calculated but are not shown in the sample output.

Two major portions of the main program are the function subprogram RAD and the subroutine EXTENS. Subprogram RAD uses the coordinate output and calculates the radius of curvature. The theory and application of RAD to the experiment to determine the local radial and circumferential radii of curvature (ie., RPHI and RLAT) is discussed in Appendix D. Subroutine EXTENS also uses the coordinate output; it calculates for each interior point on the leaflet, the straight-line lengths between the point and the four adjacent points (ie., EXUP, EXDO, EXLE, EXRI) as illustrated in figure 18 on p. 77. The main program in turn uses the length calculations to determine the local radial and circumferential surface strains (ie., STRAPH and STRALA) for each point and at each pressure. Zero strain is referenced at 0 mm. Hg.

There are two other subprograms worth mentioning at this point; EPHI and ELAT. Using stored equations* for the elastic modulus as a function of strain, the two subprograms

* 1st degree differentiation of a polynomial of a σ - ϵ curve.

return a value for the elastic modulus (ie., radial for EPHI and circumferential for ELAT) if given the respective strain. The usefulness of EPHI and ELAT comes into effect when calculating the local radial and circumferential stresses for each point on the leaflet (ie., SIGPHI and SIGLAT). This will be discussed in more detail in Part II of this study.

Variable Identifiers for Program VALVE

R is the row counter; $\text{INITR}(C,L) \leq R \leq \text{NR}(C,L)$
 C is the column counter; $1 \leq C \leq \text{NC}$
 L is the pressure load counter; $1 \leq L \leq \text{NL}$
 J is the view angle counter; $1 \leq J \leq \text{NA}$
 $\text{INITR}(C,L)$ is the initial row index for the Cth column at the Lth pressure
 $\text{NR}(C,L)$ is the maximum row index for the Cth column at the Lth pressure; therefore, the number of points in the Cth column at the Lth pressure is $\text{NR}(C,L) - \text{INITR}(C,L) + 1$
 NC is the number of columns
 NL is the number of pressure loads including the 0 mm. Hg.
 NA is the number of view angles including the 0° reference
 MA is the reference angle index; ie., $J = \text{MA}$ if $\text{THETA}(J) = 0^\circ$
 NPA is the number of possible view angles for a particular point excluding the 0° reference angle
 $X(R,C,L)$, $Y(R,C,L)$, $Z(R,C,L)$ are the three scaled Cartesian coordinates for the point identified by the Rth row, the Cth column and the Lth pressure; ie., point (R,C,L)
 $ZT(R,C,L)$ is the unscaled z coordinate of the point (R,C,L) as determined from the photographic measurement at $\theta = 0^\circ$
 CROT is the unscaled x coordinate for the axis of rotation as determined from the $\theta = 0^\circ$ photograph
 CROTS is the scaled value for CROT
 $D(R,C,J)$ is the unscaled photographic measurement of point (R,C,L) at the Jth view angle
 DS is the scaled value for $D(R,C,J)$
 $YT(R,C,J)$ is the calculated scaled value for $Y(R,C,L)$ using the $D(R,C,J)$ data
 $\text{ERRX}(R,C,L)$ is the error calculated for $X(R,C,L)$
 $\text{ERRZ}(R,C,L)$ is the error calculated for $Z(R,C,L)$
 $\text{ERRYT}(R,C,J)$ is the error calculated for $YT(R,C,J)$
 $\text{DEVY}(R,C,L)$ is the standard deviation in calculating $Y(R,C,L)$
 SUM, SUMSQ, VAR are variables used for calculating $Y(R,C,L)$ and $\text{DEVY}(R,C,L)$
 $\text{THETA}(J)$ is the Jth view angle in degrees

THETAR is the angle THETA(J) in radians
 TANTHE and SIN THE are the tangent and sine of THETA(J)
 DTHETA is the view angle step size in degrees
 PRESS(L) is the Lth pressure load in mm. Hg.; L = 1 is the
 0 mm. Hg. reference
 MAXPRE is the maximum pressure for PRESS(L) in mm. Hg.
 DPRESS is the pressure load step size in mm. Hg.
 SCALE is the scale conversion from photographic dimensions
 to actual life size dimensions
 ERRSCA is the error in SCALE
 ERRTHE is the error in THETA(J) in degrees
 ERRPRE is the error in PRESS(L) in mm. Hg.
 ERRMEA is the error in the photographic measurements; ie.,
 ZT(R,C,L), D(R,C,J) and CROT
 X1,X2,X3,X4,X5,Y1,Y2,Y3,Y4,Y5,Z1,Z2,Z3,Z4,Z5 are the coordi-
 nate arguments used for the subprograms RAD and EXTENS
 DISX,DISY,DISZ are the incremental x,y,z displacements of
 point (R,C,L-1) to (R,C,L)
 TDISX,TDISY,TDISZ are the total net x,y,z displacements of
 point (R,C,1) to (R,C,L)
 RAD is the function subprogram used to calculate radii of
 curvature
 RPHI and RLAT are the local radial and circumferential radii
 of curvature calculated using RAD
 EXTENS is the subroutine used to calculate point-to-point
 distances
 EXUP, EXDO, EXLE, EXRI are the point-to-point lengths calcu-
 lated for a point and its adjacent point using EXTENS
 EXPHI and EXLAT are the local radial and circumferential
 point-to-point lengths calculated using EXTENS
 EXPHIO(R,C) and EXLATO(R,C) are the initial EXPHI and EXLAT
 for point (R,C) at L = 1; ie., at 0 mm. Hg.
 DELEXP and DELEXL are the local radial and circumferential
 elongations for EXPHIO(R,C) and EXLATO(R,C)
 STRAPH and STRALA are the local radial and circumferential
 surface strains
 EPHI and ELAT are function subprograms used to return the
 radial and circumferential elastic moduli given the local
 radial and circumferential strains, STRAPH and STRALA
 EP and EL are the returned elastic moduli
 SIGPHI, SIGLAT, SIGNET are the local radial, circumferential
 and net in-plane stresses

Following this page is the complete program VALVE listing.

```

1      PROGRAM VALVE(INPUT,OUTPUT,TAPE5=INPUT,TAPE6=OUTPUT)
          (RIGHT)
C      CALCULATIONS FOR MUSCLE CORONARY VALVE LEAFLET NO. 3
5      DIMENSION YT(10,18,3),D(10,18,3),ERRYT(10,18,3)
          DIMENSION X(10,18,7),Y(10,18,7),Z(10,18,7),ZT(10,18,7)
          DIMENSION ERRX(10,18,7),DEVY(10,18,7),ERRZ(10,18,7)
          DIMENSION EXPHIO(10,18),EXLATO(10,18)
10     DIMENSION THETA(3),PRESS(7),NR(18,7),INITR(18,7)

          INTEGER R,C

          NA=3
          NL=7
          NC=18
          MAXPRE=120
          SCALE=0.0114
          CROT=5000
20     ERRSCA=0.00003
          ERPTHE=0.5
          ERRMEA=3
          ERPPRE=2.0
          THETA(1)=0.0
          THETA(2)=+15.0
          THETA(3)=+30.0
          MA=1
          CROTS=CROT*SCALE
          DTHETA=15
          DPRESS=20

          DO 50 L=1,NL

          READ (5,100) (INITR(C,L),C=1,NC)
          READ (5,100) (NR(C,L),C=1,NC)
100    FORMAT (18I4)
          PRESS(L)=(L-1)*DPRESS

          DO 51 C=1,NC

          NRC=NR(C,L)
          INITRC=INITR(C,L)

          DO 52 R=INITRC,NRC

          READ (5,101) ZT(R,C,L),(D(R,C,J),J=1,NA)
101    FORMAT (4(F4.0,6X))
          X(R,C,L)=D(R,C,NA)*SCALE
          Z(R,C,L)=ZT(R,C,L)*SCALE
          SUM=0.0
          SUMSQ=0.0

```

```

NPA=NA-1
60 DO 53 J=1,NA
      IF (THETA(J) .EQ. 0.0) GOTO 501
      IF (D(R,C,J) .EQ. 999) GOTO 500
65 DS=D(R,C,J)*SCALE
      THETAR=THETA(J)/57.3
      TANTHE=TAN(THETAR)
      SIN THE=SIN(THETAR)
      YT(R,C,J)=((X(R,C,L)-CROTS)/TANTHE)-((DS-CROTS)/SIN THE)
70 SUM=SUM+YT(R,C,J)
      SUMSQ=SUMSQ+YT(R,C,J)**2
      GOTO 53
500 NPA=NPA-1
501 YT(R,C,J)=999
75 53 CONTINUE
      Y(R,C,L)=SUM/NPA
      VAR=(SUMSQ/NPA)-Y(R,C,L)**2
80 DEVY(R,C,L)=SQRT(VAR)
      52 CONTINUE
      51 CONTINUE
85 50 CONTINUE
90
      WRITE (6,19)
      WRITE (6,20) MAXPRE,DPRESS
      WRITE (6,21)
95 WRITE (6,22) SCALE
      WRITE (6,23) ERPMEA,ERRPSA,ERRTHE,ERRPRE
      WRITE (6,24) CROT,CROTS
      WRITE (6,25)
      WRITE (6,26)
100 WRITE (6,27)
      WRITE (6,28)
09 FORMAT (# #,/)
19 FORMAT (1H1, #RESULTS FOR MUSCLE CORONARY VALVE LEAFLET NO. 3#, ///)
20 FORMAT (# #, #PRESSURE RANGED FROM ZERO TO #, I3, # MM. HG IN STEPS#
105 * # OF #, F5.1, # MM. HG#, ///)
21 FORMAT (# #, #COORDINATES X,Y,Z AND RADII RPHI AND RLAT ARE IN MM.#
* #, # #, # ANGLES ARE IN DEGREES AND PRESSURES ARE IN MM. HG#, /, # #,
* # ELASTIC MODULI EPHI AND ELAT ARE IN GM./SQ. MM.#, /, # #,
* # STRAINS STRAPH AND STRALA ARE IN PERCENT ELONGATION#, /, # #,
110 * # STRESSES SIGPHI, SIGLAT AND SIGNET ARE IN GM./SQ. CM.#, ///, # #,
* # NON-APPLICABLE DATA REPRESENTED BY 999.00#, ///)
22 FORMAT (# #, #THE SCALE USED IS#, F6.4, # MM./MEAS. UNIT#, /)
23 FORMAT (# #, #ERROR IN MEASUREMENTS IS#, F6.3, # SEAS. UNITS#, /, # #,
* #, #ERROR IN SCALE IS#, F7.2, # # MM./MEAS. UNIT#, /, # #, #ERROR IN

```

```

115      *,# IS#,F4.1,# DEGREES#/,# #,#ERROR IN PRESSURE IS#,F4.1,# MM. HG#
      *,//)
24  FORMAT (# #,#THE UNSCALED (X,Y) COORDINATES OF THE CENTER OF ROT#
      *,#ATION IS (#,F5.2,#,0.00)#/,# #,#THE SCALED (X,Y) COORDINATES#
      *,# OF THE CENTER OF ROTATION IS (#,F5.2,#,0.00)#,////)
120 25  FORMAT (# #,#THE ORGANIZATION OF THE RESULTS IS AS FOLLOWS#,//)
26  FORMAT (# #,#PCINT I.D.#,14X,#X#,9X,#Y#,9X,#Z#,14X,#STRAPH#,+X,
      *,#STRALA#,14X,#SIGPHI#,4X,#SIGLAT#,14X,#SIGNET#,5X,#ANGLE#,/)
27  FORMAT (# #,#COLUMN ROW#,11X,#ERRX#,6X,#DEVY#,6X,#ERRZ#,16X,#EPHI#
      *,#6X,#ELAT#,16X,#RPHI#,6X,#PLAT#,////)
125 28  FORMAT (# #,#DIAGRAM OF POINT IDENTIFICATION#)

```

130

```
DO 70 L=1,NL
```

135

```

      WRITE (6,30) PRESS(L)
30  *  FORMAT (1H1,#RESULTS FOR MUSCLE CORONARY VALVE LEAFLET NO. 3 AT#,
      *,# PRESSURE LOAD=#,F6.1,# MM. HG#,////)
      WRITE (6,09)
      DO 71 C=1,NC

```

140

```

      NRC=NR(C,L)
      INITRC=INITR(C,L)

```

```
DO 72 R=INITRC,NRC
```

145

```

      IF (L .EQ. 1) GOTO 502
      DISX=X(R,C,L)-X(R,C,L-1)
      DISY=Y(R,C,L)-Y(R,C,L-1)
      DISZ=Z(R,C,L)-Z(R,C,L-1)
      TDISX=X(R,C,L)-X(R,C,1)
      TDISY=Y(R,C,L)-Y(R,C,1)
      TDISZ=Z(R,C,L)-Z(R,C,1)

```

150

```
502
```

```

      DISX=0.0
      DISY=0.0
      DISZ=0.0
      TDISX=0.0
      TDISY=0.0
      TDISZ=0.0

```

155

```
503
```

```
CONTINUE
```

160

```

      IF ((C .EQ. 1) .OR. (C .EQ. NC)) GOTO 504
      IF ((R .EQ. INITRC) .OR. (R .EQ. NRC)) GOTO 504

```

165

```

      X1=X(R-1,C,L)
      Y1=Y(R-1,C,L)
      Z1=Z(R-1,C,L)
      X2=X(R,C,L)
      Y2=Y(R,C,L)
      Z2=Z(R,C,L)
      X3=X(R+1,C,L)
      Y3=Y(R+1,C,L)
      Z3=Z(R+1,C,L)

```

170

```

175      X4=X(R,C-1,L)
        Y4=Y(R,C-1,L)
        Z4=Z(R,C-1,L)
        X5=X(R,C+1,L)
        Y5=Y(R,C+1,L)
        Z5=Z(R,C+1,L)
180      RPHT=RAD(X1,Y1,Z1,X2,Y2,Z2,X3,Y3,Z3)
        RLAT=RAD(X4,Y4,Z4,X2,Y2,Z2,X5,Y5,Z5)
        U=SQRT(DISX**2+DISY**2+DISZ**2)
        CALL EXTENS(X1,Y1,Z1,X2,Y2,Z2,X3,Y3,Z3,X4,Y4,Z4,X5,Y5,Z5,
        *      EXUP,EXDO,EXLE,EXRI,EXPHT,EXLAT)
        IF (L.NE.1) GOTO 506
185      EXPHTO(R,C)=EXPHT
        EXLATO(R,C)=EXLAT
        DELEXP=EXPHT-EXPHTO(R,C)
        DELEXL=EXLAT-EXLATO(R,C)
        STRAPH=DELEXP/EXPHTO(R,C)*100
        STRALA=DELEXL/EXLATO(R,C)*100
190      EP=EPHT(STRAPH)
        EL=ELAT(STRALA)
        SIGPHT=(EP/0.75)+(STRAPH+0.5*STRALA)
        SIGLAT=(EL/0.75)+(STRALA+0.5*STRAPH)
        SIGNET=SQRT(SIGPHT**2+SIGLAT**2)
195      GOTO 507
        504 CONTINUE

        X2=X(R,C,L)
        Y2=Y(R,C,L)
        Z2=Z(R,C,L)
        RPHT=999
        RLAT=999
        U=SQRT(DISX**2+DISY**2+DISZ**2)
        EXUP=999
        EXDO=999
        EXLE=999
        EXRI=999
        EXPHT=999
        EXLAT=999
        DELEXP=999
        DELEXL=999
        STRAPH=999
        STRALA=999
        EP=999
        EL=999
        SIGPHT=999
        SIGLAT=999
        SIGNET=999
        ANGLE=999
220      507 CONTINUE

        WRITE (6,31) C,R,X2,Y2,Z2,STRAPH,STRALA,SIGPHT,SIGLAT,SIGNET
        WRITE (6,32) DEVT(R,C,L),EP,EL,RPHT,RLAT
        WRITE (6,09)
225      FORMAT (# #,2I5,5X,3F10.2,10X,2F10.2,10X,2F10.2,10X,2F10.2)
        FORMAT (# #,25X,F10.2,20X,2F10.2,10X,2F10.2)
227      CONTINUE

```

```

230      15  WRITE (6,15)
          15  FORMAT (# #,135 (#-#),/)
          71  CONTINUE

235      70  CONTINUE
          70  STOP
          70  END
    
```

--ENTRY POINTS--

3B	INPUTE	43B	OUTPUTE	3B	TAPESE
112B	VALVE				

--EXTERNALS--

ELAT SIN.	EPHI SORT.	EXTENS STOP.	FTNPPV. TAN.	INPCI.	INPCF.	OUTCI.	540
--------------	---------------	-----------------	-----------------	--------	--------	--------	-----

--STATEMENT LABELS--

.9	F	1161B	.15	F	1425B	.19	F	1163B	.20
.21	F	1204B	.22	F	1251B	.23	F	1260B	.24
.25	F	1332B	.26	F	1341B	.27	F	1356B	.28
.30	F	1377B	.31	F	1412B	.32	F	1428B	.33
.51	F	432B	.52	F	426B	.53	F	428B	.54
.71	F	1133B	.72	F	1125B	.100	F	1154B	.101
.500	F	364B	.501	F	368B	.502	F	366B	.503
.504	F	1017B	.505	F	745B	.507	F	1110B	.508

--VARIABLE MAP--

ANGLE	R	27427B							
CROT	R	5260B							
D	U	1643B	540						
DELEXP	R	27420B							
DISX	R	2701B						1260	
DISZ	R	5257B							
DS	P	14615B							
EL	P	27424B							
EP	R	2677B							
ERRMEA	P	5556B							
ERRSCA	P	1641B							
ERRX	P	5561B	1260						
ERRZ	U	27520B	1260						
EXLAT	R	27417B							
EXLE	P	5546B							
EXPHIO	R	27074B	180						
EXTENS	R								
FTNPPV.									
INITRO	T	27370B							

SUBROUTINE
EXTERNAL.

etc

```

1      FUNCTION RAD(X1,Y1,Z1,X2,Y2,Z2,X3,Y3,Z3)
      C      THIS FUNCTION SUBPROGRAM RETURNS A VALUE RAD AS THE APPROXIMATE
      C      RADIUS OF CURVATURE AT POINT P2 GIVEN THE COORDINATES OF THE
5      C      CONSECUTIVE POINTS P1,P2,P3
      C
      C      XJ,YJ,ZJ ARE THE COORDINATES OF POINT PJ, J=1,2,3
      C      SKL IS THE LENGTH OF LINE BETWEEN POINT PK AND POINT PL, K,L=1,2,3
      C      DPIJK IS THE DOT PRODUCT OF VECTOR IJ AND VECTOR JK
10     C      TOP AND BOTTOM ARE PARAMETERS USED TO CALCULATE RAD
      C      RAD IS THE CALCULATED RADIUS OF CURVATURE OF CURVE P1-P2-P3 AT P2

      S12=SQRT((X2-X1)**2+(Y2-Y1)**2+(Z2-Z1)**2)
      S23=SQRT((X3-X2)**2+(Y3-Y2)**2+(Z3-Z2)**2)
15     S13=SQRT((X3-X1)**2+(Y3-Y1)**2+(Z3-Z1)**2)
      DP123=(X2-X1)*(X3-X2)+(Y2-Y1)*(Y3-Y2)+(Z2-Z1)*(Z3-Z2)
      CHECK=(S12*S23)**2-(ABS(DP123))**2
      IF (CHECK .LE. 0.0) GOTO 999
      TOP=S12*S23*S13
20     BOTTOM=2*SQRT(CHECK)
      RAD=TOP/BOTTOM
      IF (RAD .GT. 10000) RAD=10000
      GOTO 998
25     999 RAD=999
      998 CONTINUE
      RETURN
      END

```

--EXTERNALS--

SQRT.

--STATEMENT LABELS--

.998	120B	.999	116B
------	------	------	------

--VARIABLE MAP--

ABS	R		INTRINSIC	BOTTOM	R	132B	
CHECK	R	136B		DP123	R	134B	
RAD	R	123B	ENTRY	SQRT.	R		B.E.F.
S12	R	135B		S13	R	140B	
S23	R	137B		TOP	R	133B	
VALUE.	R	131B		X1	R	0B	
X2	R	AU		X3	R	AU	
Y1	R	AU		Y2	R	AU	
Y3	R	AU		Z1	R	AU	
Z2	R	AU		Z3	R	AU	

```

1      * SUBROUTINE EXTENS(X1,Y1,Z1,X2,Y2,Z2,X3,Y3,Z3,X4,Y4,Z4,X5,Y5,Z5,
      * EXUP,EXDO,EXLE,EXRI,EXPHI,EXLAT)
5      C      THIS SUBROUTINE RETURNS VALUES EXUP,EXDO,EXLE AND EXRI AS THE
      C      EXTENSIONS OF POINT P2 UPWARDS,DOWNWARDS,TO THE LEFT AND TO THE
      C      RIGHT RESPECTIVELY GIVEN THE COORDINATES OF THE POINTS PJ,
      C      J=1,2,3,4,5
10     C      XJ,YJ,ZJ ARE THE COORDINATES OF THE POINTS PJ, J=1,2,3,4,5
      C      EXUP IS THE EXTENSION OF POINT P2 UPWARDS TO POINT P3
      C      EXDO IS THE EXTENSION OF POINT P2 DOWNWARDS TO POINT P1
      C      EXLE IS THE EXTENSION OF POINT P2 TO THE LEFT TO POINT P4
      C      EXRI IS THE EXTENSION OF POINT P2 TO THE RIGHT TO POINT P5
15     C      EXPHI IS THE EXTENSION OF POINT P2 IN THE PHI DIRECTION
      C      EXLAT IS THE EXTENSION OF POINT P2 IN THE LAT DIRECTION

      EXUP=SQRT((X3-X2)**2+(Y3-Y2)**2+(Z3-Z2)**2)
      EXDO=SQRT((X1-X2)**2+(Y1-Y2)**2+(Z1-Z2)**2)
      EXLE=SQRT((X4-X2)**2+(Y4-Y2)**2+(Z4-Z2)**2)
20     EXRI=SQRT((X5-X2)**2+(Y5-Y2)**2+(Z5-Z2)**2)
      EXPHI=EXUP+EXDO
      EXLAT=EXLE+EXRI
      RETURN
      END

```

--EXTERNALS--

 SQRT.

--VARIABLE MAP--

EXDO	R	A	08	EXLAT	R	A	08	
EXLE	R	A	08	EXPHI	R	A	08	
EXRI	R	A	08	EXTENS	-	-	1028	ENTRY
EXUP	R	A	08	SQRT.	R	-	-	P.E.F.
X1	R	AU	08	X2	R	AU	08	
X3	R	AU	08	X4	R	AU	08	
X5	R	AU	08	Y1	R	AU	08	
Y2	R	AU	08	Y3	R	AU	08	
Y4	R	AU	08	Y5	R	AU	08	
Z1	R	AU	08	Z2	R	AU	08	
Z3	R	AU	08	Z4	R	AU	08	
Z5	R	AU	08					

1118 PROGRAM-UNIT LENGTH

23 SYMBOLS

440008 CM STORAGE USED

.166 SECONDS

```

1      FUNCTION EPHI (STRAPH)
C      THIS FUNCTION SUBPROGRAM RETURNS EPHI AS THE ELASTIC MODULI IN THE
5      PHI DIRECTION GIVEN THE STRAIN IN THE PHI DIRECTION IE. STRAPH
C      THE CALCULATED ELASTIC MODULI IS DETERMINED AS THE SLOPE FROM A
C      STRESS-STRAIN CURVE OF A FRESH HUMAN AORTIC VALVE LEAFLET IN THE
C      PHI OR THE RADIAL DIRECTION
10     IF (STRAPH .LE. 0.0) GOTO 10
        EPS=STRAPH/100.0
15     IF (EPS-0.10) 10,14,11
11     CONTINUE
        IF (EPS-0.24) 12,13,13
20     CONTINUE
        IF (EPS-0.17) 14,15,15
10     EPHI=0.8
        GOTO 20
25     13 EPHI=11.0
        GOTO 20
14     EPHI=-3.3+43.0*EPS
30     GOTO 20
15     EPHI=-12.5+97.0*EPS
20     RETURN
        END

```

--STATEMENT LABELS--

.10	24B	.11	15B	.12	20B	.13
.14	34B	.15	42B	.20	46B	

--VARIABLE MAP--

EPHI	-	50B	ENTRY	EPS	P	65B
STRAPH	R AU	0B		VALUE.	R	67B

66B PROGRAM-UNIT LENGTH 11 SYMBOLS
44000B CM STORAGE USED .109 SECONDS

```

1      FUNCTION ELAT(STRALA)
      C      THIS FUNCTION SUBPROGRAM RETURNS ELAT AS THE ELASTIC MODULI IN THE
      C      LAT DIRECTION GIVEN THE STRAIN IN THE LAT DIRECTION IE. STRALA
5
      C      THE CALCULATED ELASTIC MODULI IS DETERMINED AS THE SLOPE FROM A
      C      STRESS-STRAIN CURVE OF A FRESH HUMAN AORTIC VALVE LEAFLET IN THE
      C      LAT OR THE CIRCUMFERENTIAL DIRECTION
10     IF (STRALA .LE. 0.0) GOTO 10
      EPS=STRALA/100.0
      IF (EPS-0.03) 10,10,11
15     11 CONTINUE
      IF (EPS-0.15) 12,13,13
20     12 CONTINUE
      C0=35.0
      C1=625.0
      C2=18750.0
      C3=390625.0
      C4=-3385417.0
      C5=45572915.0
      X0=EPS-0.03
      X1=X0-0.02
      X2=X0-0.04
      X3=X0-0.06
      X4=X0-0.08
      X5=X0-0.10
      ELAT=1.5+C0*X0
      *      +C1*X0*X1
      *      +C2*X0*X1*X2
35     *      +C3*X0*X1*X2*X3
      *      +C4*X0*X1*X2*X3*X4
      *      +C5*X0*X1*X2*X3*X4*X5
      GOTO 20
40     10 ELAT=1.5
      GOTO 20
      13 ELAT=49.0
45     20 RETURN
      END

```

--STATEMENT LABELS--

.10
.20102B
110B

.11

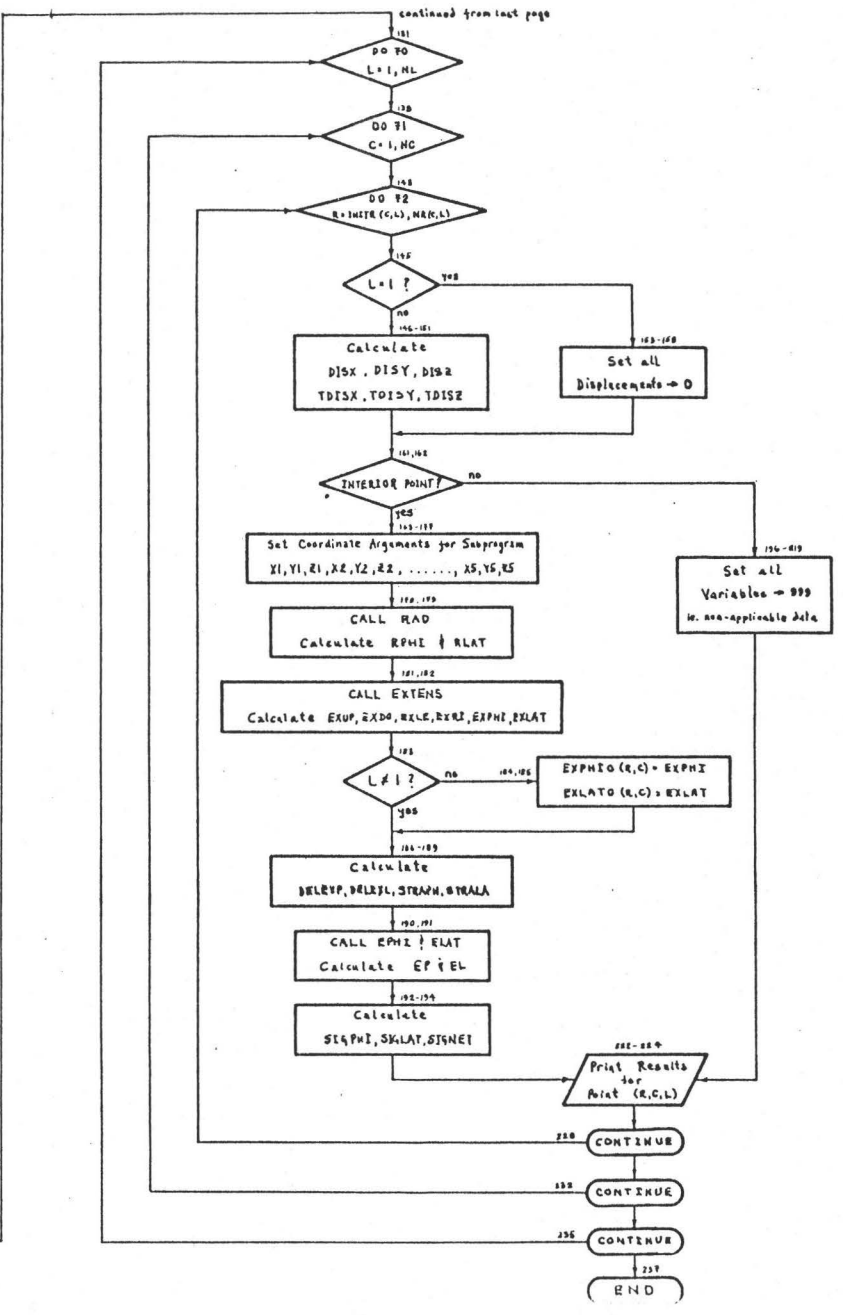
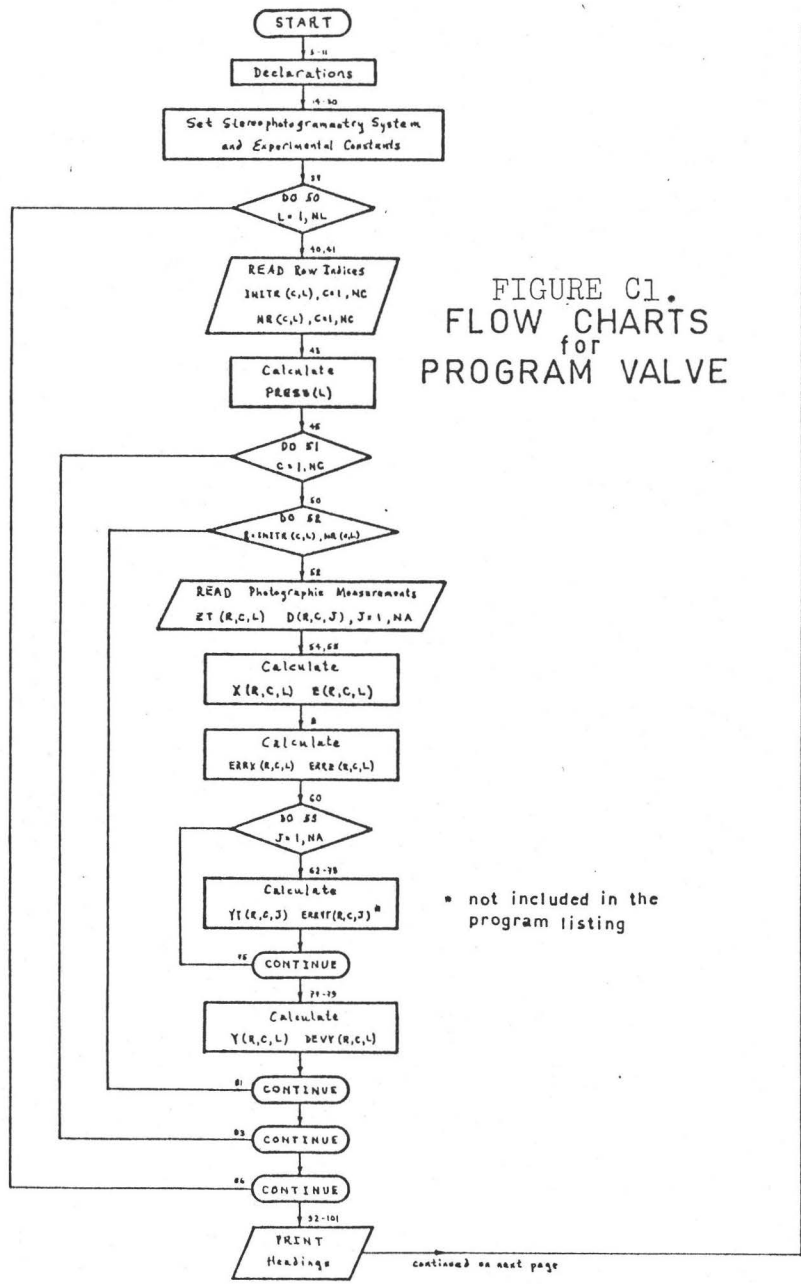
15B

.12

20B

.13

170



Preparation of the Input Data Deck

The data deck consists of the photographic measurements for a particular leaflet being analysed. It comprises of NL sub-decks, each one containing the measurements at the NL different pressure loads. Also, each sub-deck is preceded by two cards which input the initial row (ie., INITR(C,L)) and the last row (ie., NR(C,L)) in each column (C) for the pressure load (L) corresponding to the sub-deck. For example, the format for the data card entries for the 5th pressure load (ie., L = 5 and P = 80 mm. Hg.) is as follows:

1st card: NC integers representing the initial row index for each column(C) and for L = 5; ie.,

INITR(1,5) INITR(2,5) ... INITR(C,5) ... INITR(NC,5)

2nd card: NC integers representing the last row index for each column (C) and for L = 5; ie.,

NR(1,5) NR(2,5) ... NR(C,5) ... NR(NC,5)

L=5 sub-deck: consists of the measurement data for each point (R,C) at NA different view angles and L = 5;

ZT(R,C,5) D(R,C,1) D(R,C,2) ... D(R,C,J) ... D(R,C,NA)

For example, the entries for the 4th row point in the 6th column are:

ZT(4,6,5) D(4,6,1) D(4,6,2) ... D(4,6,J) ... D(4,6,NA)

and the entries for the initial point in the 9th column are:

ZT(INITR(9,5),9,5) D(INITR(9,5),9,1) ... D(INITR(9,5),9,NA)

and the entries for the last row point in the 17th column are:

ZT(NR(17,5),17,5) D(NR(17,5),17,1) ... D(NR(17,5),17,NA)

Following this page are typical output. The results that are shown are for the first two columns of points from the right coronary (RC) leaflet. Data are obtained for every 20 mm. Hg.

RESULTS FOR MUSCLE CORONARY VALVE LEAFLET NO. 3
(RIGHT)

PRESSURE RANGED FROM ZERO TO 120 MM. HG IN STEPS OF 20.0 MM. HG

COORDINATES X,Y,Z AND RADII RPHI AND RLAT ARE IN MM.
 ANGLES ARE IN DEGREES AND PRESSURES ARE IN MM. HG.
 ELASTIC MODULI EPHI AND ELAT ARE IN GM./SQ. MM.
 STRAINS STRAPH AND STRALA ARE IN PERCENT ELONGATION
 STRESSES SIGPHI, SIGLAT AND SIGNET ARE IN GM./SQ. CM.

NON-APPLICABLE DATA REPRESENTED BY 999.00

THE SCALE USED IS .0114 MM./MEAS. UNIT

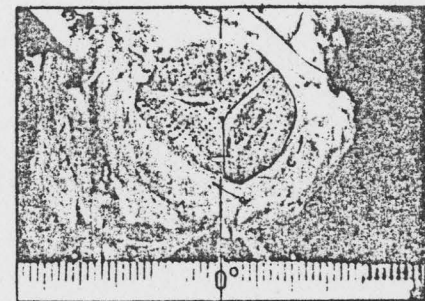
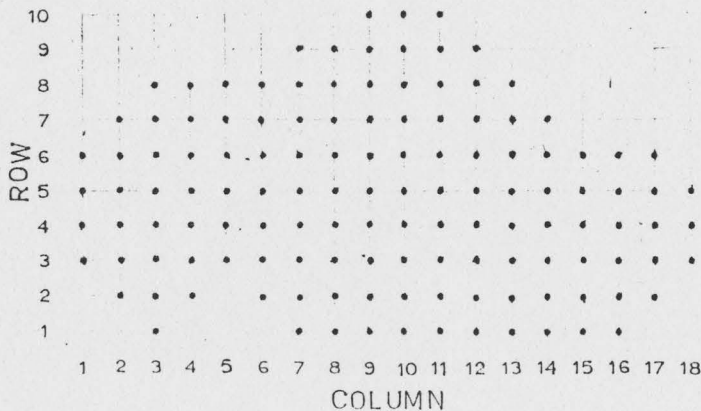
ERROR IN MEASUREMENTS IS 3.000 MEAS. UNITS
 ERROR IN SCALE IS .00003 MM./MEAS. UNIT
 ERROR IN ANGLE IS .5 DEGREES
 ERROR IN PRESSURE IS 2.0 MM. HG

THE UNSCALED (X,Y) COORDINATES OF THE CENTER OF ROTATION IS (*****,0.00)
 THE SCALED (X,Y) COORDINATES OF THE CENTER OF ROTATION IS (57.00,0.00)

THE ORGANIZATION OF THE RESULTS IS AS FOLLOWS

POINT I.D.	X	Y	Z	STRAPI	STRALA	SIGPHI	SIGLAT	SIGNET	ANGLE
COLUMN ROW	ERRX	DEYV	ERRZ	EPHI	ELAT	EPHI	RLAT		

DIAGRAM OF POINT IDENTIFICATION



C6A

RESULTS FOR MUSCLE CORONARY VALVE LEAFLET NO. 3 AT PRESSURE LOAD= 0.0 MM. HG
(RIGHT)

1	3	45.81	11.28 .07	23.26	999.00 999.00	999.00 999.00	999.00 999.00	999.00 999.00	999.00
1	4	12.67	8.86 3.02	12.67	999.00 999.00	999.00 999.00	999.00 999.00	999.00 999.00	999.00
1	5	12.67	8.86 3.02	12.67	999.00 999.00	999.00 999.00	999.00 999.00	999.00 999.00	999.00
1	6	47.31	9.14 .07	24.70	999.00 999.00	999.00 999.00	999.00 999.00	999.00 999.00	999.00

2	2	46.38	12.41 .08	22.86	999.00 999.00	999.00 999.00	999.00 999.00	999.00 999.00	999.00
2	3	46.89	11.93 .03	23.43	0.00 .80	0.00 1.50	0.00 3.41	0.00 3.95	0.00
2	4	47.38	11.30 .08	23.83	0.00 .80	0.00 1.50	0.00 2.36	0.00 25.06	0.00
2	5	47.97	10.49 .09	23.88	0.00 .80	0.00 1.50	0.00 1.59	0.00 30.70	0.00
2	6	48.21	9.70 .09	24.40	0.00 .80	0.00 1.50	0.00 2.54	0.00 10.30	0.00
2	7	48.45	9.05 .08	24.57	999.00 999.00	999.00 999.00	999.00 999.00	999.00 999.00	999.00

3	1	46.74	13.52 .06	22.17	999.00 999.00	999.00 999.00	999.00 999.00	999.00 999.00	999.00
3	2	47.42	13.06 .04	22.80	0.00 .80	0.00 1.50	0.00 3.15	0.00 1.34	0.00
3	3	47.91	12.40 .06	23.25	0.00 .80	0.00 1.50	0.00 1.05	0.00 2.17	0.00

RESULTS FOR MUSCLE CORONARY VALVE LEAFLET NO. 3 AT PRESSURE LOAD= 20.0 MM. HG
(RIGHT)

1	3	44.33	12.73 .08	22.91	999.00 999.00	999.00 999.00	999.00 999.00	999.00 999.00	999.00
1	4	12.67	8.86 3.02	12.67	999.00 999.00	999.00 999.00	999.00 999.00	999.00 999.00	999.00
1	5	12.67	8.86 3.02	12.67	999.00 999.00	999.00 999.00	999.00 999.00	999.00 999.00	999.00
1	6	46.17	10.61 .07	24.40	999.00 999.00	999.00 999.00	999.00 999.00	999.00 999.00	999.00

2	2	44.84	14.02 .05	22.23	999.00 999.00	999.00 999.00	999.00 999.00	999.00 999.00	999.00
2	3	45.43	13.56 .08	22.86	7.74 .80	2.74 1.50	9.72 2.32	13.22 3.32	18.41
2	4	45.94	12.84 .07	23.22	8.42 .80	-3.81 1.50	6.35 3.11	.80 20.93	5.99
2	5	46.55	11.91 .04	23.29	12.42 2.04	-3.62 1.50	29.85 2.01	5.19 27.37	23.31
2	6	47.03	11.14 .08	23.94	19.53 8.44	2.18 1.50	177.09 8.33	23.88 13.75	179.70
2	7	47.47	10.44 .07	24.28	999.00 999.00	999.00 999.00	999.00 999.00	999.00 999.00	999.00

3	1	45.13	15.21 .06	21.33	999.00 999.00	999.00 999.00	999.00 999.00	999.00 999.00	999.00
3	2	45.83	14.65 .03	22.04	8.79 .80	-2.62 1.50	8.85 4.35	1.55 8.13	8.03
3	3	46.40	13.97 .07	22.43	7.85 .80	-3.93 1.50	8.04 1.14	-1.21 2.17	8.04

RESULTS FOR MUSCLE COFONARY VALVE LEAFLET NO. 3 AT PRESSURE LOAD= 40.0 MM. HG
(RIGHT)

1	3	44.12	14.40 .07	22.91	999.00 999.00	999.00 999.00	999.00 999.00	999.00 999.00	999.00
1	4	12.67	8.86 3.02	12.67	999.00 999.00	999.00 999.00	999.00 999.00	999.00 999.00	999.00
1	5	12.67	8.86 3.02	12.67	999.00 999.00	999.00 999.00	999.00 999.00	999.00 999.00	999.00
1	6	45.91	11.91 .01	24.20	999.00 999.00	999.00 999.00	999.00 999.00	999.00 999.00	999.00

2	2	44.75	15.68 .03	22.29	999.00 999.00	999.00 999.00	999.00 999.00	999.00 999.00	999.00
2	3	45.37	15.14 .05	22.90	14.37 2.83	7.13 3.91	68.87 2.22	68.87 3.85	99.00
2	4	45.83	14.21 .04	23.11	11.13 1.49	-3.33 1.50	18.74 2.22	4.47 20.63	19.26
2	5	46.35	13.33 .06	23.03	11.35 1.58	-3.33 1.50	19.63 1.50	3.50 29.17	20.14
2	6	46.82	12.50 .03	23.71	24.52 11.00	4.86 2.12	395.20 6.72	4.86 24.73	395.16
2	7	47.23	11.78 .08	24.13	999.00 999.00	999.00 999.00	999.00 999.00	999.00 999.00	999.00

3	1	45.14	16.95 .03	21.38	999.00 999.00	999.00 999.00	999.00 999.00	999.00 999.00	999.00
3	2	45.83	16.22 .00	22.00	13.41 2.47	-7.85 1.50	42.86 2.39	11.70 3.13	44.27
3	3	46.40	15.44 .06	22.12	4.59 1.81	-3.30 1.50	8.27 1.73	7.00 2.97	11.20

RESULTS FOR MUSCLE CORONARY VALVE LEAFLET NO. 3 AT PRESSURE LOAD= 60.0 MM. HG
(RIGHT)

1	3	44.35	16.00 .07	23.06	999.00 999.00	999.00 999.00	999.00 999.00	999.00 999.00	999.00
1	4	12.67	8.86 3.02	12.67	999.00 999.00	999.00 999.00	999.00 999.00	999.00 999.00	999.00
1	5	12.67	8.86 3.02	12.67	999.00 999.00	999.00 999.00	999.00 999.00	999.00 999.00	999.00
1	6	46.14	13.42 .08	24.20	999.00 999.00	999.00 999.00	999.00 999.00	999.00 999.00	999.00

2	2	45.06	17.28 .06	22.46	999.00 999.00	999.00 999.00	999.00 999.00	999.00 999.00	999.00
2	3	45.71	16.61 .07	22.95	20.14 7.03	14.04 35.48	254.69 2.36	1140.65 4.24	1166.64
2	4	46.20	15.66 .01	23.20	14.95 3.13	-1.92 1.50	58.30 2.30	11.10 19.67	59.35
2	5	46.63	14.67 .04	23.03	16.94 3.98	-2.77 1.50	22.58 1.54	11.40 30.82	83.37
2	6	47.03	13.73 .00	23.71	27.13 11.00	3.50 1.54	423.69 8.76	34.65 7.61	424.93
2	7	47.42	13.00 .02	24.09	999.00 999.00	999.00 999.00	999.00 999.00	999.00 999.00	999.00

3	1	45.50	18.45 .07	21.55	999.00 999.00	999.00 999.00	999.00 999.00	999.00 999.00	999.00
3	2	46.29	17.77 .07	22.17	10.34 3.72	10.34 9.72	106.30 3.10	246.41 12.74	262.01
3	3	46.85	16.91 .06	22.32	21.75 0.00	-1.00 1.00	243.14 1.12	10.71 0.71	244.14

RESULTS FOR MUSCLE COFOMARY VALVE LEAFLET NO. 3 AT PRESSURE LOAD= 80.0 MM. HG
(RIGHT)

1	3	44.35	17.04 .04	23.03	999.00 999.00	999.00 999.00	999.00 999.00	999.00 999.00	999.00
1	4	12.67	8.86 3.02	12.67	999.00 999.00	999.00 999.00	999.00 999.00	999.00 999.00	999.00
1	5	12.67	8.86 3.02	12.67	999.00 999.00	999.00 999.00	999.00 999.00	999.00 999.00	999.00
1	6	46.00	14.10 .03	24.05	999.00 999.00	999.00 999.00	999.00 999.00	999.00 999.00	999.00

2	2	45.03	18.12 .02	22.38	999.00 999.00	999.00 999.00	999.00 999.00	999.00 999.00	999.00
2	3	45.68	17.27 .06	22.83	27.24 11.00	4.90 2.15	435.14 3.42	53.06 8.14	438.26
2	4	46.14	16.29 .01	23.09	18.67 5.61	-0.93 1.50	135.14 3.06	15.81 21.72	137.18
2	5	46.55	15.23 .07	22.88	11.06 1.46	-2.74 1.50	14.80 1.29	5.57 30.74	19.50
2	6	46.97	14.54 .00	23.54	25.39 11.00	.93 1.50	379.20 3.07	27.25 2.57	380.18
2	7	47.31	13.61 .00	23.94	999.00 999.00	999.00 999.00	999.00 999.00	999.00 999.00	999.00

3	1	45.54	19.36 .01	21.51	999.00 999.00	999.00 999.00	999.00 999.00	999.00 999.00	999.00
3	2	46.31	18.60 .07	22.12	32.38 11.00	8.50 5.09	537.20 2.54	187.59 3.81	562.21
3	3	46.76	17.34 .04	22.22	5.45 .89	-1.24 1.50	7.21 1.52	3.89 27.12	7.37

RESULTS FOR MUSCLE CORONARY VALVE LEAFLET NO. 3 AT PRESSURE LOAD= 100.0 MM. HG
(RIGHT)

1	3	44.40	18.35 .09	23.14	999.00 999.00	999.00 999.00	999.00 999.00	999.00 999.00	999.00
1	4	12.67	8.86 3.02	12.67	999.00 999.00	999.00 999.00	999.00 999.00	999.00 999.00	999.00
1	5	12.67	8.86 3.02	12.67	999.00 999.00	999.00 999.00	999.00 999.00	999.00 999.00	999.00
1	6	45.98	15.17 .07	24.09	999.00 999.00	999.00 999.00	999.00 999.00	999.00 999.00	999.00

2	2	45.14	19.43 .06	22.49	999.00 999.00	999.00 999.00	999.00 999.00	999.00 999.00	999.00
2	3	45.79	18.56 .05	22.97	37.03 11.00	7.90 4.27	601.10 3.17	150.38 4.13	619.62
2	4	46.20	17.37 .04	23.18	23.65 10.44	-1.45 1.50	326.91 2.68	22.75 21.18	326.71
2	5	46.60	16.40 .07	22.91	12.99 2.23	-2.01 1.50	36.48 1.40	8.96 23.65	37.07
2	6	46.97	15.50 .05	23.54	25.70 11.00	2.52 1.50	395.42 3.71	30.75 11.24	395.61
2	7	47.28	14.67 .09	23.91	999.00 999.00	999.00 999.00	999.00 999.00	999.00 999.00	999.00

3	1	45.60	20.50 .07	21.58	999.00 999.00	999.00 999.00	999.00 999.00	999.00 999.00	999.00
3	2	46.40	19.62 .06	22.20	26.05 11.00	5.67 2.56	453.23 3.51	67.35 5.95	453.20
3	3	46.89	18.58 .07	22.49	17.03 7.02	-1.04 1.50	91.80 2.23	18.95 23.05	92.85

RESULTS FOR MUSCLE CORONARY VALVE LEAFLET NO. 3 AT PRESSURE LOAD= 120.0 MM. HG
(RIGHT)

1	3	44.40	19.53 .06	22.80	999.00 999.00	999.00 999.00	999.00 999.00	999.00 999.00	999.00
1	4	12.67	8.86 3.02	12.67	999.00 999.00	999.00 999.00	999.00 999.00	999.00 999.00	999.00
1	5	12.67	8.86 3.02	12.67	999.00 999.00	999.00 999.00	999.00 999.00	999.00 999.00	999.00
1	6	45.94	15.98 .02	23.79	999.00 999.00	999.00 999.00	999.00 999.00	999.00 999.00	999.00

2	2	45.09	20.29 .00	22.23	999.00 999.00	999.00 999.00	999.00 999.00	999.00 999.00	999.00
2	3	45.79	19.38 .03	22.72	41.01 11.00	10.51 10.33	678.51 3.02	427.04 3.84	901.71
2	4	46.17	18.17 .01	22.91	19.00 5.93	-0.08 1.50	149.79 2.49	18.83 21.79	150.97
2	5	46.61	17.33 .07	22.55	14.61 2.59	-1.58 1.50	54.77 1.47	11.25 29.39	95.91
2	6	46.91	16.24 .03	23.26	34.77 11.00	4.45 1.91	542.54 7.79	59.72 26.99	545.10
2	7	47.20	15.36 .03	23.60	999.00 999.00	999.00 999.00	999.00 999.00	999.00 999.00	999.00

3	1	45.66	21.52 .01	21.38	999.00 999.00	999.00 999.00	999.00 999.00	999.00 999.00	999.00
3	2	46.46	20.52 .03	21.97	37.27 11.00	11.14 13.04	625.29 4.04	317.91 5.42	711.17
3	3	46.97	19.36 .02	22.23	19.32 3.29	.74 1.50	63.40 2.21	11.24 21.27	79.82

APPENDIX D

Method of Calculating the Local Radius of Curvature

In Clark et al's (1975) and Cataloglu et al's (1976) stress analyses of the human aortic valve leaflets, three-dimensional data as determined from close-range stereophotogrammetry of silicone aortic molds were fitted to a cubic polynomial equation to represent the leaflet surfaces. First and second degree differentiation of the polynomial with respect to each coordinate then give the radius of curvature at any desired point. Others have crudely approximated the leaflet surfaces with typical average homogeneous and/or isotropic curvature radii.

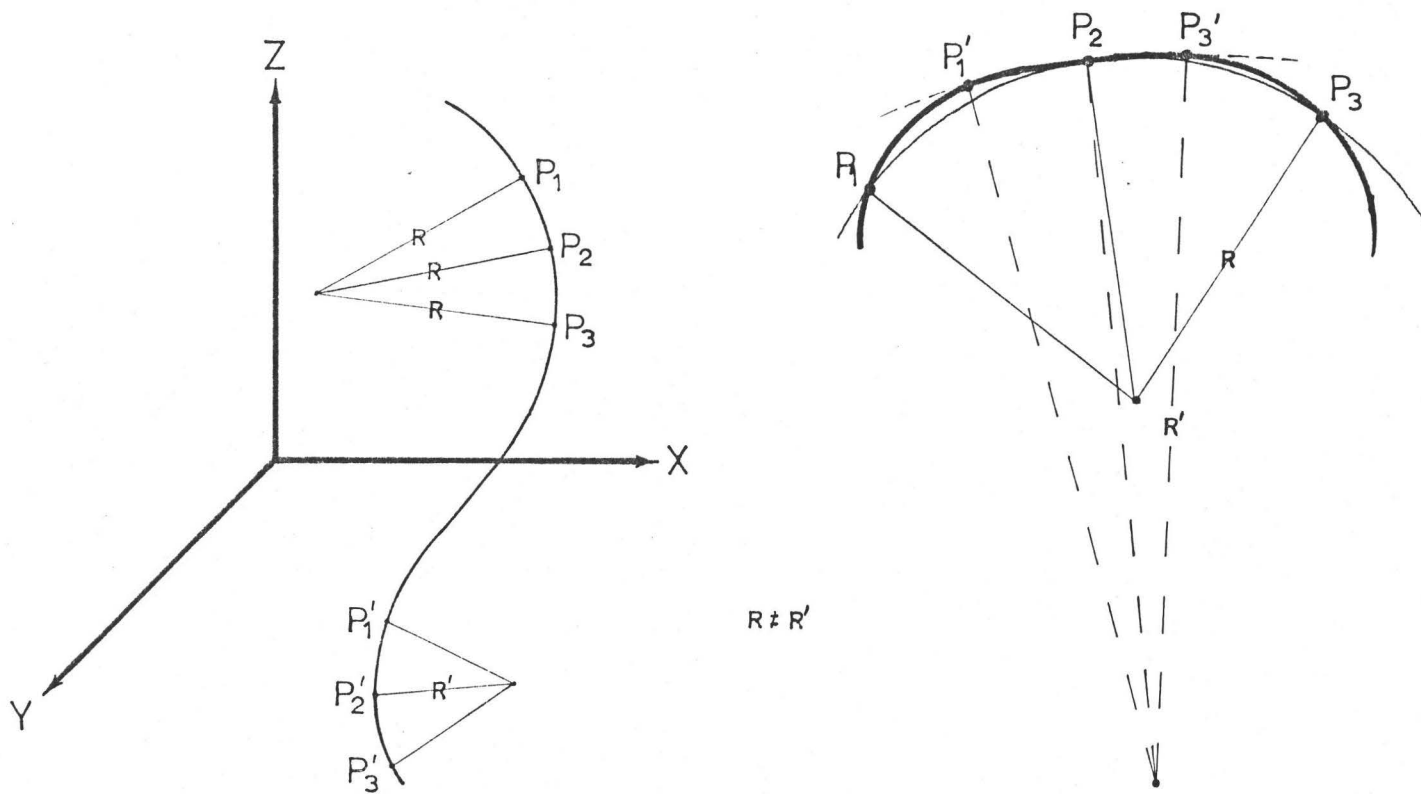
This appendix will describe a method to calculate the local radius of curvature of the valve leaflets in preferred directions; that is, as outlined by the circumferential rows and the radial columns of dots (see figure 18 on p. 77).

1. Theory

Given three randomly spaced points, say $P_1(x_1, y_1, z_1)$, $P_2(x_2, y_2, z_2)$ and $P_3(x_3, y_3, z_3)$, which lie on a monotonically-smooth curve as illustrated in figure D1a, it is desired to find the local radius of curvature (R) of the curve at the midpoint P_2 . The basis of the following derivation is the

FIGURE D1.
ILLUSTRATION of LOCAL RADII of CURVATURE, R

DEPENDENCE of R on MESH SIZE



realization that the radius of curvature for a curve at a given point may be defined as the radius of the circle which best fits the curve at that point. Three points such as P_1 , P_2 and P_3 uniquely define a circle; thus, the radius of this circle is the radius of curvature of the curve through the points. However, in fitting the "best" circle to a curve that has a changing curvature, the "best" criterion requires the points to be spaced as closely as possible. This is illustrated in figure D1b.

For the case where the three points are sufficiently closely spaced*, the derivation for R at the midpoint P_2 goes as follow. Figure D2 shows the three points lying concurrently on the curve (\mathcal{C}) and the circle (\mathcal{O}) with centre C . Points $P_1P_2P_3C$ construct triangles as shown. Perpendicular bisector CB defines the bisecting $\theta = \angle BCP_1 = \angle BCP_3$. Angles ϕ_1 and ϕ_2 are respectively the equal angles in the isosceles triangles ΔP_1P_2C and ΔP_2P_3C . The angle γ is the containing angle between the vectors \vec{l}_1 and \vec{l}_2 . The vectors between the points are defined as follows:

$$\vec{l}_1 = \overrightarrow{P_2P_1} \quad ; \quad \vec{l}_2 = \overrightarrow{P_3P_2} \quad ; \quad \vec{l}_3 = \overrightarrow{P_3P_1} \quad (1)$$

The lengths of the respective vectors are

$$l_1 = |\vec{l}_1| \quad ; \quad l_2 = |\vec{l}_2| \quad ; \quad l_3 = |\vec{l}_3| \quad (2)$$

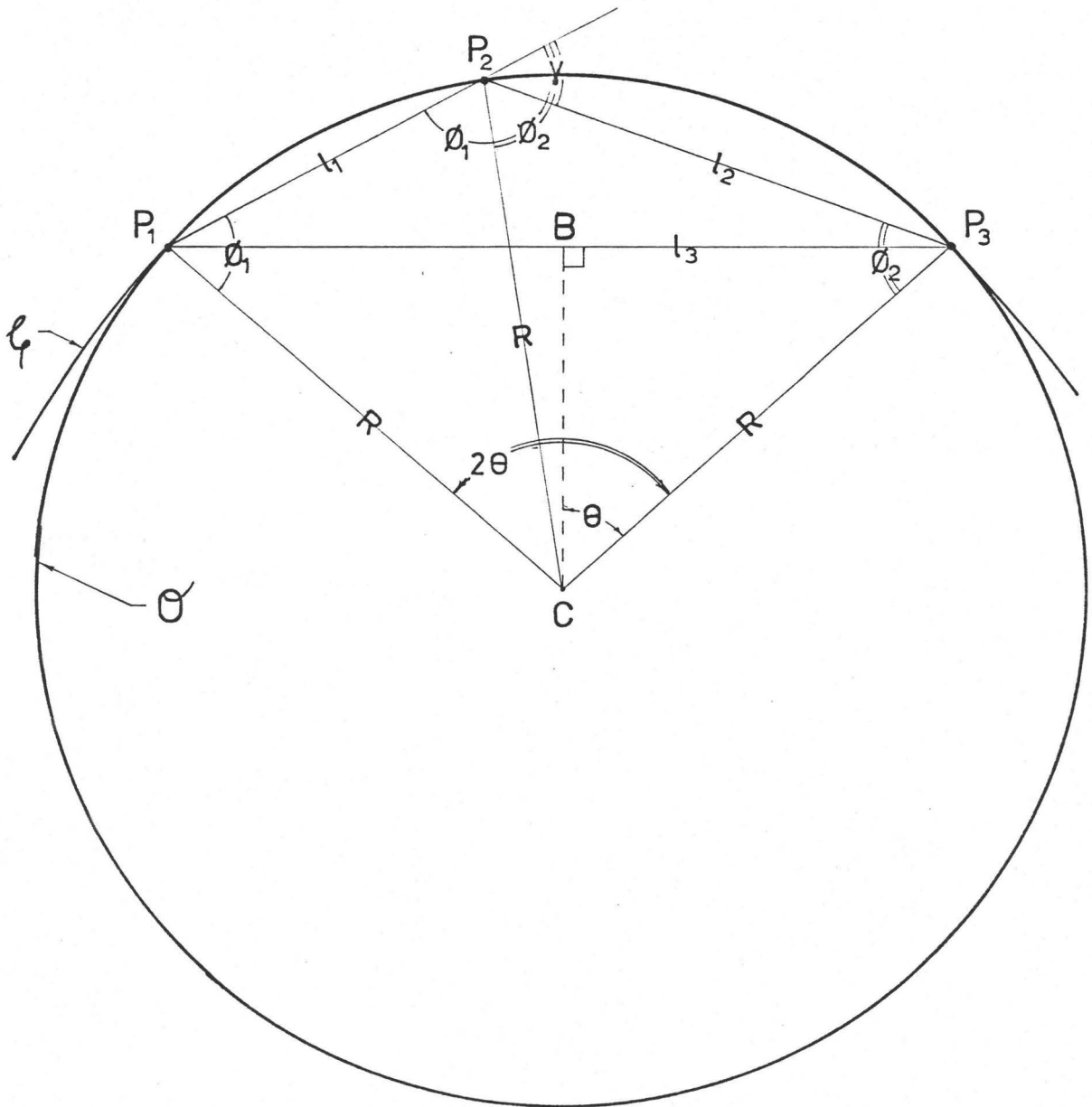
where for example,

$$l_i = \left[(x_2 - x_1)^2 + (y_2 - y_1)^2 + (z_2 - z_1)^2 \right]^{\frac{1}{2}} \quad (3)$$

* "sufficiently closely spaced" will be discussed later.

FIGURE D2.
 GEOMETRY for DERIVATION of R

D4



$$R = \frac{l_1 \cdot l_2 \cdot l_3}{2 \cdot (l_1^2 \cdot l_2^2 - |\bar{l}_1 \cdot \bar{l}_2|^2)^{1/2}}$$

$$\bar{l}_1 \cdot \bar{l}_2 = (x_2 - x_1) \cdot (x_3 - x_1) + (y_2 - y_1) \cdot (y_3 - y_1) + (z_2 - z_1) \cdot (z_3 - z_1)$$

From the two isosceles triangles ΔP_1CP_2 and ΔP_2CP_3 ,

$$\angle P_1CP_2 = 180^\circ - 2\phi_1 \quad \text{and} \quad \angle P_2CP_3 = 180^\circ - 2\phi_2 \quad (4)$$

The sum of these angles equals the angle subtended by the vector \vec{l}_3 ; that is,

$$2\theta = \angle P_1CP_3 = 360^\circ - 2 \cdot (\phi_1 + \phi_2) \quad (5)$$

$$\theta = 180^\circ - (\phi_1 + \phi_2) \quad (6)$$

From the geometry,

$$\gamma = 180^\circ - (\phi_1 + \phi_2) = \theta \quad (7)$$

From triangle ΔBCP_1 or ΔBCP_3 ,

$$\sin \theta = \frac{l_3/2}{R} \quad (8)$$

$$R = \frac{l_3/2}{\sin \theta} = \frac{l_3/2}{\sin \gamma} \quad (9)$$

Vector geometry yields

$$|\vec{l}_1 \times \vec{l}_2| = l_1 \cdot l_2 \cdot \sin \gamma \quad (10)$$

Combining equations (9) and (10),

$$R = \frac{l_1 \cdot l_2 \cdot l_3}{2 \cdot |\vec{l}_1 \times \vec{l}_2|} \quad (11)$$

By using the vector identity

$$|\vec{l}_1 \times \vec{l}_2|^2 = l_1^2 \cdot l_2^2 - |\vec{l}_1 \cdot \vec{l}_2|^2 \quad (12)$$

Equation (11) becomes

$$R = \frac{l_1 \cdot l_2 \cdot l_3}{2 \cdot [l_1^2 \cdot l_2^2 - |\vec{l}_1 \cdot \vec{l}_2|^2]^{\frac{1}{2}}} \quad (13)$$

where the dot product is

$$\begin{aligned} \vec{l}_1 \cdot \vec{l}_2 &= (x_2 - x_1)(x_3 - x_2) + (y_2 - y_1)(y_3 - y_2) \\ &\quad + (z_2 - z_1)(z_3 - z_2) \end{aligned} \quad (14)$$

2. Application to Experiment

For each interior point (P_0) on the valve leaflets, there are four other adjacent points (P_U, P_D, P_L, P_R) as shown in figure 18 on p. 77. Application of the above theory to the points P_U, P_0, P_D on the radial curve yields the radial radius of curvature, R_R at P_0 . Similarly, application of the theory to points P_L, P_0, P_R on the circumferential curve yields the circumferential radius of curvature, R_C at P_0 . In the data analysis and computer program which are described in Appendix C, these calculations are performed by a function subprogram named RAD.

A limitation of the method is its inability to determine the sense of the curvature (ie., positive or negative). But this is acceptable since the radius of curvature for any large section of the leaflets is clearly convex outwards (ie., positive R). However, if local variations on a smaller scale are desired, then the sense of the curvature is important to the understanding of the state of the valve leaflets (eg., development of compressive stresses).

A "sufficient" mesh size is defined as one that is fine enough to produce satisfactory inhomogeneous data, but yet large enough to be insensitive to measurement errors. Unfortunately, the 1 mm. mesh size used in the experiment is particularly very sensitive to measurement errors. It has already been demonstrated in Appendix B that straight-line distance calculations have errors in the order of 5% to 10%.

Therefore, the error in the numerator of equation (13) is approximately 15% to 30%. If the error in the denominator is included, the error in R as calculated from equation (13) may be 50% or more. Hence, the mesh size used in the experiment is considered "insufficient". An improvement in the accuracy of the measurements is necessary in order to retain the discreteness of the mesh size in investigating the valve leaflet inhomogeneity.

APPENDIX E

Use of Lasers to Determine Surface Strains

The technique of double-exposure holographic interferometry was first considered for determining the differential surface displacements and strains of the aortic valve leaflets. The theory and applications in engineering are well established [Haines and Hildebrand, 1966; Aleksandrov and Bonch-Bruevich, 1967; Ennos, 1968; Boone, 1969,1970,1972; Gates et al, 1969,1972; Sollid, 1969,1970,1971; Früngel and Schultz, 1970; Cook, 1971; Matsuoka et al, 1971; Bjelkhagen, 1973; Bijl and Jones, 1974; Stetson, 1976]. However, the technique has not yet been sufficiently exploited in the biomedical sciences.

Preliminary holograms were made for inflated porcine aortic valves with a 2 mW. He-Ne laser, AGFA 10E75 AH holographic plates and a Gaertner-Jong holographic table and optics. Insufficient laser output necessitated long exposure times (~30 seconds). The holograms produced were poor since 1) the aortic leaflet tissue was not particularly conducive for reflecting the red laser light and 2) the vibrations of the air-inflated valve destroyed the interferometric process. Pulsed multiple holography using a higher power laser (CO_2), which would minimize the vibration problems, was considered

next. However, this work was abandoned because of insufficient equipment. Even if the analysis was conceivable, the data measurements would have been quite formidable. It is estimated that for typical displacements and strains of the aortic leaflets, the number of interferometric fringes to be counted would be in the order of thousands. However, this difficulty should be manageable technically. Perhaps then, the pulsed multiple hologram technique should be pursued; the technique does offer a potentially very accurate means of measuring the leaflets' surface strains with minimal preparation of the valve (ie., no dotting and no molds).

Other feasible techniques, yet to be considered, are Moiré fringe techniques [Schiamarella and Durelli, 1962; Theocaris, 1964; Cargill, 1970; Stetson, 1970] and speckle photography [Archbold et al, 1970; Forno, 1975].

-
- Aleksandrov, E.B. and Bonch-Bruevich, A.M. (1967). Investigation of Surface Strains by the Hologram Technique. Soviet Physics-Tech. Physics 12(2):258-265.
- Archbold, E. et al (1970). Recording of In-Plane Surface Displacements by Double-Exposure Speckle Photography. Optica Acta 12(2):883-898.
- Bijl, D. and Jones, R. (1974). A New Theory for the Practical Interpretation of Holographic Interference Patterns Resulting from Static Surface Displacements. Optica-Acta 21(2):105-118.
- Bjelkhagen, H. (1973). Simplified Interpretation of Interference Fringes Obtained by Time Averaged Holography. Optics and Laser Technology 5(4):172-175.
- Boone, P.M. (1969). Application of Hologram Interferometry to Plate Deformation and Translational Measurements. Optica Acta 16(8):555-567.

- Boone, P.M. (1970). Holographic Determination of In-Plane Deformation. *Optics and Laser Technology* 2(1):94-98.
- Boone, P.M. (1972). Determination of Three Orthogonal Displacement Components from One Double Exposure Hologram. *Optics and Laser Technology* 4(4):162-166.
- Cargill, J.M. (1970). Moiré Method for Measuring Strains Under Welds. *Optics and Laser Technology* 2(1):154-157.
- Cook, R.W.E. (1971). Recording Distortion in Irregularly-Shaped Objects. *Optics and Laser Technology* 3(2):71-73.
- Ennos, A.E. (1968). Measurement of In-Plane Surface Strains by Hologram Interferometry. *J. Sc. Inst.* 2(1):731-734.
- Forno, C. (1975). White Light Speckle Photography for Measuring Deformation, Strain and Shape. *Optics and Laser Technology* 7(5):217-221.
- Früngel, F. and Schultz, F. (1970). Holography for Three-Dimensional Vector Analysis of Rapid Events. *Optics and Laser Technology* 2(1):32-35.
- Gates, J.W.C. (1969). Holographic Measurement of Surface Distortion in Three Dimensions. *Optics Tech.* 1(5):247-250.
- Gates, J.W.C. et al (1972). Holographic Interferometry of Impact Loaded Objects Using a Double Exposure Laser. *Optics and Laser Technology* 4(2):72-75.
- Haines, K.A. and Hildebrand, B.P. (1966). Surface Deformation Measurement Using the Wavefront Reconstruction Technique. *Applied Optics* 5(4):595-602.
- Matsuoka, S. et al (1971). Application of Holographic Interference Technique to Mechanical Studies of Polymeric Solids. *Polymer Engineering and Science* 11(1):46-50.
- Schiamarella, C.A. and Durelli, A.J. (1962). Moiré Fringes as a Means of Analyzing Strains. *Trans. Soc. Civ. Eng.*:127.
- Sollid, J.E. (1969). Holographic Interferometry Applied to Measurements of Small Static Displacements. *Applied Optics* 8(8):1587-1595.
- Sollid, J.E. (1970). Translational Displacements Versus Deformational Displacements in Double-Exposure Holography. *Optics Communication* 2(6):282-287.

- Sollid, J.E. (1971). A Comparison of Out-of-Plane Deformation and In-Plane Translational Measurements, in Developments in Holography; Seminar Proceedings, April 1971, Boston, Mass., 171-176.
- Stetson, K.A. (1970). Moiré Method for Determining Bending Moments from Hologram Interferometry.
Optics and Laser Technology 2(1):80-84.
- Stetson, K.A. (1976). Three-Dimensional Time Resolved Measurements from Holographic Records.
Optics and Laser Technology 8(4):167-174.
- Theocaris, P.S. (1964). The Moiré Method in Thermal Fields.
Proc. Soc. Experimental Stress Analysis 21(2):214-218.
- Wadsworth, N. et al (1973). Real-Time Observation of In-Plane Displacements of Opaque Surfaces.
Optics and Laser Technology 5(3): 119-123.